Investigation of Glaze Formation in Reciprocating Wear of Superalloys

Aleena James

Supervisor: Prof. Matthew Marshall

September 2023

A thesis submitted in partial fulfilment of the requirements for the degree of
Doctor of Philosophy

The University of Sheffield
Faculty of Engineering
Department of Mechanical Engineering

Abstract

High temperatures and harsh operating conditions lead to wear in aero-engine components such as the disc-blade interface. Under dry sliding conditions, metal-to-metal contact leads to adhesive transfer and wear because of their similar chemical properties. To reduce this, dissimilar material combinations can be used which reduces friction between the surfaces. However, implementing this solution can be challenging because it requires materials capable of providing both strength and resistance to heat/oxidation. This means incorporating similar elements into the alloys to meet these requirements.

An additional way to avoid metal-to-metal contact is to have an oxide layer on the surface. As sliding begins, the transient oxide layers on the surface break down due to adhesive wear. This exposes fresh metal, which then oxidises, generating wear debris in the contact area and resulting in abrasive wear. These debris particles collect in the grooves created by the abrasive wear and form a compacted oxide layer, which appears smooth and glossy under visual inspection, known as 'glaze'. The glaze layer serves as a protective coating, enhancing the durability of the interface by reducing oxidation, friction and wear, However, the effectiveness of glaze in reducing surface degradation is highly dependent on the rate of generation of glaze and the breakdown of glaze, so the balance between these is essential. Moreover, it is influenced by various operating and environmental conditions such as temperature, load, speed, humidity, and composition of materials etc. Temperature has been widely studied, however, there is limited research available on other factors like load, speed, environmental factors etc. Therefore, this study aims to investigate the influence of different factors on the formation of glaze, including contact pressure, sliding time, and historical dependence, to determine the optimal conditions for maintaining an effective glaze.

In order to carry out the above-mentioned aims, wear tests were carried out using a ball-on-flat test configuration. This study primarily investigated the effect of operating temperature and the load conditions. Initially, a similar material combination was used for both disc and the pin, then a dissimilar material combination to understand the influence of alloying elements on the glaze generation process. Finally, the history dependence of glaze was studied to understand whether having a pre-glazed surface

reduces severe wear. Both friction data and surface examinations were conducted post-test. The results have shown that temperature has a higher influence on glaze generation compared to pressure. At lower temperatures, severe adhesion and abrasions were predominant, while at higher temperatures, mild oxidation was observed. The temperature thresholds vary for different materials depending on their chemical composition. For example, nickel alloys exhibited low wear rates above 250°C, whereas cobalt-based alloys required temperatures above 400°C. The chemical composition of the layers formed at different temperatures were different and this determined the effectiveness of these layers in providing wear resistance. Dissimilar material tests indicated that a certain combination (i.e. Cobalt with Nickel based alloys) can have a positive influence by reducing surface degradation and wear rate especially when there is a higher variation among the alloying elements. The history dependence of glaze has a positive effect by reducing the severe wear seen at low temperatures to an extent however, there is no indication of no glaze layers forming. This suggests that further tests are required to confirm whether this is valid for all conditions and materials.

Finally, a wear map was produced with the input parameters such as temperature, load and the wear rate for like-on-like material tests. This allows the prediction of wear behaviour at various test combinations.

Acknowledgements

First and foremost, I would like to thank the lord almighty to enabling me to finish this thesis.

I would like to thank my supervisor, Professor Matt Marshall for his continued support, guidance and patience. I must also thank Richard Wellman, Lloyd Pallet and Glen Pattinson at Rolls Royce for their industrial support and expertise (especially in understanding the chemistry).

The technical staff (especially Chris, Dave, Luke, Oliver) in the department for helping me sort out issues with the rig/instruments and trainings. I would like to thank Mrs Kim Hyde for all the admin support. Also, my fellow PhD candidates (Eldar, Alvaro, Allan, Julian, Scott) who have helped me figure out issues with the rig, taught me how to use test rigs/systems in the department and making the lab sessions fun.

Lastly but definitely not least, a huge thanks to my amazing family- Amma, Acha, chechi, Achachen, Ochy, Appachen, Molaunty, Kunjumamma and everyone else for their love, prayers and understanding during the last few years, enabling me to achieve my goals. Thank you for being there for me always and listening when I needed to vent about things not going as planned!

I would like to express my heartfelt gratitude to everyone, whether they have directly or indirectly supported me in this journey.

Covid Impact Statement

The COVID-19 pandemic significantly impacted this research, particularly as it involved experimental study. Firstly, the closure of laboratories and research facilities during lockdown periods resulted in disruptions to data collection and experimentation, causing significant delays in the progress of this research. Additionally, travel restrictions and social distancing measures limited access to laboratories and constrained the number of people allowed inside, resulting in a lack of staff or colleagues available to provide training on equipment. This situation also led to a high demand for essential equipment such as scanning electron microscopes (SEMs), optical microscopes, and profilometers, further complicating access. Consequently, the scope of this thesis was adversely affected, as some planned experiments could not be conducted as intended, necessitating the reliance on certain assumptions in the analysis.

Table of Contents

Nomenclature

AFM	Atomic force microscopy
ASTM	American Society for Testing and Materials
BSE	Back scattered electron
c	Specific heat capacity, J/kg°C
CLA	Centre line average
COF	Coefficient of friction
EDX	Energy dispersive X-Ray
EDX	Energy Dispersive X-Ray Analysis
F_f	Friction force, N
H_s	Hardness of the softer material
HS25 or Hs25	Haynes 25
HCF	High cycle fatigue
IP	Intermediate Pressure
H	Material hardness, Pa
k	Dimensionless wear coefficient
L	Sliding distance, m
LCF	Low cycle fatigue
MML	Mechanically mixed layer
N	Newtons
N	Normal force, N
Nc	Number of contacts
r	Radius of the contact, m
SEM	Scanning electron microscope.

SE	Scattered electron
TEM	Transmission electron microscope
TTS	Tribologically transformed layers
v	Sliding speed, ms^{-1}
W	Wear volume, m^3
XRF	X-ray fluorescence analysis
3D	Three dimensional
2D	Two dimensional
μ	Coefficient of friction
ºC	Degrees Celsius
λ	Thermal conductivity, W/m.K
$λ_r$	Ratio of thermal conductivity between contacting surfaces
ρ	Density, kg/m^3

List of Figures

List of Tables

Chapter 1   Introduction

1.1   Project motivation

Friction and wear are an inevitable problem that affects all areas of engineering. Under normal conditions, good design practices with appropriate material selection and lubrication can be used to reduce the effects of friction and wear on components. However, there is a high demand for higher efficiency aero engines increasing performance; recent advances in gas turbine design involve high temperature and pressure improving thermal efficiency and power output. One of the challenges when doing this, however, is the increase in high-temperature corrosion and wear of components.

Engine components are subject to severe temperature gradients, mechanical loads, and corrosive/erosive particles. This includes erosion in the blade tips caused by sand particles, ash etc, fretting fatigue, corrosion, and oxidation [1]. Due to variations in the centrifugal load and temperature, the components expand, contract, slide and press against each other causing damage to them.

Sliding wear, in particular, is caused by the relative motion between two surfaces; this leads to various wear mechanisms such as adhesion, abrasion, oxidation, corrosion etc. causing changes in the geometry, operating performance of the components and reduction in the dynamic strength of the materials [2]. This in turn leads to safety risks and reduces the operating life of the components and the engine efficiency by weakening materials causing material loss, reducing surface hardness, changing the component geometries (such as differences in clearances) and promoting crack initiation and propagation.

The damage that occurs due to the above-mentioned mechanisms is observed in many parts within an aero engine. One such damage zone can be seen in the blade/disc contact. Both compressor and turbines are composed of several stages of blade/disc interfaces. Throughout operation, the components endure cyclic loading induced by factors such as rotational motion, which generates alternating tensile and compressive forces with each rotation. Additionally, temperature variances, particularly during engine start-up and shutdown, lead to expansion and contraction. Furthermore, aerodynamic forces, contingent upon operating conditions such as

altitude, speed, and throttle settings, contribute to this cyclic loading. These cyclic loading lead to blade/disc contact experiencing variations in centrifugal and thermal loading which then causes a combination of Low cycle fatigue (LCF) and High cycle fatigue (HCF) (see Figure 1-1). Due to the cyclic loading conditions LCF are usually associated with start-up and shutdown stages in an engine operation, where the components experience high variations in centrifugal load causing expansion and contraction of the blade producing 'larger' displacements, whereas HCF are due to high-frequency vibrations experienced by the blades during flight. These fatigue cycles initiate crack propagation, and thus premature failure of the components.
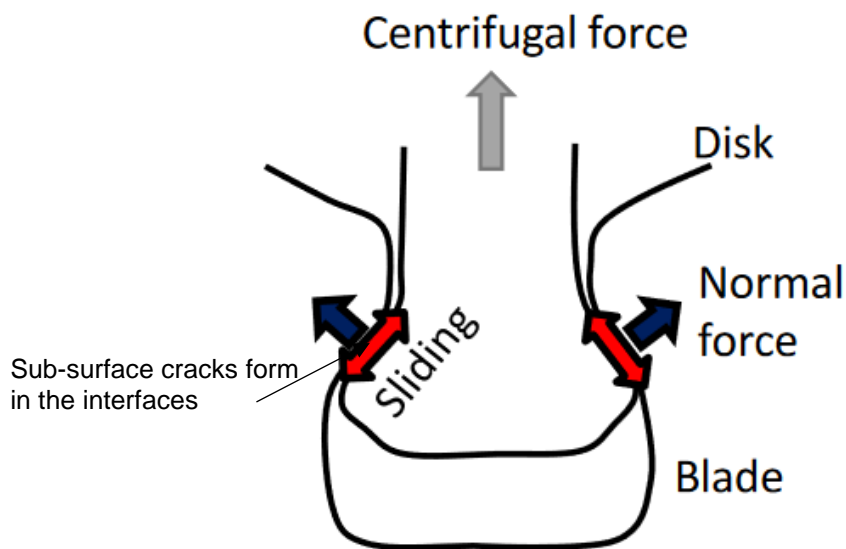
Figure 1-1: Tribological loading on the blade root/disc contact [3]

Another example of damage caused by sliding is seen in Figure 1-2, showing how a leakage path is formed in the pipe connector as a result of wear. These connectors are used within the IP turbine of the Rolls Royce Trent engines connecting service piping from the central bearing chamber to the external dressings. Pipework routes through a zone of high-pressure air, thus connectors must be able to provide adequate sealing to maintain this pressure. However, due to the vibrations and centrifugal load causing small amplitude displacements, wear is formed on the surface leading to leakage paths of high-pressure air to form [4].
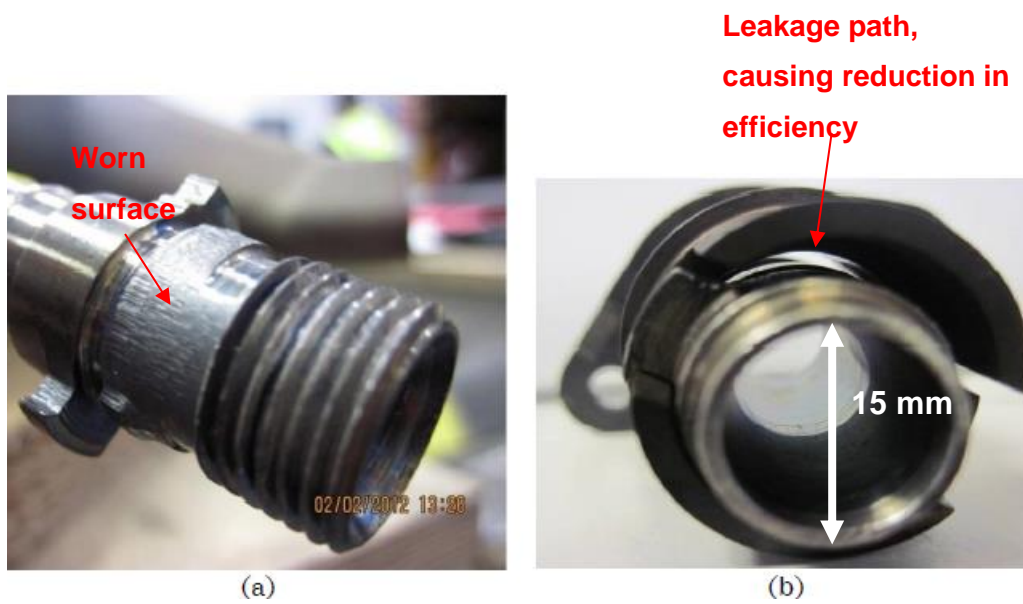
Figure 1-2: a) worn spherical seal b) resultant leakage path formed due to the wear [4]

The main wear mechanism involved in the aforementioned examples is adhesive transfer of materials between surfaces; it is more dominant in similar (chemical and mechanical properties) materials. This presents a challenge in aero-engines due to the need for heat and corrosion resistant materials limiting the material choices thus similar materials are often used. Under normal load, strong adhesive forces are observed between the contacting surfaces, and they stick together at the asperity junctions. As the surfaces move relative to each other, the asperity junctions are broken and usually, the tip of the softer surface is plucked off and adheres to the harder surface. Figure 1-3 shows the stages of adhesion between asperities and how they lead to metallic transfer and generating wear debris.
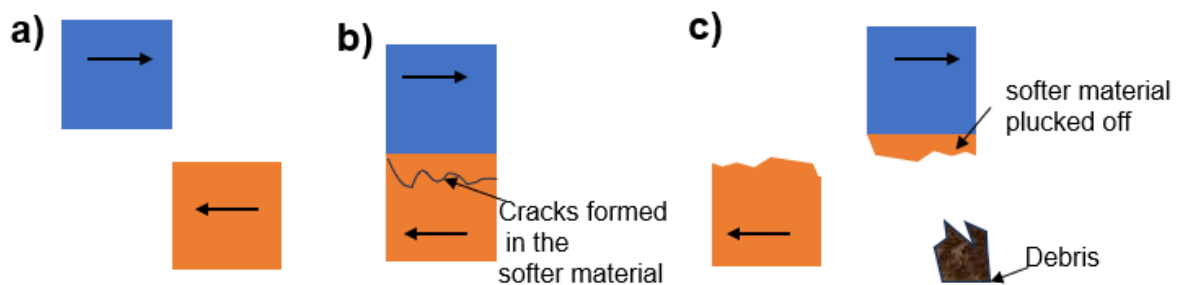
Figure 1-3: Metallic adhesive transfer process between the contacting asperities to wear debris generation [5]

Using dissimilar materials or making the surfaces harder can hinder the wear process though at extreme operating conditions such as high temperature and pressure this has not been found to be very useful as the wear rate and coefficient of friction tends to be higher. Therefore, it is better to avoid metal-to-metal contact. One way to avoid metal-metal contact is by having an oxide layer. Figure 1-4 shows how an oxide layer can act as a protective layer against wear; only a small amount of (bulk) material transfer occurs when an oxide layer is present leading to lower wear rates. Oxidation of surfaces under atmospheric oxygen conditions is a typical process, however, these (transient) oxide layers are usually thin, brittle and spall off easily with further sliding movement generating wear debris. At certain operating conditions, these debris are compacted and sintered together to form a wear protective layer called 'glaze' and this can reduce wear rate significantly. Glaze layer is a composite layer made up of wear debris which appears 'glossy' under visual inspection, and it tends to have low values of coefficient of friction. There are two ways to generate glaze; by using materials that promote glaze or by coating the bulk materials with materials which form a glaze. The process of generating glaze is thoroughly elucidated in section 2.4.5.
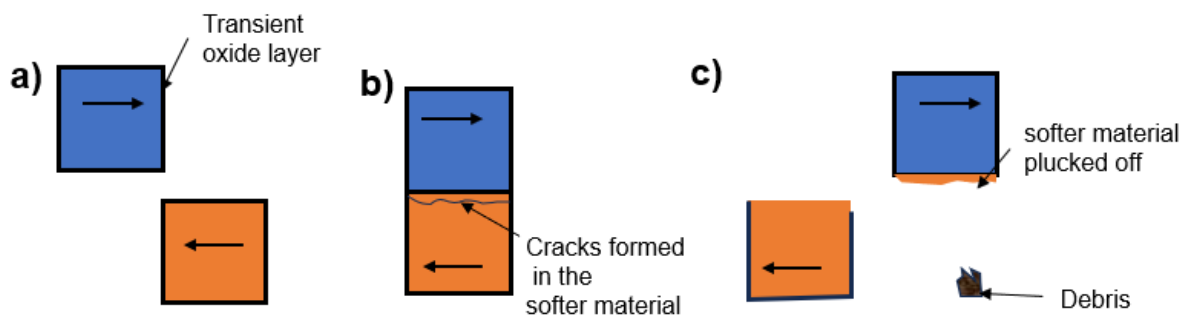
Figure 1-4: Metallic adhesive transfer process when an oxide layer is present [5]

Several methods have been adopted in recent years to promote the generation of glaze layer such as pre-oxidation of the surfaces, supplying oxide particles prior to sliding, increasing availability of oxygen, coating bulk material with glaze promoting metals etc. Coatings are the most common and reliable method and are used in various areas throughout the engine such as heat/corrosion resistant, anti-fret liner, compressor seals etc. Figure 1-5 shows some of the coatings used in turbine engines. They are applied to the bulk materials when the material properties contradict the design requirements; bulk materials are chosen so that the components have the required overall mechanical strength. Coatings are then used to enhance the surface

properties to improve the performance, especially at the contact interface so that the bulk/substrate material is protected against wear and deterioration caused by the operating and atmospheric conditions [1]. One of the ways coatings prevent bulk material damage is by having a transient oxide layer present before being in contact and once the surfaces move relative to each other, the transient layer is broken down generating oxide wear debris. These debris are further broken down and collect at the grooves. Further sliding leads to the generation of the glaze layer. However, the efficiency of glaze layer is determined by its ability to form a stable layer which is determined by a combination of operating and atmospheric conditions.

As highlighted, metallic coating systems are used to create a thin oxide layer to act as a protective layer. An important factor when considering metallic coatings is the composition and the active elements in the materials. Active elements are those that quickly form compounds with other elements present in the alloy. These elements actively participate in the alloys chemical reactions and plays crucial roles in determining the microstructure, mechanical properties, and performance of alloy materials, making it essential for detailed investigation. The primary elements in the chosen materials used in this study are Nickel, Chromium, Cobalt and Iron. If the content of the active element is too high, it leads to rapid internal oxidation and unstable glaze generation [4]. Hence, the composition of coatings needs to be in a defined range along with the appropriate of coatings operating conditions to be able to create a stable glaze layer.
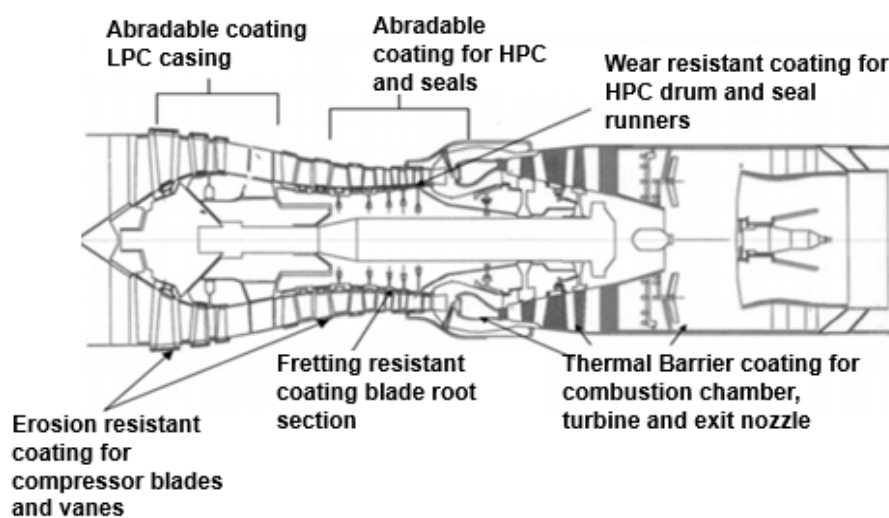
Figure 1-5: Various types of the coatings used in gas turbine *[1]*

Whilst glaze can be used to reduce wear, sliding wear is still a complex phenomenon and involves several processes such as loss of material to wear when two surfaces are in contact, adhesive transfer, diffusion of ions between surfaces and oxidation which leads to the formation and breakdown of oxide layers creating wear debris. All these processes are influenced by the operating (temperature, load, speed etc.) and atmospheric conditions (humidity, partial pressure of oxygen, presence of contaminants etc.). Nevertheless, glaze has not been investigated in detail, especially in regard to the above-mentioned conditions. Hence, this study will aid the engine manufacturers to improve their understanding of the processes involved with the formation of glaze, thus designs can be improved accordingly to minimise the wear and deterioration of components.

1.2   Aims and Objectives

The overall aim of the study is to investigate the development of glaze formation and subsequent breakdown under dry sliding conditions for Nickel and Cobalt based superalloys. The influence of various operating conditions will be studied to produce a wear map differentiating between different wear regimes and material responses and to understand fundamental drivers for glaze formation.

To achieve this the following objectives were defined:

1. Review of literature to find gaps, appropriate test methods/data to compare against etc.
2. Evaluate different design of the experiment set-up, specimen geometry, choice of test conditions etc.
3. Undertake tribological tests with similar material combinations at various operating conditions to establish the extent of factors affecting glaze generation.
4. Conduct dissimilar material tests to determine the combinations of materials that promote or hinder the glaze generation.
5. Carry out tests to analyse the history dependence to observe if there is any influence when a glaze layer is already present on the surface.
6. Produce a wear map with temperature, load and wear rate for each material combination; in order to identify preferable operating conditions.

1.3　Thesis layout

Following the introduction to this research, a review of previous studies relating to the topic is presented in chapter 2. The review focuses on the generation of a transient oxide layer during the initial stages of sliding and how this leads to the formation of a wear-resistant glaze layer. This also includes a review of the factors influencing the generation/breakdown of glaze layer. Moreover, early wear maps presenting wear test data are detailed. This review helped to form the above-mentioned aims and objectives.

Chapter 3 describes the test rig and methods used to conduct the experiments. In this study, a ball-on-flat contact configuration is used and contact modelling is carried out as well. The test materials, data acquisition methods and signal processing are detailed. This chapter also introduces test procedure and post-test analysis methods.

Chapters 4 and 5 present the experimental study of similar materials at varying temperatures and normal loads. The normal load was varied between 15 to 37.5N (i.e. 0.5-1.1 GPa) and the temperature ranges from 25^0C to 600^0C. At room temperature, interrupted tests were carried out to observe the progression of glaze layer formation. However, this was not continued for higher temperature tests due to results being significantly affected because of the changes in the contact. Chapter 6 introduces experimental data from tests conducted with dissimilar material combinations at varying temperatures and a normal load of 25N. This chapter focusses especially on the influence of alloying elements and how they promote or hinder the generation of a stable glaze layer. Chapter 7 details work carried out to examine the history dependence when a glaze layer is already present on the surface.

Finally, chapter 8 and 9 discusses the outcome of this research and future directions the work could be taken.

Chapter 2   Background theory and Literature Review

2.1   Introduction

This chapter reviews the relevant literature in dry sliding wear and the formation of glaze layer. Sections 2.2 covers the fundamentals of frictional force and the influence of asperity interaction in wear. Sections 2.3 discusses the wear mechanisms observed in sliding situations and a detailed literature review of oxidational wear and how that leads to glaze formation. Additionally, the impact of wear debris interaction is also reviewed. Several of the relevant testing methods are mentioned in 2.5. This chapter concludes with a summary of the work previously done on glaze formation and how this information will be used in the current study.

2.2   Background theory

2.2.1   Engineering Surfaces

The surfaces of solids present complex issues as there are irregularities on any surface ranging from bulk flaws to nanoscopic imperfections and friction arises due to these irregularities. The surface condition has a huge impact on the overall tribological performance of a system. They are made of peaks and valleys; the peaks or the high points of the surfaces are called the asperities. Friction and wear are a result of the nano and micro scale interactions that occur at these asperity peaks and junctions. The presence of asperities mean that the real area of contact is determined by these asperities as they usually support major loads in contacts. The true contact area is often less than 10% of apparent contact area (see Figure 2-1) [6], [10]. This leads to high stress concentrations being generated by the contacting asperities and can result in high temperatures, welding or tearing of the asperities [7] [8] [9].
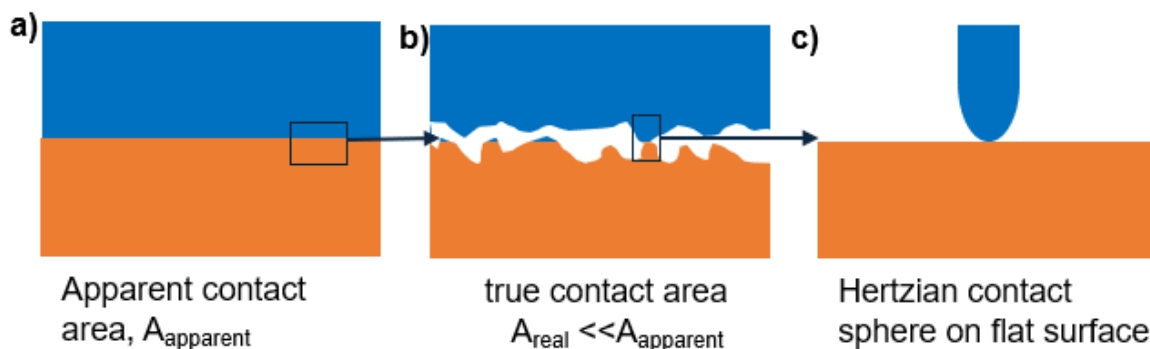
Figure 2-1: The basic concept of contact area [10]

Machined/finished components may have a surface layer which is different to the base material depending on the machining processes and the surrounding environment. Figure 2-2 shows layers in a solid surface and this contains contaminant layer, adsorbed gas layer, oxide layer and work hardened layer; oxide layer may penetrate the bulk material. Overall, the surface becomes complicated, and the formation of these layers depends on the composition of the bulk material and its surroundings. These variations in the surface layer can have major impact on the friction behaviour when two surfaces interact.
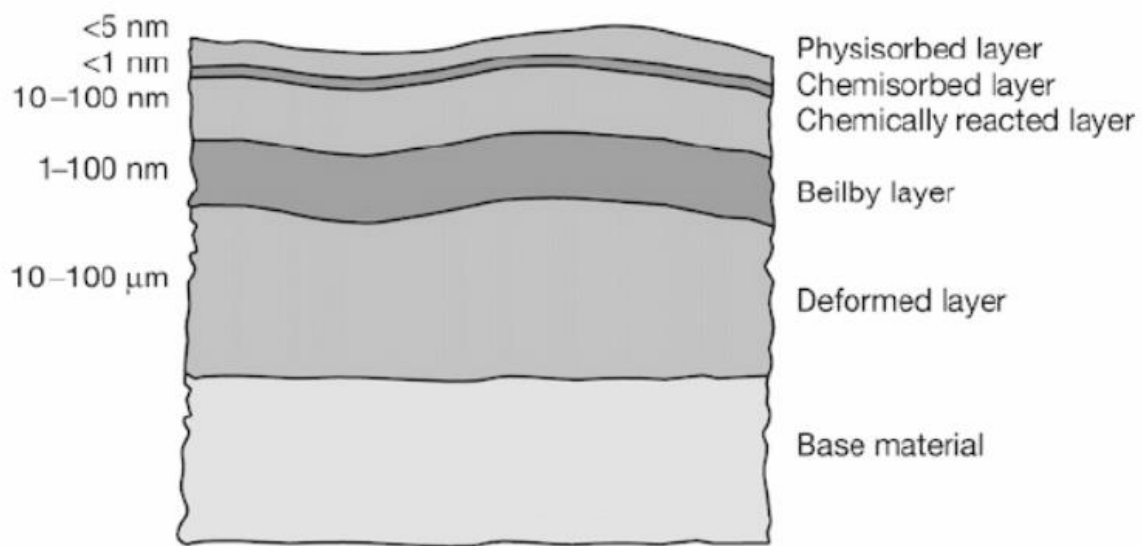
Figure 2-2: Layers with a solid surface [10]

In order to quantify the roughness of the surface, various parameters can be used such as peak to valley height, centre line average (CLA), amplitude density function, root mean square etc. CLA is one of the most used measures and it is the average deviation of the profile from the mean line. They are usually used when specifying surface finish. However, both CLA and root mean square measurements of quantifying roughness do not mean much, typically can only be used as a guide because there is a lack of sensitivity to the shape of the profile (i.e. do not provide information on local variability). These limitations can be overcome by using peak to valley height or total roughness height. Other surface roughness quantification method involves use of stylus profilometry or 3D laser scan, but comes with its own limitations. Thus, it is essential to carefully evaluate different methods according to the wear mechanism involved [12] [13]. In tribological surfaces, the roughness changes throughout the processes due to material wear.

2.2.2 Friction

Friction is the resistance to motion, when two surfaces slide over one another both lubricated and dry contacts are affected. It is manifested in many ways such as energy dissipated during relative motion (heat, noise etc.) and the friction force needs to be overcome to initiate or sustain motion. The three laws of friction (Amontons and coulomb) are [7] [9]:

- Friction force is independent of the apparent area of contact.
- Friction force is directly proportional to normal load, and it is independent of apparent areas of contact; $F_f = \mu N$, where μ is the coefficient of friction and N is the normal force.
- The coefficient of friction is independent of sliding speed. Although this is not true in all cases.

Although a wide range of research on friction has been conducted and many friction models developed, basic understanding of friction mechanisms is still lacking in information, with many unanswered questions such as how the energy is dissipated and the nano/micro scale mechanisms etc. One of the limitations when studying surfaces and tribological performance is the lack of ability to directly observe the contact interface. It is important to understand what happens in the interface and how the interface evolves especially the interaction between the nanoscale particles because the events that occur at the atomic scale has an influence on events that happen at macroscopic scale [14]. Figure 2-3 shows the different length scales of surfaces and the information that can be captured by studying at that scale. At the highest magnification scale, interactions at atomic and chemical reactions between the elements/components can be investigated, then the microscopic level surface looking at wear debris and wear scar etc. is possible.
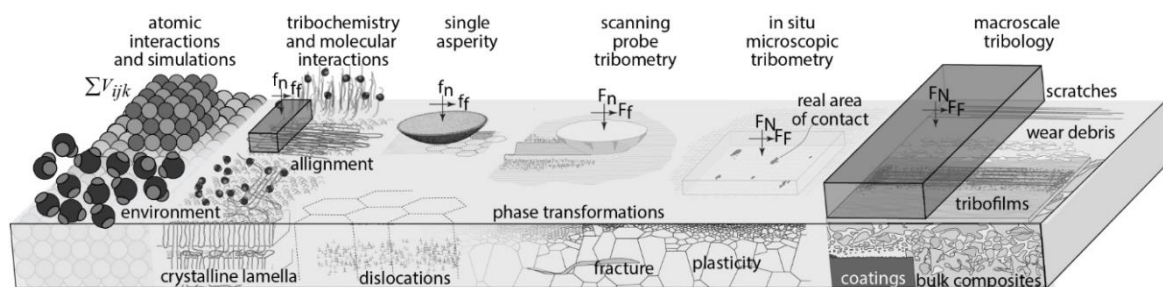
Figure 2-3: Surfaces at different magnification scale [15]

Bowden and Tabor [9] developed a more realistic theory considering the real area of contact. They pushed a steel/brass pin into an indium surface and then removed it. Two main mechanisms proposed for friction are adhesion and ploughing. They observed that the force required to separate the surfaces was greater than pushing them in, also as the surfaces separated some of the soft materials adhered to the harder material. This phenomenon is caused by adhesion. It is based on the concept that the contact is made up of many asperity contacts and the high pressure causes local welding in the contacts; these are then broken as the surfaces move relative to each other. Ploughing or plastic deformation is also caused by a hard-conical asperity ploughing into softer surface. Hence, the total friction is given by the sum of the friction arising from adhesion and ploughing.

$$\mu_{total} = \mu_{adhesion} + \mu_{deformation}$$ (Equation 2.1)

Recent studies using AFM and TEM [13] [14] has helped to understand how the debris are generated and the influence of its interactions on the friction and wear properties of the system. Single asperity studies [14] have shown that complex events occur on the surface such as the rearrangement of atoms which leads to macroscopic changes in the surface. Mishra, Inkson and Bobji [16] investigated how wear particles are formed and interact in real time using an in-situ TEM triboprobe. They noticed that, once reaching the nano hardness of the material, plastic deformation started to occur at the contact generating nanoscale wear debris. Figure 2-4 shows the formation and interaction of wear particles. Some initial particles are swept along and are removed from the wear track. Some particles are trapped; these trapped particles play a vital role in the material wear process by joining together to form elongated clusters. They observed that the wear particles roll, spin, and slide in the contact leading to changes in the friction behaviour; in particular the rolling action seems to reduce the friction. With further sliding, two mechanisms were seen with the trapped particles; they join to form clusters and then dissociate into smaller particles. The agglomeration and breakdown of clusters leads to tribofilms being formed on the surfaces and it is dependent on the number of particles, size, and geometry. Although this research gave an insight into how and what happens to the wear debris, the generation of the tribofilm is not fully understood and how the rolling motion of debris results in wear reduction [11]. Better understanding of the fundamental processes involved in friction and wear is essential to improve the performance and the life of components.
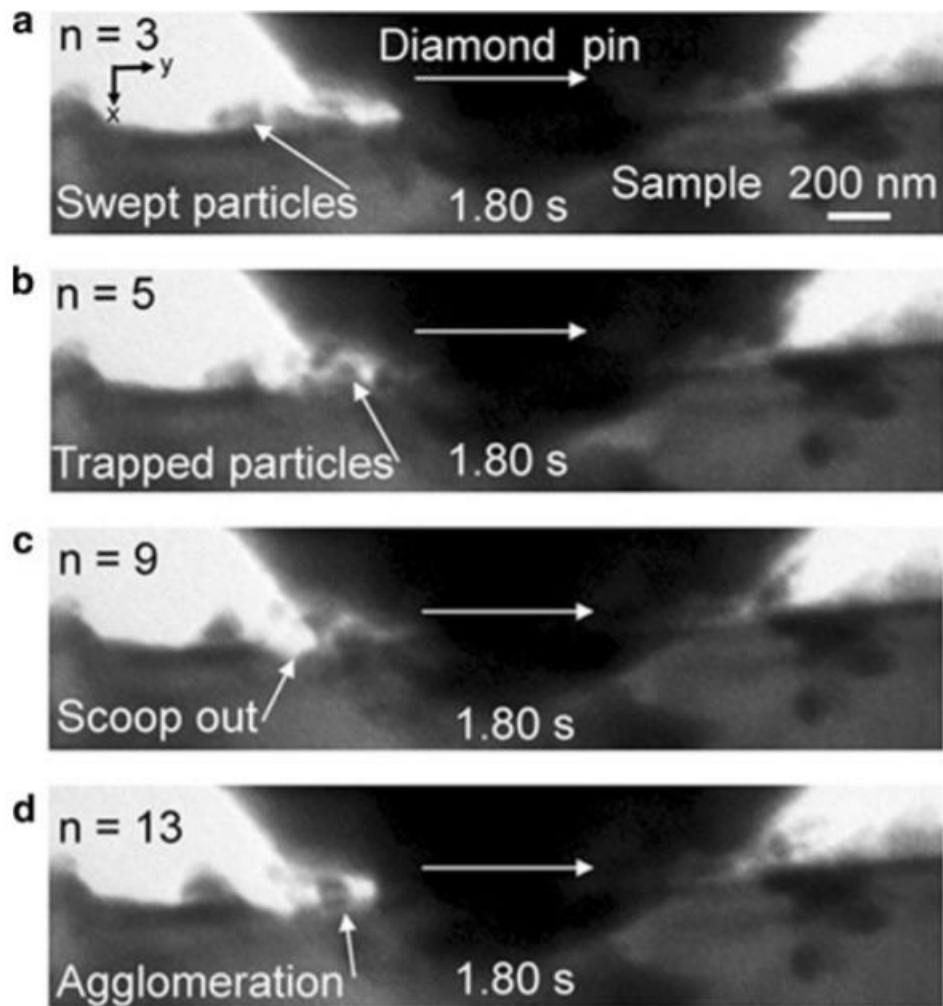
Figure 2-4: Formation and interaction of wear debris a) debris swept along and out of the track b),c) trapped particles scooping small chunks of material d) particles join together to into rounded particles of 100nm approx. [16]

2.2.3 Wear

Wear is the progressive loss of material over time because of interaction between two contacting surfaces moving relative to each other. There are various equations and models developed to predict the wear of materials. However, the most well-known equation is Archard's wear equation [17],

$$W = \frac{KNL}{H}$$
(Equation 2.2)

where W is the wear volume (m^3), K is the dimensionless wear coefficient, N is the normal load (N), L is the sliding distance (m), and H is the hardness of the materials (Pa).

Sliding wear between two metallic surfaces can cause severe surface damage. sliding wear of metal alloys is complicated as it depends on various factors such as the properties of materials involved, how it reacts with the environment, and experimental conditions. Burwell described that there are four types of mechanical wear that occur in sliding situations, and they are adhesive, abrasive, fatigue (delamination), and chemical wear. These mechanisms can operate singly or in combination [18].

2.2.3.1   Adhesive wear

Adhesive wear is when materials are transferred from one body to other. It occurs at the sliding contact between similar materials. The basic concept for adhesive wear mechanisms is that real contact between surfaces occurs at the asperities. At these junctions, bonding occurs between surface asperities. When the surfaces move relative to each other, these junctions are broken, and new ones formed. Usually, the tip is plucked off the softer asperity leaving them adhering to the harder surface. Subsequently they become loose and give rise to wear debris. High temperatures accelerate adhesive wear since the bond occurs in atomic scale and adhesive wear is usually higher during the run-in period. However, the mechanism in which wear debris are formed is still not clear due to difficulties in direct observations of the adhesive contacts.

According to Holm's findings [19], plastic deformation occurred on asperities and then they are worn away by gradual removal of atoms as surfaces slide relative to each other. On the other hand, Archard [17] proposed that wear debris are generated due to cracks being formed on the surface and fracture. Recent asperity level studies have shown both mechanisms (gradual smoothing and fracture) and it is illustrated in figure 2-5.

Aghababaei [20] [21] simulated wear debris generation using the assumption that it is produced due to two wear mechanisms: plastic deformation and fracture (see Figure 2-2). They observed that there is a critical junction size where smaller junctions have a gradual smoothing and larger junctions form debris by fracture. Although there are still many unknowns such as the influence of surface roughness, size of debris formed etc.
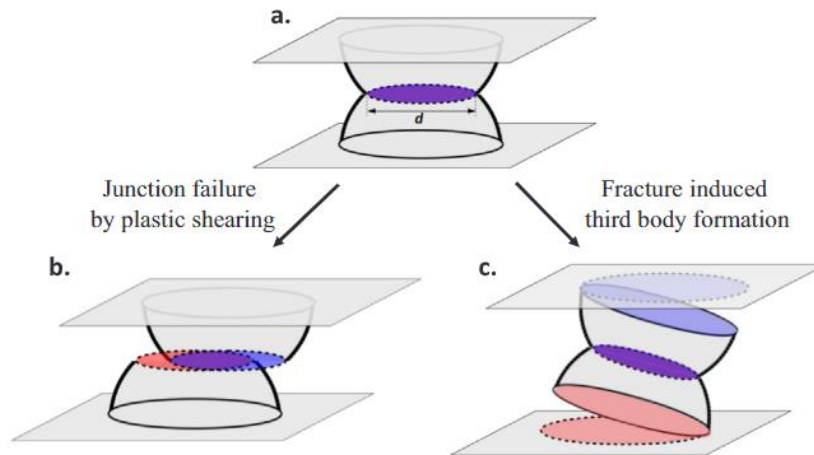
Figure 2-5: Wear debris generation mechanisms [20]

2.2.3.2   Abrasive wear

Abrasive wear occurs because of the motion relative to the surface of either harder asperities (two-body abrasive wear) or because of hard particles trapped between the surfaces (three-body abrasive wear) causing the softer asperity to be pulled out. The damage happens via plastic deformation, cutting, ploughing and brittle fracture [7]. In sliding motion, abrasive wear is usually initiated by having third body particles i.e. wear debris in the contact. Wear occurs via four mechanisms- cutting, fracture, accelerated fatigue due to repeated deformations and individual grains being pulled out by the harder particle (see Figure 2-6).
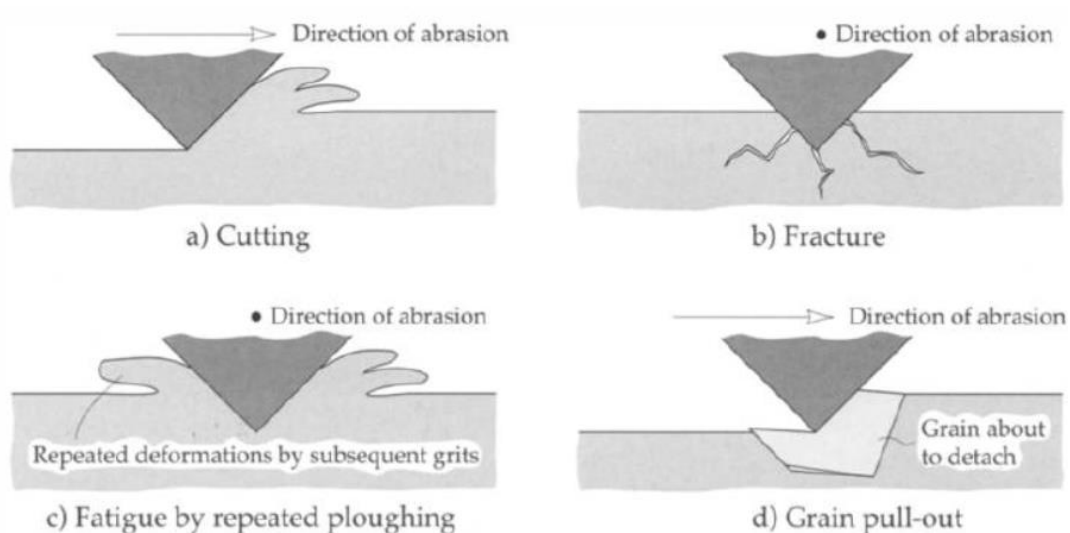
Figure 2-6: Abrasive wear mechanism [7]

2.2.3.3 Fatigue and delamination wear

Fatigue wear occurs due to repeated cyclic loading, this leads to small cracks being formed below the surface. Further deformation and loading cause the cracks to extend, propagate and join with adjacent cracks. Delamination occurs due to many deformed layers/cracks being formed below the surface layer which leads to subsurface cracks and removal of thin and long sheet like debris. Figure 2-7 shows how parallel subsurface cracks are formed in reciprocating fretting wear.
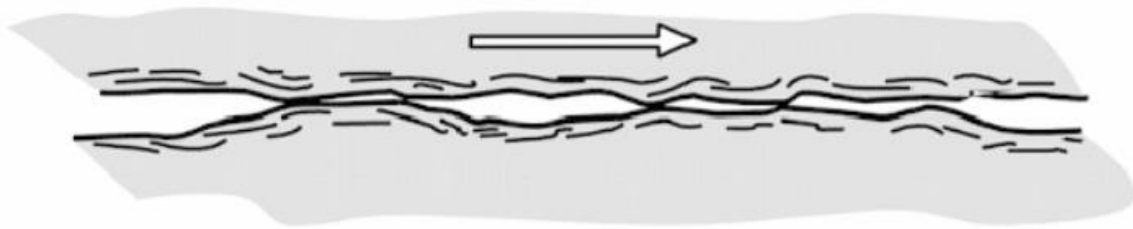
Figure 2-7: Subsurface cracks and debris formation in delamination wear [22]

2.2.3.4 Chemical wear

Chemical wear is influenced by the environmental conditions and contact mechanics in which the systems operate. Sliding action increases the surface temperature and creates surface cracks which aids chemical reactions by diffusion of active elements between the surfaces. This can eventually lead to oxidation and corrosion. Additionally, the chemical reactions can make the surface softer and weaker making it prone to crack nucleation [22]
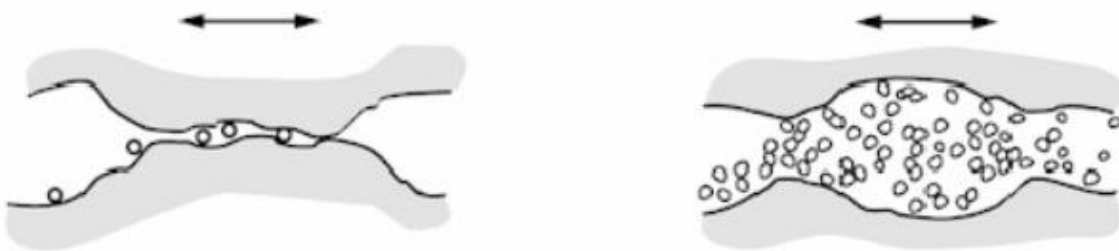
Figure 2-8: Chemical wear: how the contact geometry and debris amount changes over repeated sliding [22]

2.3 Literature review on Oxidative wear and formation of glaze

In the 1950s, Archard [17] and Hirst observed that an oxide layer appears in real areas of contact (typically a transient layer) which prevents metal-to-metal contact, leading to mild wear at a reducing wear rate by hindering the growth of welded junctions between contacting surfaces. Since the transient oxide layers are usually thin, these are broken down easily with further sliding, generating wear debris, which leads to severe adhesive and abrasive wear (due to third body) resulting in large metallic debris being produced in the contact interface. The wear debris are either removed from the contact surface resulting in a higher wear rate or retained within the wear track. Those debris that are retained in the wear track are further broken down into smaller particles and are oxidised with further sliding. These particles combine and are collected within the grooves and low points on the surface. This layer is usually called a tribologically transformed structure (TTS). Figure 2-9 shows a schematic of the evolution of TTS from generation of third body particles as a result of wear. However, it is observed on several occasions that the TTS will gradually crack giving rise to wear. This type of wear is categorised into two modes, mild (when a TTS is present) and severe wear. However, these categories are not defined clearly. Later, Quinn [23] [24] defined mild and severe wear according to the morphology and wear rate at various operating conditions. In mild oxidational wear, an oxide layer acts as a protective film which has high contact resistance and oxidised wear debris (less than 1μm) whereas in severe wear, plastic deformation and adhesive transfer is dominant with larger wear debris (between 1-100μm).

Most of the early studies [20] [21] [25] on TTS and oxide layers are conducted at room temperature. At higher temperatures, a different phenomenon was seen where a protective/lubricating layer being formed on the surface which significantly reduces wear rate. The protective layer is formed when wear debris that are retained on the surface are sintered and consolidated to form a solid layer, these layers are typically two to three times harder than the base material. This layer appears glossy and smooth under visual inspection. Thus, it can be referred to as a 'glaze' layer.
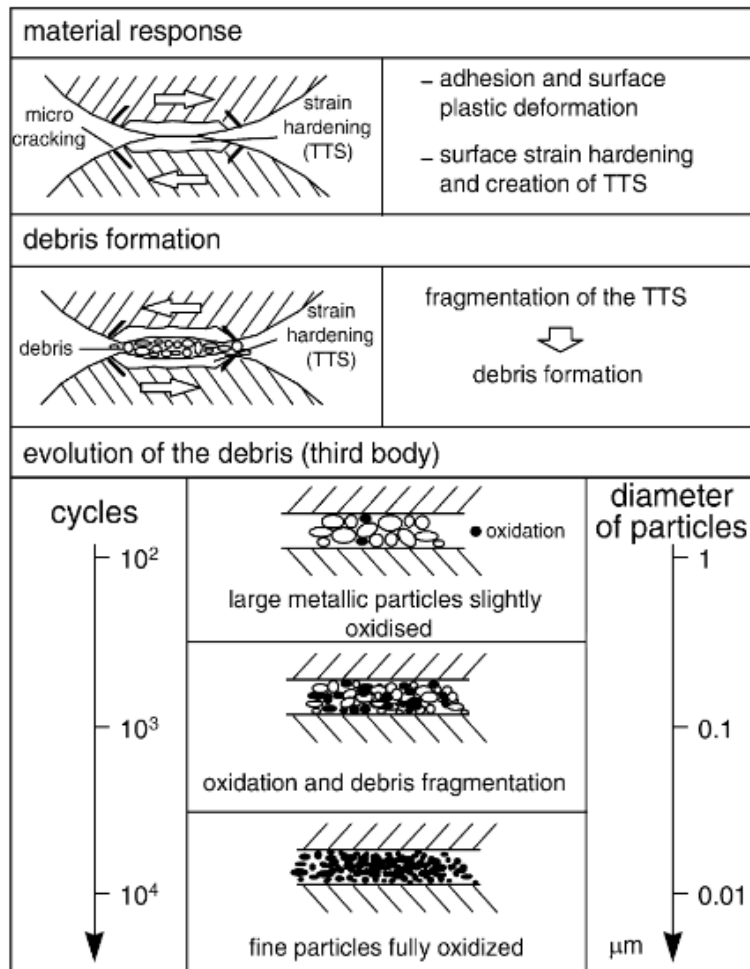
Figure 2-9: The generation and evolution of a tribologically transformed structure (TTS) [25]

Stott described three ways of oxide formation in a low reciprocating sliding setting [25]:

1. Oxidation-scrape-reoxidation: takes place in two stages. Oxidation of asperities occurs whilst in contact. The rate of oxidation depends on the material properties and its operating parameters such as contact temperature, duration, and speed. With sliding, the oxide layer is removed, exposing fresh areas of metal for further oxidation.

2. Existing oxide layer (prior to sliding) is not removed or only partially removed, so further sliding leads to compaction of wear debris leading to thickening of this oxide layer over time.

3. Wear debris generated during the initial stages are further broken down by the sliding action, this leads to new unoxidised areas of debris for further oxidation.

Each of these play a dominant role under different conditions. For example, the metallic debris mechanism is dominant at lower temperatures whereas the oxidation-scraper oxidation mechanism may be dominant at higher temperatures.

Figure 2-10 shows a schematic of how the morphology of the glaze layer changes in the steady state period as the sliding continues. Figure 2-10a shows a thin glaze layer on top of the very deformed alloy and oxides. With further sliding, glaze is broken down and deformed alloys/oxides are fractured generating more debris. Figure 2-10c, shows the glaze layer formed after a longer sliding duration. The layer below the glaze has only oxide particles, this is due to increased plastic deformation (surface cracks are formed allowing more oxygen into the alloy for oxidation) with sliding, and a rise in temperatures at the apparent area of contact due to frictional heat. The morphology varies continuously over sliding time. For instance, in the run-in period the surface just has undeformed alloy. With further sliding, surfaces start to deform due to stress, leading to cracks on the surfaces and therefore generation of wear debris [26].
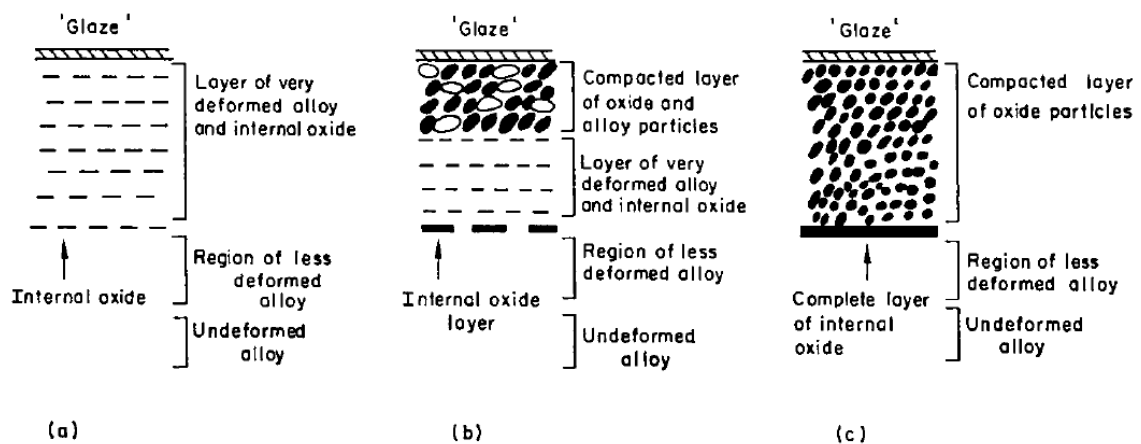
Figure 2-10: Schematic of the morphology of the glaze layer formed on Nickel alloys at elevated temperature as the sliding progresses [25].

Once a glaze layer is established, two competitive processes occur; the breakdown of layers leading to more wear debris, or further sintering and compaction to form a further thicker glaze layer. If the rate of breakdown of layers is higher than generation of glaze, wear rate will be higher. The balance between the formation and breakdown of glaze layers will dictate the wear resistance of the material combination or materials. The rate at which the formation and breakdown of glaze depends on the operating parameters, contact conditions and chemical composition of the materials/wear debris. Moreover, the effectiveness of the glaze is determined by the thickness of the

layer, and it is a product of rate of oxidation, time available for oxidation and temperature [27].
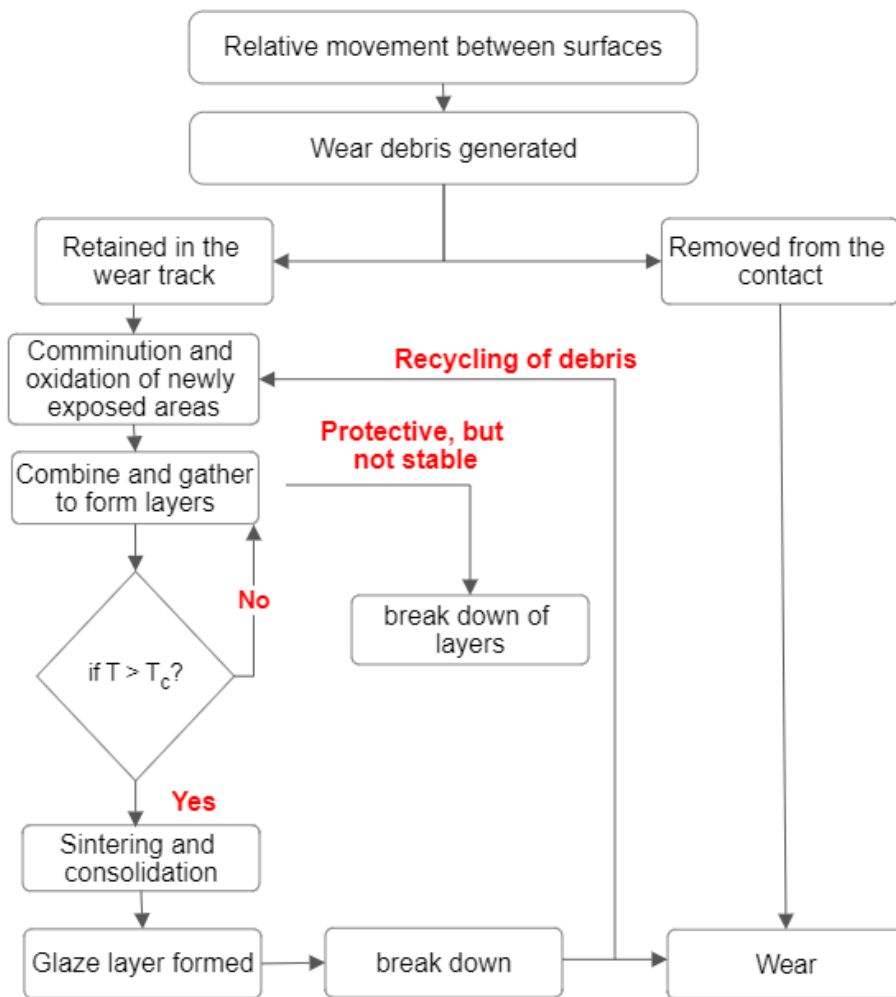
Figure 2-11: Wear process (modified version of Jiangs representation) [28]

Figure 2-11 shows what happens to the wear debris formed during sliding and the wear debris has a major influence on the subsequent wear behaviour. The wear debris are either retained in the contacting surfaces or removed from the contact. The wear debris that are retained on the surfaces can either act as a third body and cause abrasion leading to more wear or combine and form glaze layers.

Jiang, Stott and Slack [29] conducted sliding wear studies on Nimonic 80A, for the running in period or when the glaze is broken down, and the contact is essentially metal-metal leading to metallic wear debris due to adhesive transfer and delamination. They found that the debris that are not removed from the surface are broken down into smaller fragments and oxidised if appropriate environmental conditions are present.

The fine oxide particles adhere to the grooves in the contacts, and with further sliding, the particles are subjected to compression and compaction. During these processes, the fine particles are sintered together to form compacted layers of oxides, i.e. glaze. If the glaze is not stable, it can be easily broken-down releasing wear debris, this acts as a third body causing serious abrasion. A model to describe the behaviour of wear particles is described. It is supposed that a layer of wear debris is in contact with a layer of similar material wear debris, and then it is assumed that four mechanisms of movement can happen within layers. The loose wear debris at the contact surface may rotate, roll forward, skid or entrapped in the surface. Figure 2-12 shows the schematic illustration of the four mechanisms when a normal load is applied. Both rolling and rotating result in wear since they are not restricted and can freely move along with the opposite rubbing surface. When adhesion occurs with the neighbouring particle, both rotation and rolling mechanisms are restricted and the following mechanism depends on the adhesive strength and the friction force between particles. The behaviour of wear debris depends on the chemical composition, dimensions, and properties of the particles [30].
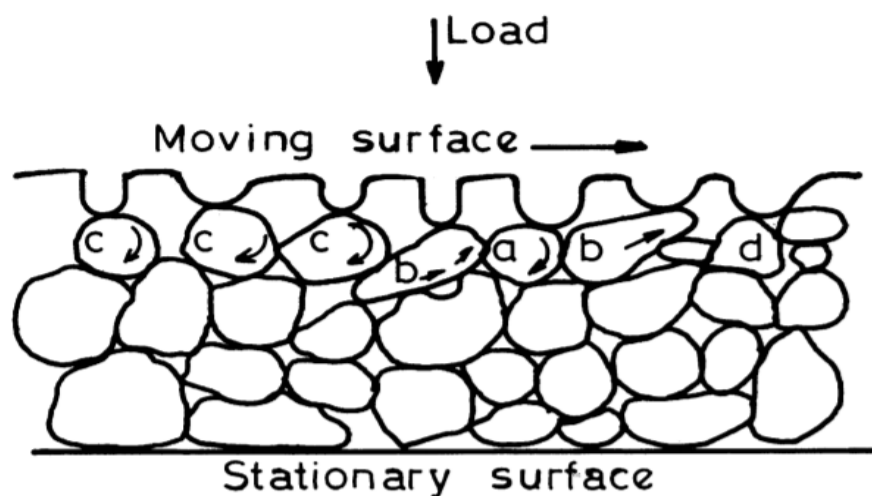
Figure 2-12: Schematic illustration of possible mechanism for relative motion of debris particles during sliding; (a)rotation, (b)skidding, (c) rolling, (d)entrapment [29]

Iwabuchi et al. [31] [32] studied the effect of supplying oxide particles to the contact prior to sliding. It was noticed that the addition of the oxide particles before sliding reduces severe wear at the run-in period because of the quicker formation of the oxide layer reducing the metal-metal contact. However, it was easily broken down because of not having enough oxide particles; a critical number of particles were needed to

form a stable glaze. The critical amount is determined by the balance between the rate of breakdown and glaze layer formation. Additionally, the composition of the supplied particles needs to be considered for the stable generation of a glaze layer. The rate of reduction in wear rate depends on the load and surface roughness. The critical value increases with increasing load and increasing the surface roughness reduces the time it takes to form a stable layer since the grooves on the surface act as a particle accumulation site and aids the compaction process.

Finally, Hiratsuka and Muramoto [33] investigated the effect of wear debris in wear mode transition when a copper pin was rubbed against an iron disc. Before the transition to mild wear, the debris generated were large metallic particles, whereas, after the transition, the wear debris were found to be fine black oxides. When the debris were removed from the contacting surface, the transition to mild wear does not occur due to no glaze layer being formed. As the load is increased, the time taken for transition increases however, the coverage of glaze is also increased with applied load. Increasing speed at low loads had minimal effect on the time taken for the glaze to form, but as the operating conditions are increased, the time taken also increases.

As highlighted in the preceding discussion the formation and breakdown of glaze is influenced by various factors; this includes the material composition, operating and environmental impacts. Each of these plays a vital role and having the right combination of parameters has a significant effect on the formation of stable glaze. For instance, in order to form a stable glaze layer, it is necessary to allow diffusion of active elements into the contact surface and the rate of diffusion depends on the temperature, which in turn is influenced by the load and speed (through the addition of flash temperature).

2.3.1 Factors influencing glaze formation

2.3.1.1   Contact conditions

Temperature is one of the main factors that influence the rate of glaze generation and the efficiency of the layer. It affects the kinetics of the oxidation process and thus the glaze formation process. The microstructure of the glaze layer and the rate at which they are formed is highly dependent on the temperature. This is because oxidation of debris/metals occurs due to the diffusion of ions into the surface and the rate of oxidation increases exponentially with an increase in temperature [30]. Additionally,

sliding increases surface temperature which leads to softening and melting (at extreme conditions) of surface layers. This is further accelerated by high sliding speed and load.

Most metals and alloys have a critical temperature, above this, the wear rate becomes significantly lower due to a stable glaze layer being generated. The critical temperature depends on the chemical composition of the debris/materials and the operating conditions. The maximum temperature it can reach depends on the melting points of the contacting surfaces [34].

Since the temperature has such a significant influence in the formation of glaze, it is essential to take the flash temperature into consideration when deciding the total surface temperature, which is determined by the ambient temperature plus the flash temperature contributions. Flash temperature occurs close to the true area of contact where energy is dissipated creating a short period of very high temperature compared to the bulk temperature, even reaching melting points of material under certain conditions. Being able to predict the flash temperature can provide significant information on changes in the mechanical and tribological properties of the contact. Several analytical models to predict the flash temperature rise have been developed considering the contact geometry, material properties, operating variables etc. Two of the most used models are Archard and Kuhlmann-Wilsdorf model [35]. Archard's model works for mild wear conditions and is not reliable at high loads and speeds. It is based on the heat flow between contacting surfaces. Unlike Archard's model (only circular contact), the Kuhlmann-Wilsdorf model allows both circular and elliptical contacts to be modelled, moreover, it can also use dissimilar material combinations. Kuhlmann-Wilsdorf's flash temperature for unlubricated wear for circular and plastic contact between asperities is given by [35]:

$$\Delta T_0 = \frac{\mu v (\frac{\pi N H_s}{N_c})^{1/2}}{4\lambda_1 (\frac{1}{Z_0} + \lambda_r)} \qquad \text{(Equation 2.3)}$$

where μ is the coefficient of friction, v is the sliding speed, N is the normal load, H_s is the hardness of the softer material, N_c is the number of contacts, λ_1 is the thermal conductivity of the softer surface, λ_r is the ratio of thermal conductivities between the

two surfaces, r is the radius of the contact, d is the density and c is the specific heat capacity.

$$Z_0 = \frac{1}{1 + v_r/3} \qquad \text{(Equation 2.4)}$$

$$v_r = \frac{v}{\lambda/rdc} \qquad \text{(Equation 2.5)}$$

As seen from the above equation, flash temperature is highly influenced by the load, sliding speed and material properties. However, the accuracy of this model is dropped by the difficulties to find/measure the number of asperities and true area of contact.

Lancaster [27] studied brass on hardened steel using a pin-on-disc device at various temperatures, loads, and speed conditions. It was found that at low speeds, the severe to mild wear transition is dependent on the time available for oxidation (because the effects of frictional heating are negligible) whereas, at higher speeds, the transition depends on the rise in the contact temperature due to frictional heating. The transition from severe to mild wear occurs after the critical temperature is reached. The critical temperature is defined as the mean temperature over the apparent area of contact and is not affected by the source of heating (either frictional or external). It depends on the combined magnitudes of load and speed. Additionally, critical temperature increases as the load is increased, meaning a higher rate of oxidation is required at higher loads to generate a stable oxide layer. Conversely, when the speed is increased, the critical temperature lowers due to an increase in frictional heating. Even in the absence of frictional heating, a glaze layer is formed as long as a critical load/speed limit is reached and the rate at which the glaze is formed is dependent on the time available for oxidation and compaction of the debris. Morphological examination has shown that there are smooth brown or black patches on the surfaces, i.e. glaze. Once the sliding conditions are considerably higher than the critical values for wear mode transition, a uniform and thick glaze is formed due to the rate of oxidation being higher than the rate of breakdown of the layers.

Experiments conducted by Jiang [36] at 20°C, 150°C and 250°C have shown the effects of critical temperature. Although compaction of the wear debris occurred at 20°C (critical temperature is not reached), it did not sinter to form a glaze layer. At

150°C, some glaze areas were seen but there was a large area of non-glaze region. This means that the temperature is close to critical temperature, but still limited sintering occurs. At 250°C, a clear and stable glaze layer is observed.

A similar study by Jiang et al [29] investigated the effect of temperature and wear debris in the wear process during dry sliding conditions by studying nickel alloys in a pin-on-disc rig setup at temperatures 20, 150 and 250°C. It was found that wear rate is reduced at the higher temperature. However, when the temperatures are varied rather than kept at a constant temperature, the wear rate was higher due to more wear particles being generated. This is mostly due to the time it takes for sintering and compaction at different temperatures. For instance, when the temperature is reduced to 150°C from 250°C, the rate of sintering and compaction reduces, so it takes longer to form a stable glaze layer leaving loose wear debris at the contact, since higher amounts of debris are formed at higher temperatures, i.e. 250°C. Excess time is required to compact these debris. Therefore, this debris can act as third body particles causing abrasion. However, they did not go to higher temperatures than 250°C to see if the rate of compaction and sintering would increase to a higher rate than debris generation.

The applied normal load and the sliding velocity are the next important factors as they influence the wear rate through changes in the surface temperature as mentioned in Equation 2. The friction coefficient decreases with increasing pressure. Typically, at higher load, the flash temperature increases to a significant extent owing to a higher level of frictional heat generated at the contact surface.
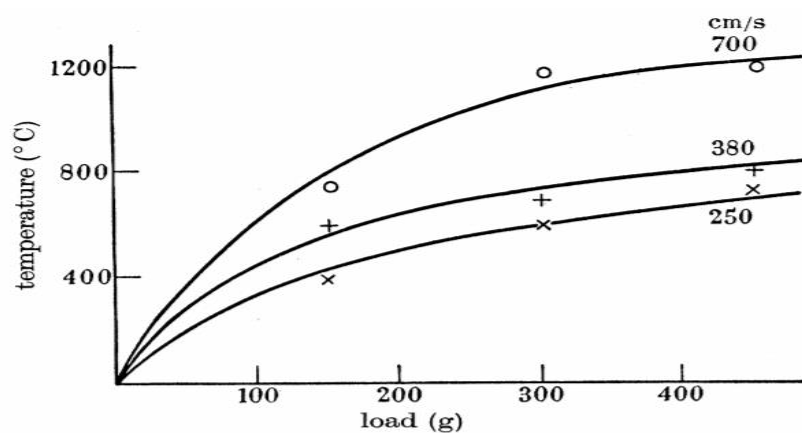
Figure 2-13: Variation in surface temperature due to flash temperature rises at different normal loads and sliding speed [37]

Early studies on surface temperature during sliding by Bowden and Thomas [37] have found that both load and speed influenced the surface temperature. Figure 2-13 shows the surface temperature as a function of load at varying speeds from a sliding wear test of steel against glass; as the load and temperature is increased, the surface temperature also increased. Material properties such as melting point defined the maximum temperature; except when the oxides are already present on the surface, in that case, the metals burn leading to very high temperatures.

Similarly, Jordan and Stott [38] investigated the influence of load and substrate hardness on the establishment of glaze layers by using high-speed steel/ high chrome steel against a carbon steel disc at high temperatures (500-600°C) and loads of 10,15, 20N (i.e. an average contact pressure of 0.34 – 0.5 GPa). As the load is increased, the size of the wear debris particles increased. They found that it is harder for the larger debris to be collected into the grooves in the surface hindering the glaze layer formation. The effect of hardness was more obvious with the temperature variations. For instance, when the temperature was 500°C the debris particles formed were harder compared to those formed at 550°C, leading to more abrasion, increasing the overall wear rate.

Li et al. [39] studied the effect of sliding speed on the generation of oxide debris and wear mechanisms involved with Ti–6Al–4V alloy against steel. The tests were carried out between 0.5 – 4 m/s and normal load between 10-50N (average pressure of 0.34 – 1.5 GPa). An increase in the contact temperature was observed with the increase in speed, this led to an increased rate of oxidation of the debris. Low levels of glaze were seen at the lowest speed, i.e. 0.75m/s, due to not having enough debris for the compaction and thus generation of the layer. More recently, Zhang et al. [40] investigated the wear resistance of ZG42CrMo under various sliding speeds and load conditions at ambient temperature. They observed that as the load is increased the wear rate increases due to the formation of larger abrasive wear particles. However, as the speed is increased with load, the wear rate increases initially with a higher amount of wear debris forming, but once a critical load and speed are reached the wear rate decreases because of the rise in surface temperature which led to the formation of a protective oxide layer.

As discussed before, there are several factors affecting the glaze layer formation and many authors have sought to explore multiple factors in combination. An investigation conducted by Alkelae and Fouvry [41] studied the influence of various parameters such as temperature, sliding lifetime, load, amplitude, and frequency on nickel alloys Waspaloy (counter body) and René125 (as the sample). As the sliding duration is varied, a cyclic evolution of the wear rate is observed with an initial decrease in wear rate due to the glaze, it then increases because of the breakdown of the glaze and the cycle repeats. As the load and the amplitude are increased, an increase in the wear volume and larger wear debris are generated which are removed from the sliding interface before they are broken down into smaller fragments. This led to a larger wear scar. With increasing amplitude, the glaze was found to be stable until 120µm (having a glaze thickness of 35 µm), afterwards glaze is broken down due to fatigue. With the increase in frequency, there is a significant increase in the wear rate. Although a stable glaze layer is seen, it is immediately broken down generating more wear debris leading to a higher wear rate because of not having enough time to form a thick layer. However, the test temperature was only up to 400°C; higher temperature tests are necessary to investigate the evolution of the microstructure as there will be changes in the oxide phases.

Tests conducted by Wohltat [42] investigated the influence of various parameters such as material, load, temperature, frequency of sliding (speed), and history dependence on the generation of glaze. Studying the dependence of history is an important factor in an aerospace context since the temperature profile varies in a flight cycle such as during take-off/landing and cruise. Three materials were studied (MarM002, Inconel 718, Inconel 713) at temperatures between 400°C to 700°C. They found temperature as the dominant parameter in the generation of glaze; with stable glaze formed above 500°C and a reduction in both coefficient of friction and wear width. With regards to the material type, alloys with a lower content of chromium (Cr) had better glaze generation capability making MarM002 (9%) the best followed by Inconel 713 (12%) and Inconel 718 (19%). Both load and frequency had a similar effect, hindering the glaze process as they are increased. With an increase in load (12.5 to 50N) and frequency, larger wear debris were formed increasing wear volume. Also, increased frequency led to the removal of wear debris from the wear track at the same time increased speed aided to break down the debris into smaller fragments. Finally, pre-

glazed surfaces had a positive effect by reducing the coefficient of friction faster (i.e. lower number of cycles). They carried out two tests; 1) a combined test where a stable glaze was generated at 700°C, then the same samples were tested at a lower temperature (600°C) and 2) simple test without preoxidation at 600°C. It was seen that it takes a lower number of cycles to generate a glaze on the pre-glazed surfaces. For instance, it only took around 580 cycles for a pre-glazed Inconel 713 against the Inconel 718 surface to generate a glaze, whereas the same material combination (without preoxidation) took around 1800 cycles to generate a stable glaze. So, the pre-glazed surfaces can help generate glaze as the temperature is lowered (i.e. cruise).

2.3.1.2   Environmental conditions

The operating environment has a major role in dictating how the glaze is formed on the interacting surfaces. The presence of an active gas will create an adsorption layer which reduces the adhesion forces between the contacting surfaces. Jiang and Stott [43] investigated the influence of partial pressure of oxygen in an oxygen/argon mixture at temperatures between 20-600°C. An increase in partial pressure of oxygen reduced the wear rate owing to the reduction in the size of the wear debris and the increased number of wear debris. Thus, making the agglomeration and compaction process faster. This is due to both mechanical and chemical effects; as the partial pressure of oxygen is increased, there are more oxygen atoms available to react with the deformed surface layers and debris creating more oxidation. Additionally, the time required to have mild wear decreased with an increase in the partial pressure of oxygen. The wear rate was found to be independent of the partial pressure of oxygen once the critical temperature is reached (in this case, 400°C).

Moving away from the level of oxygen, Klaffke [44] investigated the effect of relative humidity and normal load on the friction and wear behaviour of steel at an ambient temperature of 25°C. Relative humidity of dry (5%), normal (45-55%) and moist (100%) conditions were used and normal loads between 1 to 10N. As the relative humidity was increased from dry to moist, there was a decrease in the wear rate, this was due to more oxygen available for oxidation from the water vapour. As the load was increased, the wear rate increased due to the higher loading of the asperities leading to more plastic deformation. Between load and relative humidity, the load had a more significant role in the production of glaze layers. Humidity acts as a lubricant and slows

down the severe wear process. However, the author did not investigate the influence of temperature, microstructure of the layers and sliding speed on the glaze formation.

2.3.1.3   Microstructure and chemical composition

As outlined in the previous sections, wear debris plays a significant role in the generation of a wear-resistant glaze layer. Thus, studying morphology and the chemical nature of the debris would be of great importance to fully understand the behaviour of these layers. Previous studies have found that two processes dominate the generation of the glaze layer [30]; oxidation of the wear debris and sintering of the debris to form a compacted layer. Oxidation is promoted by the flash temperature rises and the plastic deformation caused by the sliding action which leads to surface cracks and porosity allowing oxygen atoms to diffuse into the bulk material. Sintering is led by the diffusion capacity of the elements in the metals to move from one to the other.

Xin, Wang and Li [45] studied the microstructure of the subsurface caused because of fretting wear of Inconel690 against stainless steel. Their investigations found that the subsurface was made of five layers; a top oxide layer with nickel chromite and iron oxide, then a mixed oxide layer with fine grains of nickel oxide and chromium oxide, below that a tribologically transformed structure (TTS) with no oxides but recrystallised structure, plastically deformed layer with cracks allowing oxygen diffusion and finally the bulk material. A higher concentration of oxygen was found on the top layer, and it was reduced in the sublayers. This corresponded to the grain size with fine nanoparticles in the top layer with an increase in the sub-layers. TTS was found to have very little or no oxygen concentration. These layers were also observed in the studies conducted by Stott, Lin and Wood [19] during high temperature wear tests in nickel alloys (C263, Incoloy 910, Nimonic 75 and Nimonic 108). They observed a thin composite glaze layer; the chemical composition differed at different temperatures. Nickel oxide was dominant in all alloys up to 400˚C and above 400˚C nickel chromite was the dominant compound.

Likewise, Viat et al. [46] attempted to find the role of alloying elements in the formation of glaze in a cobalt-based alloy (Haynes 25, HS25). So, they compared the tribological behaviour of HS25 to pure chromium, cobalt and nickel (since they are the main alloying elements in HS25). They observed that only cobalt was able to produce a similar glaze layer as HS25. They suggested that it was because cobalt had a better

diffusion capability, and the thickness of glaze is dependent on the sintering process. Sintering can only take place if the atoms can diffuse and create bonds on the surface. They concluded that glaze formation is more kinetically driven than thermodynamically.

Progressing from Viat's studies, Dreano et al [47] studied the microstructure of the glaze layer formed during the fretting of Haynes 25 against alumina. They observed three oxide layers (see Figure 2-14) with a transient oxide layer before sliding, as the sliding progresses a mixed oxide layer, and finally a stable glaze layer with mixed oxide sublayer. The chemical composition of each layer was different. The transient oxide layer is rich in chromium due to its capability to diffuse easily into the surface and react with oxygen. The mixed oxide layer is mainly composed of a chromium oxide layer with traces of other elements such as cobalt, nickel, tungsten, and manganese. A higher amount of oxygen was also present due to the cracks in the surface. This chromium-rich mixed layer is removed by further sliding leading to a chromium depletion in the layers and oxidation of cobalt. Cobalt oxides diffuse easily compared to chromium oxide creating a cobalt-rich gaze layer meaning cobalt has better sintering capabilities. However, both of these studies were carried out on a point contact for simplification, need to conduct studies on more representative contacts to fully understand the behaviour of these materials.
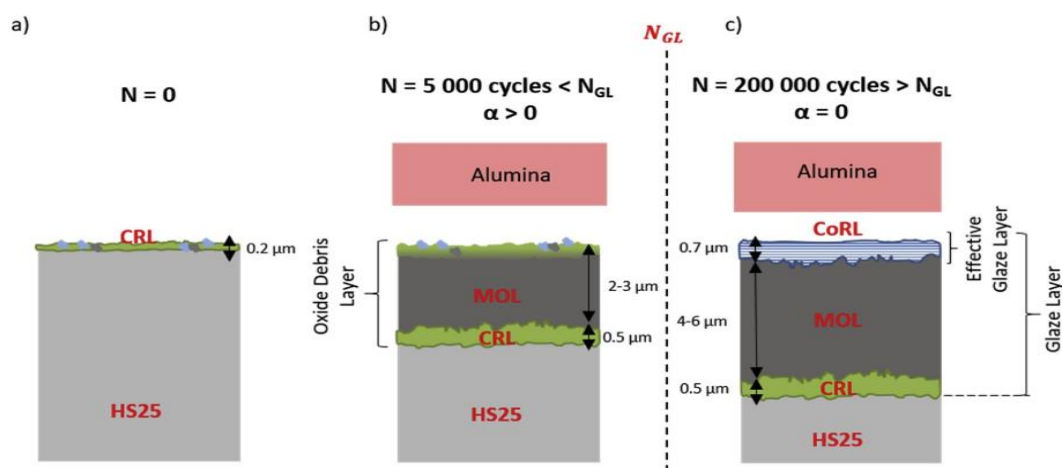
Figure 2-14: Schematic illustration of the chemical composition of the tribological layers formed during HS25 [47]

In summary, although superalloys are known for their high wear resistance and strength, the extreme conditions under which they operate present several challenges, including surface fatigue, fretting wear, and limited options for high-temperature lubrication, adhesion, and abrasive wear. Additionally, they often have a high coefficient of friction, which can increase energy consumption and reduce efficiency, ultimately impacting overall performance. The heat generated by friction can accelerate material degradation processes, potentially shortening component lifespan. Therefore, managing friction in superalloys is crucial. Figure 2-15 illustrates wear coefficients under various sliding conditions, indicating that similar materials result in high wear coefficients. Thus, investigating different materials and their compatibility is necessary.
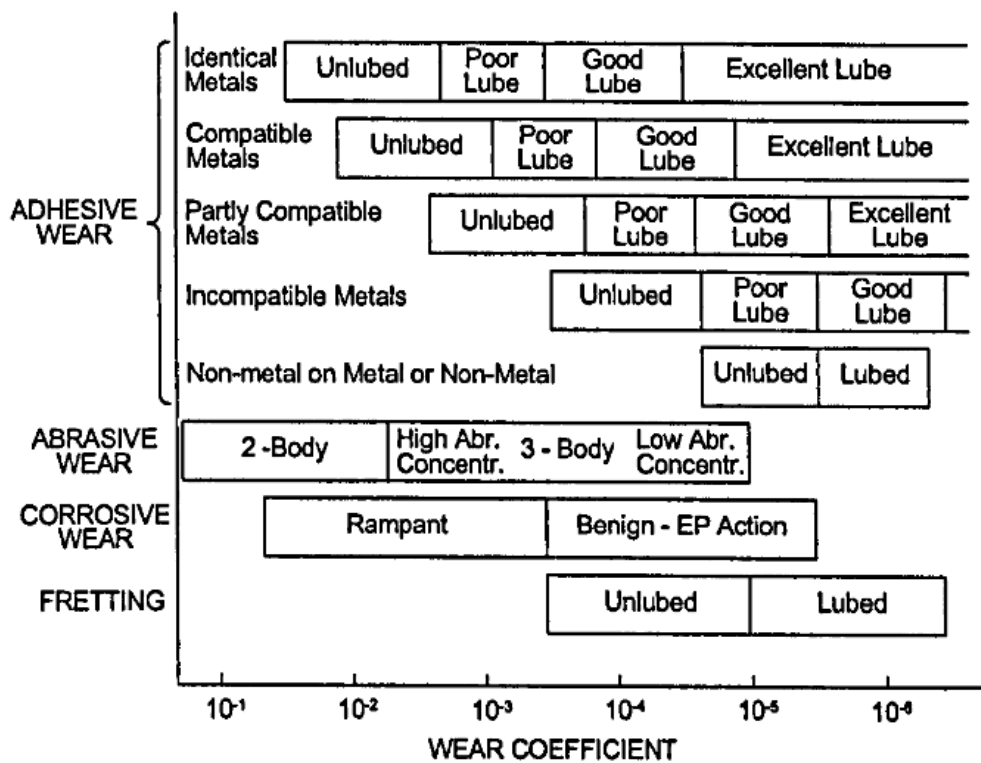
Figure 2-15: Wear coefficient in various sliding conditions [48]

2.4   Wear maps

Just as understanding the factors influencing wear, it is also useful to look at different methods of presenting the experimental data collectively from the various tests, allowing comparison and prediction of material response. There are various methods

of characterising the friction and wear response of a tribological system. The most common ones are the coefficient of friction, wear rates and morphological examination. However, this is limited in the information it can provide since it only provides information relating to particular situations such as sliding speed, load, temperature etc and it does not provide information on tribological characteristics such as wear mechanisms. This is due to the difficulties in presenting different types of wear data and the complex wear processes involved. This can be compensated by using a wear map.

A wear map is a two-dimensional or three-dimensional map representing wear data. A wear map identifies and summarises the tribological response of a combination of materials and operating conditions, also the map can allow the prediction of the wear mode or the response of the contact interface for a particular operating condition. This includes wear modes maps, mechanisms, operating parameters, and material [50].
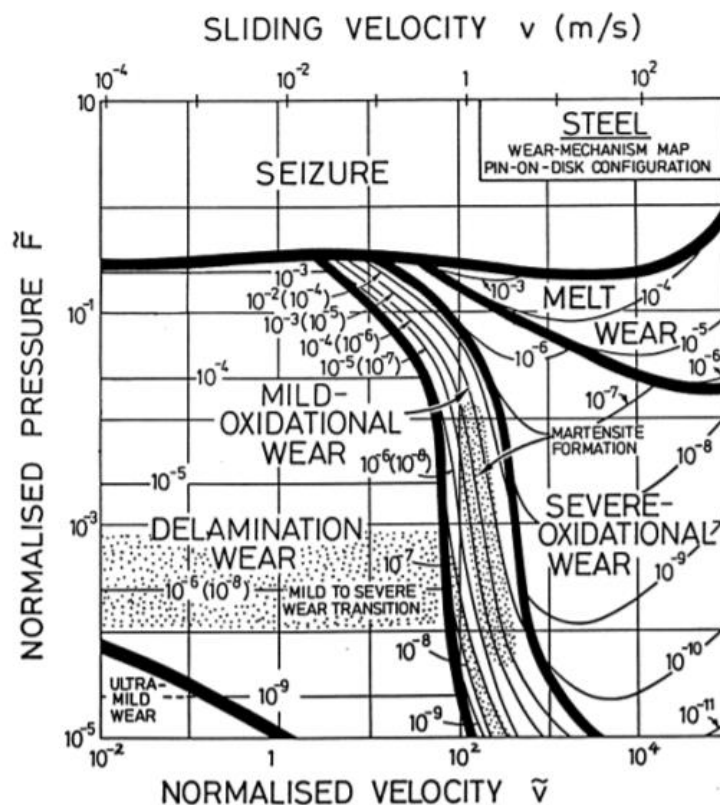
Figure 2-16: Lim and Ashby's wear map [50]

One of the earliest attempts at creating a wear map was done by Okoshi and Sakai [51]. They created a 3D wear map showing the behaviour of steel and brass in sliding conditions. Most of the early wear maps just included the wear modes and they did not provide any details on the mechanisms observed. Wear mechanisms were first introduced by Tabor showing the dominant wear mechanisms for a given set of conditions. Lim and Ashby [50] created collated data for steel-steel contact in sliding to create a 2D wear map, displaying both wear modes and mechanisms (see Figure 2-16) using normalised pressure and sliding speed on the axes. The main objective was to allow the prediction of wear mechanisms and modes for a given set of operating conditions. However, the complex processes and factors that influence wear make this difficult. They characterised a zone of mild and severe oxidative wear with mild wear ranging from sliding speeds of 0.6 to 60 m/s and a wide range of normal pressure. Anything above the range of mild wear conditions, they considered it to be severe wear.
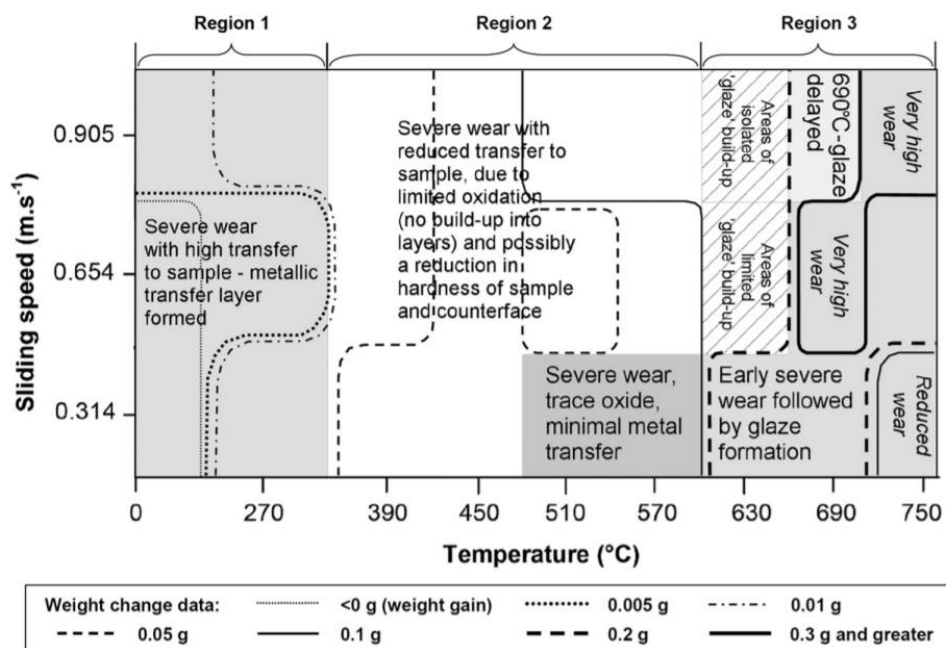
Figure 2-17: Wear map for nickel alloys with weight loss and glaze details [52]

Inman and Datta [52] generated a wear map using the high temperature sliding wear data between Incoloy MA956 and the Incoloy 800HT. As seen in Figure 2-17, the map is divided into three regions: 1) severe wear with a high rate of adhesive transfer, 2) severe wear with reduced rate of adhesive transfer due to unstable or thin oxide layer formation and 3) glaze region occurring between 630 and 750˚C. Although the map is informative for a range of speed and temperature conditions with the change in mass

information, the effect of the load is not presented. Since sliding speed and normal load are interdependent, both influences the surface temperature. This in turn has a major impact on the generation of glaze making the map a little ineffective.

Since glaze formation is influenced by a range of factors, having a wear map with just two variables would not provide enough information to predict the wear response of a system. As such further development is needed in order to incorporate more details when mapping. Therefore, it will be beneficial to generate a 3D wear map with temperature, pressure, and speed data to highlight the formation of glaze and how to reduce wear using the appropriate conditions; moreover, the effect of surface temperature rises and the quality (whether it is stable and the thickness) of glaze layer at certain conditions need to be mentioned. These gaps in the wear maps are also linked to the fact that glaze is not studied in detail and the complexity involved with sliding wear and glaze formation.

2.5   Testing methods

As mentioned in previous sections, glaze layer formation and breakdown are very much dependent on the operating and environmental conditions and the ability to retain wear debris in the contact. Therefore, it is essential to design tests in such a way that the debris are retained as much as possible to improve the quality of the results.

The most common and basic wear test used to analyse the glaze formation is ball on flat reciprocating tests. Using this configuration is useful in controlling the operating parameters and environmental conditions by adjusting the temperature, vibrations, load, and humidity. This test setup was used in most of the previous studies; however, it has poor debris entrainment along with small contact geometry causing significant drops in the pressure as wear occurs. This results in a point contact where the contact area is concentrated at a single point, typically occurring between curved or irregular surfaces creating extremely high contact pressures and localised stress concentrations (see Figures 2-18 a and c). The next step would be conducting tests using a flat-on-flat contact configuration as it allows better debris. One of the challenges with this type of contact is that it is difficult to get the alignment accurate. The contact pressure in a line contact is spread over a larger area compared to a point contact, reducing localised stress concentrations (see Figure 2-18 b). The final step

would be conducting tests using a more representative contact condition such as the fan blade rig at the University of Sheffield.
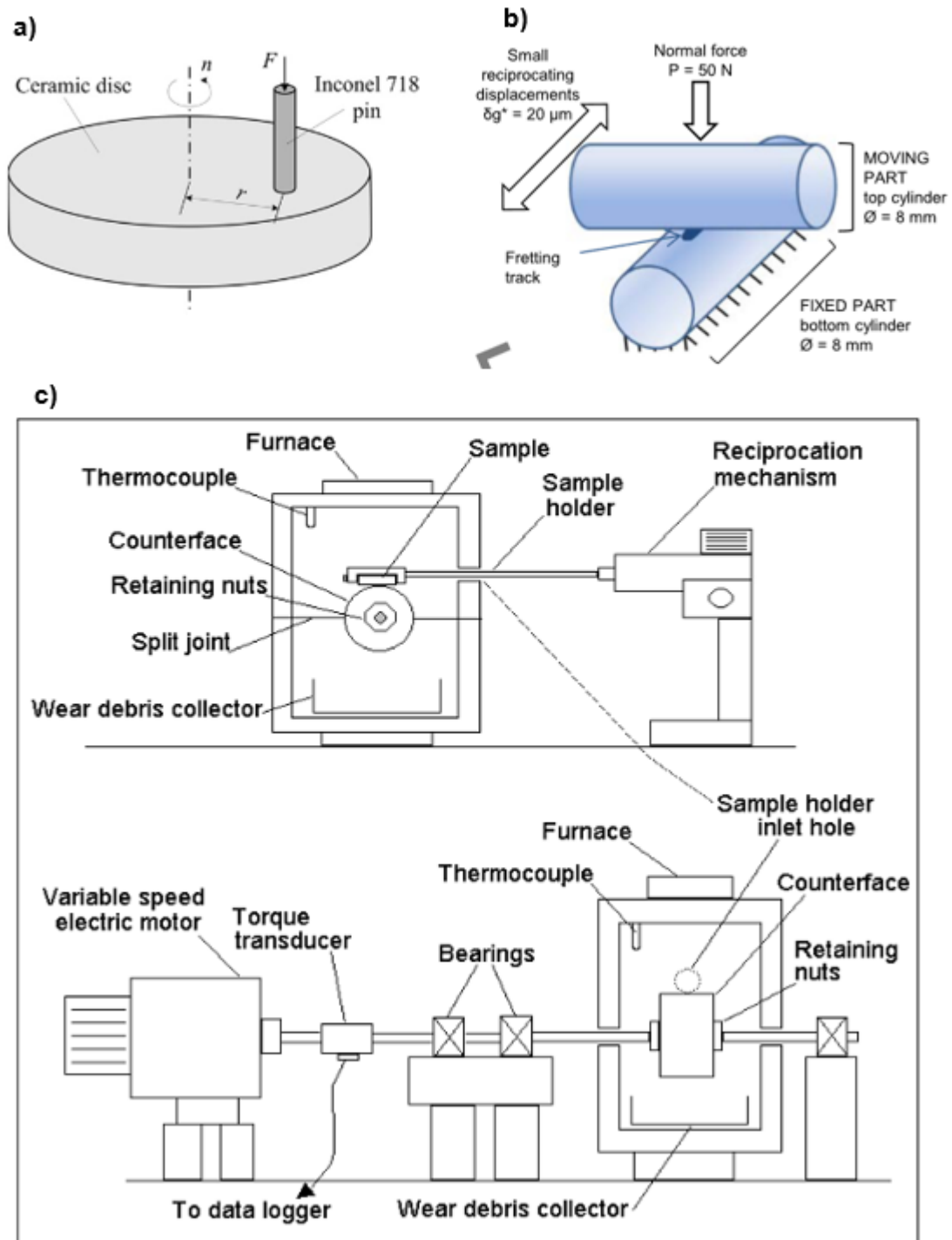
Figure 2-18: Different test arrangements, a and c: pin on disc contact [53] [52] flat-on-flat contact [54]

The fan blade rig at the University of Sheffield (Figure 2-19) allows more complex geometries to be tested and has good alignment meaning it has good force distribution without vibration. This rig provides oscillatory movement in the vertical direction through a hydraulic actuated system. This rig accommodates two stationary disc specimens and a blade specimen, and can have temperatures between room temperature (RT) and 600°C. The blade is pressed against the disc samples at a constant horizontal load up to 1200N; at the same time, the fretting is initiated to simulate the effects of vibration (See Figure 2-20 left). As seen in Figure 2-20 right, this configuration allows two contact points so letting good debris entrainment and it would self-align. Since it is a disc on flat contact the drop in pressure was slow compared to ball on flat (this was observed in previous tests in the rig [55]. The main advantage of this rig is that more representative contact seen in aero engines can be tested such as the blade/disc interface.
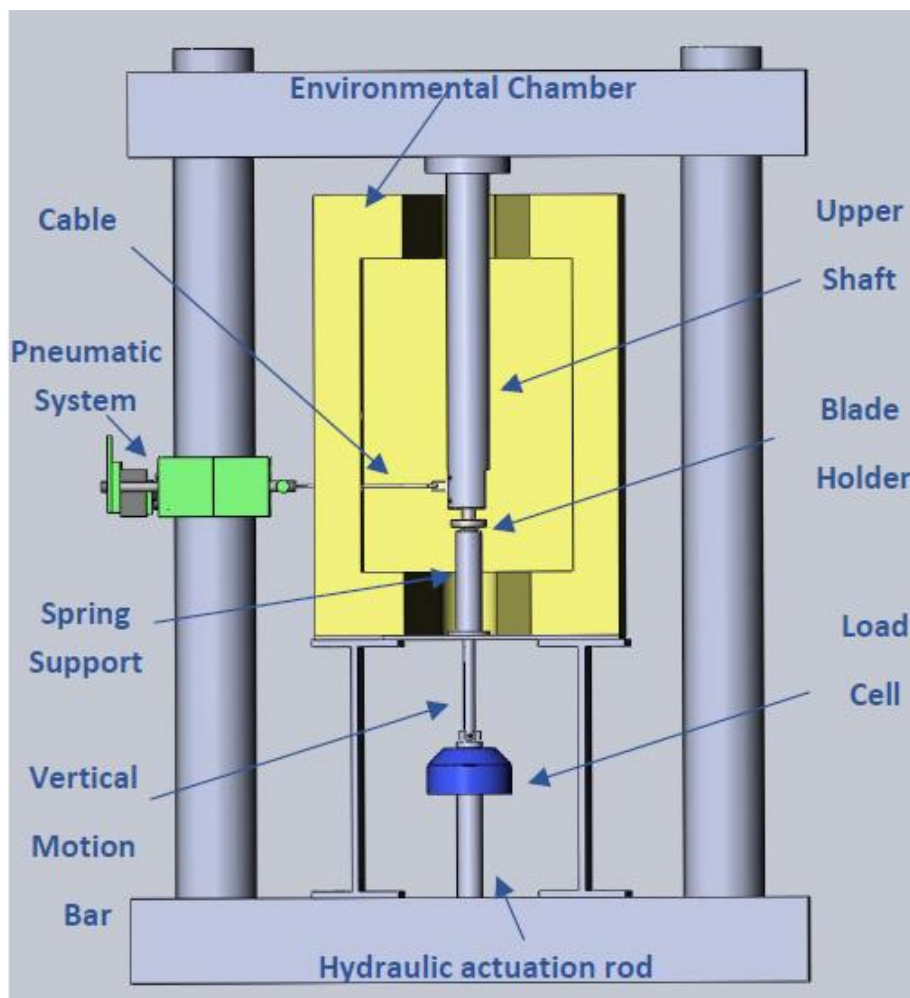
Figure 2-19: Sheffield University fan blade rig [55]

From the review of the studies on glaze and the testing methods, it is evident that debris entrainment and the changes in contact geometry is vital when designing experiments. As such, simple tests on the tribometers can help to determine the effects of surface temperature rises and the effects of load and speed on the wear response and coefficient of friction. Although some vital information is obtained from these tests, as they are not representative of the real geometries and conditions that are observed in engines. In turn, these tests can be combined with more representative rigs such as the University of Sheffield rig to study fan blade disc interface, as it mimics the geometry and debris entrainment of an actual blade/disc contact.
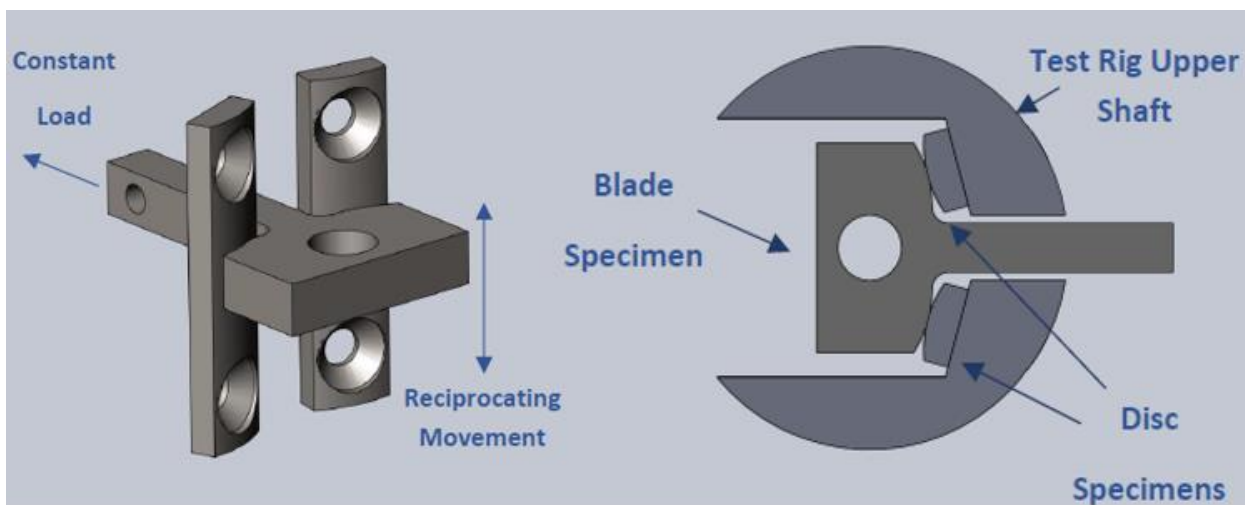
Figure 2-20: Loading and relative movement of the specimens (left) contact arrangement within the rig (right) [55]

2.6   Summary

Sliding wear involves complex process and four main wear mechanisms are observed in dry sliding situations: adhesion, abrasion, delamination, and oxidation. Using dissimilar materials and making the surfaces harder can reduce the wear rate however this is not very practical in extreme operating conditions such as high temperature and pressure. Therefore, functional surfaces such as glaze that develop their own wear resistance offer a solution. This reduces severe wear by preventing metal-to-metal contact. To reduce the severe rate, it is vital to reduce the time it takes for the severe to mild wear transition by accelerating the formation of wear and producing a stable thick layer. Therefore, several methods have been attempted previously to promote glaze generation on the contact interface such as pre-oxidation, supplying oxide debris in the contact, coatings bulk material etc. These have been found useful but not

effective enough. This is due to glaze layer generation being influenced by various operating and environmental conditions and it is only generated when a critical threshold is reached, making it harder to predict the efficiency of the layers formed. Moreover, getting the right conditions that promote glaze generation rather than hinder the process is also vital.

The contacting surfaces undergo continuous plastic deformation due to the repeated sliding action, which leads to the generation of wear debris. Further sliding leads to fragmentation, agglomeration, and compaction of debris into the grooves in the surfaces creating a glaze layer. However, this process involves various steps and are influenced by many factors.

The most important factor that determines the rate at which the glaze is formed is temperature followed by the speed and load. Glaze layer is generated once a critical temperature is reached, and it is highly influenced by the load and sliding speed because high loads and speed conditions create flash temperature on the surface. It is unclear how wear rate changes for a certain combination of temperature, load and speed conditions, and indeed the best combination to have a more effective glaze. Additionally, the microstructure of the surface and atmospheric conditions plays a significant role. Although many studies have included the influence of temperature, they have not discussed the combined effect of temperature, pressure, and speed and the other conditions that have an influence on the glaze such as humidity, partial pressure of oxygen etc. Hence, a detailed understanding of the effect of these parameters on the overall wear rate and the coefficient of friction is required. Moreover, these parameters are interdependent such as the surface temperature controls the rate of oxidation and diffusion of active elements etc, this in turn has an impact on the microstructure. Even though extensive work has been done on understanding the microstructure and its role in reducing wear rate, it has not been done for the material combinations studied in this study, and the change in the microstructure depends on the aforementioned parameters.

In the present research, various temperature, load and test duration will be studied and their effect on other parameters and the overall wear. This will be done by looking at the changes in the microstructure and morphology of the contacting surfaces and wear volume. Additionally, wear maps can be used as a useful tool to represent and

predict tribological response and a detailed wear map for the formation of glaze does not exist. So, a 3D map with pressure, speed and temperature would be of great advantage to identify the best conditions to improve the efficiency of the glaze, as a wear map allows prediction of wear response for a particular material combination and operating variables, the information from this study can be used in the future.

Previous research has shown that having a pre-glazed surface will reduce the wear rate, this needs to be further investigated to understand if this will be an effective option to reduce the severe wear. Also, one of the ways to prevent adhesive wear is to use dissimilar materials, therefore it will be interesting to study how different material combinations would behave especially the diffusion of active elements on the rate of glaze generation and whether moving to dissimilar materials reduces initial severe adhesive wear, whilst still promoting glaze formation for an appropriately selected material pair.

Finally, having reviewed previous studies and the gaps in the knowledge on the generation of an effective glaze layer, it is important to understand the fundamental factors and combinations of factors that promote or hinder glaze generation. Therefore, experiments will be done on simple geometries and test conditions (such as a ball on flat on a tribometer) to fully understand the impact of operating conditions. The experiments on tribometers are really useful since they are readily repeatable and can use simple geometries, avoiding complications such as alignment issues.

Chapter 3   Methodology

Chapter 3 introduces the methodology of the experimental study of the formation and breakdown of glaze. The chapter begins with explaining the test configuration, followed by the materials and contact modelling explaining the sample geometry chosen for the study. The latter part of the chapter describes data analysis methods and details the various surface characterisation methods such as imaging the wear scar, chemical analysis of the surface, image processing etc.

3.1 Introduction

Although the literature review gives an insight into glaze formation, it is not fully applicable to this study since tests were carried out under different conditions such as the material combinations and operating parameters. Many of the previous studies on glaze formation have been conducted using a pin on flat/disc test configuration to obtain essential information. Similarly, the contact configuration preferred for these tests is a reciprocating ball-on-(flat)disc. This configuration is mostly adopted in tribological studies because it is relatively simple allowing more control over variables, so tests can be carried out to study the influence of a wide range of variables such as normal load, stroke length, frequency, temperature, test duration, and relative humidity. Additionally, it is more efficient at avoiding misalignment issues, therefore, high contact pressures can be achieved with a reduced normal load. Though the pin wears throughout the test making it difficult to maintain the initial contact conditions (i.e., high pressure), with careful design of the pin, relatively stable conditions can still be achieved throughout the test. A reciprocating mode is chosen rather than unidirectional sliding because wear debris retention and use of these debris are essential in glaze generation. These tests involve a flat and a spherically ended sample, sliding against the flat sample. Usually, the flat sample is stationary while the ball sample reciprocates in back and forth sliding motion, and the load is applied vertically downward through the ball sample [56] [57]. Friction and wear measurements can be easily obtained, and repeated tests under the same conditions can be done readily. This makes these types of tests ideal so that the fundamental driving factors of glaze can be studied easily with simple geometry, and can provide reasonable control on other variables.

3.2   Test materials

This section describes the materials studied in the ball- on- flat tests, chosen based on the knowledge found in the literature review.

Aero engines demand materials capable of withstanding high temperatures, pressure, and stress while remaining lightweight. Commonly used alloys in aero engines include titanium, nickel, high-strength steels, and cobalt-based alloys. These alloys are selected based on the specific material and mechanical requirements of each component. For example, titanium alloys offer excellent corrosion resistance, while nickel and cobalt-based alloys provide high temperature and oxidation resistance. In this study, nickel and cobalt-based alloys are chosen due to their frequent use in the applications outlined in Chapter 1.

The materials selected were Inconel 718, Haynes 25 and C263 since they are frequently used in aerospace applications as they contain a high percentage of nickel, chromium and cobalt providing high temperature and corrosion resistance capabilities. The chemical composition and properties of each material can be seen in Tables 3-1 and 3-2.

Both Inconel 718 and C263 are Nickel-based alloys whereas Haynes 25 is a cobalt-based alloy. Although these materials contain similar alloying elements, the weight of the elements vary, with this likely to affect the composition and strength of the glaze layer formed because the rate of diffusion and oxidation of elements differs for each element, in turn making these a good choice. Some of the alloying elements include chromium (aids in the generation of a stable oxide layer and corrosion resistance), cobalt (provides strength to nickel), aluminium, titanium, iron, copper, tungsten, carbon, and molybdenum. Inconel 718 is the most used nickel alloy in gas turbine engines; hence it will be best to find out the glaze formation in these [55]. The process of creating these materials is similar, as all three rely on solid solution strengthening to dissolve various alloying elements into a nickel or cobalt matrix. Subsequently, they undergo a series of heat treatments and cooling to dissolve any secondary phases and remove impurities. The literature review suggests that the performance of glaze varies depending on the material, so looking at different materials aids in deciding the best material. Also, previous studies have shown similar materials provide a consistent and reproducible glaze to varying levels on various materials/combinations, therefore

it would be ideal to start with materials that generate glaze, and results can be compared to validate them.

Materials	Chemical composition (%)									
	Ni	Cr	Co	Fe	W	Mo	Nb	Ti	Mn	Cu
C263 [58] [59]	49.3	20	20	0.7	-	5.8	-	2.2	0.6	0.2
Haynes 25 [60]	11	21	47.4	3	13.1	1	-	-	1.5	-
Inconel 718 [61] [62]	48	18	>1	18	-	3.0	5.25	0.85	0.35	-
Traces of elements such as Al, P, B, Si, C, S are also present.										

Table 3-1: Chemical composition (weight, %) of the alloys used in the test.

Properties	C263	Haynes 25	Inconel 718
Density (kg/m^3)	8360	9130	8190
Thermal conductivity (W/m.K)	14.26	10.5	11.4
Specific heat capacity(J/kg°C)	461	403	435
Thermal diffusivity (m^2/s)	4.0E-06	2.8E-06	3.2E-06
Elastic modulus (GPa)	205	225	200

Table 3-2: Mechanical and physical properties of the test materials

3.3   Contact modelling

As discussed in Chapter 2, temperature, pressure, and speed play a significant role in glaze generation and breakdown. Hence, it is important to carefully choose the appropriate conditions to run the experiments to have an appropriate insight. Therefore, contact modelling was carried out to understand the influence of different contact radii on the load and how wear affects the pressure.

Hertz contact modelling was used to model the pressure changes in the contact as the radius of the pin is varied. The variables used in the modelling are described in Table 3-3 [63] [64]. Since all the materials have a similar elastic modulus and Poisson's ratio, only Inconel 718 is used to model the contact.

Radius (mm)	3.8, 6.35, 12.7, 20
Normal Load (N)	25
Elastic modulus (GPa), E [61]	200
Poisson's ratio,v [61]	0.294

Table 3-3: Variables used in the contact modelling calculations carried out for Inconel 718

The ball-on-disc contact arrangement gives a point contact, the equations used to calculate the pressure are detailed below.

The ball on flat/disc contact arrangement gives a point contact, the Hertz equations were used to calculate the pressure.

$$\text{Reduced radius, R}' : \frac{1}{R'} = \frac{1}{R_1} + \frac{1}{R_2} \qquad \text{(Equation 3.1)}$$

$$\text{Reduced elastic modulus, E}^*: \frac{1}{E^*} = \frac{1-v_1{}^2}{E_1} + \frac{1-v_2{}^2}{E_2} \qquad \text{(Equation 3.2)}$$

The contact will be a circular radius, it is given by:

$$\text{Contact area dimension, } a = \sqrt[3]{\frac{3PR'}{4E^*}}, \qquad \text{(Equation 3.3)}$$

where P is the normal load.

$$\text{Maximum contact pressure, } p_o = \frac{3P}{2\pi a^2} \qquad \text{(Equation 3.4)}$$

$$\text{Average contact pressure, } p_{average} = \frac{P}{\pi a^2} \qquad \text{(Equation 3.5)}$$

For the contact modelling, it was assumed that the wear scar generated was spherical and has a diameter of 4mm. Then, the wear volume equation as detailed in ASTM G133 was used to calculate the new radius, R_1.

$$v_p = \frac{\pi h}{6}[3D^2 + h^2] \qquad \text{(Equation 3.6)}$$

$$h = R - \sqrt{R^2 - \frac{D^2}{4}} \qquad \text{(Equation 3.7)}$$

where v_p is the wear volume, D is the diameter of the wear scar, R is the pin radius. As the wear volume serves as the independent variable in this model, assumed a

range of volumes and applied them in the Equation 3.6 to compute a 'new diameter' for each volume. Subsequently, this 'new diameter' was used as an input in Equation 3.6 to determine the new pin radius.

The calculated 'new radius, R_1' was added to the initial radius which was then used for further calculation of contact pressure.

Figure 3-1 shows the variations in maximum and average contact pressure as the radius and the normal load is varied. As the radius increases both the maximum and average pressure decrease. With the increasing applied load, the pressure on the contact increases. The reduction in contact pressure is especially important because during the tests (with sliding) the pin wears increasing the radius leading to a reduction in the contact area and pressure.
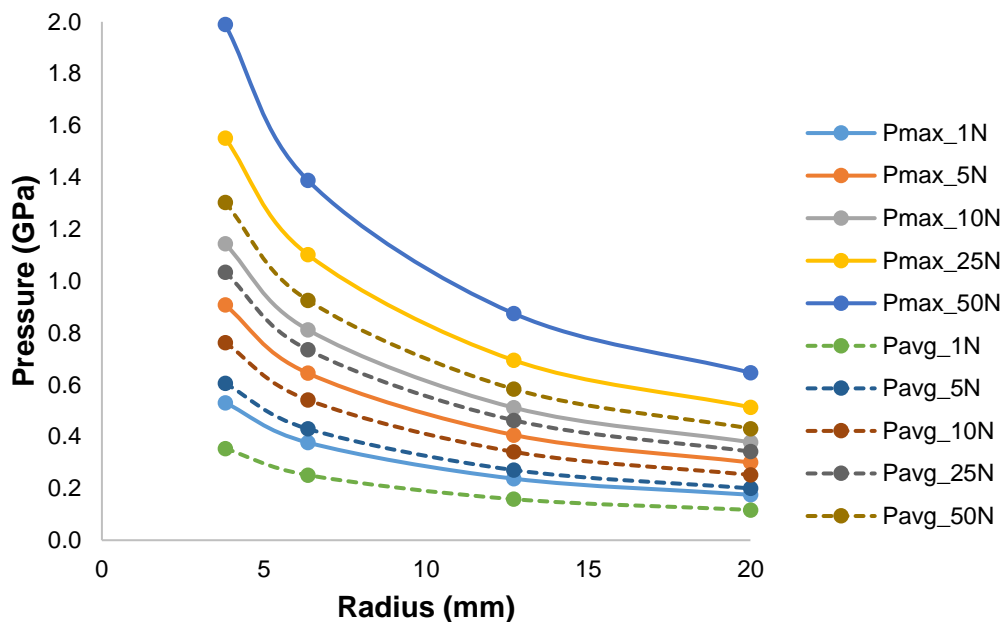
Figure 3-1: The variation in average and maximum pressure as the normal load and radius of the pin are increased.

Therefore, it is essential to see the difference in the contact dimension as the pin wears. To model the 'new' pressure as the pin wears, the wear volume was assumed (from the literature for similar tests and parameters) and the geometry of the wear scar was to be spherical. This allowed the calculation of the new radius using the volume of sphere equation which was then used to calculate the new pressure [56] [65] [66] [67] [68].

Radius (mm)	Average contact pressure (GPa)				
	1N	5N	10N	25N	50N
3.80	0.354	0.605	0.762	1.035	1.304
6.35	0.251	0.430	0.541	0.735	0.926
12.70	0.158	0.271	0.341	0.463	0.583
20.00	0.117	0.200	0.252	0.342	0.431

Table 3-4: Summaries the average contact pressure at various radii and normal load

Figure 3-2 shows the ratio between average final pressure and the initial pressure against the wear volume when the applied normal load is 25N. As seen in the figure, there is a greater drop in the pressure at the lowest radii (i.e. 3.8mm and 6.35mm); dropping to less than 70% of the initial pressure. But, with the initial radius of 12.7mm and 20mm, the rate at which the pressure is dropped is reduced and it should be able to keep 80% of its initial pressure over the duration of a test. Maintaining as much as the initial pressure is crucial because the high pressure in the contact influences the surface temperature which in turn has the most impact on the glaze generation. This ensures stable conditions are achieved for the tests.
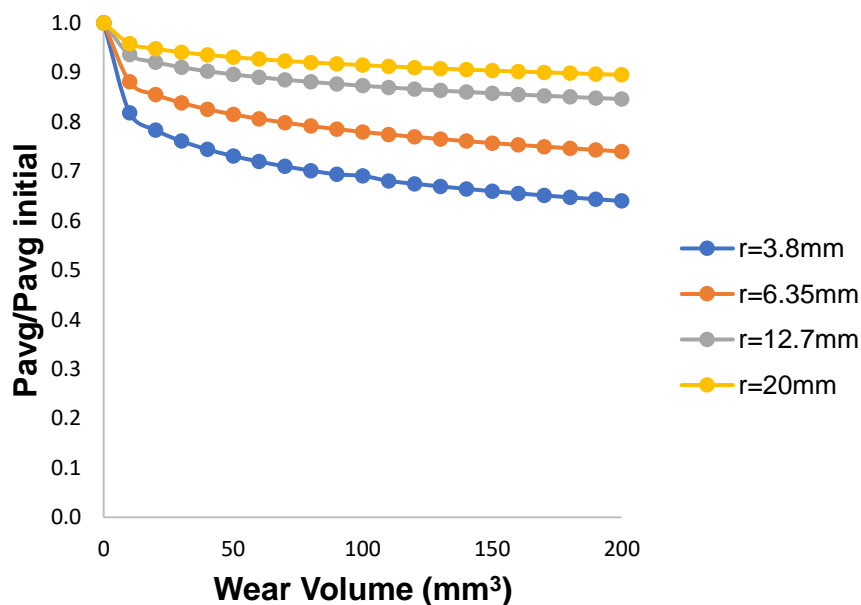
Figure 3-2 The pressure variation as the pin wears for different radius

From Figures 3-1 and 3-2, it is concluded that a pin with an end radius of 12.7mm will be used for the studies as this would provide an initial maximum pressure of 0.71 GPa and average pressure of 0.47GPa when a normal load of 25 N is applied. The normal load of 25N was used for contact modelling (that would produce an average pressure of 0.47GPa) because literature has shown that good glaze is produced under these conditions [29] [42] [55].

3.3.1 Flash Temperature calculations

Flash temperatures are calculated to get an insight into the changes in the temperature for the test conditions used in this study. Kuhlmann-Wilsdorf's method is used, however there are some inaccuracies due to the inability to directly measure some of the parameters such as the hardness of the oxide and the number of contacts.

Kuhlmann-Wilsdorf's flash temperature for unlubricated wear for circular and plastic contact between asperities is given by [29]:

$$\Delta T_0 = \frac{\mu v (\frac{\pi N H_S}{N_c})^{1/2}}{4\lambda_1(\frac{1}{Z_0}+\lambda_r)} \qquad \text{(Equation 3.8)}$$

where μ is the coefficient of friction, v is the sliding speed, H_s is the hardness of the softer material, N_c is the number of contacts, λ_1 is the thermal conductivity of the softer surface, λ_r is the ratio of thermal conductivities between the two surfaces, r is the radius of the contact, d is the density and c is the specific heat capacity.

$$Z_0(v_r \leq 2) = \frac{1}{1+\frac{v_r}{3}} \qquad \text{(Equation 3.9)}$$

$$Z_0(\geq 2) = \frac{9/8}{v_r^{\frac{1}{2}}+\frac{1}{8}^{1/2}} \qquad \text{(Equation 3.10)}$$

$$relative\ velocity, v_r = \frac{v}{v_o} \qquad \text{(Equation 3.11)}$$

$$characteristic\ velocity, v_o = \frac{K(\pi N H)^{\frac{1}{2}}}{P^{\frac{1}{2}}} \qquad \text{(Equation 3.12)}$$

where N is the number of contacts

Since this is done for like-on-like combinations, λ_r is 1 and it is assumed that the oxides have a hardness of 9 GPa. Table 3-5 shows the parameters used in the calculation; the material properties are from the In718 data.

Normal load, P (N)	25
COF	0.4
Hardness, H (GPa)	9
velocity, v (m/s)	0.0417
Thermal conductivity, K (W/m.K)	11.4
density, ρ (kg/m^3)	8170
specific heat capacity, c (J/Kg.K)	435
Thermal diffusivity, K (m^{2}s^{-1})	3.207E-06

Table 3-5 The parameters used to calculate contact temperature between a like on like material combination.

Number of contacts	10	20	40
Contact temperature, T_0 (ºC)	**60**	**42.17**	**31.25**

Table 3-6 The changes in the contact temperature as the number of contact points are varied

Table 3-6 shows the rise in contact temperature for the conditions described in table 3-5. As seen in Equations 3.7 to 3.11, the accuracy of these temperature is highly dependend on the CoF and the number of contacts as well.

3.4 Methodology

3.4.1 Test equipment

The ball-on-flat reciprocating wear tests were performed on the Phoenix TE77 reciprocating tribometer. The pins are attached through an upper specimen holder, connected to an oscillating arm. The flat specimen (lower) is clamped on a dry mounting plate. The moving upper (specimen) was loaded against the fixed lower specimen through a lever mechanism which is triggered by a geared servomotor. Figure 3-3 shows the schematic diagram of the experiment set-up, and Figure 3-4 shows the arrangement of samples in the holder. Once the samples are secured on to the respective holders and are in position, the normal load is applied by turning the dial, then speed and frequency are set on the controller. The tests can be initiated once the software used for data capture is switched on, followed by pressing the 'run' button on the controller. This begins the test by moving the oscillating drive in a back-and-forth motion, so the pin rubs against the flat disc.

The tangential load is measured by a load cell attached to the lower specimen holder; data is downloaded via using LABVIEW, National Instruments. This is later processed to determine the coefficient of friction (COF) by dividing the tangential force (F_f) by the normal force (N).
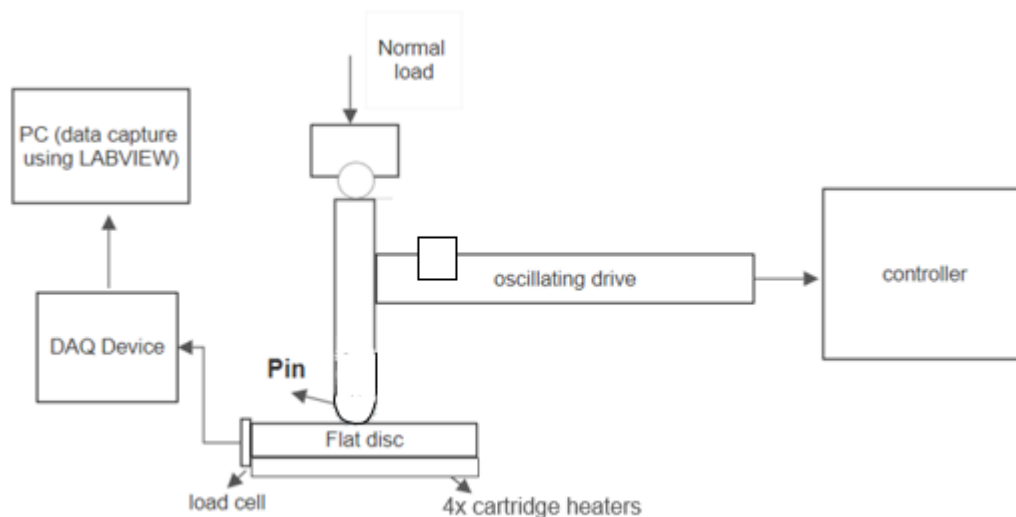
Figure 3-3: Schematic diagram of the rig
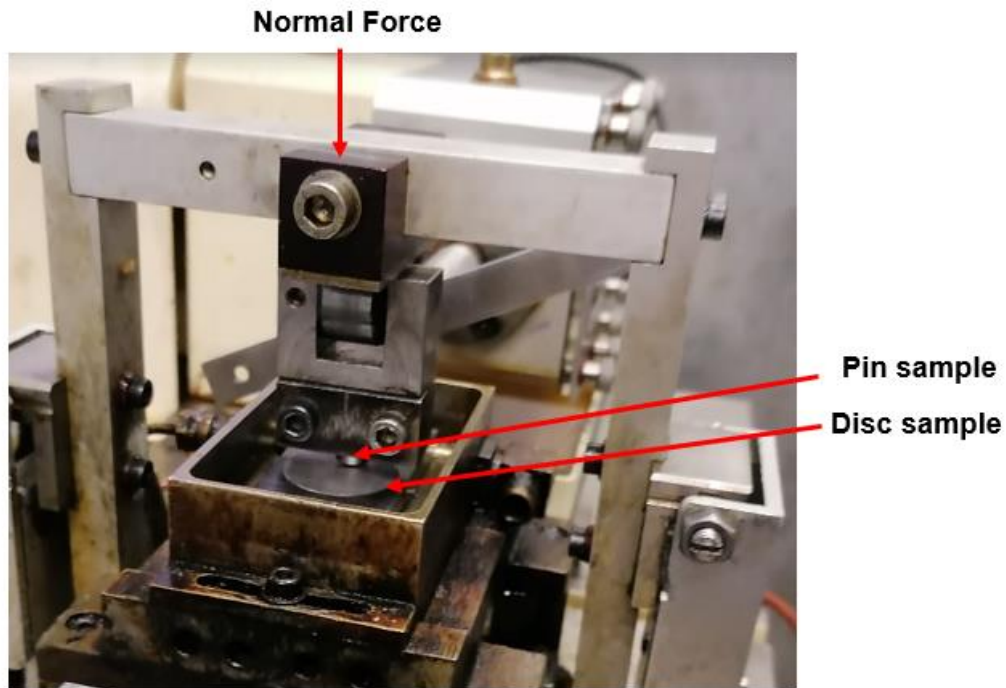
Figure 3- 4: Sample arrangement for ball on flat test

3.4.2 Test parameters

The alloys used in the ball on flat tests were Inconel 718, C263 and Haynes 25, nickel and cobalt-based alloys with high strength, thermal and corrosion resistant capabilities. A like-on-like material combination was used in the initial studies since the results were needed to understand the fundamental factors affecting glaze formation. The pin specimens had a domed end with a radius of 12.7mm to achieve the appropriate pressure requirement (as seen in Section 3.3) and the flat specimens were 25.4mm in diameter and a thickness of 5mm (see Figure 3-5 and 3-6). The pins oscillated with a stroke length of 2.2mm at a frequency of 8.3 Hz. These parameters were used since it was commonly used in the literature so that the results could be compared against the existing data. These conditions have generated a glaze layer on similar alloys previously [24,34,35]. Each test was carried out for 30,000 cycles. However, constant sliding velocity could not be maintained since it is a reciprocating motion, and the speed was zero at the end of each stroke when the direction of motion changed, returning to steady state quickly. In the ball on flat tests, initially the normal load (15 N, 25N, 37.5N) was the only parameter that was varied, keeping all the other

conditions that influence the formation of glaze the same such as temperature, humidity, speed etc. Although later tests went on to investigate the role of temperature.
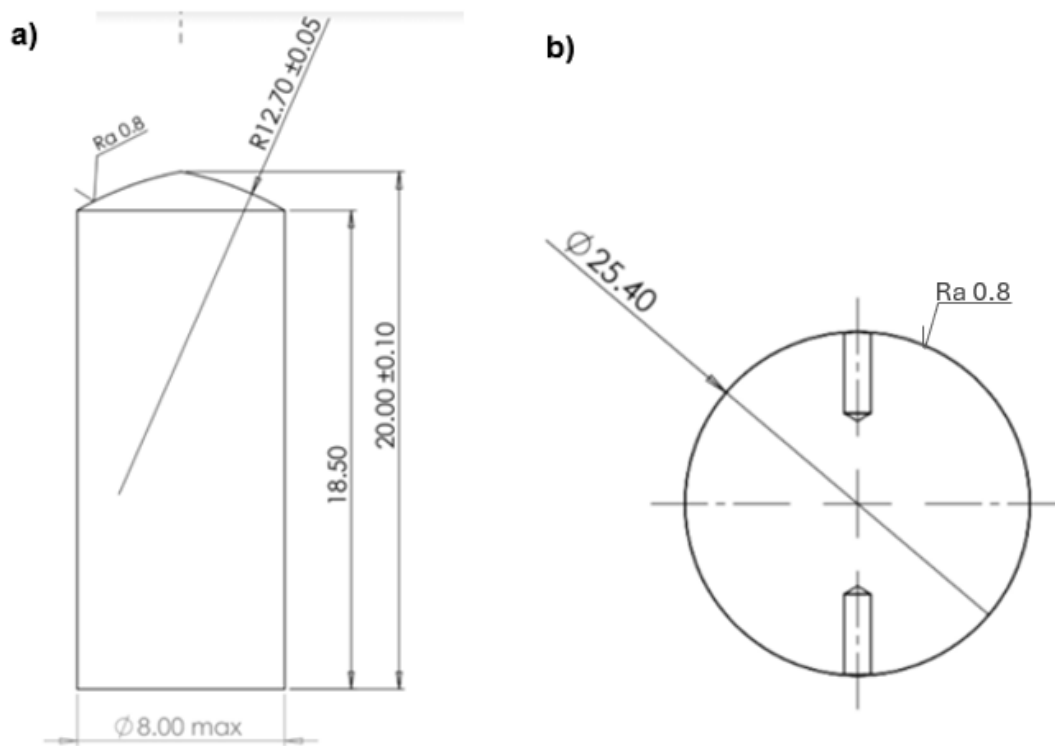
Figure 3-5 Dimensions of the samples used in the test a) pin b) disc
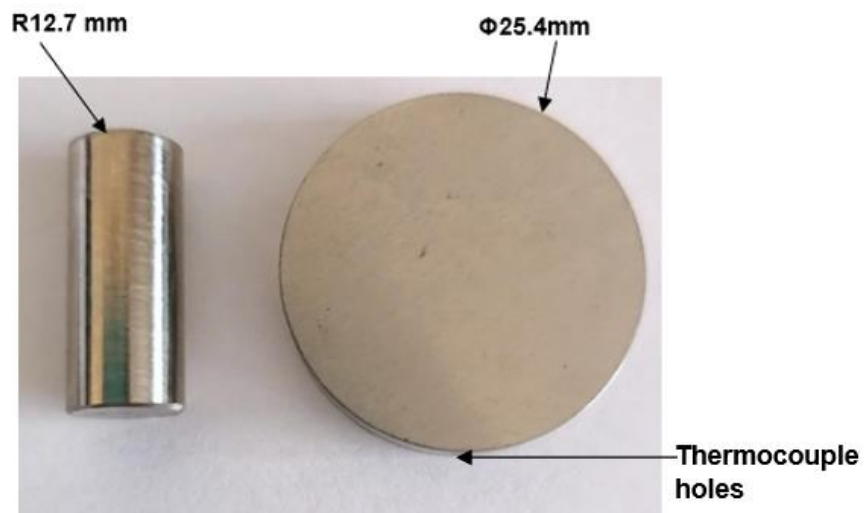
Figure 3-6 The pin and disc sample

In the latter tests, the samples were heated using 4x200W (resistance) heating cartridges which are positioned underneath the bottom sample holders, and monitored using a K-type thermocouple placed on the samples through the holes in the sample. The thermocouples are placed on the side of the samples rather than near the contact to minimise the effects of frictional temperature rise. The heaters are controlled using a PID controller (Omega Platinum series, CN32Pt) allowing independent control of the temperature.

To reduce the effects of pre oxidation, the temperature was raised to the 'set' value as quickly as possible. To reduce the effects of pre oxidation, the temperature is raised to the 'set' value as quickly as possible. The test is only commenced once the temperature is stabilised i.e. the temperature variations are within ±3°C. During this investigation the 'set temperature' was maintained throughout the test to observe the influence of temperature independent of other factors. The graph showing fluctuations in the temperature as the test progresses can be seen in Appendix 3a. Tests were conducted at various temperatures ranging from room temperature to 600°C. At the end of the test, the machine and heaters were switched off together.

The chosen normal load conditions provided an average contact pressure of 560, 710 and 810 MPa, meaning there was enough data to compare the effect of load with upper and lower bounds. These contact pressures had been used previously to reproduce the severe operating conditions in aero engines.

Load (N)	15,25,37.5
Frequency (Hz)	8.3
Stroke length (mm)	2.2
No of cycles	30,000
Temperature (°C)	Room temperature (22 – 25), 200, 400, 600

Table 3-7: Ball on flat reciprocating test parameters

To investigate the rate of glaze generation with sliding time, some additional tests were carried out where the tests are interrupted at every 5000 cycles. This allowed observation of progression of wear scar and identify any trends in glaze formation and breakdown at various conditions.

3.4.2.1   Dissimilar materials tests

The test parameters used in the dissimilar material study can be seen in Table 3-8. The methodology and experiment setup are described in 3.4.1. The combinations were chosen in a way that the material that is less likely to form a glaze are chosen as the disc since discs will be able to retain debris better. Also, the pin material is selected because they are found to generate more debris, which is studied to determine whether an increased availability of debris has a beneficial effect.

Load (N)	25
Frequency (Hz)	8.3
Stroke length (mm)	2.2
No of cycles	30,000
Temperature (˚C)	400, 600
Material combination	• In718 pin and Haynes 25 disc • C263 pin and Haynes 25 disc • In718 pin and C263 disc

Table 3-8 Details the test parameters and the material combinations used in the dissimilar material tests

3.4.2.2   Pre-glaze tests

A like on like material combination is used to study the history dependence at a normal load of 25N. In order to achieve glaze on the surface, the pin samples were rubbed against the disc samples first at a high temperature (i.e. 600ºC), this was then checked using a USB microscope to ensure a glaze is actually formed. Th pre-glazed sampled were then tested at a lower temperature (i.e. 25ºC).

Although, these tests are not fully representative of the engine conditions and contacts, some of the parameters represented harsher engine conditions such as the high contact pressure, and it is important to understand the limits of load where a good glaze can be generated to be effective against wear. As the demand for higher efficiency engines remains constant, it drives the need for tighter dimensional tolerances and operation under more demanding conditions, including higher temperatures and loads. An example of such contact can be seen in Figure 3-7, where a blade/disc is presented. The range of pressures mentioned have been previously

seen to generate a good glaze thus a comparison can be made. Also, the highest load is significantly greater than in the engines so severe cases could be tested.
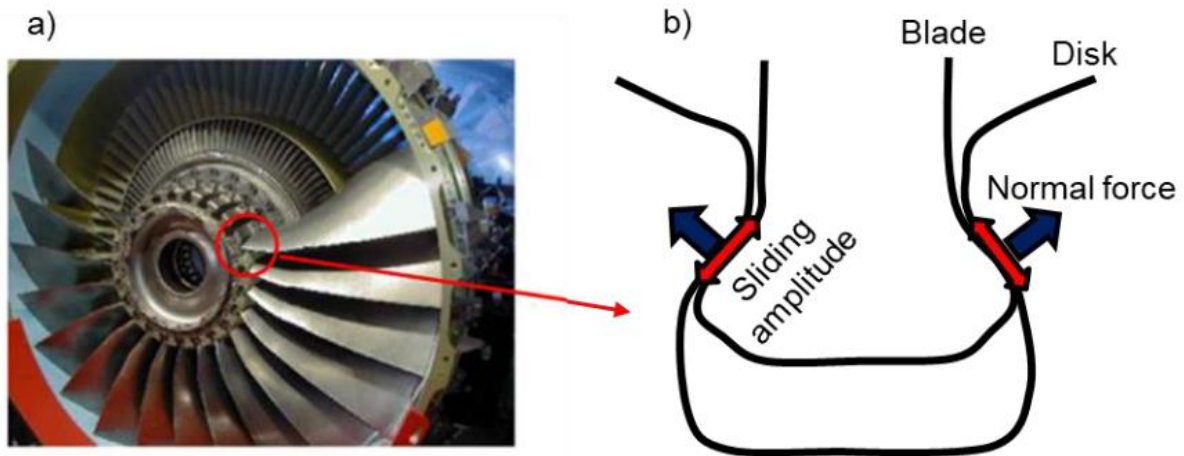
Figure 3-7 a) Illustration of a turbine engine; b) Fretting wear process at the blade/disc contact [38]

During all of the tests, the load cell continually recorded the tangential load. The results from these tests were used to calculate the coefficient of friction so that the evolution of COF could be observed by checking if the COF values would stay stable once the glaze is formed or if there is a change in the COF when the glaze layer is broken down by further sliding. The wear tests were repeated three times under the same conditions.

3.4.3 Data analysis

As noted, the tangential force and displacement data were recorded using Labview, this helps to understand the behaviour and evolution of friction as the tests progressed.

The Tangential force data were processed using MATLAB to obtain the coefficient of friction. The tangential force was divided by the normal force to determine the COF. COF was calculated to allow comparisons of tests carried out under different loading conditions. For illustration purposes only positive values of COF is shown in the results. An example of the raw data and the processed can be seen in Figure 3-8. A moving average is used to smooth the data, making trends more evident and helping to avoid anomalies. It effectively reduces noise by smoothing out fluctuations and irregular behaviour in the data. By averaging values over a window of time, the high-frequency components of the noise are dampened, resulting in a cleaner signal. The calculation involves finding average for the series of data points in the defined window or the time period and the process continues as you slide the window along the data series, generating a series of moving average values. A moving average with an interval of 620 points (representing one cycle) is used, it is adopted since it is a known approach to represent trends in the data (ASTM G115-10 Standard Guide for Measuring and Reporting Friction Coefficients) [69] [56].
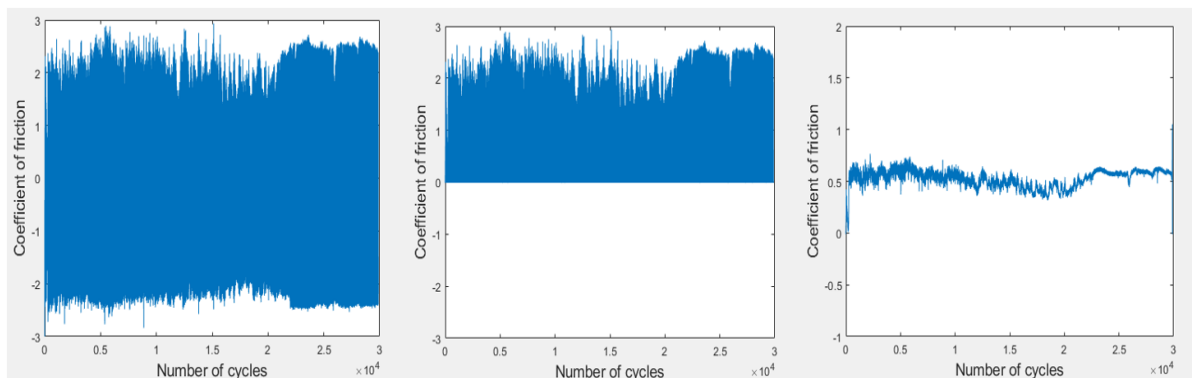
Step 1: Raw friction data

Step 2: A code (COF_data(COF_data < 0) = 0;) is applied to eliminate the negative values

Step 3: moving average with a window size of 620 is applied to get this graph

Figure 3-8 Raw COF and processed COF data obtained from Inconel 718 against Inconel 718 test at a normal load of 37.5N.

To ensure that the gross slip regime is achieved during the tests and the contact has not seized, analysis of the fretting (hysteresis) loop is essential. Figure 3-9a shows an ideal fretting loop in the gross slip regime. The shape of the loop can be used to determine the regime for example, in the gross slip regime, the loop has a parallelogram shape with the displacement measured equal to the slip amplitude and the slope of the sides proportional to the stiffness of the rig [71]. Figure 3-9b shows a fretting loop obtained from the Inconel 718 test at a normal load of 37.5N. Although the loop has an overall parallelogram shape (as seen in Figure 3-9a for the ideal scenario), the slight variation is due to the stiffness of the rig. Additionally, the peak values of tangential forces, especially towards the end of the stroke are due to the development and interaction of wear debris as a result of wear [72] [73] [74]. However, since the overall parallelogram shape is achieved, this means that the force is in the opposite direction to sliding, and the energy is dissipated in the contact.
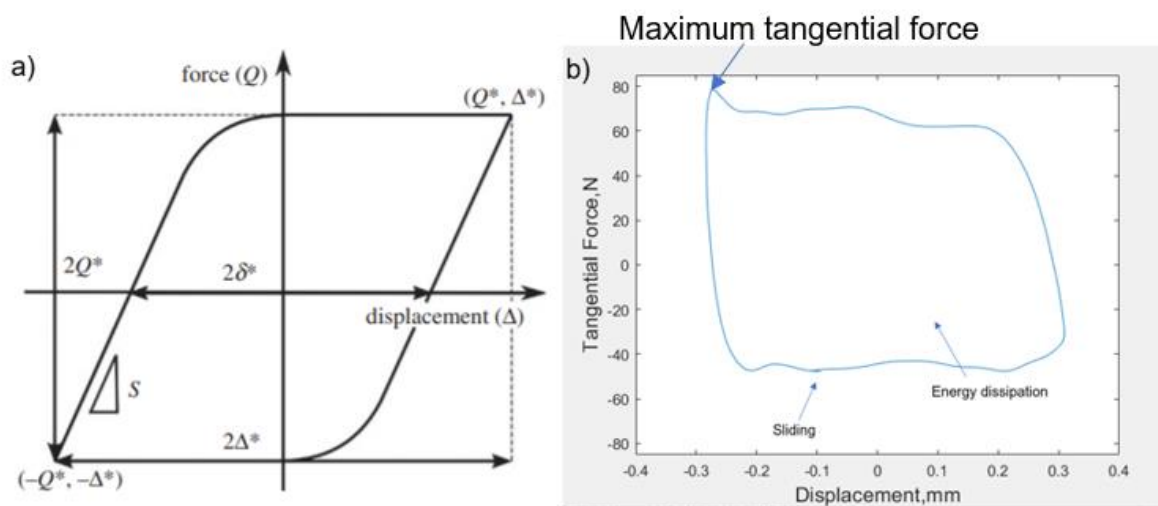
Figure 3-9 a) an ideal fretting loop in gross-sliding regime b) fretting loop for one cycle from the tests conducted at a normal load of 37.5N and using Inconel 718 against Inconel 718

Similarly, Figure 3-10 shows the variations in the force and displacement in one cycle. As seen in the figure, there is a small period where the contact is stationary (the irregularities/slopes are due to the stiffness of the system), followed by gross sliding. The areas inside the loop represent the energy that is dissipated.

In processing the data, the fretting loops at different stages of the test were also assessed. This was done to confirm that the contact was stable, and the results are valid. Figure 3-11 shows the segmented average loop observed at 1000, 10,000 and

20,000 cycles for C263. It can be seen from the figure that at the lowest normal load (i.e. 15N), the loops are distorted and unstable, however, the trend is only seen during the initial cycles making the data acceptable.

This could be due to the vibrations in the rig being dominant at lower loads leading to variations in the contact. However, at the normal load of 25N and 37.5N, the fretting loops are more stable and similar to Figure 3-11a, where the loops were stable at each stage with a slight change in the shape due to the changes in the COF as the test progresses, this will be further discussed in the results section. This trend is observed regardless of the material used (as seen in Appendix 3b).
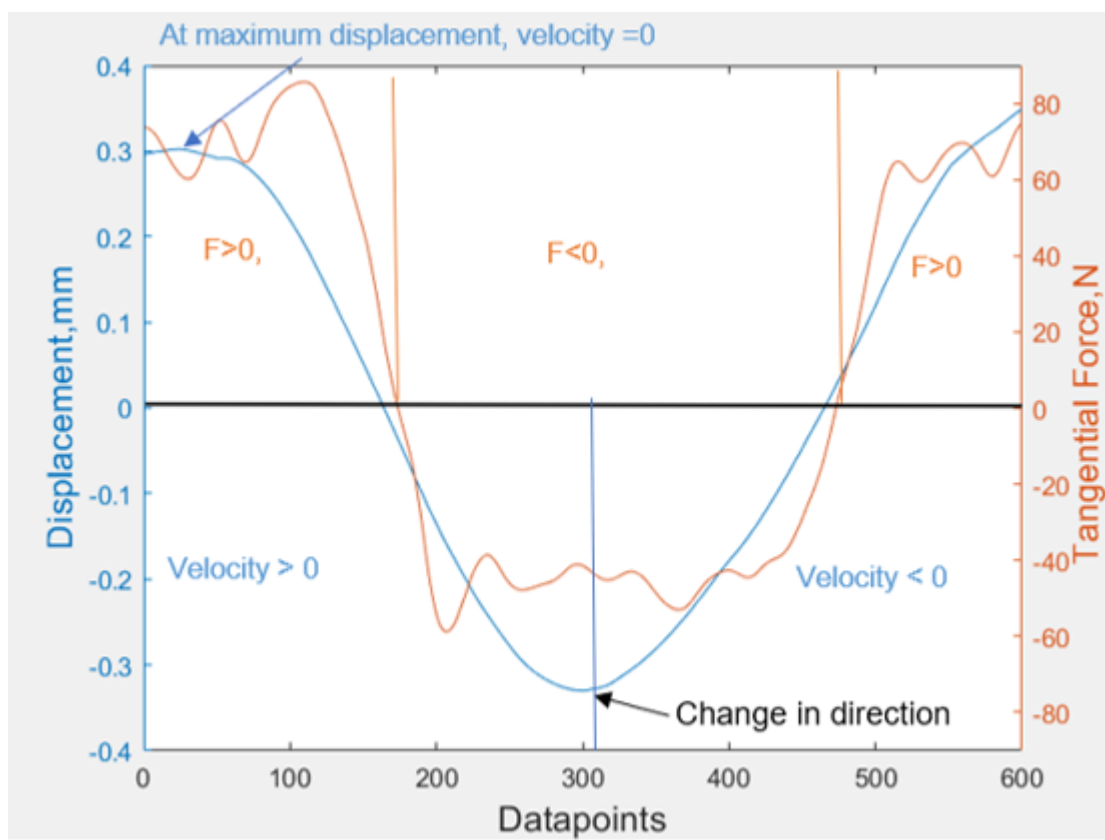
Figure 3-10 The variations in tangential force and Displacement in one cycle (data from Inconel 718 against Inconel 718 test at a normal load of 37.5N)
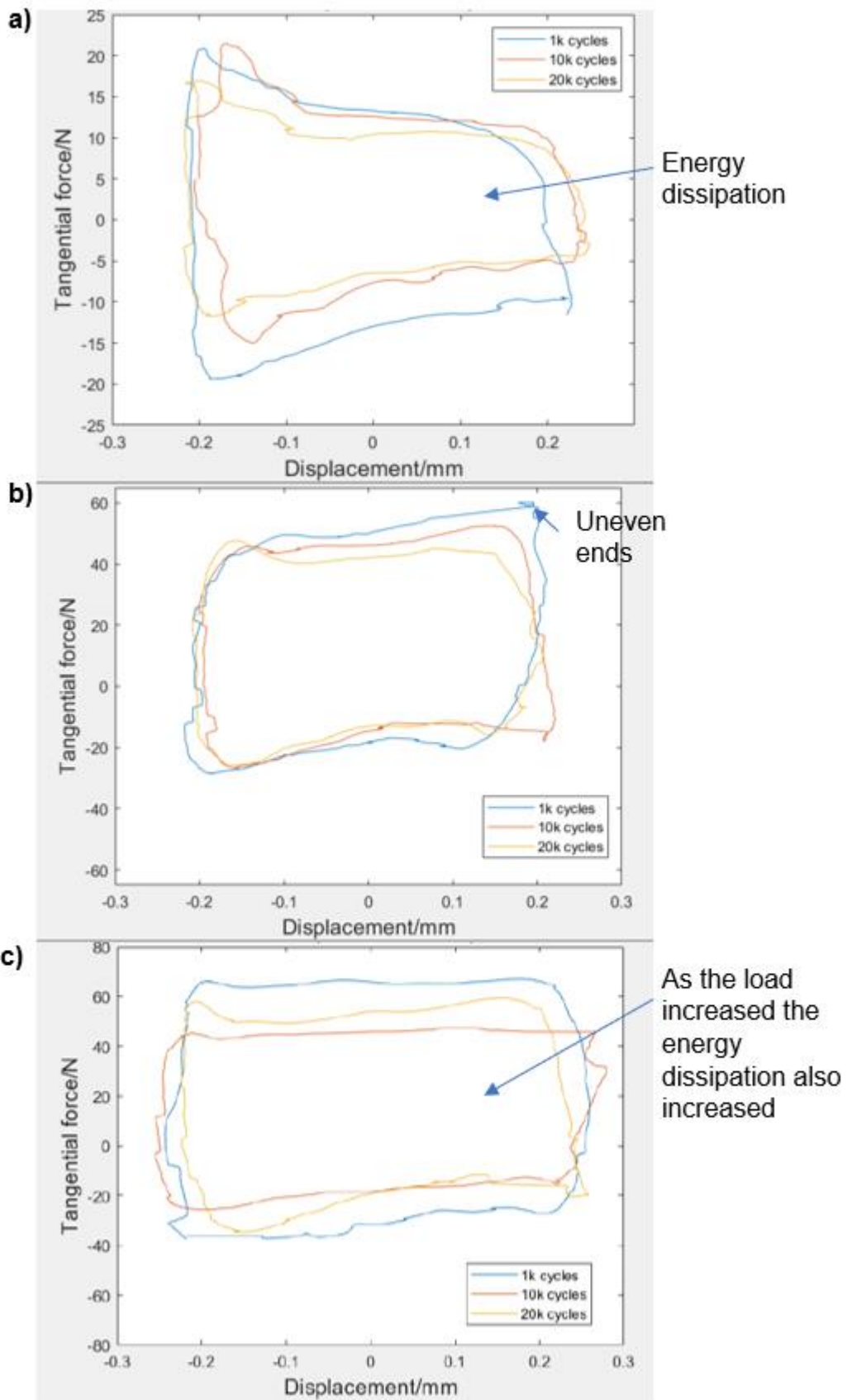
Figure 3-11 Average fretting loop of 50 cycles at various stages of the C263 test (1000-1050, 10000-10050,20000-20050 cycle) a) normal load of 15N, b) normal load of 25N, c) normal load 37.5N

3.4.4 Surface characterisation methods

Post-test samples were investigated to characterise changes in the surface conditions. The technologies and equipment used in surface characterisation are listed here with a short explanation of the preparation, processing, and interpretation. Figure 3-12 shows a flow chart with all the analysis methods undertaken to analyse the test samples. Firstly, the optical images of the wear scar are obtained using a USB microscope and the Alicona. These images are then post-processed to obtain wear volumes and surface roughness etc. The regions of interest were identified from the optical images, these were then further analysed using SEM images that were used as a guide for elemental analysis and detailed profilometry.
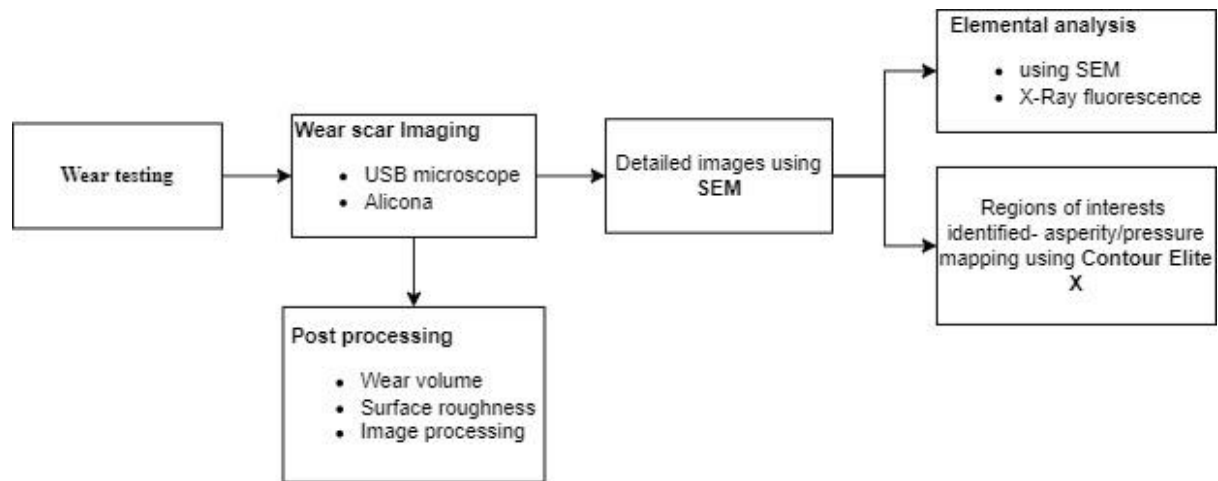
Figure 3-12 Flowchart showing all the analysis methods undertaken

3.4.4.1 Optical images of the wear scar

The images of the wear scar produced form the tests conducted in the TE77 reciprocating wear tester are taken using Alicona Infinite Focus SL, using a 5x magnification lens. These images were used to assess different wear mechanisms and any key surface features. Additionally, this allowed easy comparison of characteristics between different samples tested under various load conditions.

The images of the wear scar during the interrupted tests were captured using a USB powered microscope (Jiusion 40) for easy access and this could be connected to any PC. This ensures that contact conditions are not changed (especially the wear debris) throughout the test.

3.4.4.2   Image processing

Images of the wear scar obtained using the USB microscope and Alicona were processed for quantitative measurement of the glaze coverage. For this analysis, the glaze is identified by the regions where a 'black' oxidised region is present.

Image segmentation techniques are applied to extract/highlight the features on the image. Image segmentation is a process where an image is divided into regions or categories and each pixel is assigned to a category depending on the interested features [75] [76]. There are several methods of segmenting an image such as shape analysis, intensity thresholding, background detection/subtraction etc. Intensity thresholding and background subtraction are the methods used to process the wear scar images.

The images are processed using the image processing toolbox app in MATLAB. Figure 3-13 summarises the image processing techniques and steps used to process the wear scar. A combination of manual and semi-automated segmentation techniques is used since each image has a different brightness and contrast level.
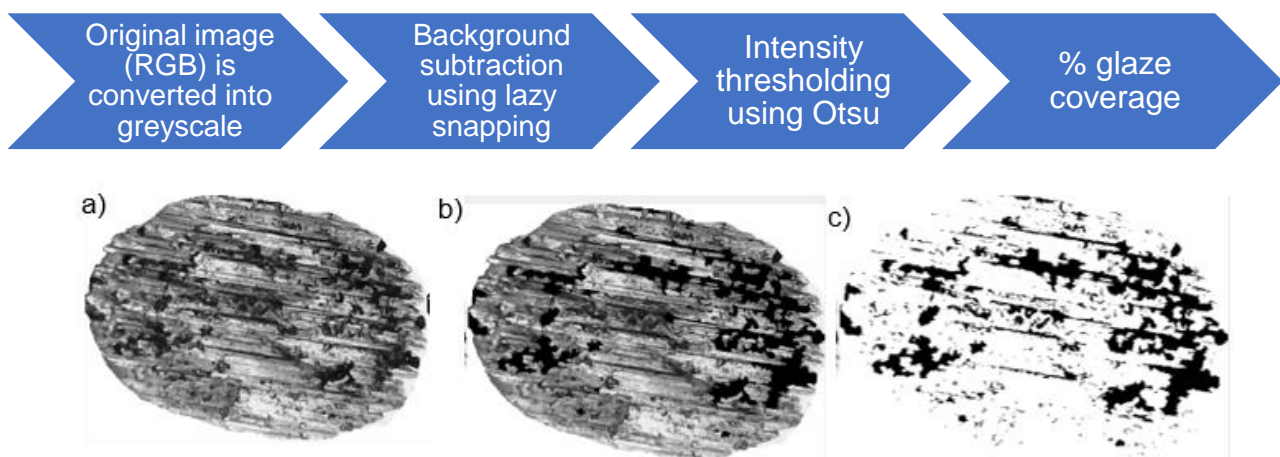
Figure 3-13 a) greyscale image prior to the segmentation process b) image once background separation is applied using lazy snapping c) final binarised image after intensity thresholding

Initially, the original image is converted into a greyscale image (see Figure 3-13a), this is then used for the segmentation process. Once the images are converted, an interactive image segmentation technique called Lazy snapping (Graph cut) is used to standardise the images, where both background and foreground (i.e. glazed regions) can be specified [77]; the output from the segmentation process is a binarised image

or a masked image. This separates the background from the foreground, highlighting the glazed regions. An example of a masked image can be seen in Figure 3-13b where the black oxidised regions are emphasised compared to the original greyscale image. This method is applied because of its flexibility (especially when the image settings are varied from one image to another) and ease of use with instant visual feedback.

The masked image from the background separation is then used as an input image for intensity thresholding (Otsu thresholding). It is an effective way to transform the image into its binary equivalents by assigning the pixels into groups. The Otsu thresholding method is where the image is segmented using a single threshold value. This method is applied in MATLAB by assessing the histogram of the image and selecting an ideal threshold value. The images present a bi-modal distribution with two peaks representing background and foreground; the optimal threshold value is chosen by calculating and evaluating the variance. This leads to a binary image being produced (as seen in Figure 3-13c).

Finally, the binarised image is used to calculate the coverage of the glaze by evaluating the number of 'black' pixels in the image. This analysis is conducted to understand how the oxides are formed and detached during subsequent sliding, thus there are some inaccuracies are present with this analysis. The assumptions include that only 'black' regions are oxide layer, the 'black' region could be loose debris on the contact or not well bonded etc.

3.4.4.3   X-ray fluorescence analysis (XRF)

X-ray fluorescence analysis was a non-destructive and quick method for the chemical analysis of the samples without any material preparation using the diffraction of x-rays. When compared with EDX spectroscopy, this technique is relatively simple and takes less time to acquire the results since the chamber does not need to evacuate before producing results and is also non-destructive.

The X-ray fluorescence machine used is a Fischerscope X-Ray XAN 250 with an excitation voltage of 50kV passed through a nickel filter. To ensure that the noise is reduced to an acceptable level, sixty seconds is allowed per measurement. Figure 3-14 shows the settings used and the processed data obtained from the area of interest (using 50kV). One of the main limitations of using this method is that it cannot detect lighter elements as the emitted radiation is absorbed by the air and usually detects

between sodium to uranium. This means that the availability of oxygen cannot be detected using this method, thus oxidation effects cannot be determined [78] [79] . The XRF analysis are carried out after optical microscopy for initial analysis to identify any trends or major changes in the composition of the layers produced by the sliding.
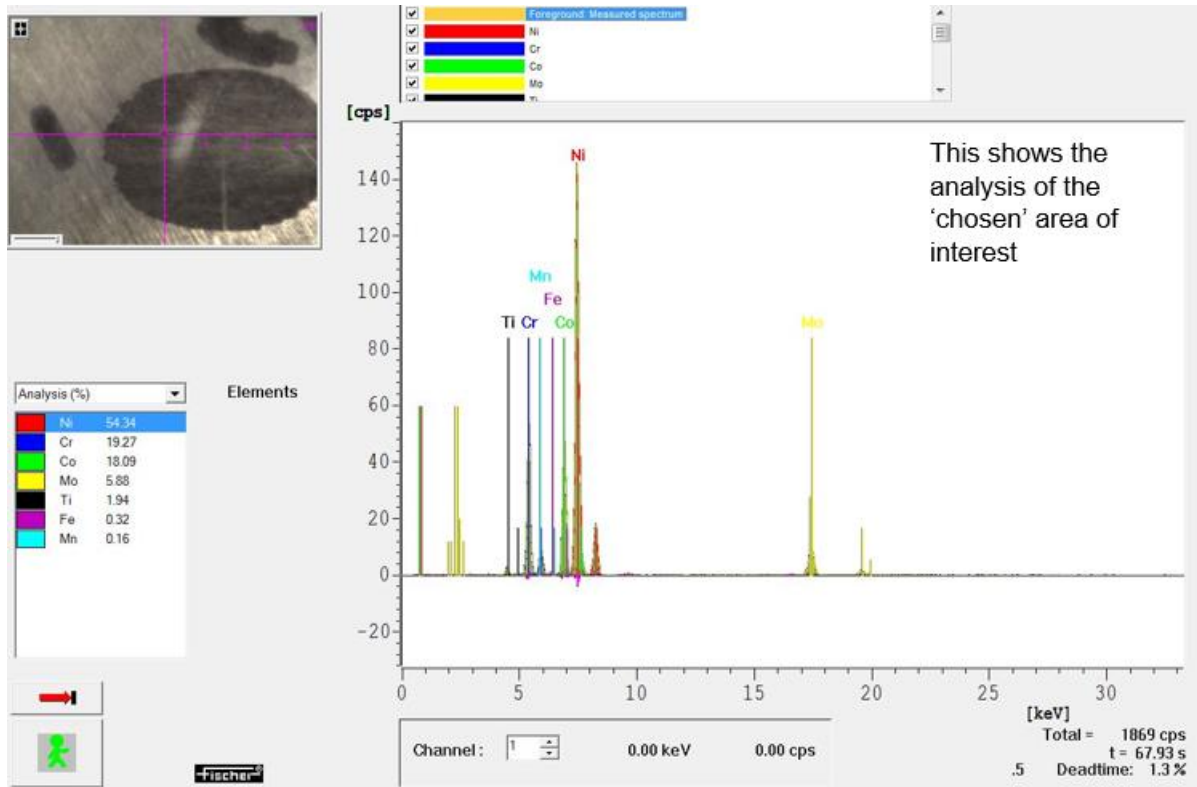
Figure 3-14 Data obtained from the X-Ray fluorescence analysis of the specified area of interest

3.4.4.4 Scanning electron microscope (SEM)

A Hitachi TM3030 Plus SEM was initially used to obtain high magnification, detailed images of the surface in order to evaluate the topography (to evaluate wear mechanisms) and cross-sectional (to identify whether there are dominant layers/elements within the layers as the test conditions are varied). This was beneficial in understanding the influence of alloying elements on glaze formation. Two main techniques used to scan the surface are backscattered electron (BSE) and Scattered electron (SE). BSE is used for acquiring compositional images whereas SE is used for topographical information. The Hitachi TM3030 Plus SEM has a mixed SE/BSE

feature where both topographical and elemental information can be viewed, where the darker regions in the micrographs represent elements with higher atomic mass. The scars were observed at a magnification of x1000.

A Inspect F50 SEM was used for the Energy-dispersive X-ray (EDX) spectroscopy to understand the overall distribution of the elements that make up the layers formed on the surface because of repeated sliding. Regions of interests are identified from the optical images of the wear scar.

An example of a result from EDX analysis can be seen in Figure 3-15. From the area of interest, several regions were then chosen for analysis. The areas chosen for analysis are where there is glazed or 'black' oxidised region, signs of initial/broken down glaze and metallic wear ('silver/grey') regions. As seen in the figure, there is a higher percentage of oxygen in the glazed region indicating that there is more oxide present.

3.4.4.5   Non-contact profilometer

The images obtained using the Alicona InfiniteFocusSL profilometer were then also analysed using the Alicona Measuresuite. It is used to measure volume loss and surface roughness.

A Contour Elite X optical profilometer is used to examine the surfaces to measure nanometre roughness, this allows to investigate the influence of contacting asperities (contact map of the surface can be produced) using a x20 magnification lens.
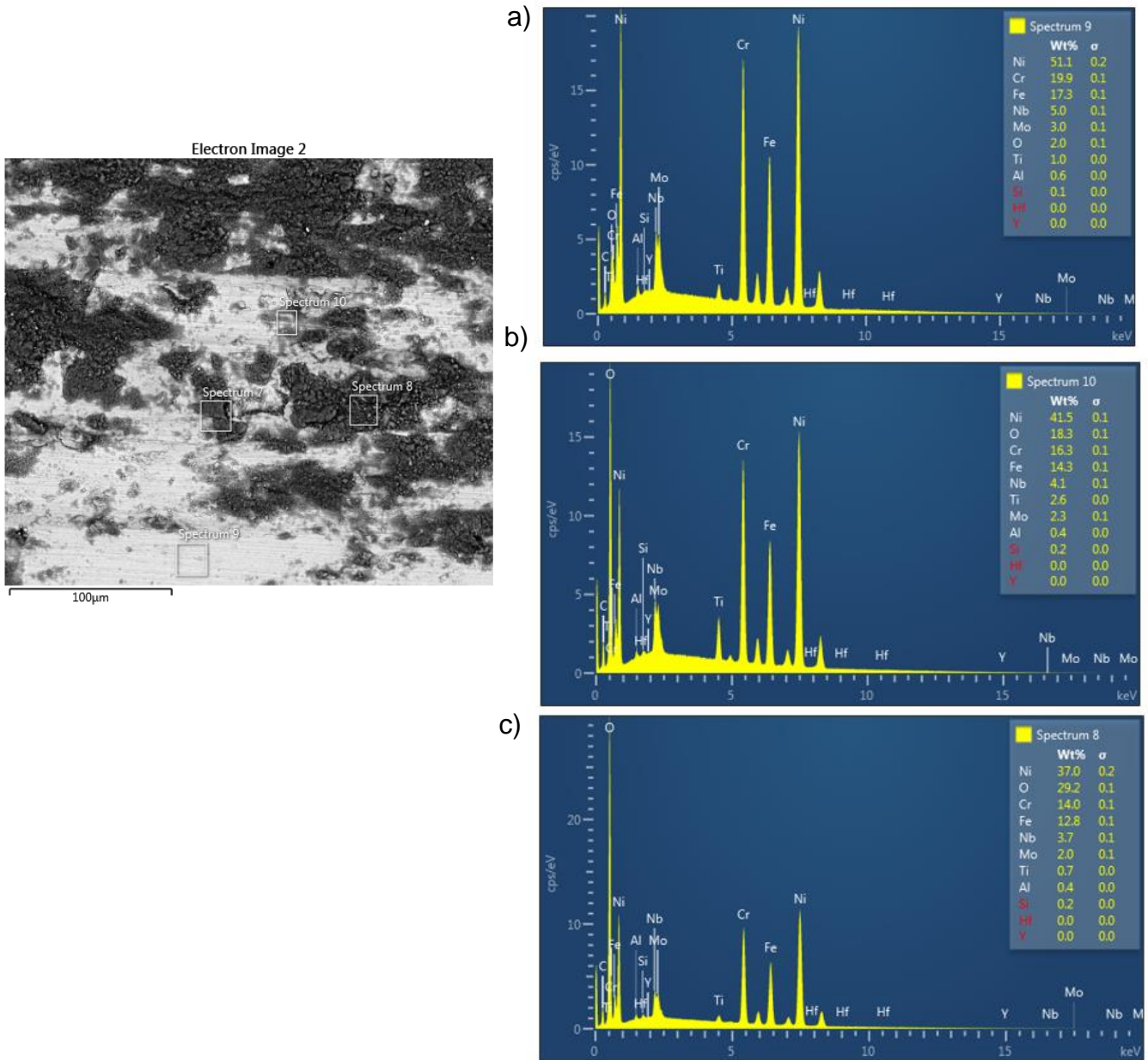
Figure 3-15 Example of a result obtained from EDX analysis. Regions of interests were chosen a) metallic wear b) starting to glaze c) glazed/oxidised regions

3.4.4.6 Sectioning and material preparation:

Following on from surface images, the samples were sectioned to examine the changes in the sub-surface layers and the thickness of any specific layers formed as a result of glaze generation. Examining the cross-section has significant importance as this can confirm how the specific elements play a role in the glaze generation and if there are any changes in the microstructure that either aids or hinders the process.

The post test samples were sectioned in the middle of the wear scar groove to observe the sub-surface changes. The cut was made using a precision cutting saw (Buehler-IsoMet). The cut samples are then cold mounted with epoxy resin. Hot mounting is not used to prevent the damage that could happen under high temperature and pressure used in the mounting press.

The mounted sample was then ground and polished using Buehler-AutoMet machine. The process and the lubricants are detailed in Table 3-9. The material preparation processes were done according to the Buehler material preparation and analysis guidelines [80]. After each step, the surface was inspected for damage using an optical microscope.

Process step	Abrasive Media and lubricant		Force (N)	Speed (rpm)	Time (s)
	SiC Paper Grit	Lubricant			
1	P600	Water	35	300	60
2	P1200	Water	35	300	60
3	P2500	Water	35	300	60
	Polishing Suspension		Force (N)	Speed (rpm)	Time (s)
4	6μm diamond		35	300	300
5	1μm diamond		35	300	180
6	0.04μm colloidal silica		35	300	300

Table 3-9 details the grinding and polishing procedures

Chapter 4   Room Temperature tests

This chapter focusses on the results from the wear tests conducted at room temperature and varying normal load conditions. Firstly, a wear scar analysis of the three different materials tested at different loads is presented, followed by the coefficient of friction analysis and surface topography.

Sample material	Normal load (N)	Temperature (ºC)	Stroke length (mm)
Inconel 718	15, 25, 37.5	22-25	2.2
C263	15, 25, 37.5	22-25	2.2
Haynes 25	15, 25, 37.5	22-25	2.2

Table 4-1 The test conditions used in the room temperature tests.

4.1   Wear scar analysis

The wear mechanisms are identified with images of the wear scars. Figure 4-1 – 4-5 show the wear scars obtained at various loads (15, 25 and 37.5 N) for Inconel 718, C263 and Haynes 25 samples post 30,000 cycles of reciprocating sliding. The scars are characterised with parallel abrasive grooves interspersed with black oxidised areas of glaze; grey/silver areas represent the exposed metal caused by metallic wear. The coverage of glaze on the wear scar has become more evident with increasing load.
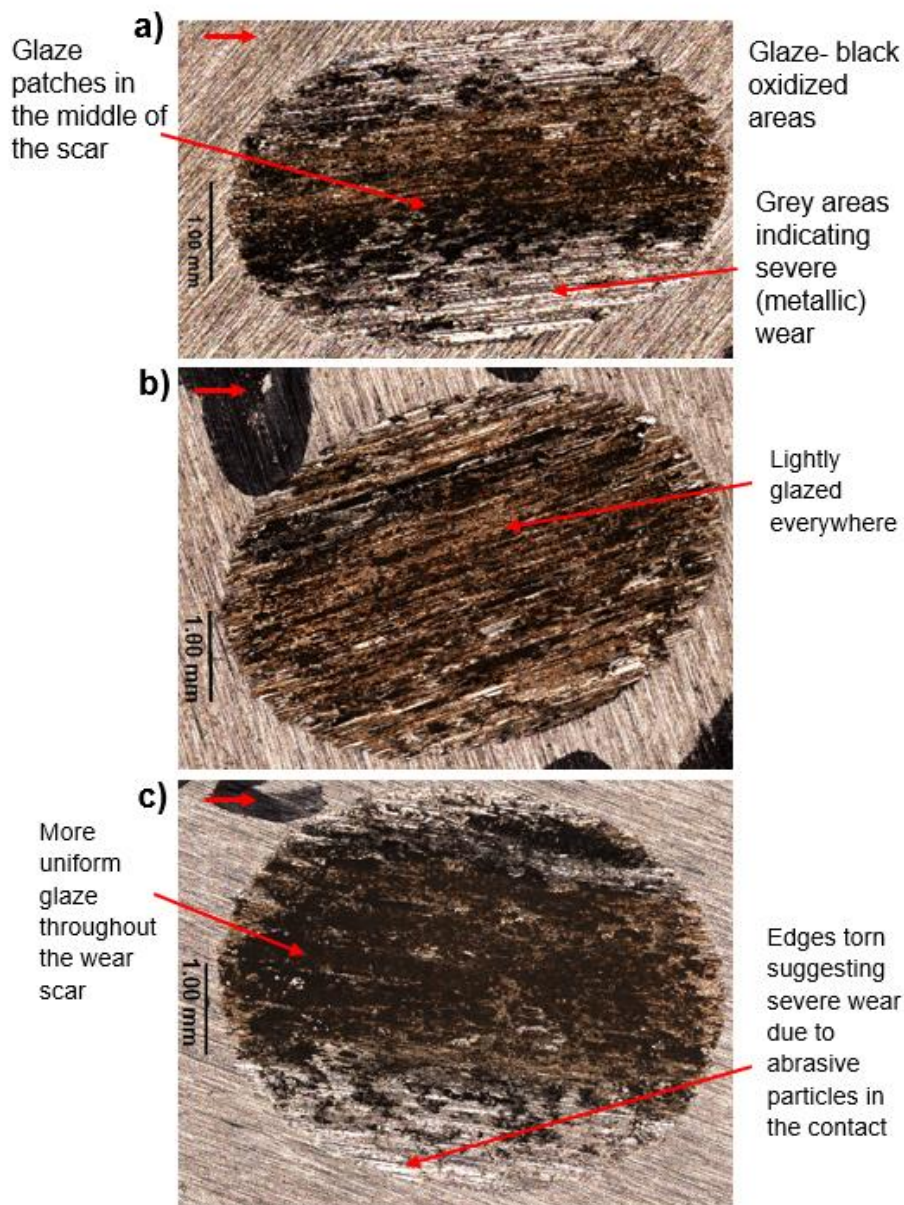
Figure 4-1 Wear scar produced on Inconel 718 disc samples at various loads over 30,000 cycles, sliding direction is indicated by red arrow on the scar image a)15N b) 25N c)37.5N
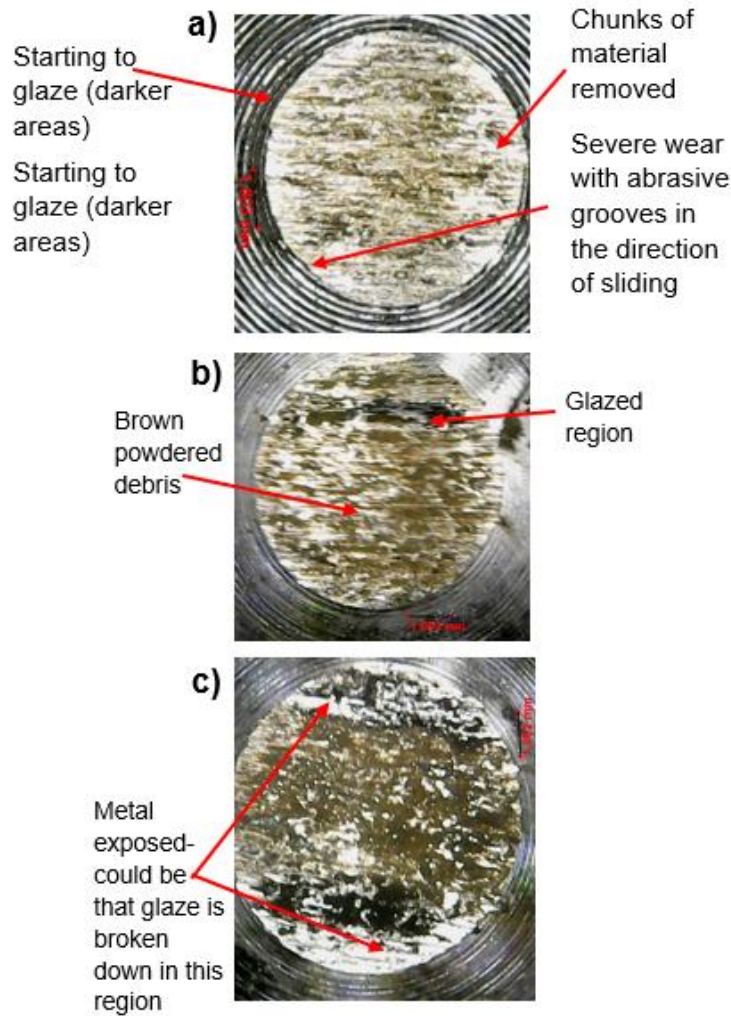
Figure 4-2 Wear scar produced on Inconel 718 pin samples at various loads over 30,000 cycles, a)15N b) 25N c)37.5N

On the Inconel 718 samples at the lowest load (i.e. 15 N), black oxidised regions are visible in the middle of the wear scar with grey areas exposing fresh metal waiting to be oxidised. The grey areas suggest a region of severe wear due to the initial metal-metal contact. On the pin, evidence of severe wear can be seen with small chunks of material removed from parts of the wear scar. As the normal load is increased more glazed areas can be seen, however, a small amount of metal exposure is still visible with light glaze everywhere on the wear scar. On the pin, brown powdered debris then starts to be visible with some glazed regions. When the applied load is at its highest load (37.5N), a thick extensive glaze is generated with little metal exposed on the edges. It is seen that the edges of the wear scar are torn indicating severe wear or abrasive wear due to the third body abrasion in the contact from the debris (wear

debris are thought to be harder than the bulk material because it would have been oxidised). Moreover, the width of the wear scar and the number of debris generated has increased as the normal load is increased. It can also be observed that at higher loads the debris produced were larger in size compared to a lower load (i.e., 15N). Additionally, the brown coloured powdered debris (probably due to the increase in temperature with load) were not compacting and was displaced out of the contact, this was observed on all load conditions.
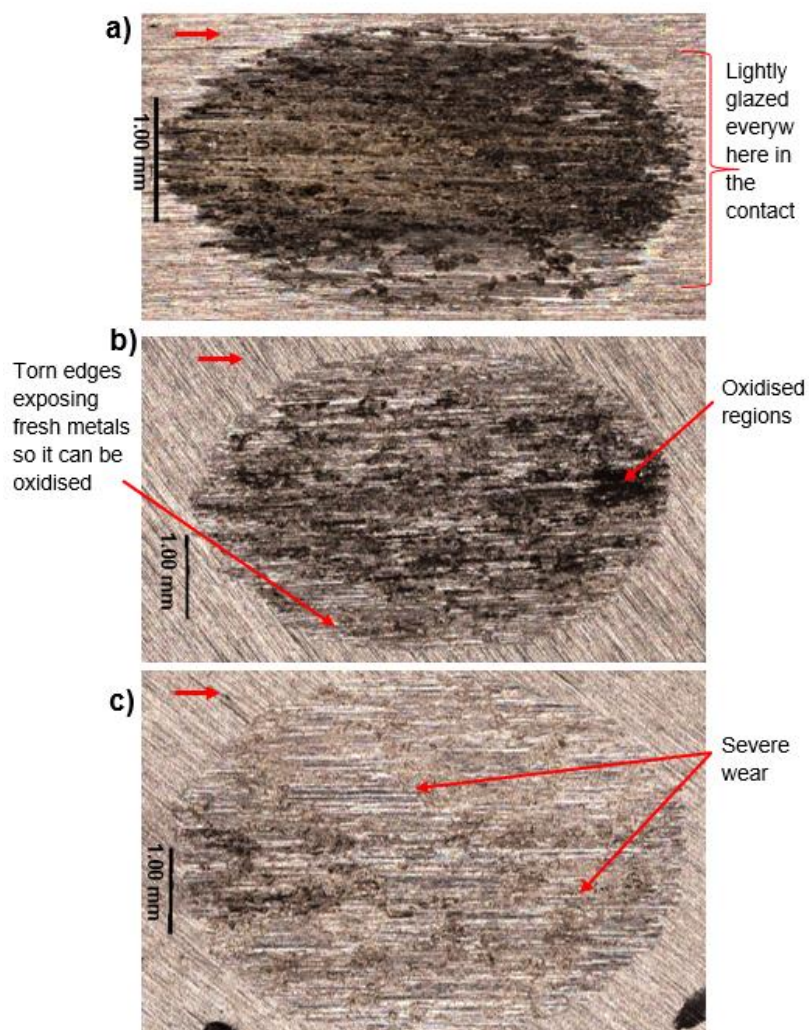
Figure 4-3 Wear scar produced on C263 disc samples at various loads over 30,000 cycles, sliding direction is indicated by red arrow on the scar image a)15N b) 25N c)37.5N

a) Severe wear- little or no glaze at all

b) Glaze beginning to form in the middle of the wear scar

c) More even coverage of glaze
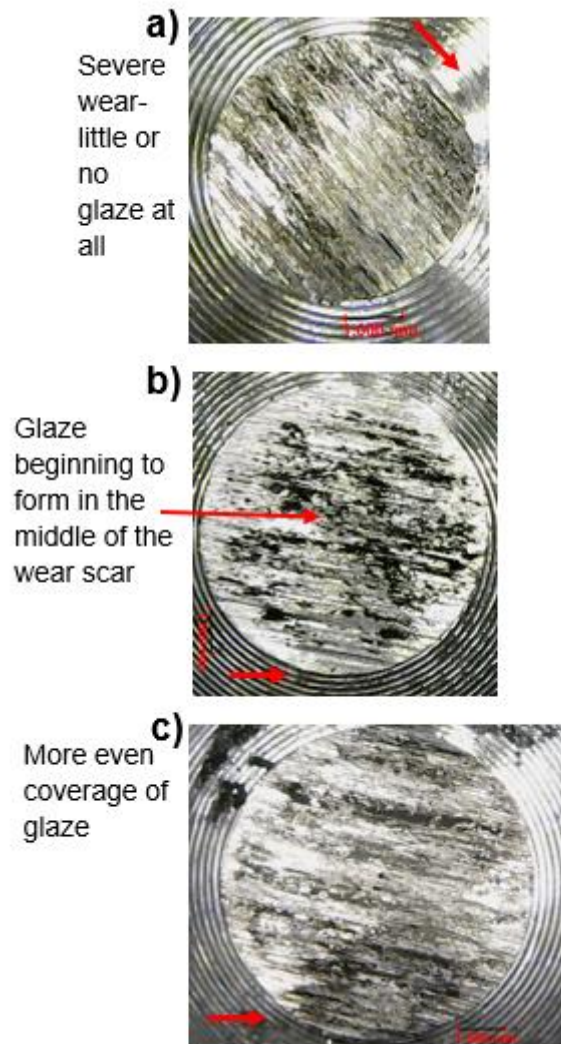
Figure 4-4 Wear scar produced on C263 pin samples at various loads over 30,000 cycles, sliding direction is indicated by red arrow on the scar image a)15N b) 25N c)37.5N

Similarly, on the C263 tests, (see Figures 4-3 and 4-4), a light patchy glaze is formed with little metal exposure. Torn/worn edges are also visible on the wear scar indicating abrasive wear due to the debris being in the contact. In contrast to Inconel 718, the coverage of glaze is lower on the C263. As seen in Figure 4-5, the Haynes 25 samples produced a slightly different wear scar compared to Inconel 718 and C263: with long striations and little oxidised regions. Also, the size of the wear scar is small when compared to Inconel 718 and C263.
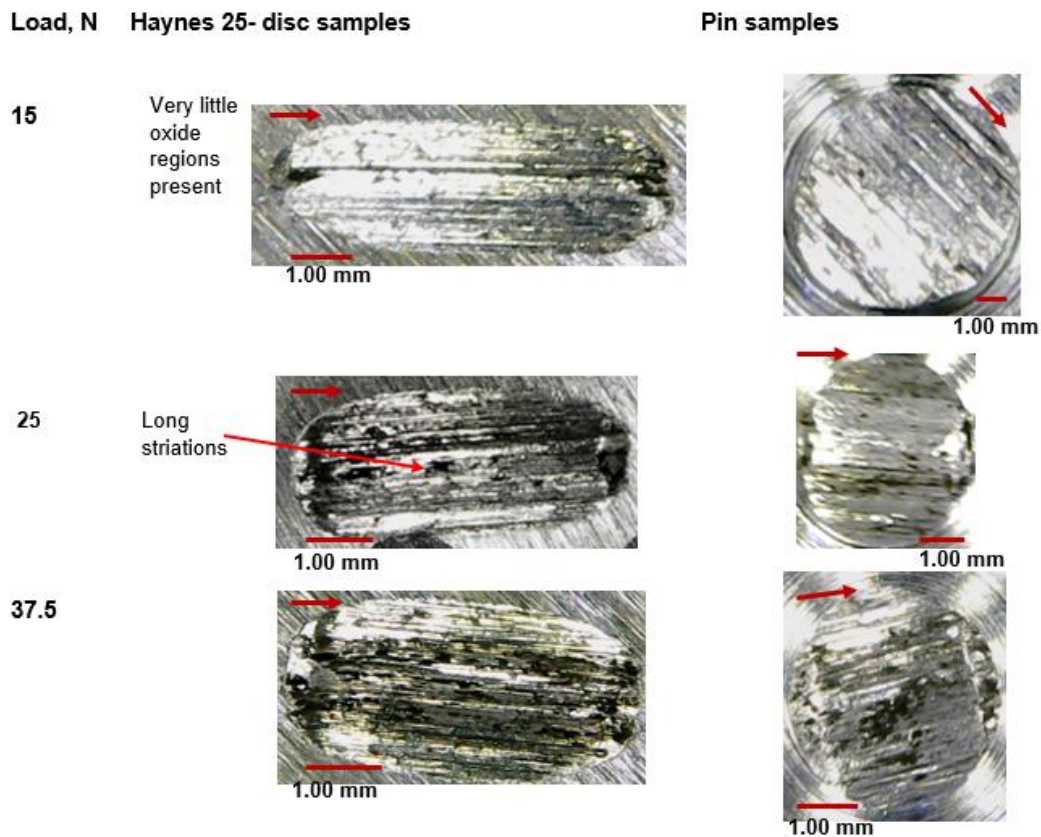
Figure 4-5 Wear scar produced on Haynes 25 pin and disc samples at various loads over 30,000 cycles, sliding direction is indicated by red arrow on the scar image

Between the three materials, extensive patches of glaze are seen on Inconel 718. However, C263 has started to form a more uniform glaze on the entire contact even at the lowest load, whereas, on the Inconel 718, the glaze is only found in the middle of the contact. However, common for all materials, the width of the wear scar and size of the debris increased as the load is increased, and at higher loads, it was observed that a greater number of debris were pushed out of the contact rather than being retained within the contact so the wear rate will be higher, this is likely because there is not enough time between cycles for the debris to be broken down into smaller fragments and oxidised.

4.1.1 Wear volume

The images obtained using Alicona InfiniteFocusSL instruments at 5x magnification were post-processed using the Alicona Measuresuite software to extract volume loss. It was also calculated using the mass loss measured on a Sartorius Micro Lab scale. Figure 4-6 shows the average wear volume from the disc samples for the repeated tests with the standard deviation.

The wear volume increases with the applied normal load. However, the rate at which the volume is increasing is different for different materials. The volume loss of Inconel 718 is almost twice when compared to C263 at each load condition, and significantly lower on Haynes 25. This further supports the role of wear debris in the glaze generation process; where the different scar seen on the Haynes 25 could be due to not having enough debris to generate a surface layer compared to the other materials.

The repeated tests showed variability, this was expected due to the various factors that are involved with the formation of glaze, with Inconel 718 showing higher standard deviations. This further supports the uncertainties involved with the formation of glaze due to the involvement of various factors such as flash temperature, the role of debris, microstructure of the materials etc. Here, the discussion focuses on volume loss; however, mass loss would have been a more precise measure, considering that the debris contains oxides, leading to discrepancies in the calculated volume loss.
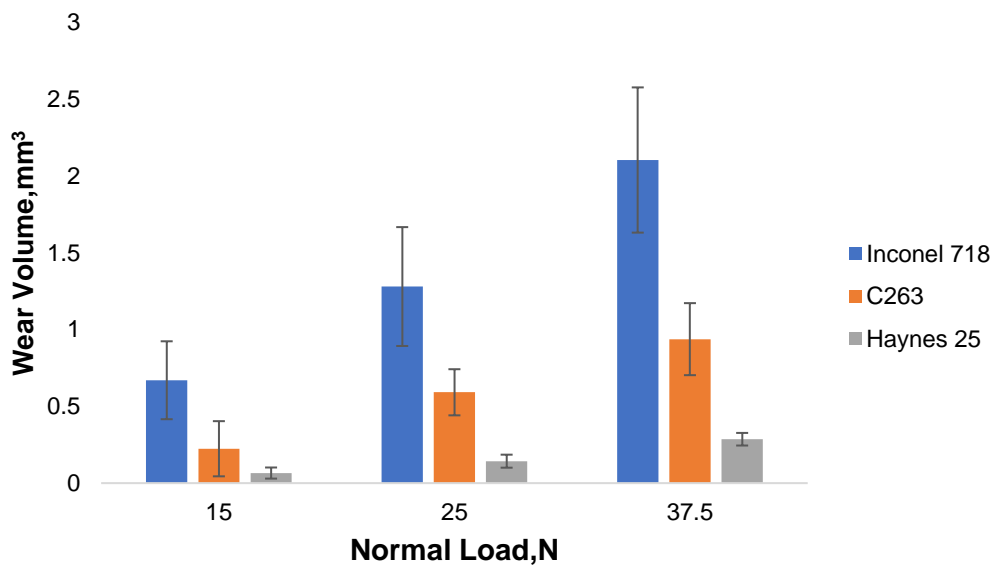
Figure 4-6 The average volume loss from the disc with the variability (standard deviation) in the results highlighted, measured using the Alicona Measuresuite software

4.1.2 Interrupted tests

To investigate the influence of time and the progression of glaze/wear, the tests were interrupted at every 5000 cycles and an image of the wear scar was recorded. Figures 4-7 to 4-9 show the wear scars from the interrupted tests. The surfaces were not cleaned before imaging in order to preserve the nature of the surfaces, especially the wear debris.

For Inconel 718, the glaze coverage has increased with time and load. Especially around the edges where there is more wear debris present. It can be seen that as the load is increased the rate at which the layers are formed is also increased (glaze starting to be visible at lower cycles), for example, there is very little black oxidised regions at 15 and 25N compared to 37.5N where the layers are starting to form all over the wear scar rather than just the edges.

For C263, the scars show a slightly different trend compared to Inconel 718, where the glaze is forming even at lower loads (15N) and there are more signs of severe wear at higher loads with less coverage (37.5N). C263 glazes at a faster rate than Inconel 718 at 15N. A slightly different trend is seen on the Haynes 25, showing more surface damage and little or no glaze generation at all load conditions. The extent of surface damage can be seen at the normal load of 25N and 5000 cycles where there is ploughing caused by the debris. Moreover, a higher amount of unoxidised (silver) debris was observed to be pushed out of the contact zone on the Haynes 25 samples when compared to other materials.

On both Inconel 718 and C263, the coverage of glaze increases over time, this indicates more time is needed for the transition, and there is more debris available to be compacted into a surface layer. As the loads are increased, the time it takes to form glazed regions is reduced. For instance, in Inconel 718, there is better and even coverage at 20000 cycles when the normal load is 37.5N compared to 15N. However, on Haynes 25, no oxidised regions are seen suggesting more energy and time are required to generate a glaze layer.
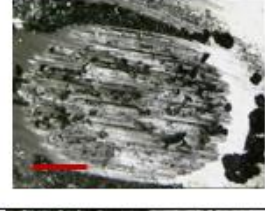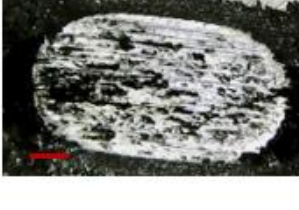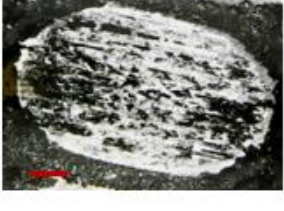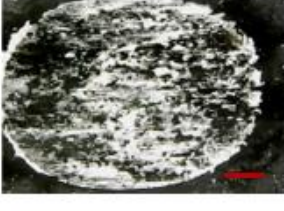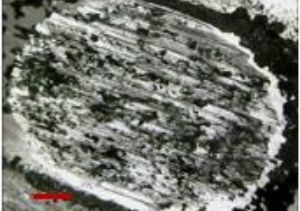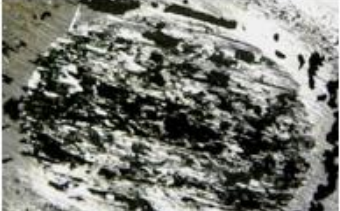
Inconel 718	15N	25N	37.5N
5k			
10k			
15k			
20k			
25k			

— Represents 1.00mm

Figure 4-7 Wear scar images obtained In718 tests by interrupting the tests every 5000 cycles to observe the evolution of glaze formation
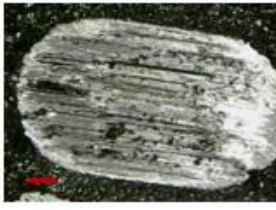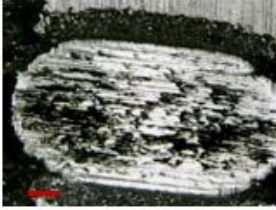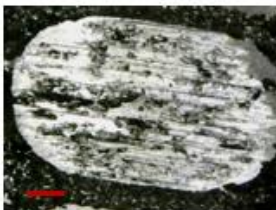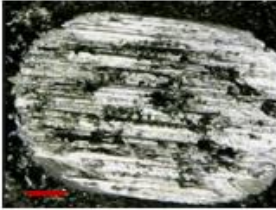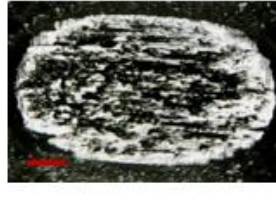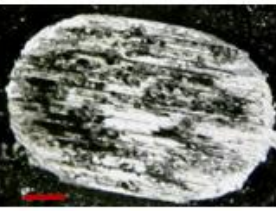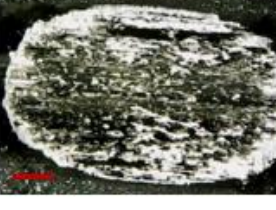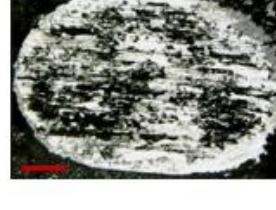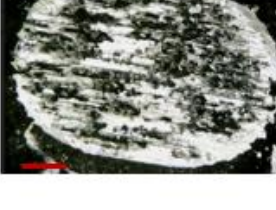
C263	15N	25N	37.5N
5k			
10k			
15k			
20k			
25k			

— Represents 1.00 mm

Figure 4-8 Wear scar images obtained C263 tests by interrupting the tests every 5000 cycles to observe the evolution of glaze formation
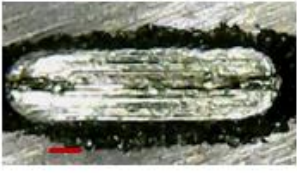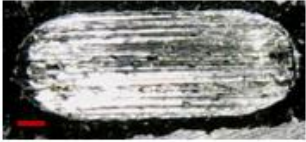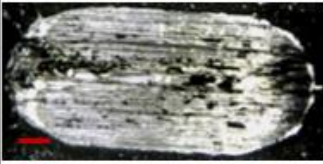
Figure 4-9 Wear scar images obtained Haynes 25 tests by interrupting the tests every 5000 cycles to observe the evolution of glaze formation

4.2 Evolution of coefficient of friction

The changes identified in the glaze formation has also made an impact on the friction observed on the wear scar.

Figure 4-10 shows the average COF after 30,000 cycles for Inconel 718 and C263 samples. This was calculated using the tangential load measured using the load cell, with apparent friction calculated as tangential load, F_f / Normal load, N. The calculated COFs are valid since a gross sliding regime is achieved as seen in the fretting loops (see section 3.4.3) As seen in the graph, as the normal load is increased, the average

COF is decreasing. The rate at which the reduction occurs is different for various loads and materials. For instance, the rate at which the COF is dropping is greater between 15 to 25N compared to 25 to 37.5N. this is seen on both materials. Between materials, Inconel 718 has lower COF values than C263. This links with the glaze observed on the wear scars, more coverage on the Inconel 718. The error bars on the chart shows the standard deviation. On the other hand, the COF for Haynes 25 stayed constant.
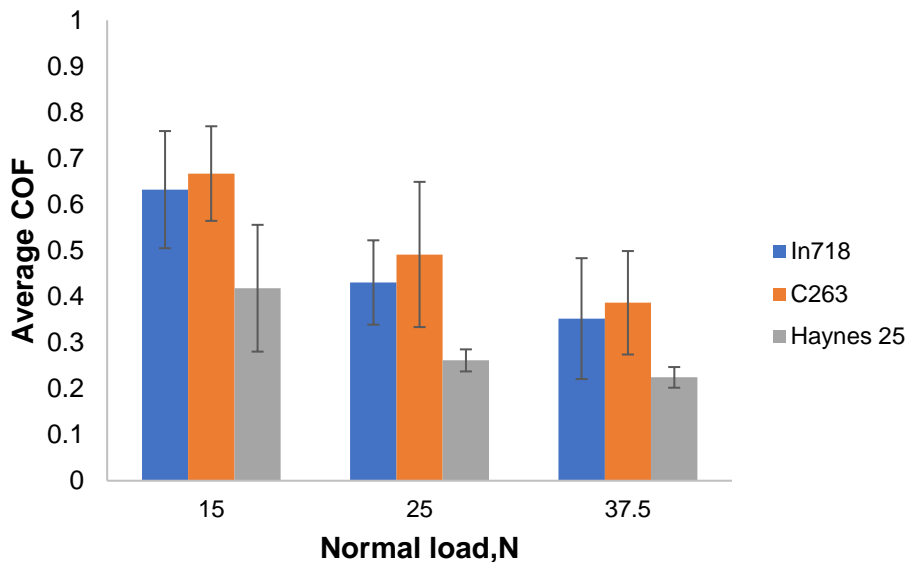
Figure 4-10 Average COF against applied normal load for the 30,000 cycles

To understand how the COF changes throughout the test, the evolution of relative COF over the sliding duration is shown in figure 4-11. However, as shown in Appendix 4a, the initial COF changes with load prior to the possibility of glaze formation. This in turn suggests that the COF is changing with load as consequence of rig dynamics, as opposed to any effects due to glaze generation. Therefore, to eliminate the test rig effects, the COF were plotted relative to the initial COF. In order to better visualise the trends in the COF because of glaze generation. As shown in Figure 4-11, at the lowest load (i.e. 15N), there is no change in the COF of C263 whereas on the Inconel 718 a slight decrease in the COF over time is seen. At higher loads (i.e., 25 and 27.5N) the drop in the COF is more evident with time. The COF is falling at a higher rate with increased load. However, the In718 data shows more variability, likely to be due to the higher amount of wear observed leading to interactions with debris. Moreover, some interruptions in the COF can be seen (especially on C263 samples at 25N), where COF has increased after 12,000 cycles suggesting disruptions in the glaze formation

and the layers are broken down with further sliding. Additionally, it takes less time for the COF to drop as the load is increased. For example, C263 samples at a normal load of 25N, takes approximately 8000 cycles to observe a change in COF whereas, at 37.5N, the COF drops around 6000 cycles. The starting points of COF at a normal load of 15N is not identical with the 25N and 37.5N, this could be due to the instabilities in the rig as discussed in section 3.4.3. Haynes 25 has shown similar rig effects (see Appendix 4a), however, there is no drop in the COF as seen with Inconel 718 and C263 and the rise in COF is likely due to surface damage.
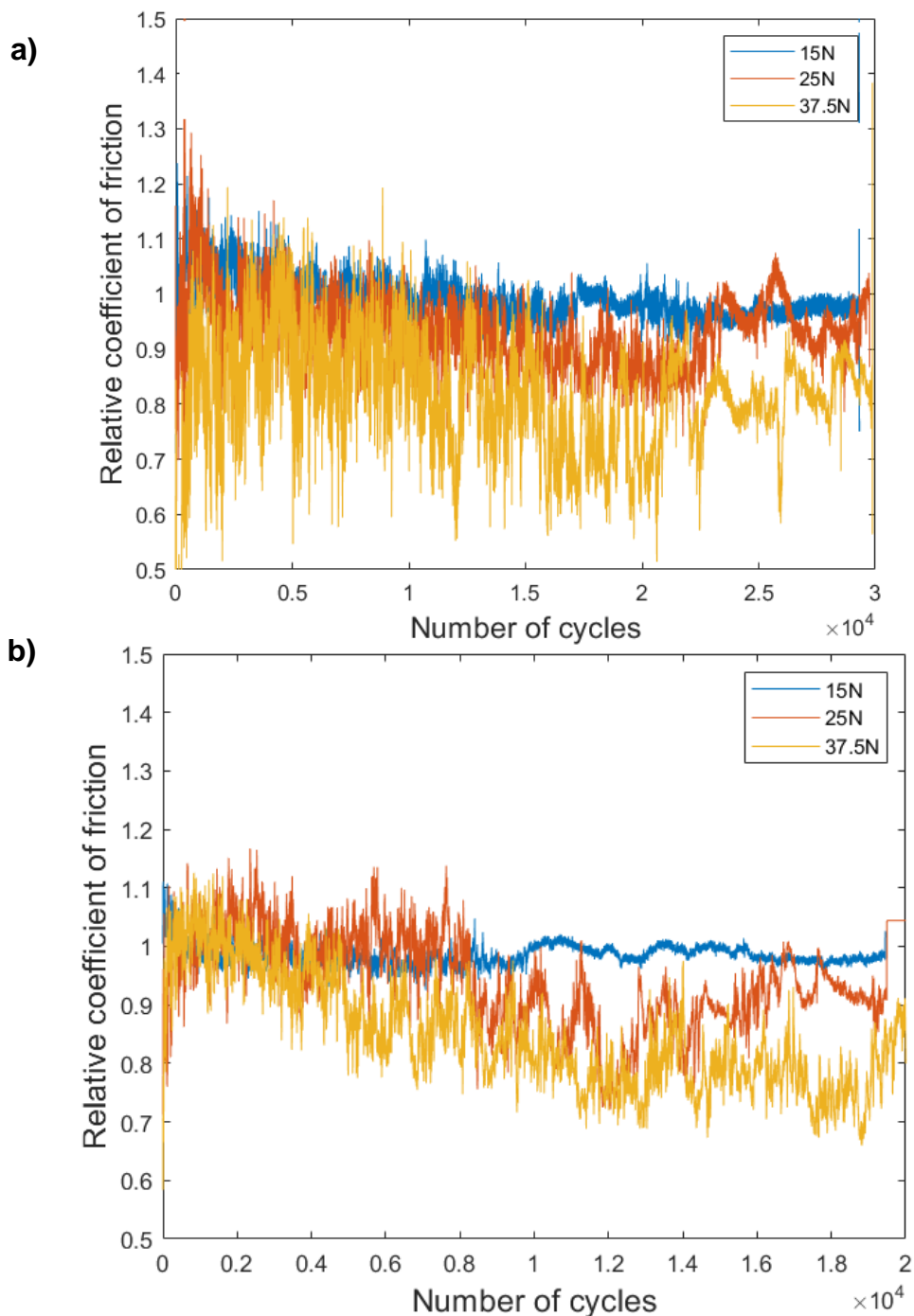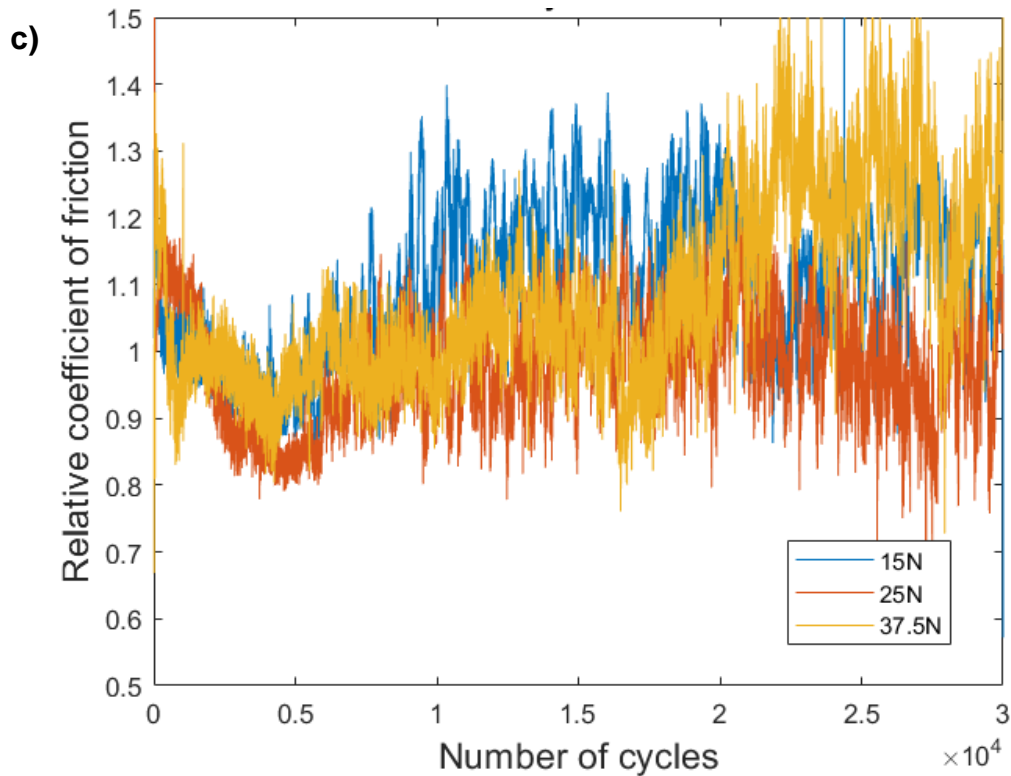
Figure 4-11 The evolution of relative COF as the tests are progressed a) In718 b)C263 c)Haynes 25

In summary, whilst some changes are seen over time in a given test, with COF dropping, corresponding with glaze formation in some cases, as well as with this tendency of COF increasing with load. With In718 and C263, this was significantly less than initially suggested once test rig effects were calculated.

Figure 4-12 illustrates the relative COF of all three materials under the same load (i.e., 25N). This allows visualisation of the similarities and differences in COF as the test progresses. Both In718 and C263 exhibit a similar trend with an overall reduction in COF due to the prevention of metal-to-metal contact. This was expected, as these materials have similar chemical compositions and hardnesses. Conversely, a distinct trend is observed for Haynes 25, likely attributable to different elements in the alloy

composition leading to high friction. This is also reflected in the wear scar images where mechanical wear was predominant.
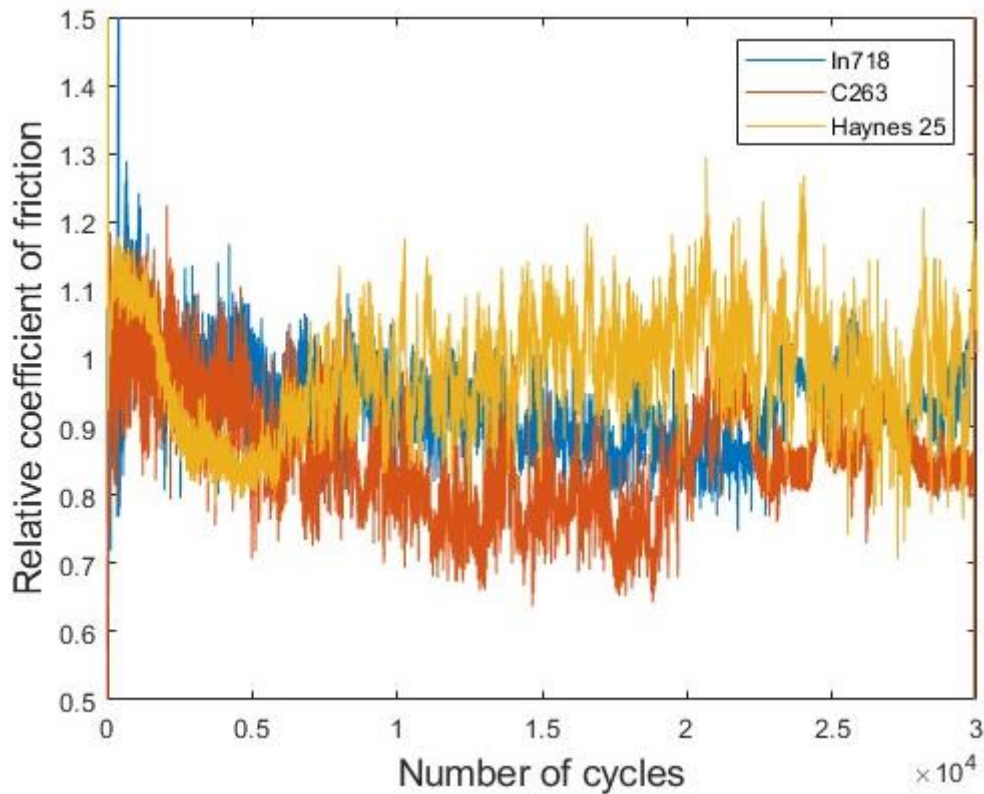
Figure 4-12 shows the evolution of COF at a normal load of 25N for all three materials at room temperature

4.2.1 Interrupted tests and glaze coverage

The evolution of COF was further investigated using the data from the interrupted tests.

Figure 4-13 shows the average relative COF for every 5000 cycles and the percentage glaze coverage at the end of every 5000 cycles. The percentage coverage of the glaze is calculated by processing the images using the image processing toolbox in MATLAB (see Section 3.4.4.3).

The results show that the glaze progressed with time and load. Although there is a rise in the percentage glaze coverage, at 15N, there is not an evident change in the relative COF for both Inconel 718 and C263. The variations in the friction and coverage could be due to the formation and breakdown of glaze layers suggesting the layers generated are thin and are easily broken down with further sliding.

As the load is increased, there is a slight rise in COF for both materials which contrasts with results seen from the continuous tests where there was a slight drop in the COF with glaze formation. The difference in the trends seen could be due to the challenge with interrupting the tests, altering the contact conditions.

It should also be noted that the relative COF for the interrupted tests should only be used to study the trends rather than using it as an absolute value due to the inaccuracies in the starting point after each interruption (see Figure 4-14). The vertical lines on the graph represent the interruptions, as seen there is a change in the start position once the plint is restarted. Overall, these tests give an insight into the glaze generation process and how the surface layers are easily broken and likely not sintered properly, although the COF data generated appears less accurate.

Variation in the data is not carried out as the inaccuracies are already mentioned due to the interrupting nature of these tests. The tests are conducted solely to observe surface changes as the testing progresses, eliminating the need for repetition.
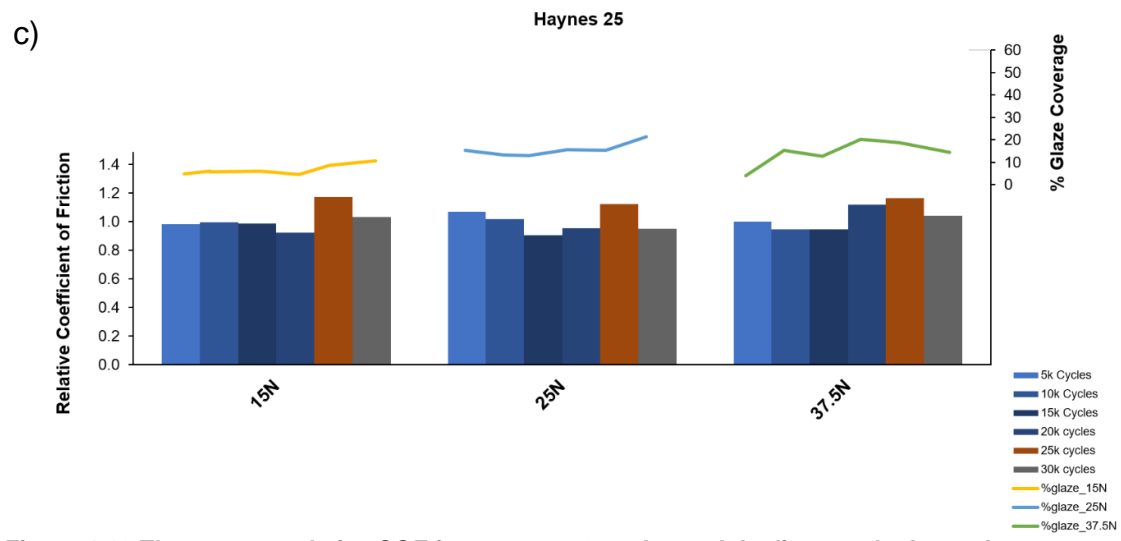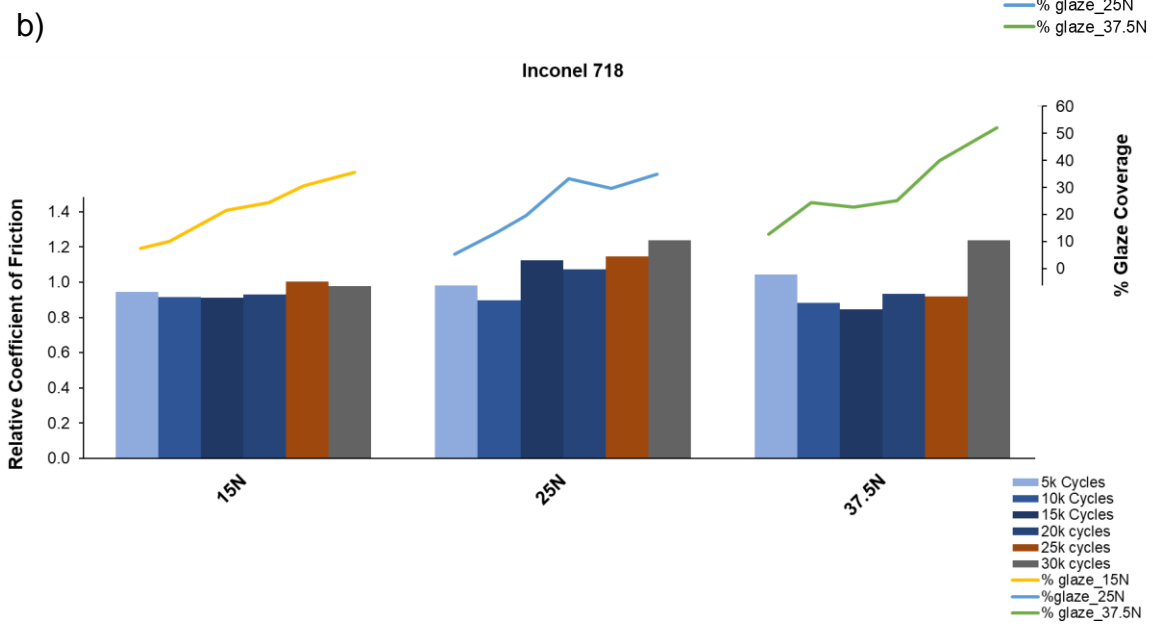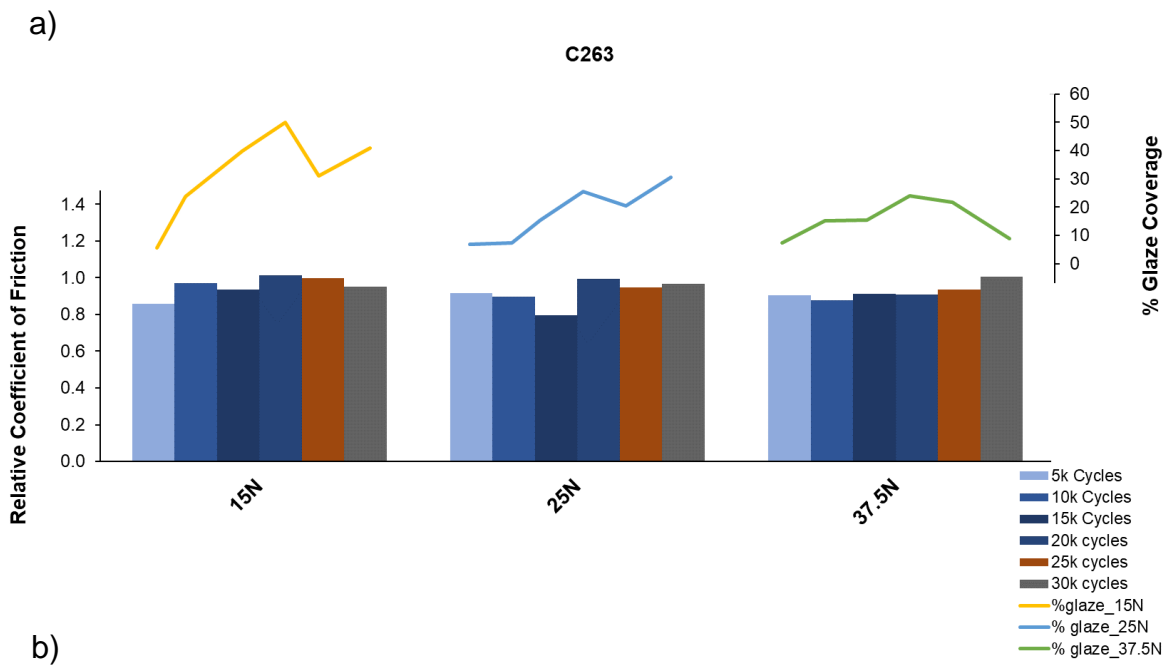
Figure 4-13 The average relative COF for every 5000 cycles and the line graph shows the percentage coverage of glaze at the end of 5000 cycle a) C263 b) Inconel 718 c) Haynes25
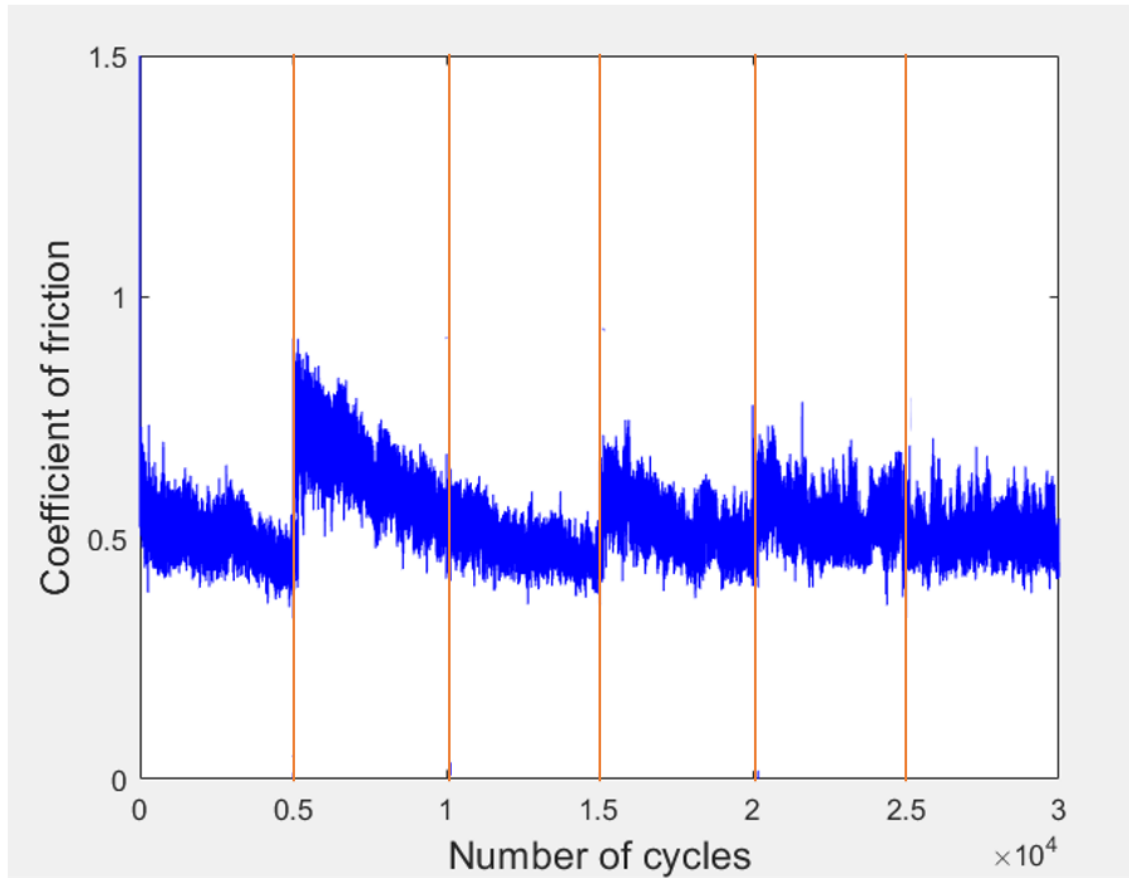
Figure 4-14 The variation in starting COF as the rig is restarted after the interruption at 5000 cycles

4.3 Surface topography

Changes in the friction coefficient were identified when a substantial apparent glaze occurred, so it is necessary to further investigate the glaze areas. Thus, the wear scars are examined using SEM, then initial elemental analysis using the X-Ray fluorescence, and finally to see the effect of oxidation, Energy Dispersive X-Ray Analysis (EDX) was performed.

4.3.1 SEM images

SEM images were obtained using the Hitachi TM3030 Plus SEM using a backscattered electron (BSE) and a scattered electron (SE) beam at 15kV.

Figure 4-15a, shows the SEM images obtained from the three regions. At Area A, a glazed region with wear debris being collected in the low points on the surface. at Area B where the layers are just starting to form, the amount of debris present are

considerably lower than Area A. Also, the debris on Area A is fine and smaller in size compared to Area B. Finally, at Area C where there is no glaze seen, metallic wear can be seen with parallel abrasive grooves caused by the debris interaction. A very little amount of debris is present suggesting no glaze is formed. Figure 4-15d shows a wear scar from Inconel 718 sample tested at 15N. Three regions of interest are highlighted in the image where Area A is where there is a black oxide layer is present, Area B where layers are starting to form and Area C where there no glaze/oxide layer present with just metal exposed.
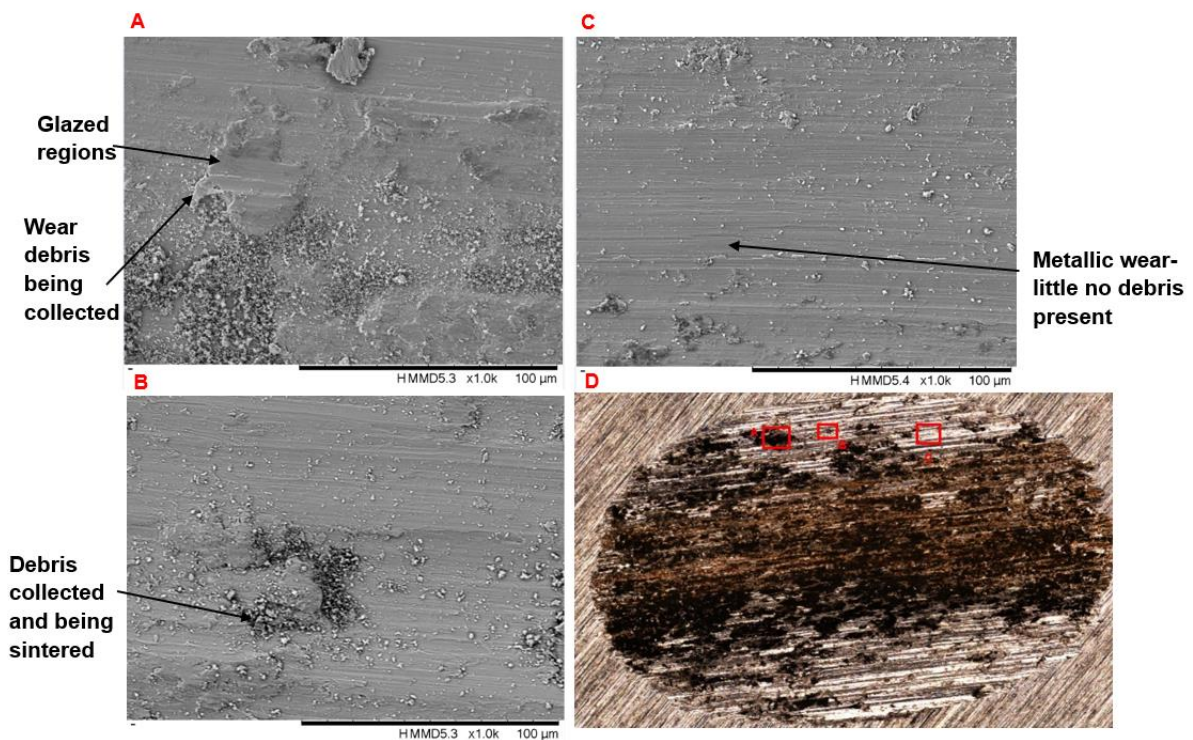
Figure 4-15 Wear scar obtained from Inconel 718 test at 15N; a,b,c) shows the x1.0k magnified images of the areas highlighted in 'd'.
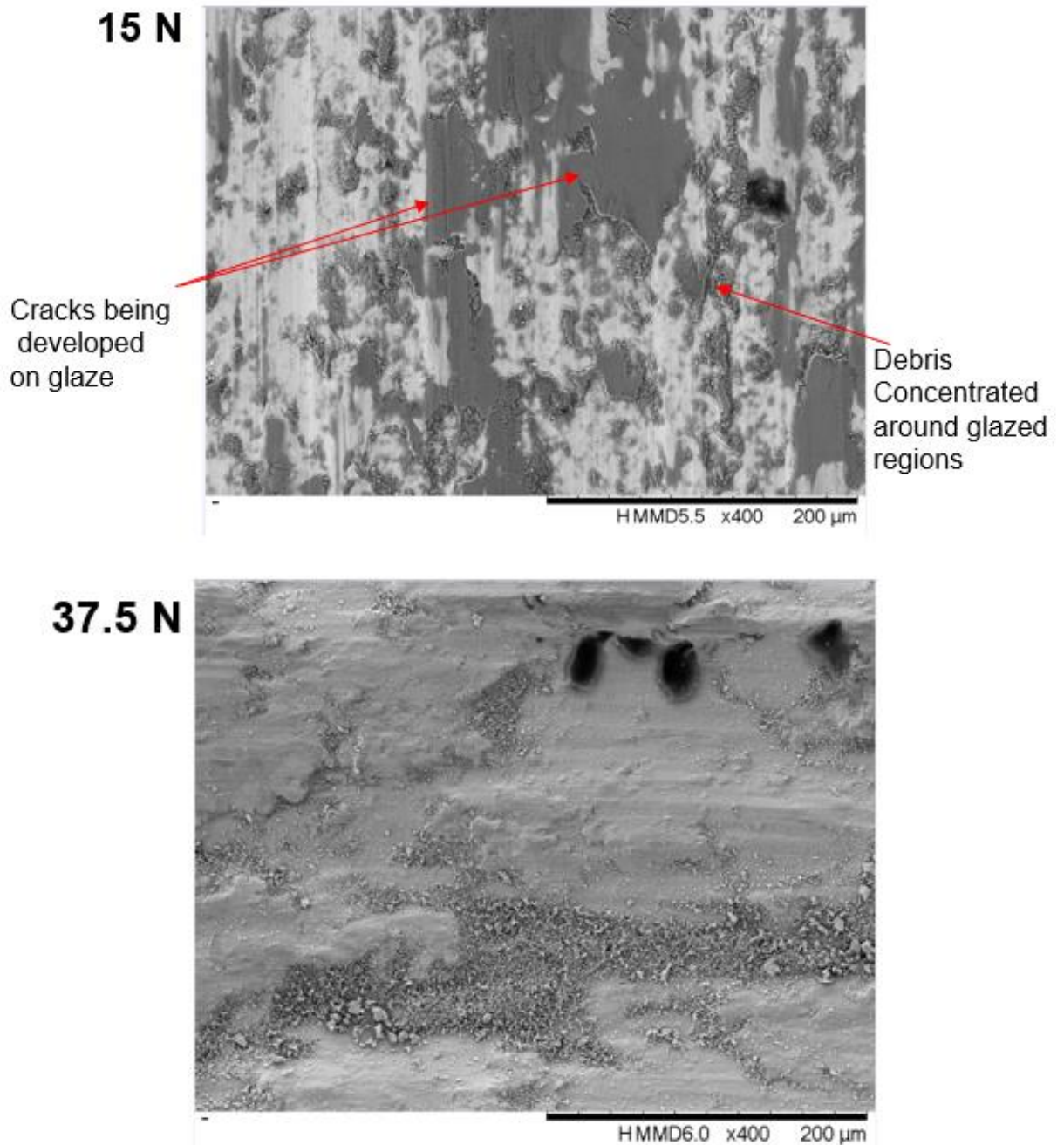
Figure 4-16 C263 samples after test a) at a normal load of 15N b) normal load of 37.5N

Figure 4-16 shows C263 samples tested at a normal load of 15N and 37.5N. At lower loads, the layers formed are very patchy and not uniform with several cracks on the layers. The debris are concentrated around the layers. At higher load, the layers appear to be more stable (fewer cracks) and with finer debris. However, a strongly bonded surface layer is not present on any materials and the 'glazed' or the black oxidised region appears to be loosely compacted wear debris. This is highlighted by the 'rougher' surface layers, as an effective glaze layer has a 'smooth finish' and glossy appearance.

Figure 4-17 shows the Haynes 25 sample at 37.5N. A clear distinction in the wear scar can be seen when compared to Inconel 718 and C263. The surface looks 'rough' with a lower volume of layers being formed (see sections 4.3.3 and 4.3.4). This suggests that no transient layers are being formed and the surface primarily consists of abrasive wear damage. The extended, streaked layers represented in the figure illustrate mechanical wear resulting from adhesion and abrasion. The presence of black regions on the surface indicates the initiation of oxide formation within the layers and debris.
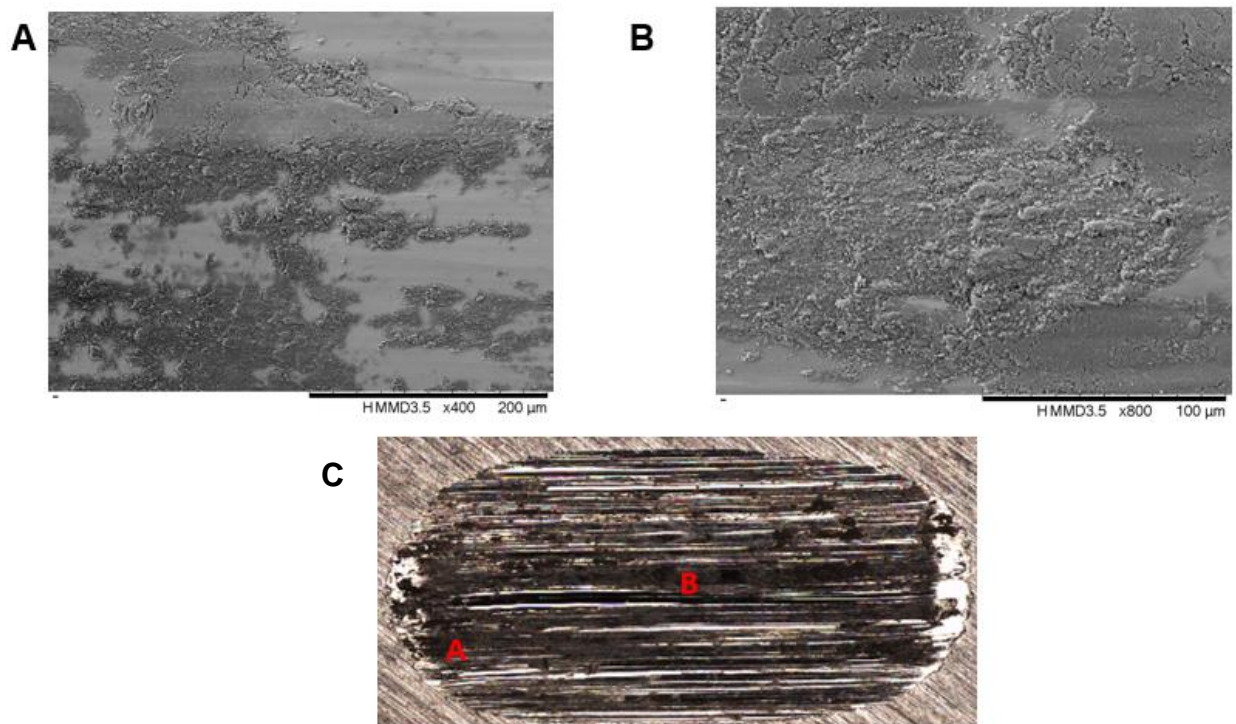
Figure 4-17 Haynes 25 at 37.5N a) at a magnification of x400 b) glaze region at a magnification of x800 c) optical images showing the areas of interest
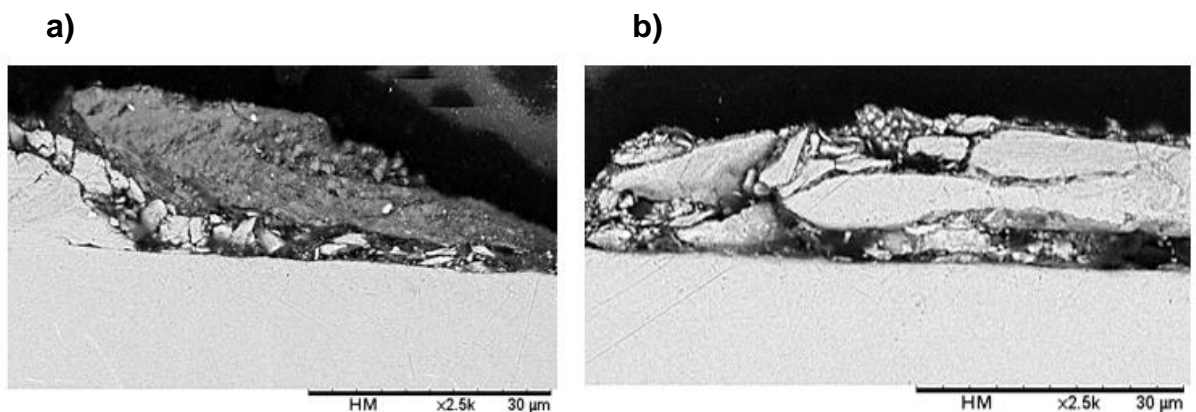
Figure 4-18 Cross sectioned images of the post test disc samples a) Inconel 718 b) C263

Figure 4-18 shows cross sections of the post-test disc samples. The exhibits regions of compacted debris with large cracks. This indicates the layers formed are not stable but prevents severe adhesive wear due to metal-metal contact.

4.3.2 Elemental analysis

As discussed in chapter 2, the effectiveness of the glaze is dependent on the chemical composition of the glaze. In order to observe if there were any major changes or trends in the chemical composition, the samples were analysed. The results for Haynes 25 are not included here as there was no oxide layer present (see Appendix 4c for details).
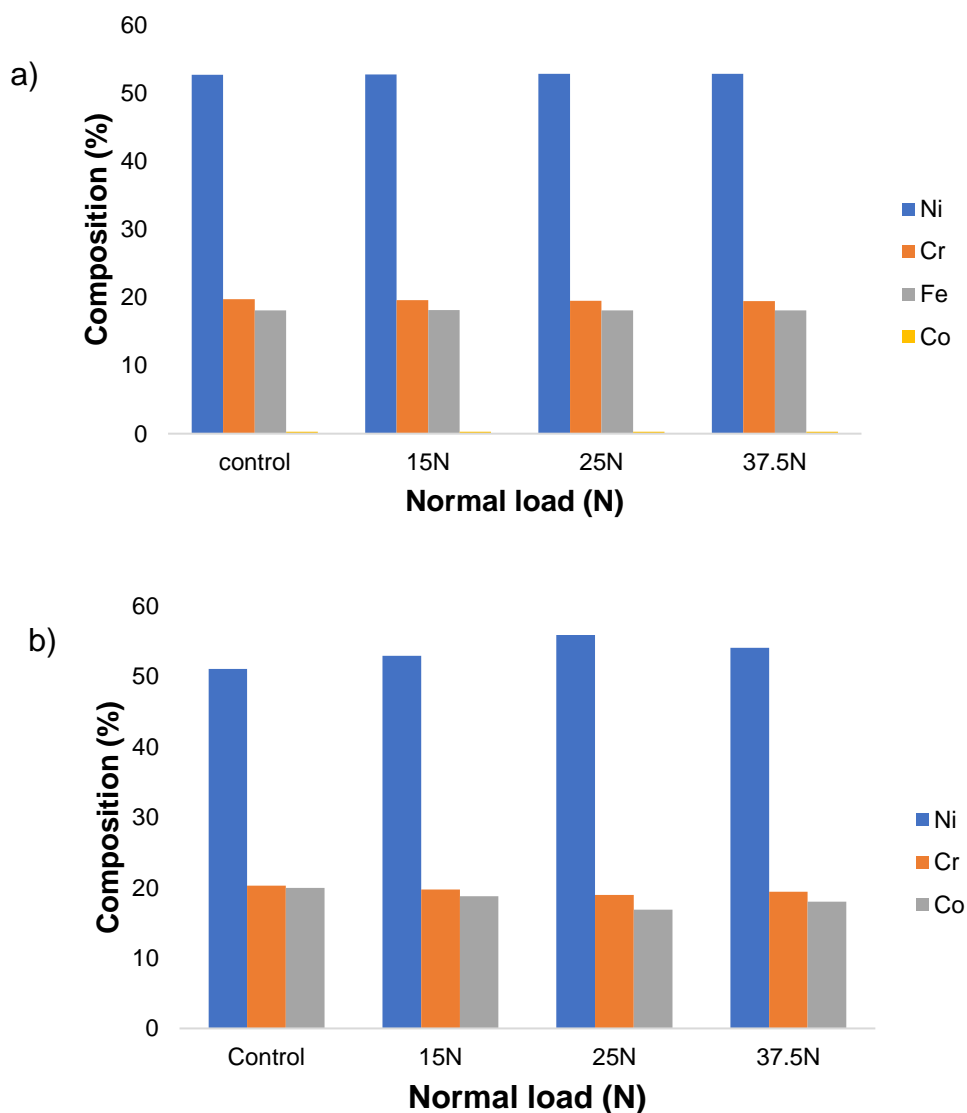
Figure 4-19 X-Ray florescence analysis of samples at an excitation voltage of 50kV a) Inconel 718 b) C263. The data is collected from glazed regions within the wear scar

Figure 4-19 shows the results from the X-Ray fluorescence analysis of the samples after the test showing the chemical composition of the compacted layer on the surface. The measurements are taken from the 'black oxide' regions of the surface. Measurements were taken from a new/untested sample as a control and for comparison. The spectra are analysed against a chosen set of elements (i.e. the elements that makes up most of the material). The elements chosen are Ni, Cr, Fe, Nb, Mo, Ti, Co, Mn. Since the amount of some elements such as Nb,Mo, Ti,Mn is so small and did not change as much at different test conditions, the results are not presented here.

As seen in the table and the graph, the percentage of Ni has increased as the load increased for both materials, this is more evident for C263. The amount of Cr in both materials has decreased slightly; however, the percentage of Co has shown a different trend on both materials where on C263 the amount of Co has gone down to 18.79% and 16.87% from 19.96% at the lowest loads, as the load is increased to 37.5N the Co content has started to increase. The changes in the Co content on the Inconel 718 is not too significant as it has not changed much. These results highlight that diffusion of active elements maybe happening.

A two-way ANOVA is carried out to see the significance in data between different elements and within the same element. Twenty measurements have been taken from each sample. No significant differences were observed within the same element (p=0.42); however, significant differences were seen between different elements (p=0.00067).

C263	Control	15N	25N	37.5N
Ni (%)	51.07	52.96	55.90	54.10
Cr (%)	20.27	19.72	18.96	19.44
Co (%)	19.96	18.79	16.87	18.03

Table 4-2 The weight composition (wt%) of glaze layer from C263 samples

IN718	control	15N	25N	37.5N
Ni (%)	52.69	52.74	52.85	52.86
Cr (%)	19.75	19.59	19.51	19.47
Fe (%)	18.10	18.15	18.10	18.12

Table 4-3 The weight composition (wt%) of glaze layer from IN718 samples

One of the limitations of X-Ray fluorescence analysis is that the effects of oxidation are not visible since it does not detect lighter elements such as O and N, thus making it difficult to determine the type of oxide formed which is key in glaze formations. Therefore, EDX analyses were performed in order to further analyse the samples, with regions of interest once again identified from the optical images (glazed regions, starting to glaze regions and no-glaze regions).

Table 4-4 shows the percentage of main alloying elements from the different regions on the scar. As seen in the table, there is a higher percentage of oxygen in the glazed region indicating that there is more oxide present. The oxygen content has increased with the normal load. However, on the C263 samples, the oxygen content has reduced as the load is increased, which links with glaze observed on the wear scar (i.e. it was less dense with even coverage on the surface as load progressed when compared to IN718).

IN718					
		Ni	Cr	O	Fe
	Control	46.4	18.0	2.3	15.8
15N	no glaze	47.4	18.6	3.0	16.4
	Initial glaze	39.9	15.6	17.2	13.8
	glaze	38.2	14.8	19.9	13.2
25N	no glaze	51.11	19.9	2.0	17.3
	Initial glaze	41.5	16.3	18.3	14.3
	glaze	37.0	14.0	29.2	12.8
37.5N	no glaze	49.9	19.4	5.0	16.9
	Initial glaze	41.5	16.2	19.2	14.6
	glaze	37.9	14.7	27.1	13.3
C263					
		Ni	Cr	Co	O
	Control	49.3	20.7	19.9	0.7
15N	no glaze	48.8	20.0	19.1	3.5
	Initial glaze	48.3	17.1	14.5	10.9
	glaze	43.4	10.8	5.1	32.6
25N	no glaze	49.7	19.9	18.4	2.5

	Initial glaze	60.5	13.8	6.2	8.7
	glaze	60.3	12.5	4.4	13.4
37.5N	no glaze				
	Initial glaze	50.9	14.6	8.4	15.4
	glaze	57.0	12.9	5.6	13.2

Table 4-4 The data from the EDX compositional (wt%) analysis of various regions from the wear scar, highlighting how the compositions have changed.

The relative changes in the elements can be used to study the composition as the operating conditions are varied. This is particularly relevant as the effectiveness of the glaze layer depends on the chemical composition as this determines how well the layers are sintered. Different elements have different diffusion and sintering properties, therefore the balance between the elements changes at different operating conditions and this controls the composition of the glaze. Table 4-5 shows the ratios between the main alloying elements that make up the glazed regions. The ratios between Ni, Cr and Fe are used to observe changes in Inconel 718 composition as they are the main alloying elements, whereas the C263 Ni, Cr and Co are examined. For Inconel 718 the ratio between Ni and Cr is almost constant with the control at all load conditions suggesting that no adhered sintered glaze layers are formed. Moreover, as highlighted by the SEM images (Figure 3-26), the layer on the Inconel 718 is compacted wear debris. Conversely, on C263 an interesting trend can be seen between Ni, Cr and Co. A Ni-rich oxide layer is formed with the highest Ni content at 25N. But as the load is increased, Co content has started to increase suggesting diffusion of Co into the contact.

Inconel 718			
Load,N	Ni/Cr	Ni/Fe	Cr/Fe
Control	2.58	2.94	1.14
15	2.58	2.89	1.12
25	2.64	2.89	1.09
37.5	2.58	2.85	1.11

C263			
Load,N	Ni/Cr	Co/Cr	Ni/Co
Control	2.38	0.96	2.48
15	4.02	0.47	8.51
25	4.82	0.35	13.7
37.5	4.42	0.43	10.18

Table 4-5: The ratios of the main alloying elements as the tests are progressed.

4.3.3 Contour Elite

The surface topography of the post test samples was acquired using the Bruker Contour Elite using x20 lens. Figures 4-20 to 4-22 shows the 3D figure of the surface and the profile. The 'red' regions represent the high points on the surface and 'blue' regions represents the low points on the surface.

Figure 4-20 shows the Inconel 718 samples at varying load. As the load is increased, a more continuous layer is seen; this could be new oxide layers are forming preventing adhesion or third body abrasions resulting in a rougher surface. The measurement at the highest load shows a platelet thickness of 12µm whereas at the lowest load (i.e. 15N) the layers very much scattered and thickness is less than 6µm. The results from the C263 samples can be seen on Figure 4-21. The layers have a thickness of around 8µm and with increasing load more even layers are seen. Unlike Inconel718 and C263, Haynes 25 displays a different trend with no layers forming.
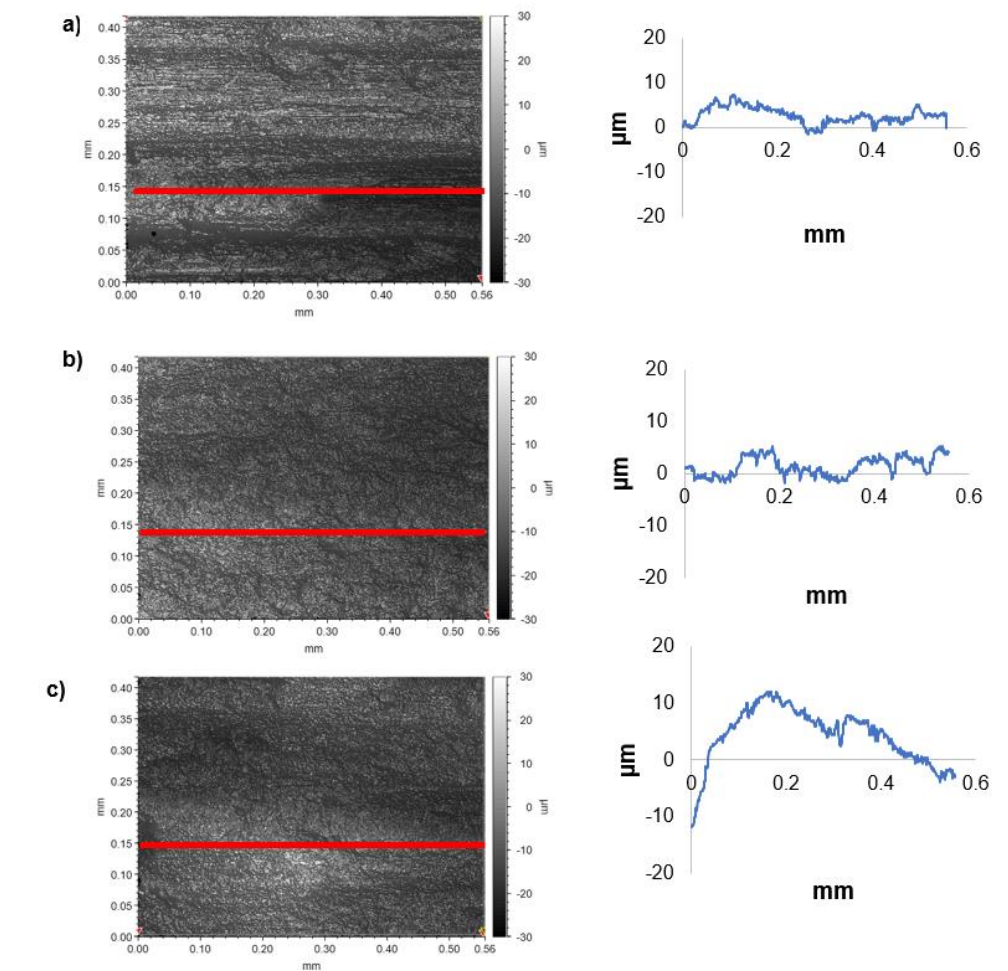
Figure 4-20 2D image of the surface and the profile for In718 samples tested at a)15N b)25N, c)37.5N
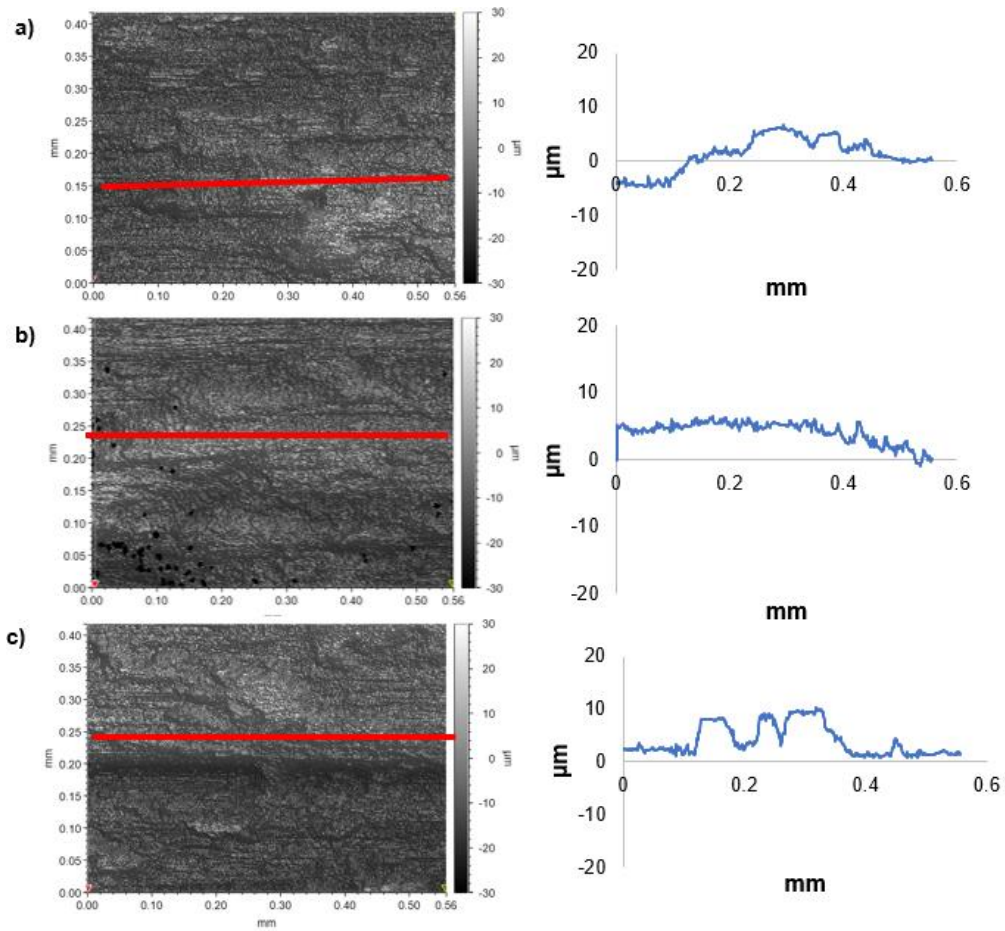
Figure 4-21 2D image of the surface and the profile for C263 samples tested at a)15N b)25N, c)37.5N
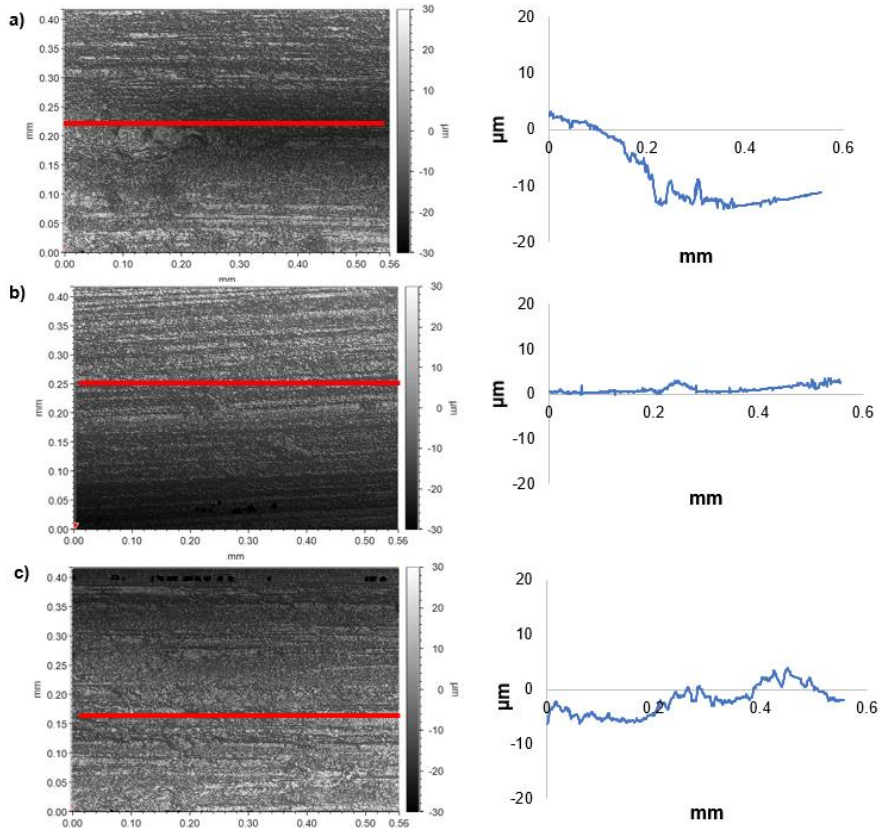
Figure 4-22 2D image of the surface and the profile for HS25 samples tested at a)15N b)25N, c)37.5N

4.3.4 Surface profiles

Figures 4-23 to 4-25 shows the surface profile and statistical data from the wear scars at a normal load of 25N. The red line on the wear scar is where the profile is taken from. Table 4-6 shows the average roughness values across the profile.

Figure 4-23 shows the surface profile from the In718 samples, a rough region can be seen with varying surface depth values. This suggests the presence of compacted oxides or accumulated debris within the abrasive grooves. Towards the end of the profile, a less varied region is observed with overall lower depths, likely to be due severe wear and abrasions causing either transient layers to be broken down or the absence of debris accumulation. A similar trend in is seen in C263, a peak is observed. This is due to the black oxidised region (as seen in the wear scar) which is due to oxide collection or compacted oxide layer. An entirely distinct profile is seen on the Haynes 25 sample (see figure 4-25) where a similar depth is observed throughout the profile. This suggests the absence of layers formed and indicates ongoing severe wear. Likewise, the average roughness values for both In718 and C263 exhibit similar values, while lower values are observed for Haynes 25. This shows the presence of distinct wear mechanisms seen on these materials.
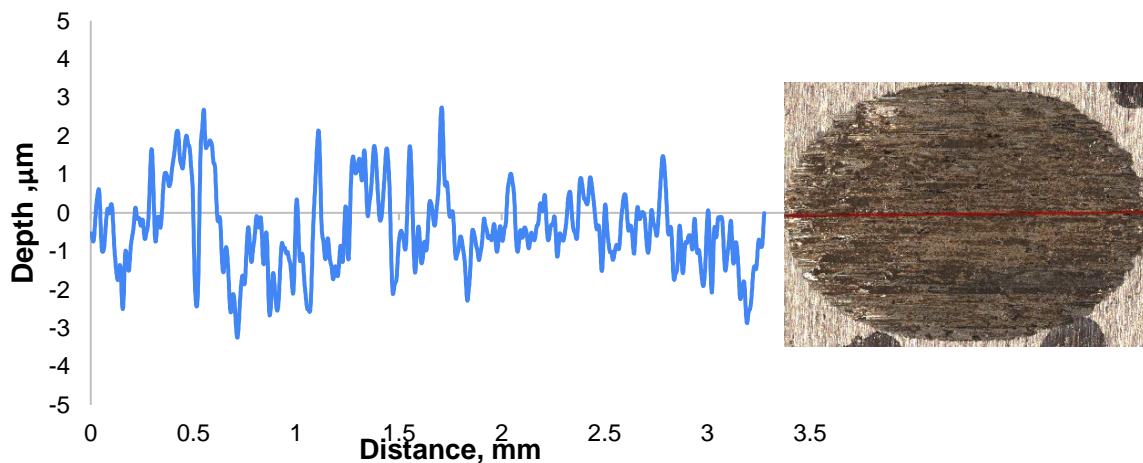
Figure 4-23 Surface profile from In718 disc samples at a normal load of 25N post 30,000 cycles at room temperature. The corresponding wear scar with red line indicating the profile path (left)
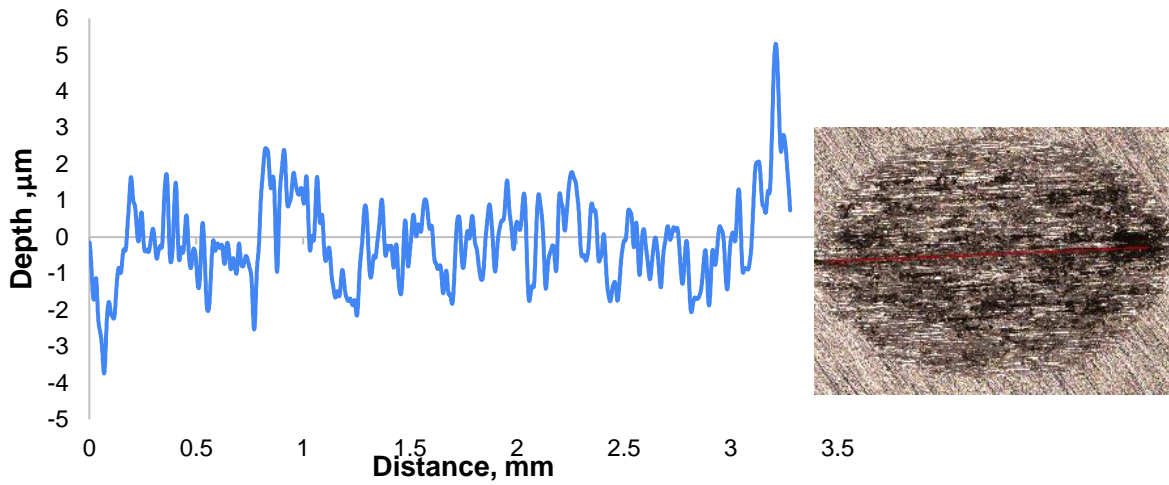
Figure 4-24 Surface profile from C263 disc samples at a normal load of 25N post 30,000 cycles at room temperature. The corresponding wear scar with red line indicating the profile path (left)
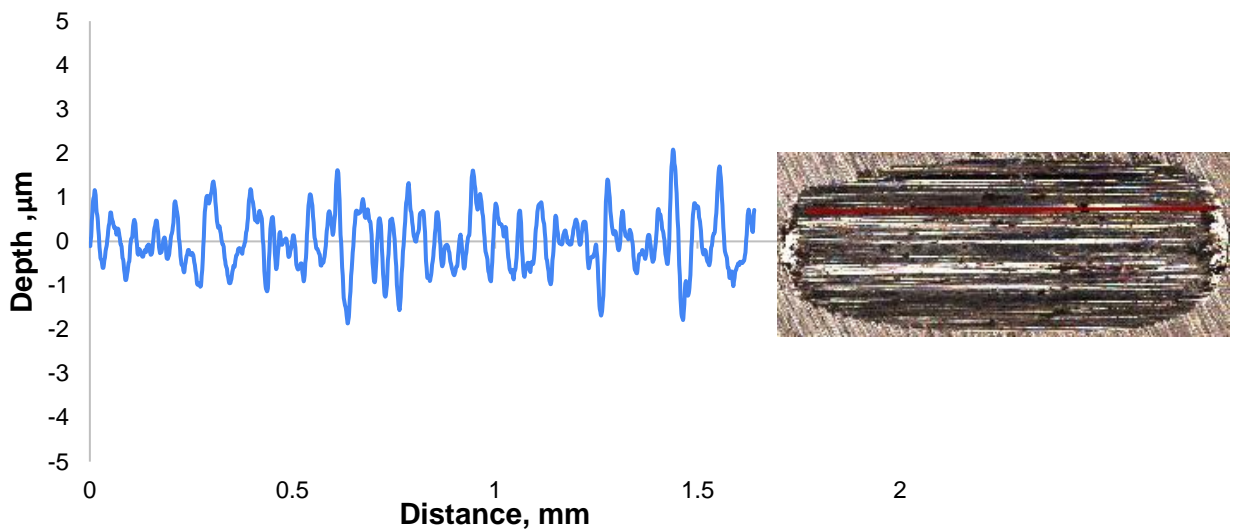
Figure 4-25 Surface profile from Haynes 25 disc samples at a normal load of 25N post 30,000 cycles at room temperature. The corresponding wear scar with red line indicating the profile path (left)

	R_a	R_q	R_z
In718	0.942	1.155	4.505
C263	0.901	1.171	4.949
Haynes 25	0.517	0.646	3.199

Table 4-6: The average roughness data from the regions of interest highlighted in figures 4-23 to 4-25.

4.4   Discussion

The tests conducted at room temperature highlight the influence of load and material on glaze generation. Haynes 25 likely did not form a glaze layer because the chemical composition of the surface layers has not changed, additionally the oxidation/diffusion rate of the elements that it is composed of have a higher activation energy, further supporting a view that diffusion has not taken place, therefore it is not discussed further [81]

For the other two materials, as the normal load was increased, a positive response is seen with more coverage of the glaze. A drop in the average COF values is also observed with more glaze. Similarly, the differences seen in the surface between C263, and Inconel 718 are discussed here.

4.4.1   Influence of load

The main wear mechanism observed on the wear scars are abrasive grooves with oxide layers on top; where there are no oxidised layers, evidence of severe metallic wear is also seen. As seen in Figures 4-1 to 4-4, there is a general trend where the formation of glaze has been positively influenced by the increasing load. As the load is increased, the coverage of the surface by 'black' oxidised regions has also increased. This could be because the surface temperature has increased with the load so more sintering and oxidation of debris occur, which leads to better compaction and formation of a stable glaze layer. Previous research has shown that there is a critical load/speed combination, together with the critical temperature where a stable glaze layer is generated [24] [82] . Between the two materials, C263 forms a more uniform glaze (black-oxidised regions on the surface) at lower loads suggesting that C263 may have a lower pressure threshold compared to Inconel 718. However, the coverage decreases at the highest load, this may be due to layers being broken down easily due to the critical load being above the threshold. Therefore, the rate of breakdown is higher than the generation of glaze. The drops in COF (Figure 4-11) highlight that the layers are being generated but it is not seen on the surface as it is broken down easily with further sliding.

Although the glaze coverage improved with increasing load, the volume lost has also increased. The volume lost from the Inconel 718 is almost twice as C263 even though a denser glaze is seen on the Inconel 718, likely to be because of the differences in

the chemical composition of the layers formed on the surface. As the load was increased, larger debris was generated. This means that it takes longer to break down the debris into fine fragments for compaction and some of the debris are displaced out of the contact. Since the glaze formation is very much influenced by the wear debris, with higher load, the availability of more debris resulted in increased glaze formation. This could also mean that the availability of debris could be a limiting factor at lower load conditions.

A slight drop in the average COF can be seen with increasing load. Between the materials, a similar trend is observed, with a greater drop between 15 to 25N compared to 25 to 37.5N. Inconel 718 has a slightly lower COF than C263, this could be due to increased coverage or more debris available for compaction.

It should also be noted that glaze starts to form at the edges first compared to the middle, this is probably because there is more debris available at the edges (it is supported by the shape of the fretting loop; the distortions in the shape towards the end of the stroke suggesting there is more wear debris available at the edges.). The influence of debris availability and glaze formation can be seen in Figure 4-15, where a greater volume of debris (and finer debris) is seen when a glaze is present.

Finally, there is a lot more variability in the glaze generated on the pins, this is likely due to contacts inability to retain debris and it is expected with the hemisphere pin.

4.4.2 Influence of number of cycles

A similar trend to varying normal load is observed with increasing the number of cycles. Over time, the coverage of glaze has increased and a decrease in the relative COF can be seen in Figure 4-11.

With more time two factors influence the results; there is increased availability of debris and there is more time available for the 'larger' debris to be broken down into smaller fragments and oxidised to be sintered.

The evolution of COF with increasing time (see Figure 4-11) shows that as the load is increased, it takes less time for the COF to drop. This is due to the increased surface temperature which leads to more oxidation and sintering of the debris. Also, over time the availability of debris increases as a result of wear, therefore it would not be a limiting factor in generating the layers. even though there is an overall increase in the

glaze, the material loss appears progressive and COF reduction is minimal, leading to questions regarding the type of glaze formed.

4.4.3 Influence of alloying elements

The composition of the oxide layer was analysed using X-ray fluorescence (XRF) and SEM-EDX to investigate the influence of alloying elements. It can be seen that the content of Ni has increased on both materials, meaning that the layers formed are nickel-based. The percentage of Co and Cr has decreased when compared to the control (i.e. pre-test). However, on the C263 samples, the Co has started to rise after 25N.

Though, this trend was not observed in previous studies where a glaze layer was achieved [83] [46]. Previous studies have shown that an effective glaze is a Cr or Co-based layer with a smooth, glossy finish. Also, Cr has a higher oxidation rate than Co, so a Cr oxide layer could be seen before an effective glaze is formed on the surface [46] [26]. The results from the EDX measurements have shown the variations in oxide content at different regions of the wear scar. As the coverage increases there is more oxygen content indicating the role of oxide debris.

One of the reasons for this is likely to be the differences in operating conditions such as the load and the speed. This leads to changes the type, size and shape of the debris formed. It was seen earlier in chapter 2 that the debris properties have a huge impact on the glaze formation [26], causing differences in the surface damage such as the plastic deformation and cracks which acts as the diffusion pathway. Another reason for the variations in the results could be due to not reaching the critical temperature where the rate of formation is greater than the breakdown of the layers. The flash temperature rises are calculated and can be seen in Section 3.3.1, where only a minimum effect is seen at these loads and for Ni-based alloys the critical temperature is usually around 400°C [26] [30], this suggests that the observed glaze/oxide layer could be a transient oxide layer (which provides some protection) but easily broken down with further sliding. The rate of glaze formation depends on the oxidation and diffusion rate of the atoms. Both of these factors are very much influenced by temperature. The slightly different pattern in the C263 behaviour suggests that the critical threshold temperature/pressure may be lower than Inconel

718 and the subsurface deformations may be different to Inconel 718 allowing more diffusion of elements.

The proportion of the main alloying elements in the IN718 has not changed at different load conditions. This means that very little diffusion of the atoms has happened, leading to poor sintering of the debris creating a non-effective glaze layer. In essence, the layer present on IN718 is unbonded, compacted oxidised wear debris. On the other hand, C263 had a varying trend in the alloy composition, where the oxide layer is mainly composed of Ni and Cr. At the normal load of 25N, the oxide layer is Ni-rich with low Co content. But as the load is increased, the percentage of Co has increased suggesting more diffusion. However, the overall dominance of Ni and Cr is due to their lower activation energy, meaning they have a higher oxidation rate compared to Co. Further, the activation energy of Ni is almost half the activation energy of Cr, this is the reason why the transient oxide layer is rich in Ni.

The data from the elemental analysis has indicated that the layers formed on the C263 samples are transient oxide layers, as previous studies have shown that transient oxide layers are Ni and Cr based. This provides some protection from further damage; however, the transient layers are thinner than an effective glaze layer. Moreover, the Ni and Cr had poor adhering and sintering properties thus the layers are easily broken down making it hard to increase the thickness of the oxide layer [5] [84]. This also supports the drop in wear performance with increasing load, more load breaks down transient oxide layers and flash temperature rises are not high enough to initiate diffusion of active elements.

This correlates well with the volume losses data where the wear volume of Inconel 718 is almost twice as C263. Inconel 718 has no protection as there is not even a transient layer generated. Although there is a rise in wear volume with the increased load, the rate at which C263 is losing is lower than Inconel 718 because the transient layer helps to avoid metal-metal contact protecting the surface.

Moreover, it is also expected to form a Cr oxide layer before a Co-based layer because Co has a higher diffusion rate than Cr. Since sintering is very much dependent on the ability of atoms to diffuse into the surface; once Cr oxides are pushed out of the contact/surface Co forms a more stable glaze layer [3] [85]. It is also interesting to note that even though the percentage of Ni and Cr are similar in both Inconel 718 and C263,

a transient layer is not seen with Inconel 718. This could be because of the presence of Fe in Inconel 718 or due to the differences in the microstructure of the materials. Fe has lower activation energy than Ni however, at lower temperature Fe_2O_3 is formed which does not adhere to the surface. At higher temperatures, the presence of Fe enhances tribological properties due to the formation of Fe_3O_4 [85] [86].
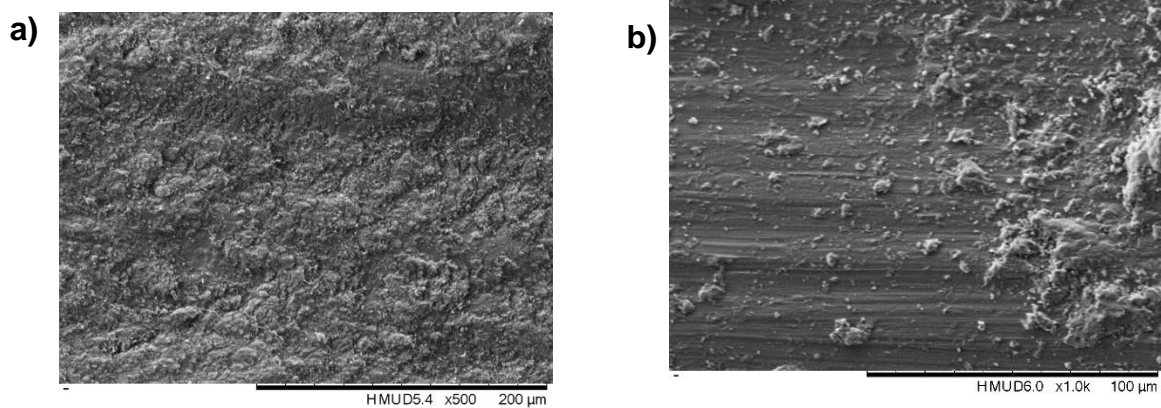
Figure 4-26 SEM image of the sample at 37.5N where a 'black' oxide region as present a) Inconel 718 b) C263

It can be concluded from the X-Ray fluorescence and EDX analysis of the samples and the images, that the 'black oxide' layer seen on the surface of both the Inconel 718 and C263 samples is not a glaze layer, and instead it is either an oxide layer (C263) or compacted debris (IN718) providing some protection but only for a short period of time. This is evidenced by Figure 4-11, where the COF has not reached a constant value, keeps changing throughout the tests, and suggests that the oxide layer easily broken downs. Additionally, the black oxide regions on the wear scar do not show a glossy surface (see Figure 4-26). Figure 4-18 further supports that a protective layer is not generated whereas the drops in COF data is due to less adhesions as metal to metal contact is prevented by the debris layers in the contact.

4.5 Summary

The aim of this chapter was to present the results from the room temperature tests at varying normal loads and understand the influence of pressure on the glaze formation.

- IN718 has shown an increased coverage of glaze compared to C263 and Haynes 25, however, the volume lost was almost twice for IN718 compared to C263. The more detailed wear scar images acquired using SEM has shown that the 'black' oxidised regions on the In718 samples were compacted debris that are not

sintered. Whereas a transient oxide layer is formed on the C263 providing some protection over a short period of time. This is especially interesting since both In718 and C263 have similar hardness. Finally, Haynes has shown evidence of mechanical wear and there is no oxide layer present.

- Interrupted tests have helped to understand how the layers are broken down easily with further sliding.

- At low load, the availability of debris may be a limiting factor whereas at higher load the time available for oxidation and compaction of the debris be the limiting factor.

- Even though the load contributes positively towards the temperature rises, the flash temperature calculations show that it is not significant enough to reach the threshold temperature for these materials.

- There is no protective layer formed on IN718, whereas a transient oxide layer composed of Ni and Cr, is present on C263. This highlights the importance of conducting tests at higher temperature to confirm whether the influence of both thermodynamics and the oxidation kinetics in the formation of glaze layer.

Chapter 5   Elevated temperature tests

This chapter focusses on like-on-like material combination sliding tests at a range of temperatures and load conditions. The temperatures ranged from 200 to 600ºC and the loads were varied between 15-37.5N. The post test samples were analysed using various methods. Initially non-destructive analysis was carried out using optical microscopes and SEM and COF was used to study the friction behaviour of different materials. Finally, the samples were sectioned to observe how the microstructure has impacted as the load and the temperature were varied.

5.1　Introduction

In the previous chapter, the significance of the role of contact pressure and the alloying elements on the glaze generation at room temperature are detailed. It is clear from the results that the effectiveness and the thickness of the glaze depends on the composition of these layers as various elements possess different sintering and oxidation capabilities. Another important factor that influences glaze generation is the temperature by affecting the oxidation and sintering processes. As previously seen in Chapter 2, the temperature can be raised by two means- by increasing the bulk temperature using an outside source or increasing the contact temperature by making changes in the contact pressure or speed. The room temperature tests, and flash temperature calculations as seen in Chapter 4 and Section 3.3.1 indicate that increasing contact pressure and contact temperature rise has minimal effect on the glaze generation process thus not providing any wear resistance. Therefore, temperatures will be raised through an external source for this investigation.

The two main processes involved in glaze generation are oxidation and sintering of the debris. Both of these have a positive influence with increasing temperature. Thus, investigating the influence of temperature is necessary to observe whether the rate of a specific process (i.e. oxidation or diffusion) that leads to glaze generation is equally or more affected by the increased temperature.

5.2 Inconel 718

5.2.1 Wear scar analysis

5.2.1.1 Wear scars

Figures 5.1 to 5.3 show the wear scars obtained during elevated temperature tests on In718 samples taken using the Alicona optical microscope with x5 lens. The tests were carried out at 200 to 600°C at varying normal loads.
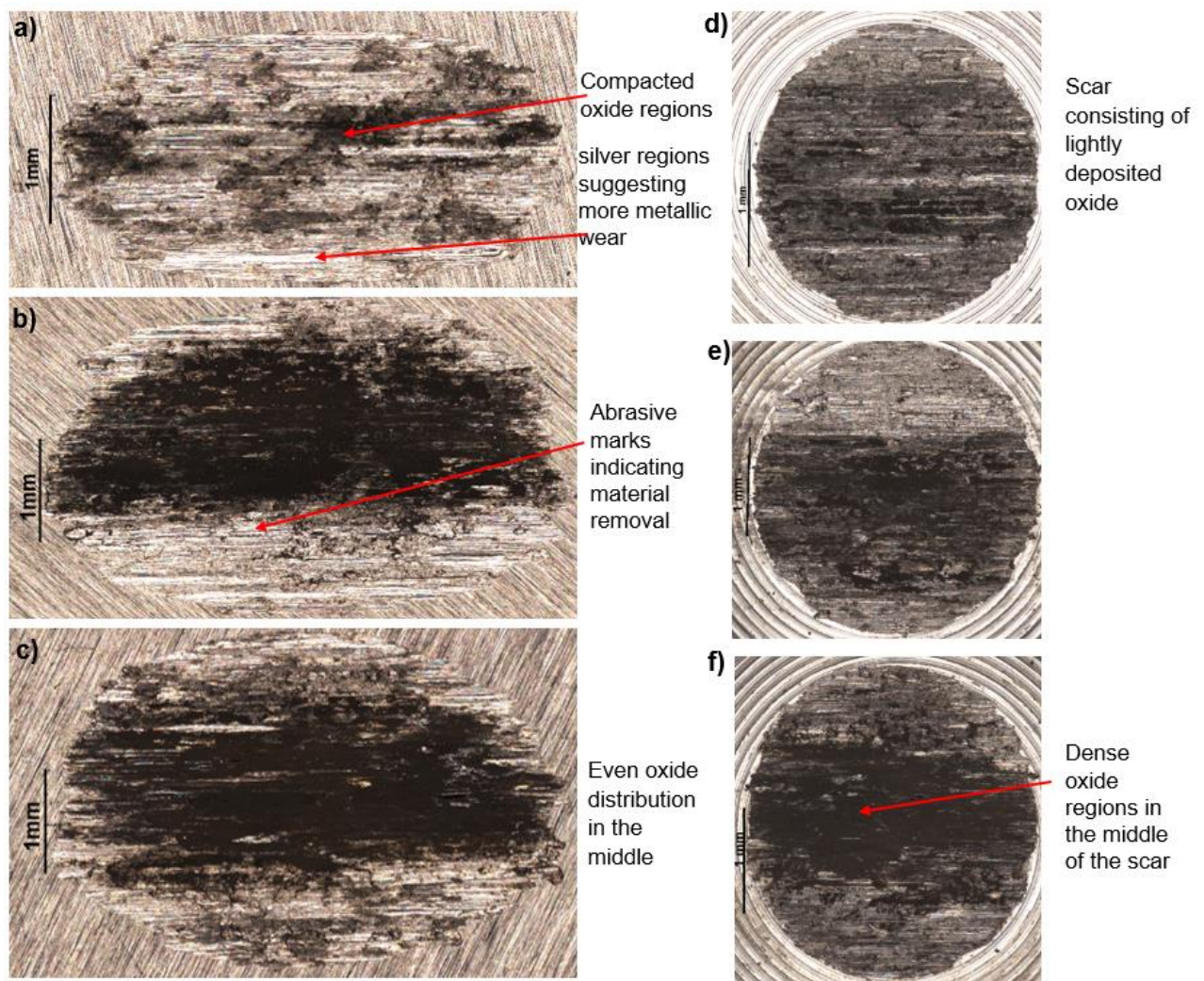
Figure 5-1 Wear scar produced on Inconel 718 disc and pin samples at various loads over 30,000 cycles at 200ºC. a,b,c are scars from the disc samples at a normal load of 15,25 and 37.5N respectively. d,e,f are from the pin samples at a normal load of 15,25 and 37.5N respectively.

Figure 5-1 shows the wear scars from tests conducted on In718 at 200°C at a normal load of 15, 25 and 37.5N. As seen in the figure, the coverage of oxidised region on both the pin and disc has increased as the load is increased. At the lowest load i.e.,15N, the glazed regions are localised and the silver/grey regions suggesting severe metallic wear. The abrasive grooves can be seen with a bright silver shade or light brown shade. The (silver) abrasions have no oxides present on the surface whereas the light brown are regions where there is a thin layer of oxide present. As the load is increased, the oxide coverage has increased suggesting glazed regions. A similar trend is seen on the pins. The oxides are evenly distributed on the pin at all loads with an increased thickness (scar exhibiting a brighter contrast) at higher loads.
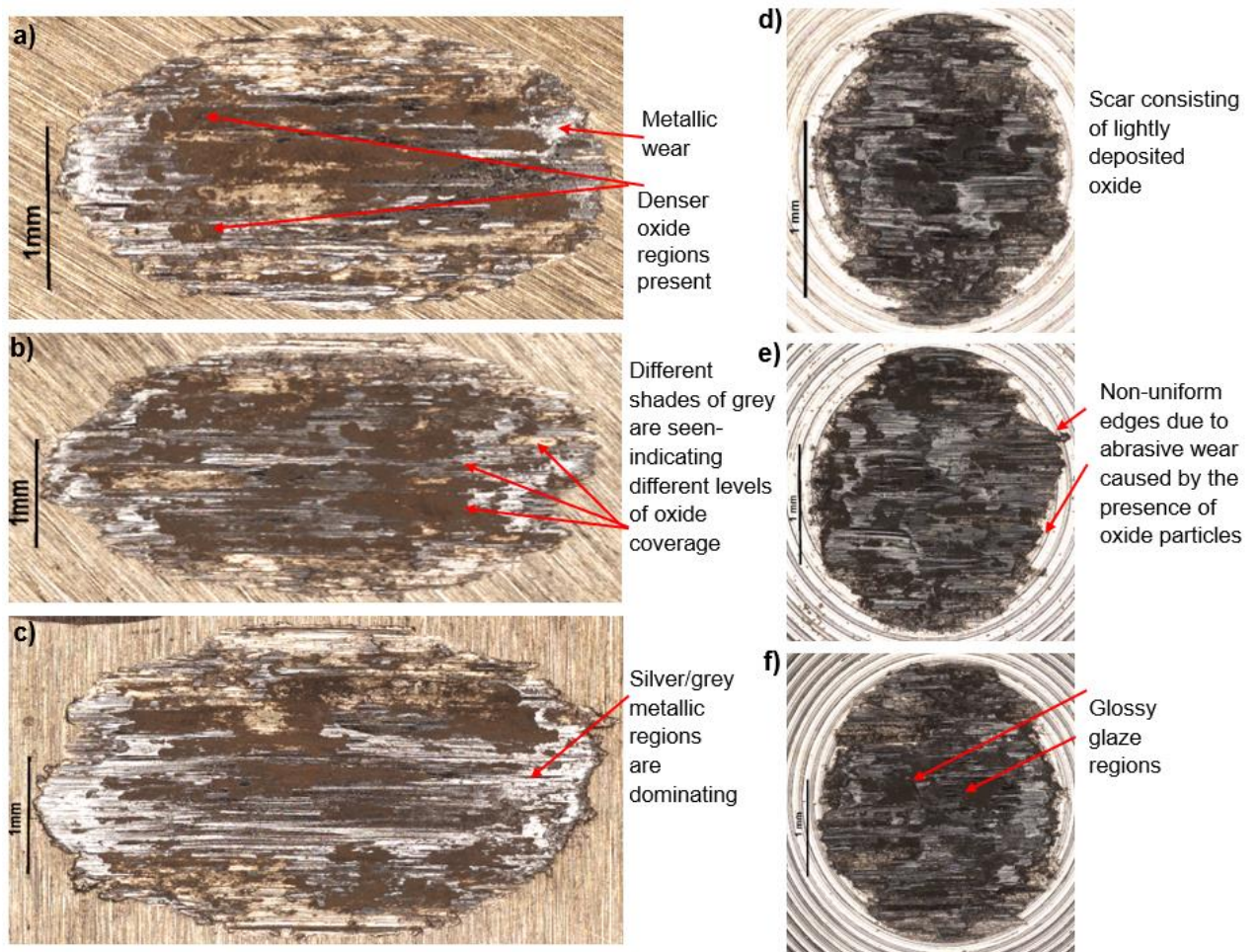
Figure 5-2 Wear scar produced on Inconel 718 disc and pin samples at various loads over 30,000 cycles at 400ºC. a,b,c are scars from the disc samples at a normal load of 15,25 and 37.5N respectively. d,e,f are from the pin samples at a normal load of 15,25 and 37.5N respectively.

The wear scars from 400˚C tests can be seen on Figure 5-2. At the lowest loads, i.e. 15 and 25N, the coverage has increased with increasing load. However, at the highest load of 37.5N, there is evidence of lost oxide regions highlighted by the silver/grey regions. This is likely to be that the failure threshold has been reached thus the layers are easily broken down at higher loads. The edges on the pin are worn suggesting abrasive wear due to the interaction with the oxidised and unoxidised wear debris. The raised shoulders on the pin scars indicate high contact stresses, which could have also triggered the glaze breakdown. Figure 5-3 shows the wear scars from the 600˚C tests. Images of the pin wear scar has shown evidence of less wear compared to the lower temperatures as the edges show less signs of abrasive wear. Both at 400ºC and 600ºC, dense black glossy regions are observable with brown coloured compacted debris, meaning that the debris are in the process of being sintered on top of the existing glaze regions. Also, an even coverage of oxide is seen at 400˚C and 600˚C. The size of the wear scar has significantly reduced with increasing test temperature.
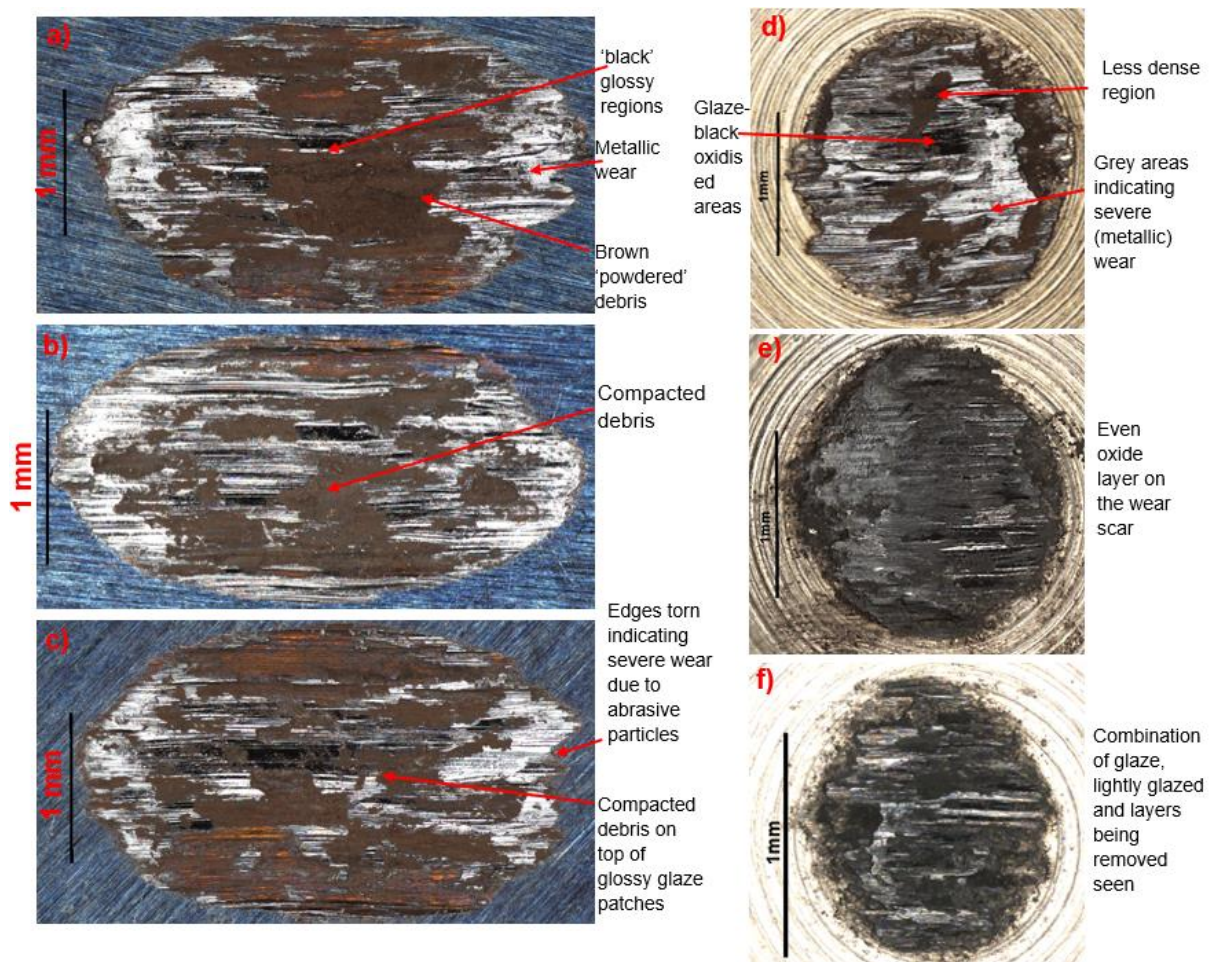
Figure 5-3 Wear scar produced on Inconel 718 disc and pin samples at various loads over 30,000 cycles at 600ºC. a,b,c are scars from the disc samples at a normal load of 15,25 and 37.5N respectively. d,e,f are from the pin samples at a normal load of 15,25 and 37.5N respectively.

Between the different load conditions used, a major difference is seen at 200ºC where the coverage has increased with increasing load. Whereas at the higher temperature, the load dependency on the glaze coverage is not as obvious suggesting that the applied load is not affecting the glaze generation as much as at lower temperatures.
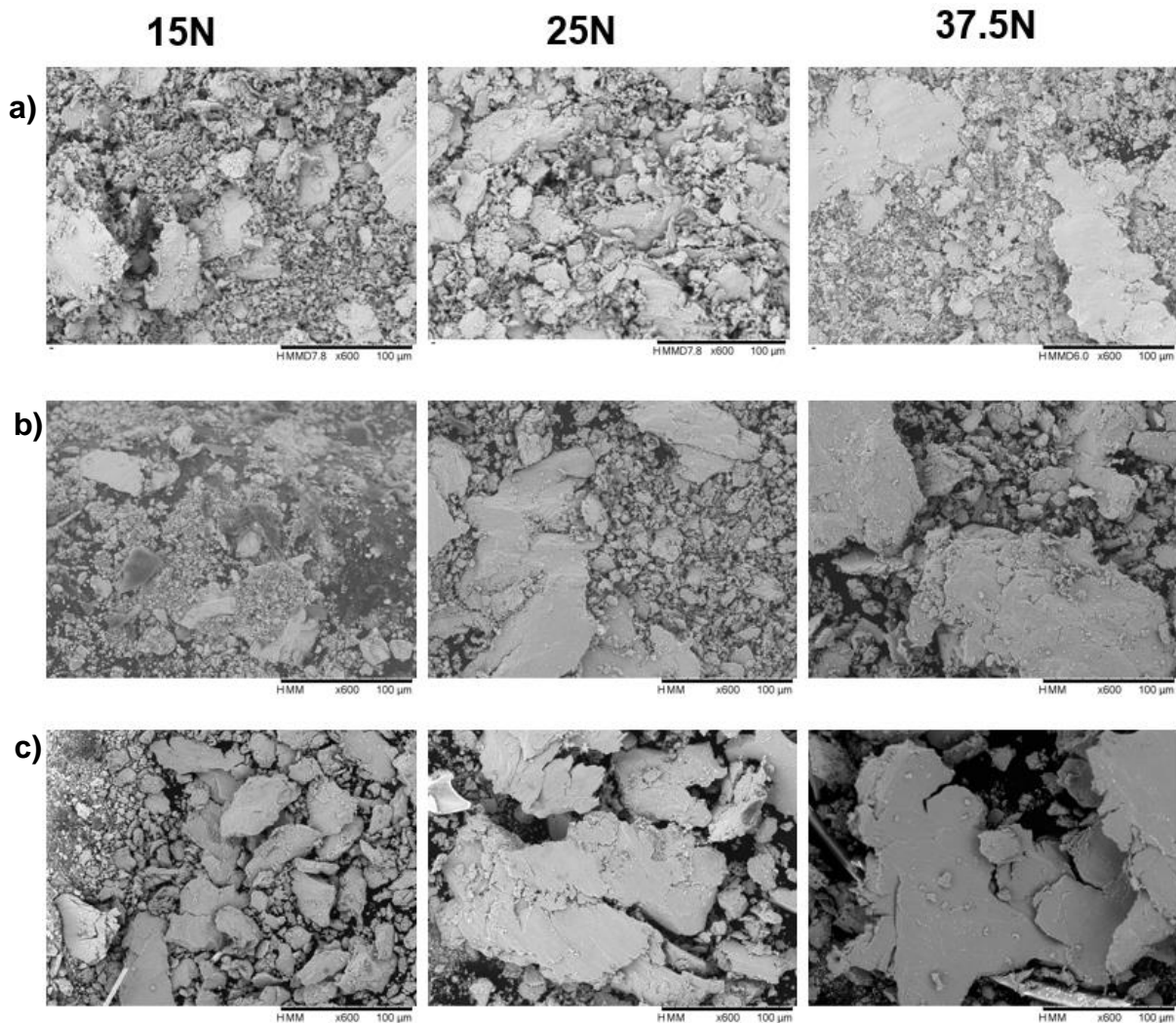
Figure 5-4 Wear debris from the different tests conducted at various loads and temperatures where a) 200ºC, b) 400ºC, c) 600ºC

Figure 5-4 shows the wear debris at various loads and temperatures. As seen in the figure, with increasing load, the size of the debris considerably increases. This phenomenon is likely due to higher loads causing greater levels of plastic deformation, leading to the formation of cracks and subsequent removal of material. This adversely affects glaze generation, as larger debris takes longer to break down into smaller fragments, thus lowering the rate of sintering. Also, it is more likely to be ejected from the contact zone [87] [88]. Between the temperatures, there is an increase in the size

of the debris, this is because as the temperature increase the surface softens and melts causing more surface damage.

5.3.1.2   Wear volume
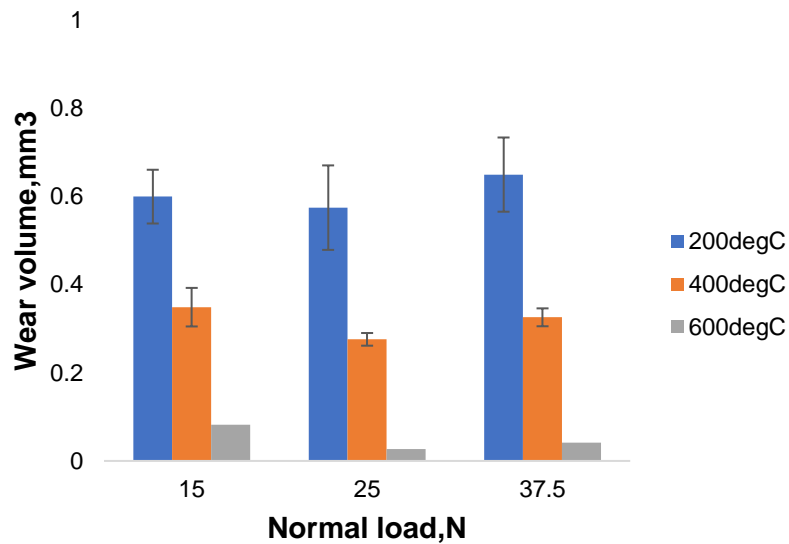
Figure 5-5 The volume lost at tests conducted at 200,400 and 600ºC at varying load on In718 like on like contact.

Figure 5.5 shows the total wear volume lost at different high temperature tests at varying loads on In718. As seen in the figure, there is an evident drop in the wear volume as the temperature is increased.   Between 200ºC and 400sºC, the wear volume has dropped to 50% when compared to 200ºC. This is likely due to increased oxidation and sintering of the debris with higher temperature resulting in glaze being formed on the surface providing wear resistance.

Between the applied load conditions, it is interesting to see that there is a drop in the wear volume at the lower temperatures and a slight increase in wear volume between 25 and 37.5N. This is likely to be influenced by the size of the debris generated at higher load. 'Larger' debris (see Figure 5-4) are produced as the applied load is increased, which means that it will take longer for the debris to be broken down and sintered into a glaze. Also, some of these debris are pushed out of the contact.

5.3.2 Evolution of coefficient of friction

The evolution of relative COF as the test progresses is illustrated in Figures 5-6 to 5-8. Different responses can be seen as the temperature and the applied load are altered.

Figure 5-6 shows the relative COF at various loads from the tests conducted at 200˚C where the COF at the higher load exhibits a similar trend consisting of regions of stable and unstable COF. However, a different trend is seen at the lowest applied load of 15N. At the lowest load, there is an overall increase in the relative COF with sharp peaks and drops suggesting formation and breakdown of oxide layers causing the abrupt changes in COF. At the higher loads (i.e. 25 and 37.5N), the evolution of COF as the test progresses follows a similar trend with stable COF seen for 3000 to 5000 cycles before there is a rise in COF. The lowest overall COF is observed at the intermediate applied load (25N) with stable COF lasting for around 5000 cycles. This suggests that it may have reached its critical load threshold level and above this load the oxide layers are broken down easily or that the wear debris produced are larger making it harder to sinter. Overall, at 200˚C, the COF continually fluctuated even after long sliding periods, this indicates periods of metal-metal contact and layers being broken down generating abrasive wear particles in the contact.

Figure 5-7 shows the progression of COF at 400˚C tests. As seen in the figure, a similar trend is seen at various load conditions; initially there is sharp rise in the COF, followed by peaks and stable COF regions. There is an overall decreasing trend with maximum COF reaching at the lowest load and minimum at the intermediate load of 25N. Even though a steady state COF is seen at all load conditions, the duration varies. For example, at a normal load of 15N, the COF is only stable for ~2,500 cycles whereas at 25 and 37.5N, the COF is stable for approximately 10,000 and 6,000 cycles respectively. Moreover, at the highest applied load, the COF decreases from a high value and reaches stable value at a faster rate than lower loads meaning it takes less time to generate wear protective layers at higher load. This is likely to be due to increase in temperature with applied load increasing the rate of oxidation and sintering. However, it should be noted that the layers are broken down faster (~6,000 cycles) at the highest load and is ultimately less effective.

The evolution of the relative COF from the 600°C can be seen in Figure 5-8. The lower loads present an overall drop in the friction whereas at the highest load, the relative COF has increased. The COF is stable for almost half of the test duration at 600°C suggesting the layers formed are protective.

One of the main notable differences between the test at different temperatures is that at the lower temperatures (i.e. 200°C and 400°C) the relative COF is unstable with sharp peaks and drops suggesting the layers are broken down creating debris. At the highest temperature the COF is staying stable for a long period of time suggesting that the glaze formed on the surface is protecting against further wear. The lowest COF is seen at the intermediate load of 25N at all temperatures. This is indicating that oxidation/sintering is not the only factors affecting the glaze formation. It is also influenced by the size and the type of debris formed under various testing condition.
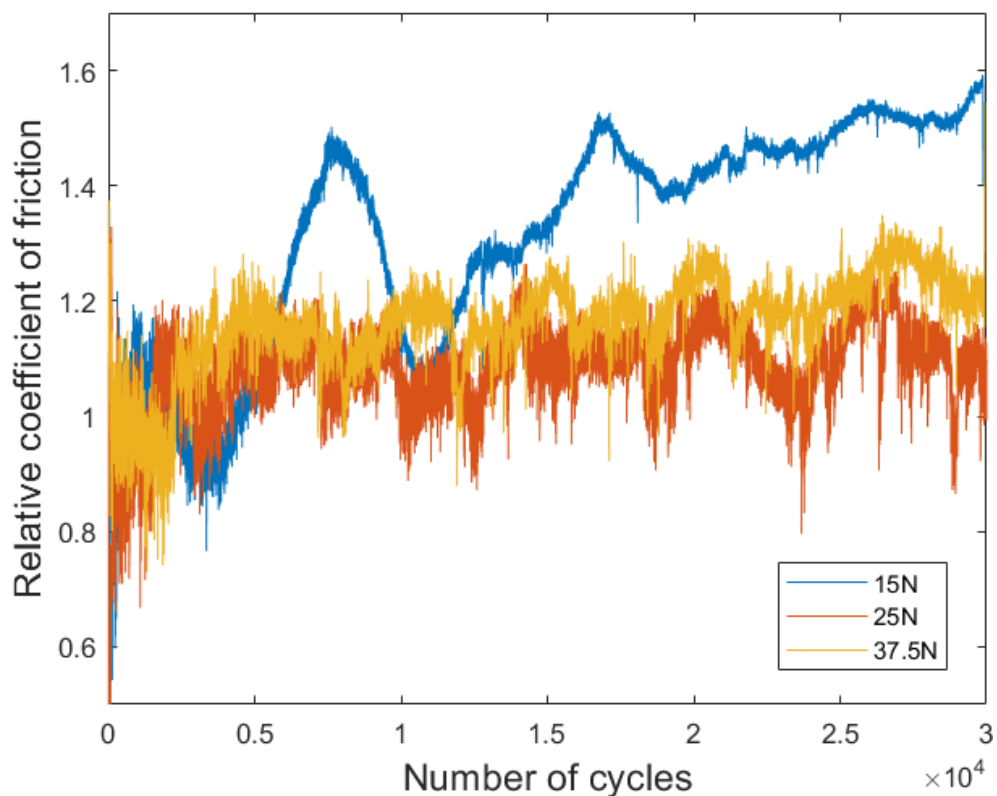
Figure 5-6 The evolution of relative COF as the test progresses at 200°C at a normal load of 15, 25 and 37.5N
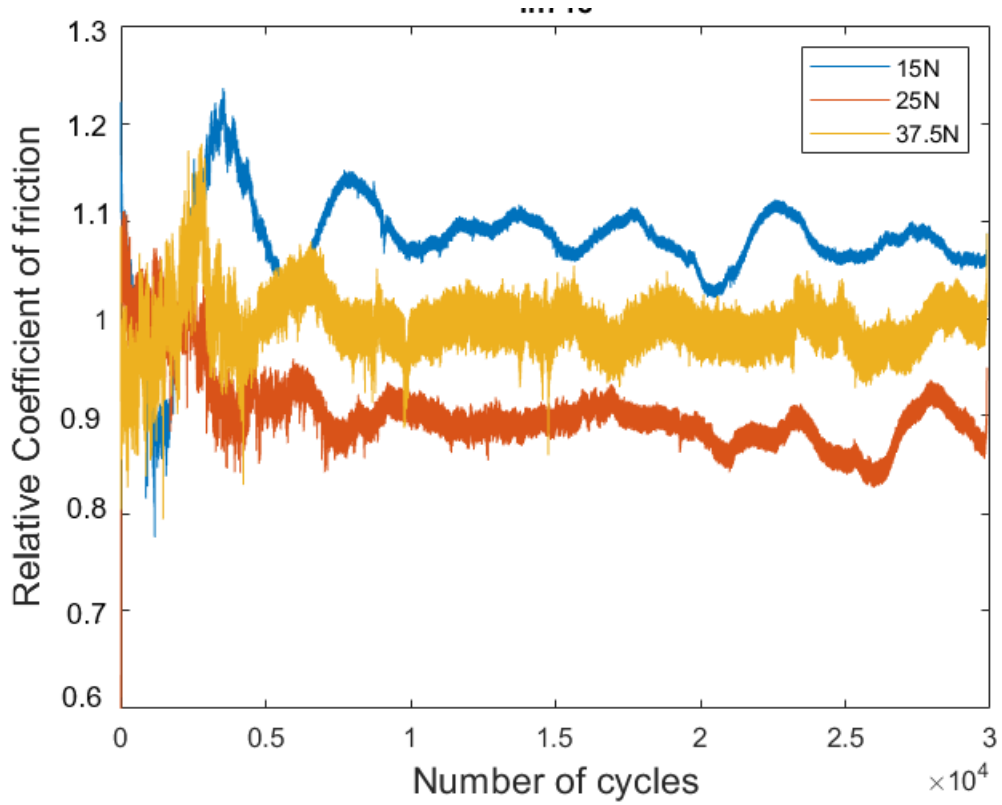
Figure 5-7 The evolution of relative COF as the test progresses at 400˚C at a normal load of 15, 25 and 37.5N
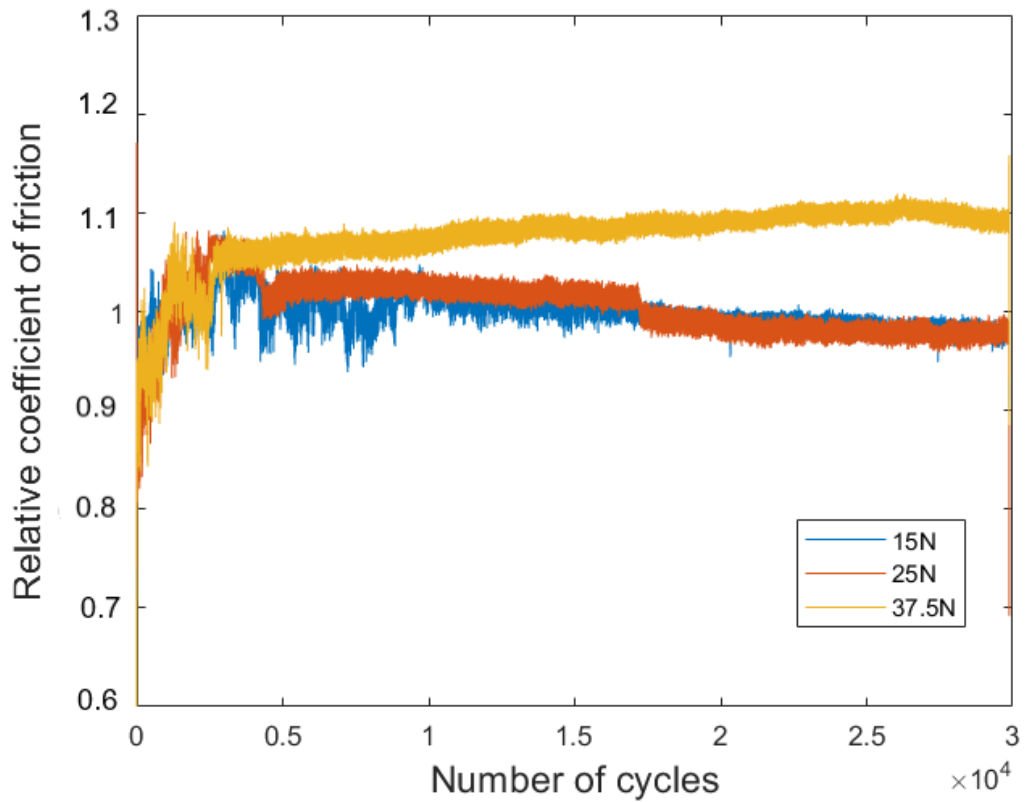
Figure 5-8 The evolution of relative COF as the test progresses at 600˚C at a normal load of 15, 25 and 37.5N

5.3.3 Surface topography

5.3.3.1 SEM Images

Figures 5-9 and 5-10 shows the detailed images of the wear scar at x1000 magnification at various load and temperatures.
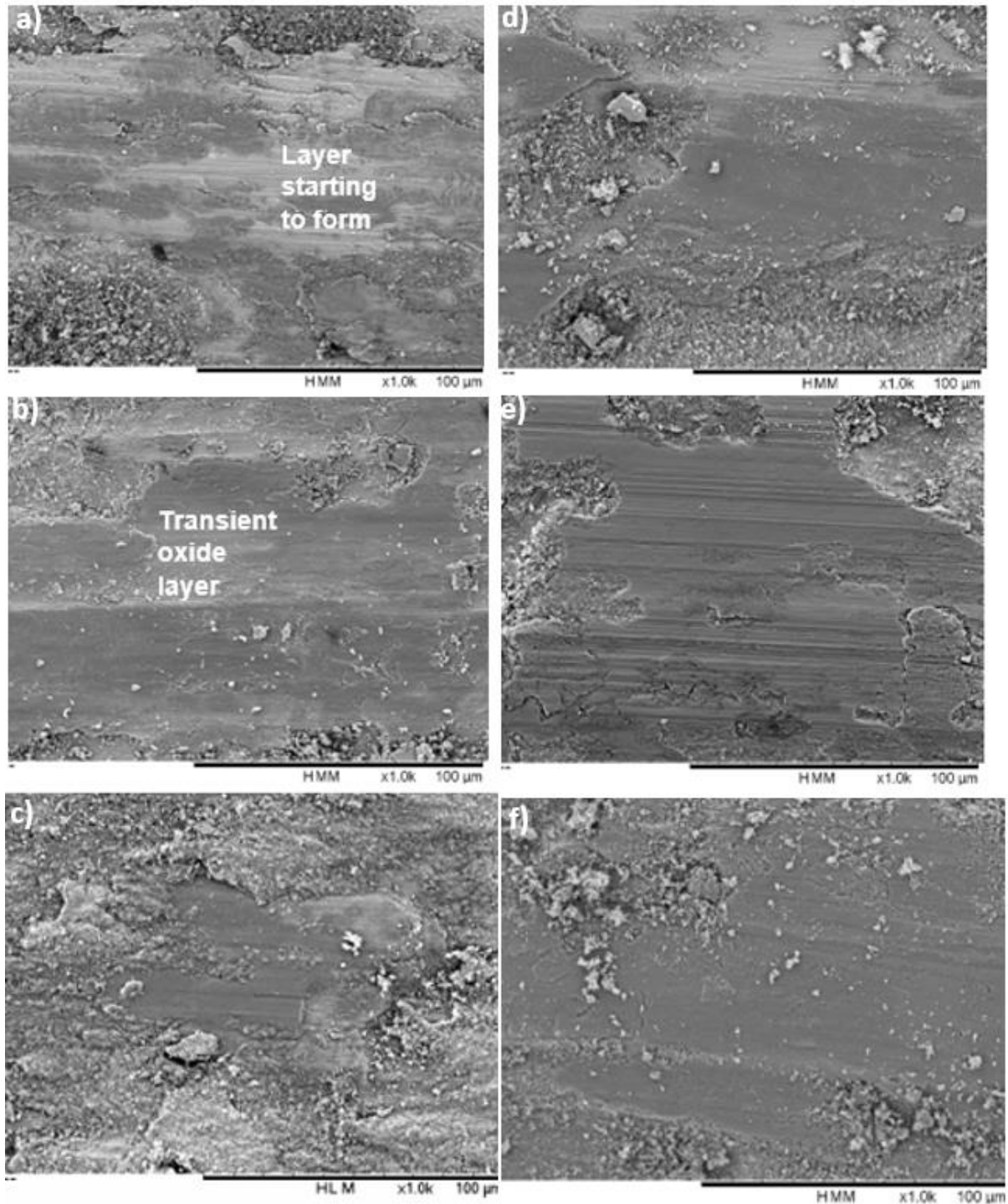
Figure 5-9 Detailed SEM images using a mix of BSE and SE detector at x1000 magnification of the wear scar. a,b,c from 200⁰C tests d,e,f from 400⁰C tests.
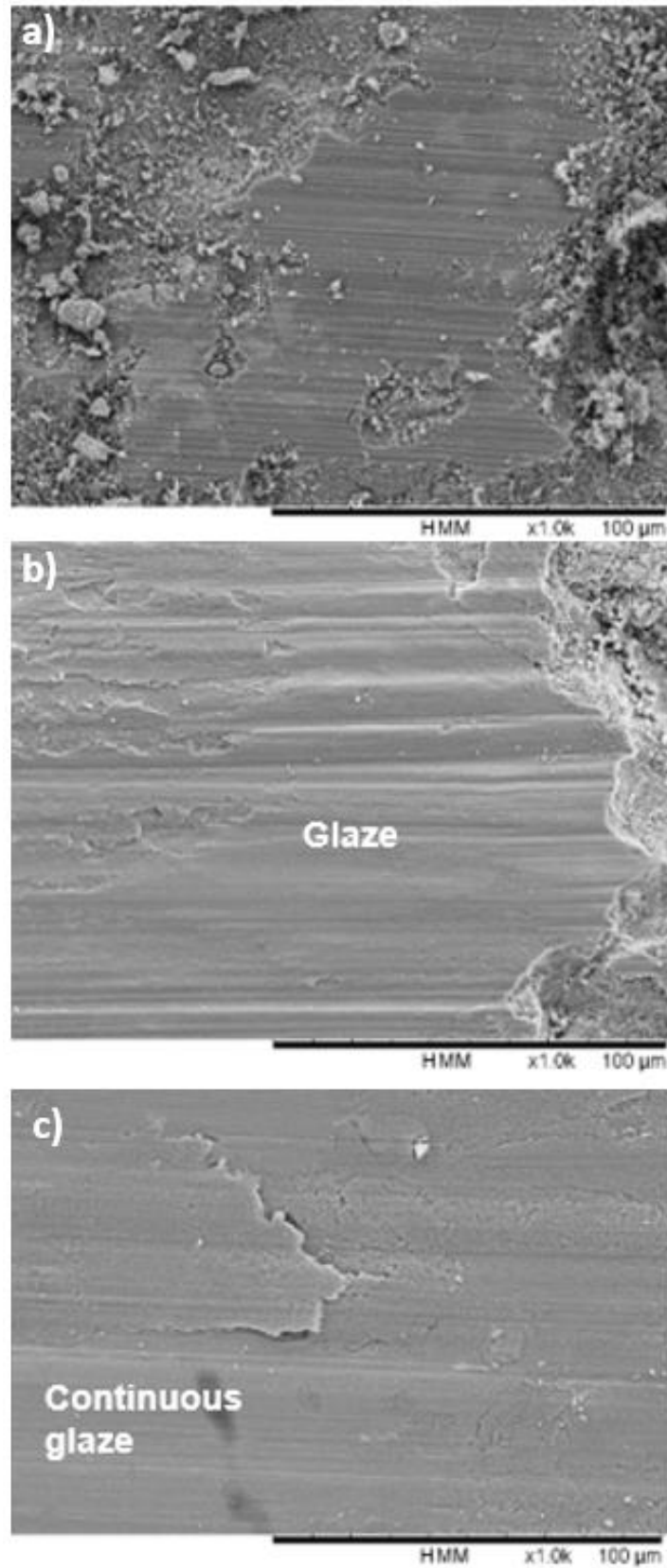
Figure 5-10 Detailed SEM images using a mix of BSE and SE detector at x1000 magnification of the wear scar. a,b,c from 600ºC tests

Very different wear features are observed at different test conditions with major differences to be seen with changing temperatures and load. At the lowest temperature, the wear scar displays adhesion and debris to be compacted/sintered. As the load is increased at 200°C, a 'smoother' layer is beginning to form. At the edges of these layers, there is a high concentration of small debris indicating compaction and sintering are happening to increase the coverage of glaze. At the intermediate temperature of 400°C, glaze layers can be seen especially at 25N, however cracks can be seen on the surface indicating the layers formed are thin and not effective. At the highest temperature, a continuous glaze layer can be seen with some adhesion at the normal load of 37.5N.

Figure 5-11 shows the sectioned SEM images of the In718 sample post test at varying temperatures and a normal load of 25N. As seen in the figure, distinctive layers can be seen at each temperature with varying thicknesses. At 200ºC, there is a thick mechanically mixed layer (MML) seen above the bulk material. This layer is formed from compaction of debris during the severe wear stage at the initial periods of sliding. Generally, this layer consists of both oxide and unoxidized debris. It can also be observed that the layers are detaching, and materials are being removed form the bulk material, this indicates that the layer formed at 200ºC has not adhered properly. As the temperature is increased (i.e. 400ºC), the main difference is that the thickness of the layers has increased, and three different layers are noticed. MML can be split into two sections where the layer adjacent to the bulk material consists of 'larger' debris and MML with 'smaller' debris are seen. followed by a compacted debris layer and a thin layer of glaze is also visible. The compacted debris layer indicates that more debris are to be sintered into a glaze layer. As the temperature is further increased, a more uniform layer can be seen with a continuous glaze as the top layer. The shows that with increased temperature there is sufficient energy available to sinter the debris layer (as seen at 400ºC) and the thickness of glaze has increased suggesting further damage can be prevented as the rate of breakdown of the layers are lowered.
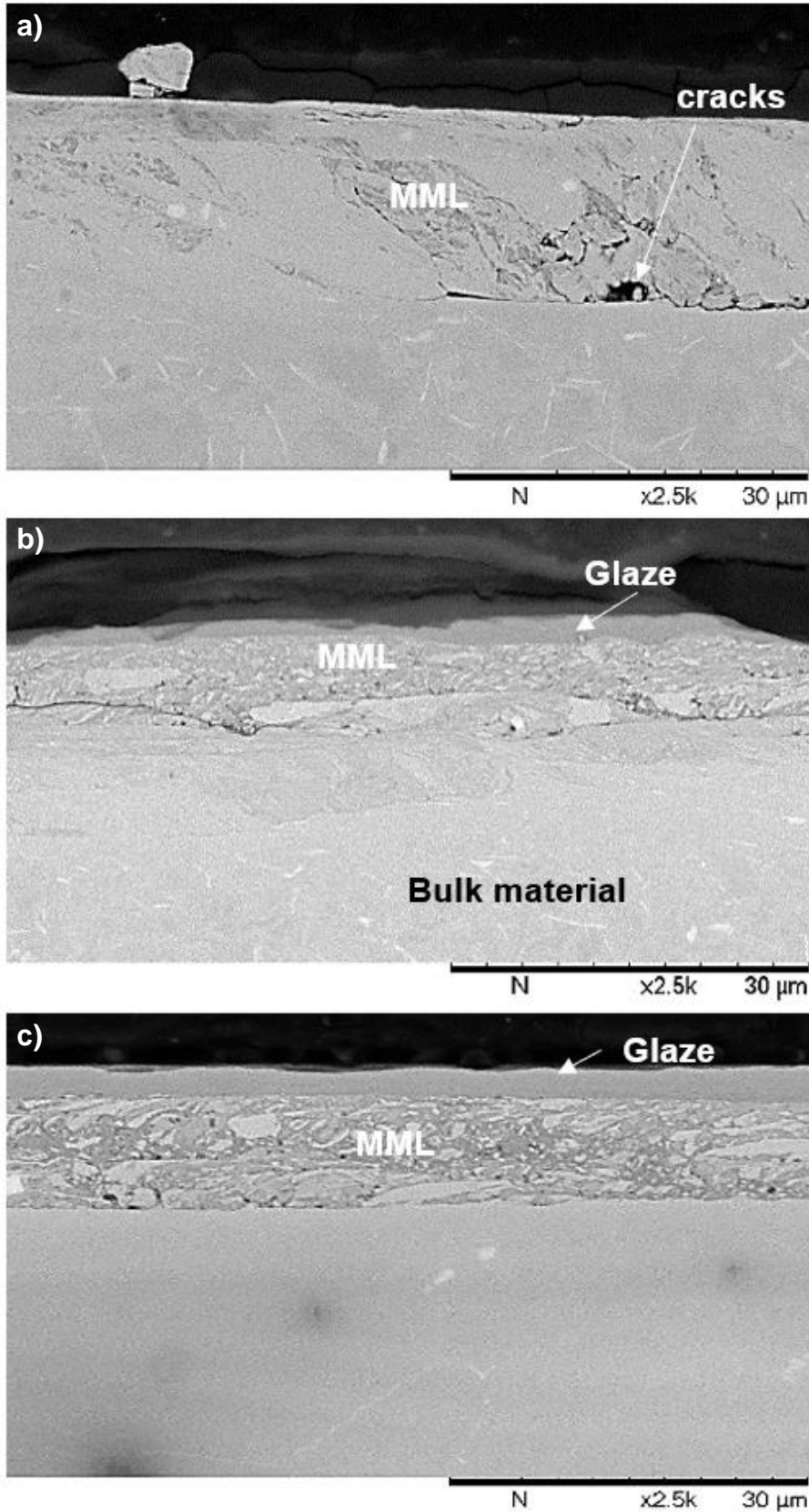
Figure 5-11 The cross sectioned images of the In718 wear scar at varying temperature after sliding for 30,000 cycles at a normal load of 25N a) at 200˚C, b) 400˚C and c)600˚C.

5.3.3.2   Chemical analysis

As previously discussed in the earlier chapters, the effectiveness of the glaze layers is determined by the composition of these layers. So, SEM EDX analysis were carried out to study the variations in the composition as the temperature and applied load is varied. The relative ratios between the main alloying elements are used, calculated from the wt% of elements on the surface layers.

Table 5-1 shows the ratios of the surface layers formed. The pre-test surface ratios are indicated by the control. As seen in the table, for Inconel 718 there are no major changes in the ratios especially between the various loads at 200˚C. There is a minor rise in the Ni/Cr and Ni/Fe ratio indicating an increase in the Ni content. Moreover, the Cr/Fe has increased slightly at the highest load suggesting Fe depletion. There is a rise in the percentage of Ni on the surface when compared to the control values at 400˚C. At 15N and 37.5N, the Cr/Fe ratio is quite stable, but, at the intermediate load of 25N, the Cr/Fe has fallen to 0.66 from 1.03 indicating that there is a Fe dependency. This could be a contributing factor in the trends observed in the COF as the overall drop in the COF was greater at intermediate load as Fe oxide has better adhesive properties than Cr and Ni oxides. At the highest temperature, a minor fall in Ni is observed and a rise in both Cr and Fe. This is likely to be because the diffusion and sintering rate of Cr is higher as there is more energy available. The Cr/Fe shows there is a drop in Cr content at the lowest load and has increased at the higher load conditions.

Normal load, N	Ni/Cr			Ni/Fe			Cr/Fe		
	200˚C	400˚C	600˚C	200˚C	400˚C	600˚C	200˚C	400˚C	600˚C
Control	2.58	2.84	2.84	2.86	2.94	2.93	1.14	1.03	1.03
15	2.89	3.06	2.33	2.93	2.86	2.02	1.01	0.93	0.87
25	2.89	3.28	2.24	2.94	1.85	2.54	1.02	0.66	1.13
37.5	2.85	3.16	2.50	3.54	2.80	2.70	1.24	0.91	1.08

Table 5.1 Elemental ratios from the SEM EDX analysis

5.3.3.3 Surface profiles

Figure 5-12 show the surface profiles obtained from the tests conducted at 200°C and 600°C under a normal load of 25N. In Figure 5-12a, the surface profile at 200°C exhibits a nearly uniform depth across the wear scar, as evidenced by the optical image on the left. This can be attributed to the presence of a lightly oxidised region covering the entire scar. The average height of the oxidised patch measures approximately 1 mm, with minimum values indicating areas where oxide or material has been removed.

A slightly different pattern appears at the higher temperature, as shown in Figure 5-12b. Here, a stable region is observed at the centre of the scar, surrounded by varying heights at the scar's edges. This stable region corresponds to the glazed region seen in the optical image. Between the different temperatures, at elevated temperatures, the oxide or glaze regions exhibit greater height compared to lower temperatures. This is due to increased oxidation and sintering of the debris, resulting in the accumulation of multiple layers over each other.
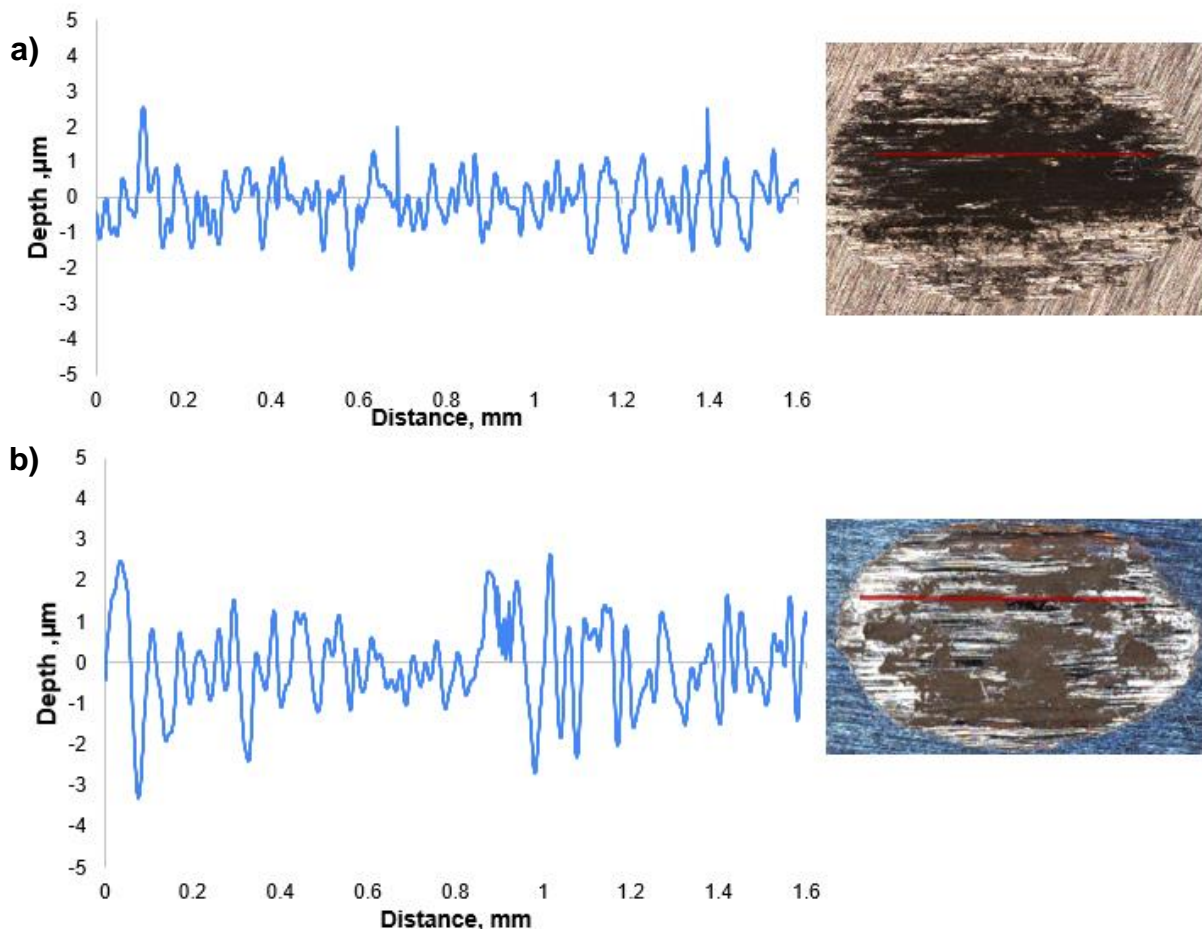
Figure 5-12 Surface profile from In718 disc samples at a normal load of 25N post 30,000 cycles at a) 200ºC b)600ºC. The corresponding wear scar with red line indicating the profile path (left)

5.4   C263

5.4.1   Wear scar analysis

5.4.1.1   Wear scars

Figures 5-13 to 5-15 shows the post test wear scars (both pin and disc) obtained from C263 tests.
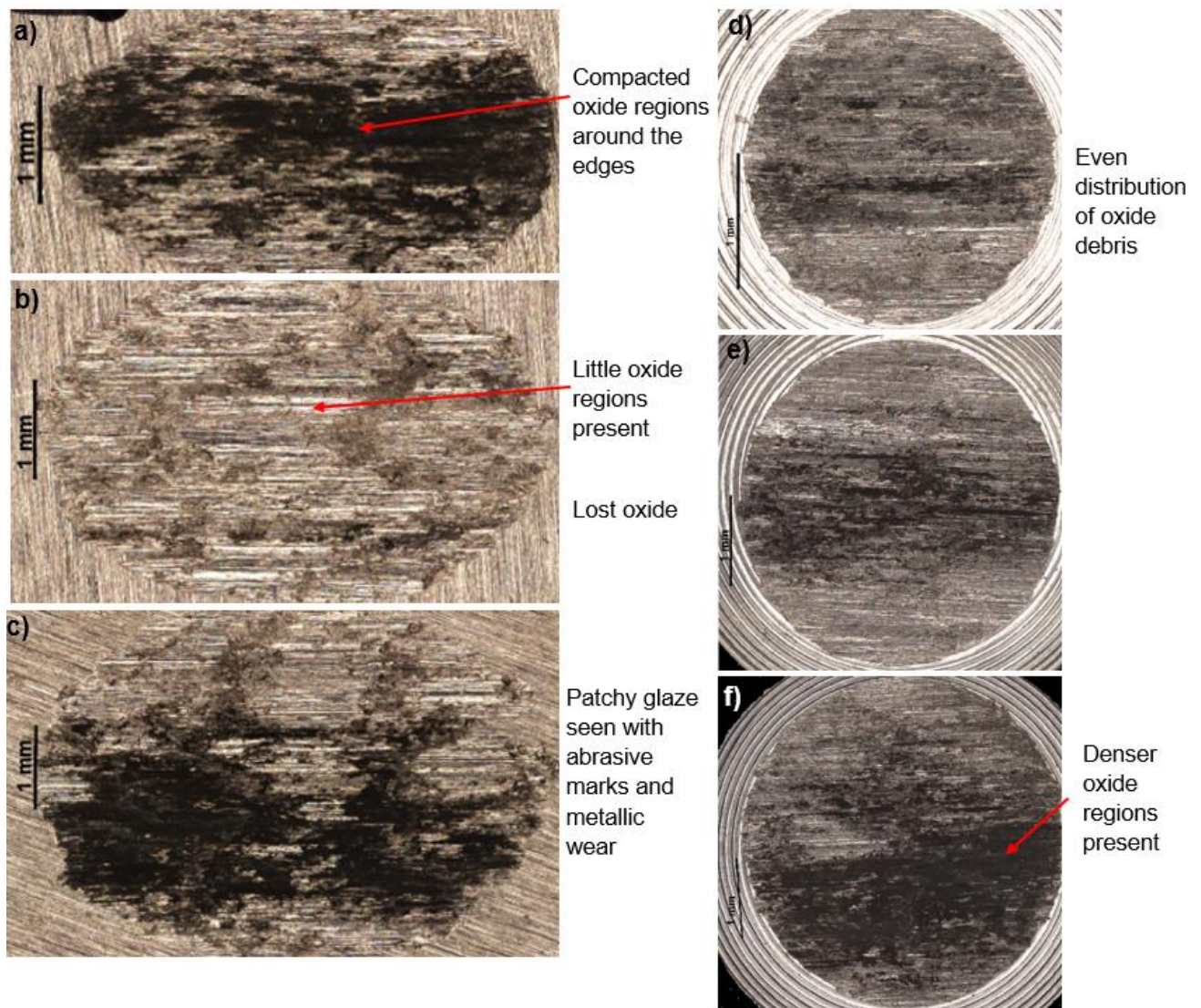
Figure 5-13 The wear scar obtained from 200ºC tests on C263 like on like combination over 30,000 cycles. The images are acquired using x5 lens. a,b,c are scars from the disc samples at a normal load of 15,25 and 37.5N respectively. d,e,f are from the corresponding pin samples at a normal load of 15,25 and 37.5N respectively.

The wear scars from the 200ºC tests can be seen on Figure 5-13. The disc scar displays a higher variability in the oxidised regions with more coverage at 15N and 37.5N. The 'black' oxidised regions are patchy and covering less than 50% of the scar at all load conditions. At the intermediate load of 25N, very few oxidised regions can be seen. This suggests that the transient oxide layers may be broken with further sliding resulting in metallic wear due to metal-metal contact. On the pin scar there is an even distribution of oxide at all load conditions. Also, the edges of the scar are more rounded meaning there is less abrasive wear due to debris interaction.
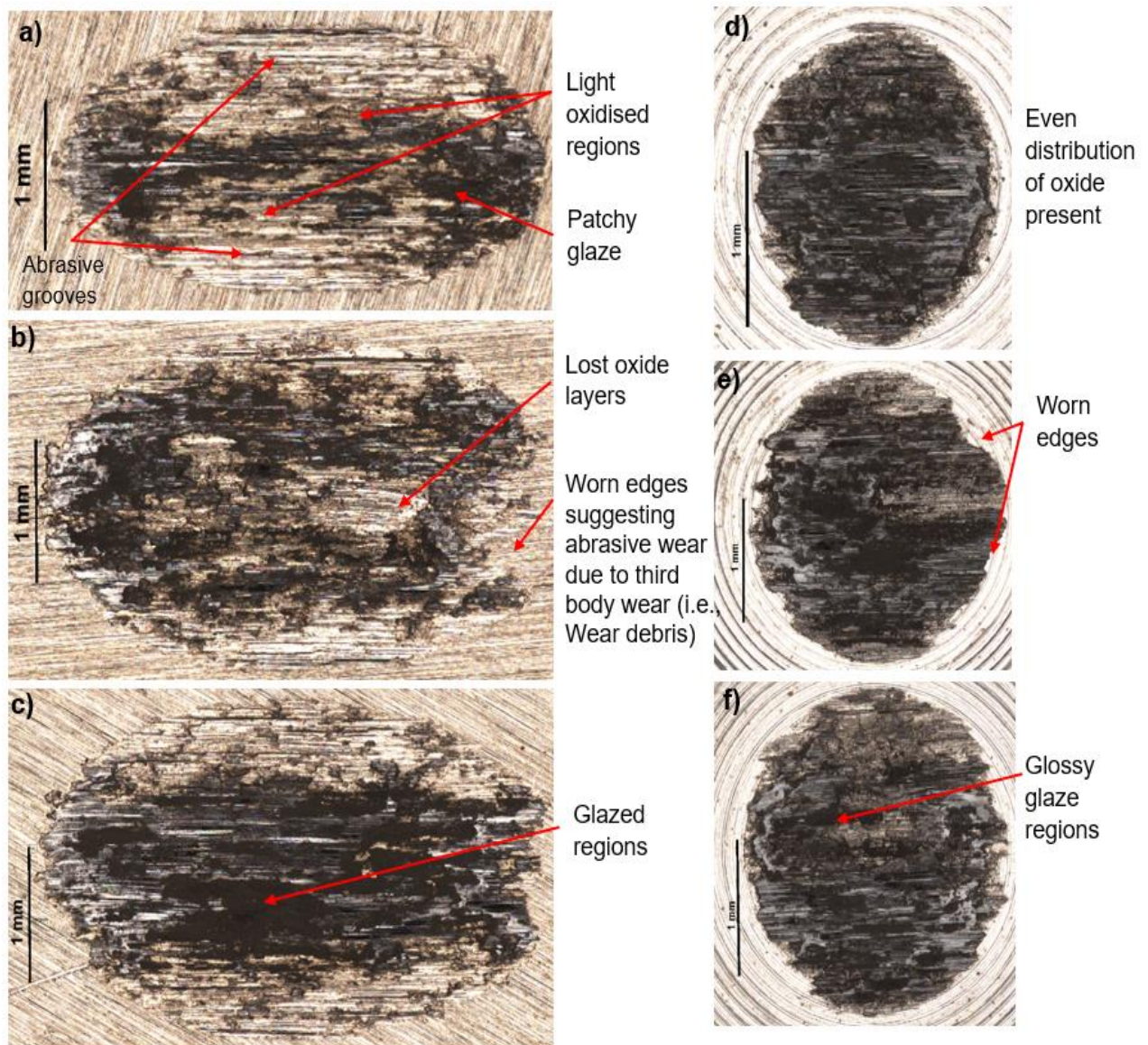
Figure 5-14 The wear scar obtained from 400ºC tests on C263 like on like combination over 30,000 cycles. a,b,c are scars from the disc samples at a normal load of 15,25 and 37.5N respectively. d,e,f are from the corresponding pin samples at a normal load of 15,25 and 37.5N respectively.

Figure 5-14 shows the wear scars from the 400ºC tests. With the increasing applied load, the oxide coverage has increased. However, at the lower loads the oxide layers are patchy and not continuous indicating wear has occurred. At the highest load, smooth/glossy regions are seen in the middle of the scar. This is due to glaze layers are being generated at higher temperatures as there is more energy available for the oxidation of debris and diffusion of active elements into the surface. Moreover, at the highest load, the surface undergoes a higher degree of plastic deformation, resulting in dislocations/defects in the crystal lattice. These areas of defects act as sites of stress concentrations leading to sub-surface cracks being formed [89] [90]. These cracks provide pathways for the movement of atoms or molecules, facilitating diffusion processes within the material, increasing the diffusion rate and allows more oxygen diffusion into the metal for oxidation. Similarly on the pin, there is an even distribution of oxide with glossy/reflective regions at higher loads.
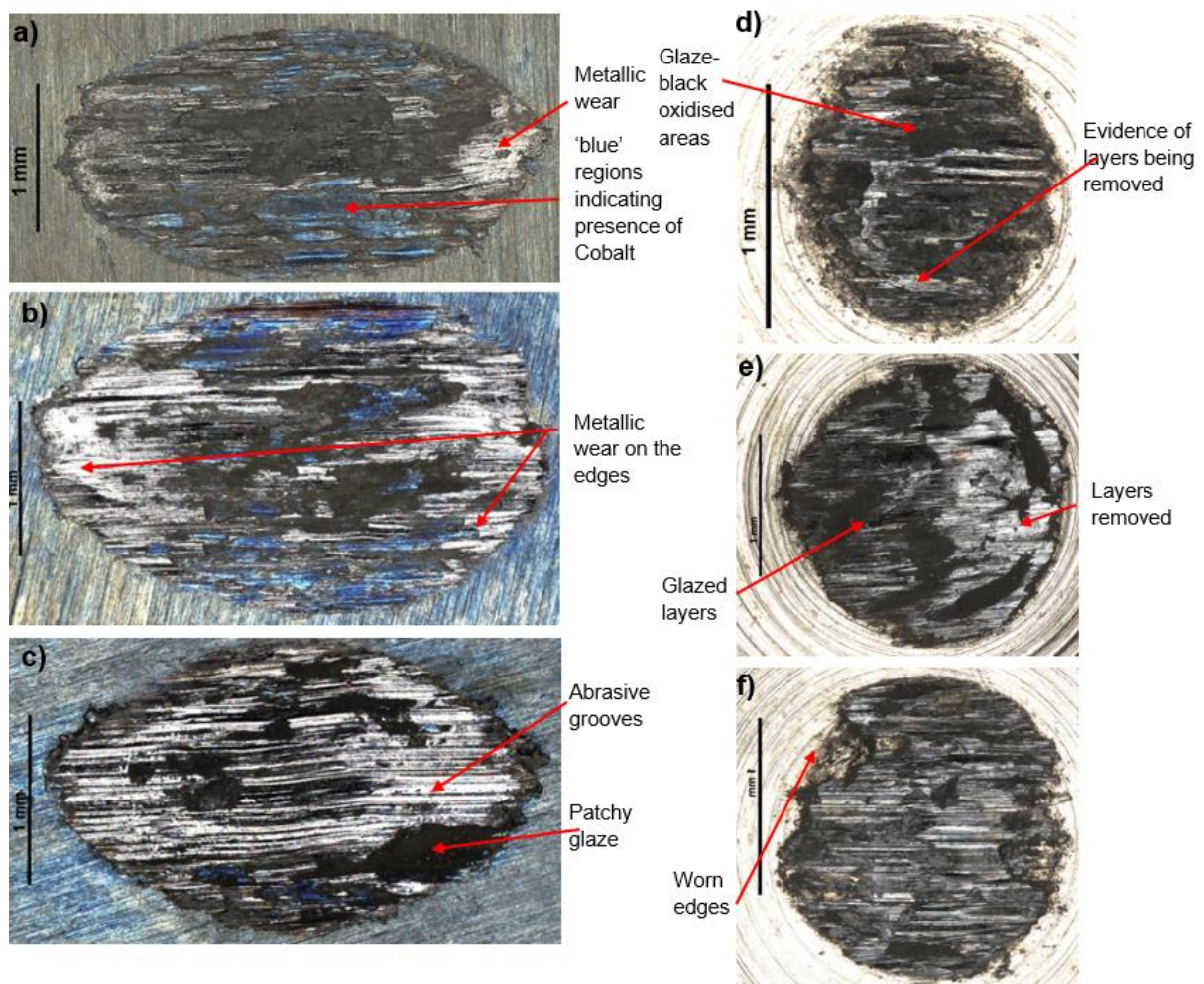
Figure 5-15 The wear scar obtained from 600ºC tests on C263 like on like combination over 30,000 cycles. a,b,c are scars from the disc samples at a normal load of 15,25 and 37.5N respectively. d,e,f are from the corresponding pin samples at a normal load of 15,25 and 37.5N respectively.

At the highest temperature of 600°C (see Figure 5-15), the wear scar diameter and width are smaller when compared to lower temperatures. There are some 'blue' regions on the surface indicating the presence of cobalt, meaning cobalt has diffused into the surface due to more energy being available. Although, there are abrasion marks, running in the sliding direction, the islands of glazed regions are extremely smooth and reflective even on the optical images. However, on the pin scar, the edges of the scar seem to be worn, likely to be due to abrasion from the oxide debris.

A clear distinction in the wear scar can be seen at various temperatures. As the temperature is increased, the oxide/glazed regions appear to be smoother and glossy; also, the wear scar dimensions have considerably decreased indicating the layers formed are wear resistant and protective. Even though increasing load appears to be advantageous (especially at the lower temperatures), it does not seem to be the major influencing factor in glaze generation at the highest load as little variation is noticed on the wear scar.
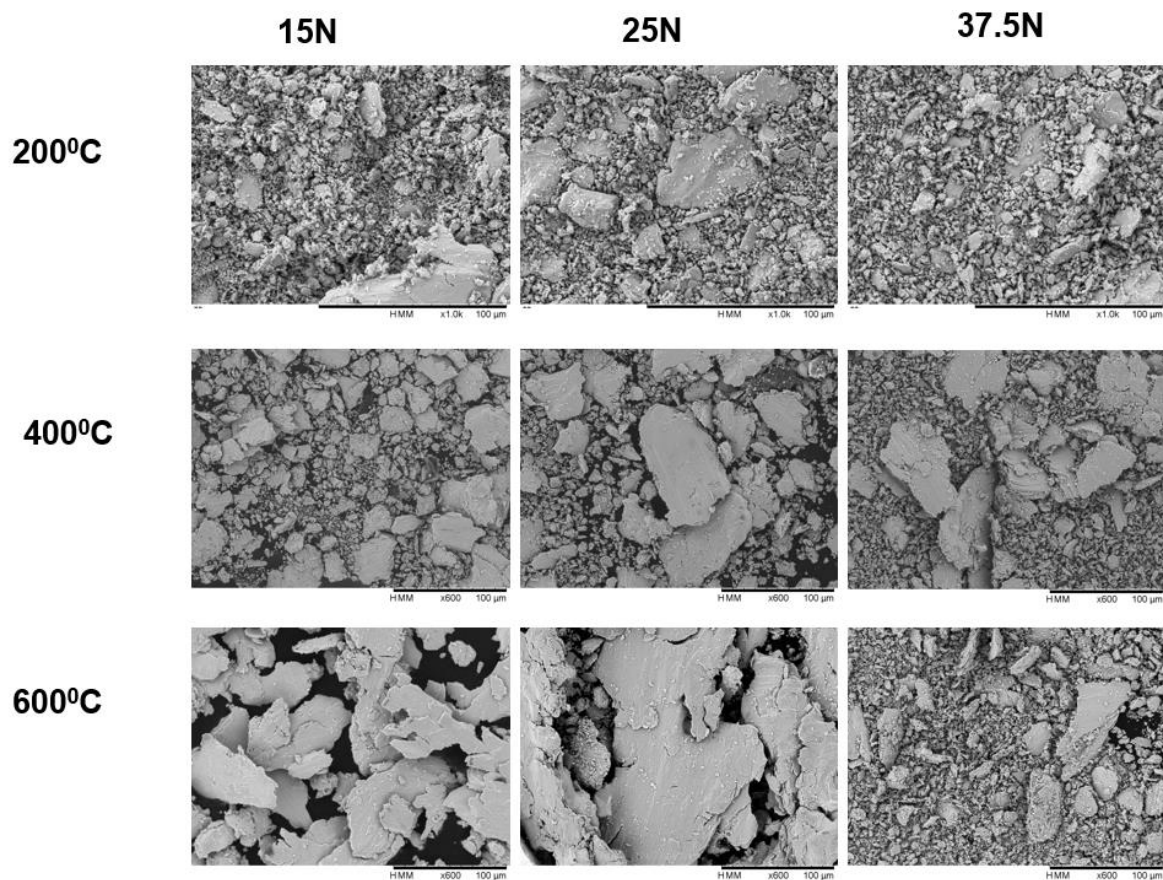
Figure 5-16 SEM image of the wear debris from the C263 like on like tests at varying temperatures and normal load.

Figure 5-16 shows the wear debris at various loads and temperatures. As seen in the figure, with increasing load, the size of the debris considerably increases, more evident at the highest temperature. As previously explained, this is due to the higher degree of plastic deformation experienced at higher loads leading to 'larger' debris being produced.

5.4.1.2   Wear volume

The total volume lost is measured by weighing the pre and post test samples. As seen in the Figure 5-17, at the lower temperatures, the volume lost is significantly higher than at 600ºC. The results from 200ºC follows a linear trend, as the load is increased the wear volume has also increased. This is likely to be that the oxide layers formed at this temperature are transient which are not wear resistant and easily broken down producing more wear debris. This in turn acts as third body wear particles abrading into the surface causing more damage. Since the surface experiences higher stresses under high loads, cracks are formed leading to large chunks of material being removed, thus the debris formed at higher loads are 'larger' than at lower load conditions. The larger debris takes longer to be broken down into fine particles to be sintered and some of the debris are pushed out of the contact increasing the volume lost.

A different trend is observed at 400ºC and 600ºC where there is a slight rise in wear volume between 15 and 25N and a drop in volume between 25 and 37.5N. At the lower load conditions, it appears that the layers formed are not as efficient as at higher loads in protecting the surface. Whereas at the highest temperatures, the influence of increasing load is more evident, a significant drop is seen at higher loads suggesting glaze is better and counteracts increased wear due to higher load. The rate at which the volume has reduced is different for both temperatures. There is a higher drop at 400ºC because the rise in flash temperature may have aided in achieving the activation energy for the some or all of the active elements involved.
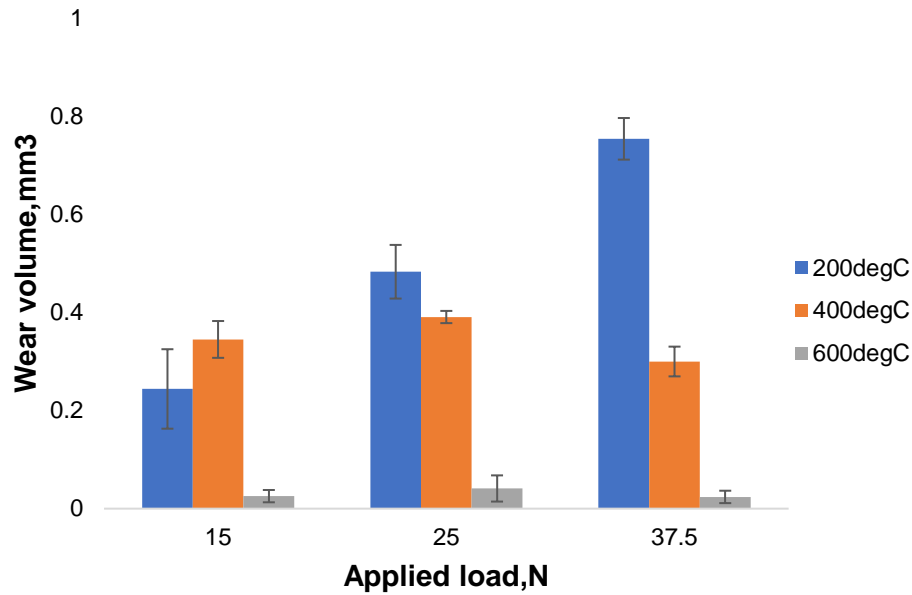
Figure 5-17 Volume lost during the various temperature and load conditions

5.4.2 Evolution of coefficient of friction

As was the case for In718, the friction characteristics for C263 have evolved as the tests progressed due to the formation and breakdown of the surface layers. Figures 5-18 to 5-20 show the variations in the relative COF at various temperatures and load conditions.
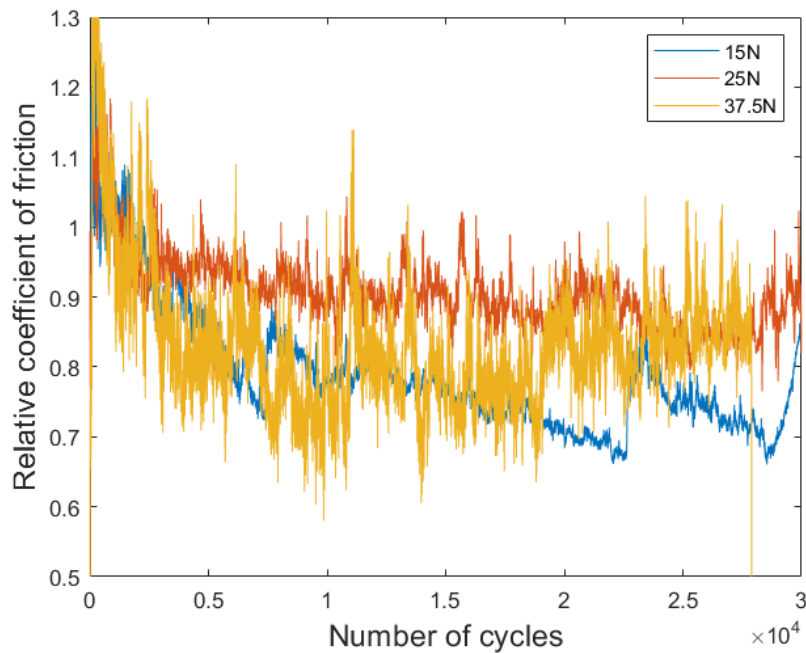
Figure 5-18 The evolution of relative COF over 30,000 cycles at 200˚C at a normal load of 15, 25 and 37.5N on C263 like on like combination
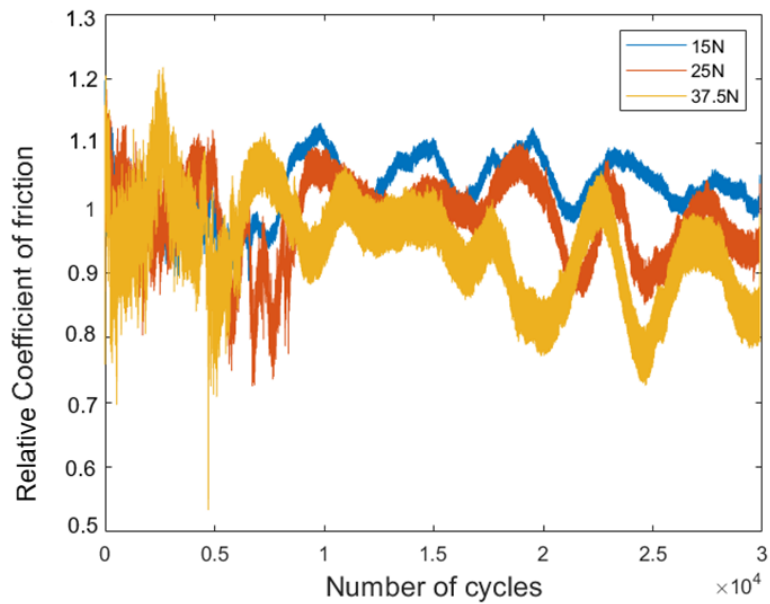
Figure 5-19 The evolution of relative COF over 30,000 cycles at 400˚C at a normal load of 15, 25 and 37.5N on C263 like on like combination
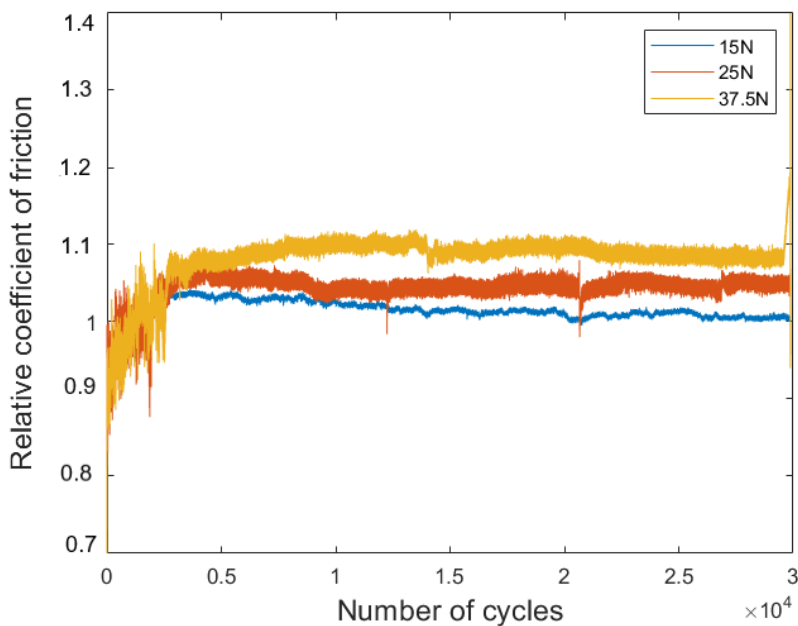
Figure 5-20 The evolution of relative COF over 30,000 cycles at 600˚C at a normal load of 15, 25 and 37.5N on C263 like on like combination

Figure 5-18 shows the evolution of relative COF at 200˚C where there is an overall decreasing trend with increasing duration. However, the rate at which the drop in COF is seen is different at various load conditions. The greatest fall in COF is noticed at the lowest load of 15N where the COF has dropped to around 70% from the initial value. Though, the COF shows an unstable characteristic with abrupt peaks and drops. The minimum is seen at the intermediate load of 25N with an overall drop of only 90% from

the initial value. Even though the overall COF is greater at 25N, a stable COF is established for the longest duration when compared to 15 and 37.5N. This behaviour in COF is unexpected as the wear scar shows very little oxide on the surface, this could be that the layers were broken down with sliding. At the highest load of 37.5N, a sharp reduction in COF is observed initially followed by stable regions where the COF is steady for approximately 10,000 cycles.

The friction response at 400°C is seen in Figure 5-19 where the overall COF has dropped as the load is increased. Although not to the same degree seen at 200ºC, regions of stable COF lasting for 6,000 cycles at the highest load and 2000-3000 cycles at lower loads are observed. At the higher loads (i.e., 25 and 37.5N), an abrupt rise in COF between 17,000 and 21,000 cycles, likely caused by third body wear due to an increase in wear debris. Another notable point is that some of the subsequent peaks in COF are lower than the previous suggesting that not all of the oxide layers are broken down proving some protection. Overall, at the lower temperatures, the COF appears to be unstable.

Finally, Figure 5-20 shows the relative COF at 600ºC. Unlike the lower temperatures, a very stable COF is seen at 600ºC. As the load is increased, there is an overall rise in the relative COF, likely to be due to adhesion between the rubbing surfaces. As seen in Figures 5-12 and 5-13, as the load increases, there is not an evident difference in wear scar or the volume, suggesting that the glaze layers formed at this temperature must be wear resistant and similar in composition. Steady state COF is observed for more than half of the test duration at all load conditions.

Between the temperatures, distinctive friction characteristics are observed as the applied load is varied. Different temperatures have shown regions of stable COF, although the duration varies considerably. While wear protective layers are developed at 200 and 400°C, they were only able to provide protection for a brief period of time as further sliding action has broken down the layers enabling metal-metal contact contributing to an increase in wear volume and more damage, whereas at the highest temperature stable COF is noticed although there is an overall rise in the COF which will be discussed later.

5.4.3 Surface topography

5.4.3.1   SEM images

Figures 5-21 and 5-22 shows the detailed SEM images obtained at x1000 magnification from the 'black' oxidised regions. It is apparent from the figure that as the test temperature is increased, a smooth surface can be seen with very fine oxide debris. At 200ºC, the surface appears to be rough, with material being removed at higher loads and compacted debris at lower loads. At lower loads, compacted debris indicates that the layers are just beginning to form whereas at 37.5N, the layers are broken down with 'larger' debris. At 400ºC, smoother layers are starting to appear. At the lowest load, abrasive marks with some adhesions can be seen. As the load is increased, the abrasive marks have started to disappear. At 600ºC, a continuous glaze (smooth surface) is observed, however, at the higher load, cracks and material removal is seen. This trend is reflected in the relative COF data as well, where at the highest temperature an overall rise in COF is observed, likely to be due to debris interaction as the layers are removed with further sliding.

Figure 5-23 shows the sectioned images of the wear scar from C263 like-on-like tests at a normal load of 25N. The images shows that different layers are generated at various temperatures. At 200ºC, the scar exhibits a debris layer with no oxide layers present. This suggests that the severe abrasive wear is occurring, leading to debris being released into the contact, and the energy is not sufficient enough for sintering. As the temperature is increased, large debris are observed on the top, a thin compacted debris layer can be seen. Although, compacted debris are seen, the glaze layers are not present, possibly due to not having enough energy to form or that the appropriate elements have diffused to the contact. The highest temperature shows the highest variation where a thick layer of glaze noticed on the topmost layer followed by a MML. The thick glaze is probably generated due to the having reached the activation energy and the appropriate elements being present which aids the compaction and sintering process ensuring the new glaze layers have strong bonds preventing further damage.

Figure 5-21 SEM images obtained from the oxidised regions on the C262 samples at x1000 magnification. a,b,c from 200⁰C tests d,e,f from 400⁰C tests.

Figure 5-22 SEM images obtained from the oxidised regions on the C262 samples at x1000 magnification. a,b,c from 600⁰C tests
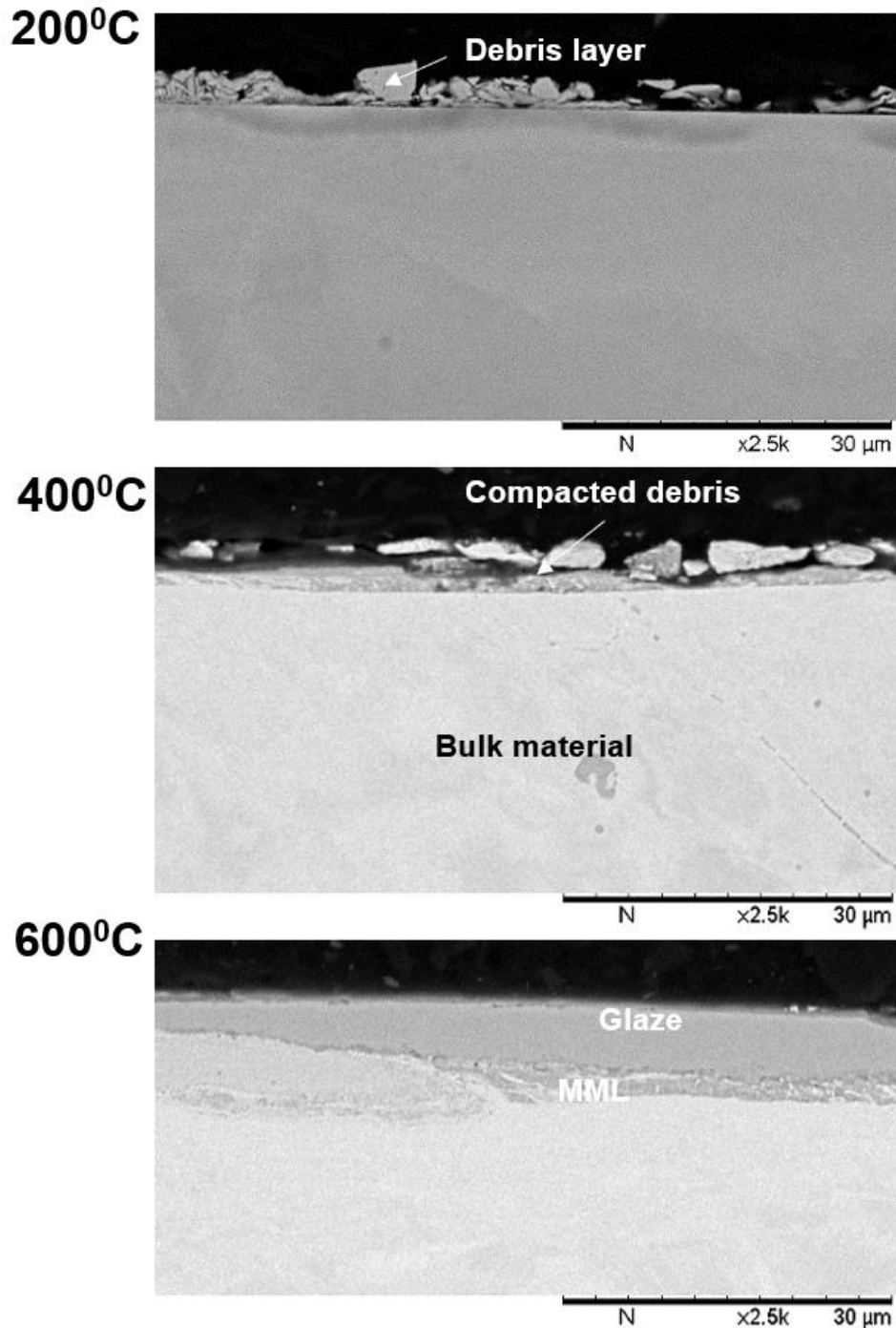
Figure 5-23 Cross sectioned images of the C263 samples at various temperatures at a normal load of 25N.

5.4.3.2 Chemical analysis

As seen in Table 5-2, the ratios of the main alloying elements have been stable as the load is varied at a specific temperature. At 200 and 400ºC, there are only minute changes in the composition, as the layers formed are transient oxide layers which are hard to detect due to being a very thin. The ratios shows that there are no major changes in the composition; the layers are made up of NiCr. This correlates well with

the friction characteristics seen in Figures 5-13 and 5-14 where the steady state COF is only seen for a short period of time, and the wear volume is seen to increase at higher temperatures. Although there is a rise in the Cr on the surface, Cr and Ni has poor sintering and adhering properties thus an effective glaze is not achieved. This is likely to be causing the layers to be easily broken down with further sliding. Moreover, the additional debris generated as the layers are broken down, acts as abrasive wear particles promoting more wear.

At the highest test temperature (i.e. 600ºC), Co/Cr ratios show a Co dominancy where the percentage of CO has increased, this is likely to be because both the temperature and load condition provides enough energy to reach the activation energy of Co resulting in diffusion into the surface.

Normal load, N	Ni/Cr			Ni/Co			Co/Cr		
	200˚C	400˚C	600˚C	200˚C	400˚C	600˚C	200˚C	400˚C	600˚C
Control	2.40	2.40	2.41	2.52	2.52	2.56	0.95	0.95	0.94
15	2.38	2.69	2.54	2.52	1.48	2.16	0.94	1.82	1.18
25	2.11	2.41	2.45	2.52	2.56	2.19	0.83	0.94	1.12
37.5	2.26	2.52	2.46	2.51	2.66	2.21	0.90	0.95	1.11

Table 5.2 Ratio of active elements on the surface obtained from SEM EDX analysis of C263 samples at various temperatures and load conditions

5.4.3.3   Surface profiles

Figure 5-24 shows the surface profiles from 200˚C and 600˚C tests at a normal load of 37.5N. As seen in figure 5-24a, the profile starts off stable and then dips and peaks in the graph is observed. The stable region is due to an oxide layer present as represented by the wear scar; the drops are due to the lost oxide regions. Figure 3-24b shows the scar from the 600˚C tests, a more stable profile is seen throughout the scar. Between the two temperatures, at higher temperature, the stable region lasts longer than lower temperature, this indicates that the layers forming are not broken off

and 'smoother' for these regions than the severe wear region (grey/silver regions on the optical image)
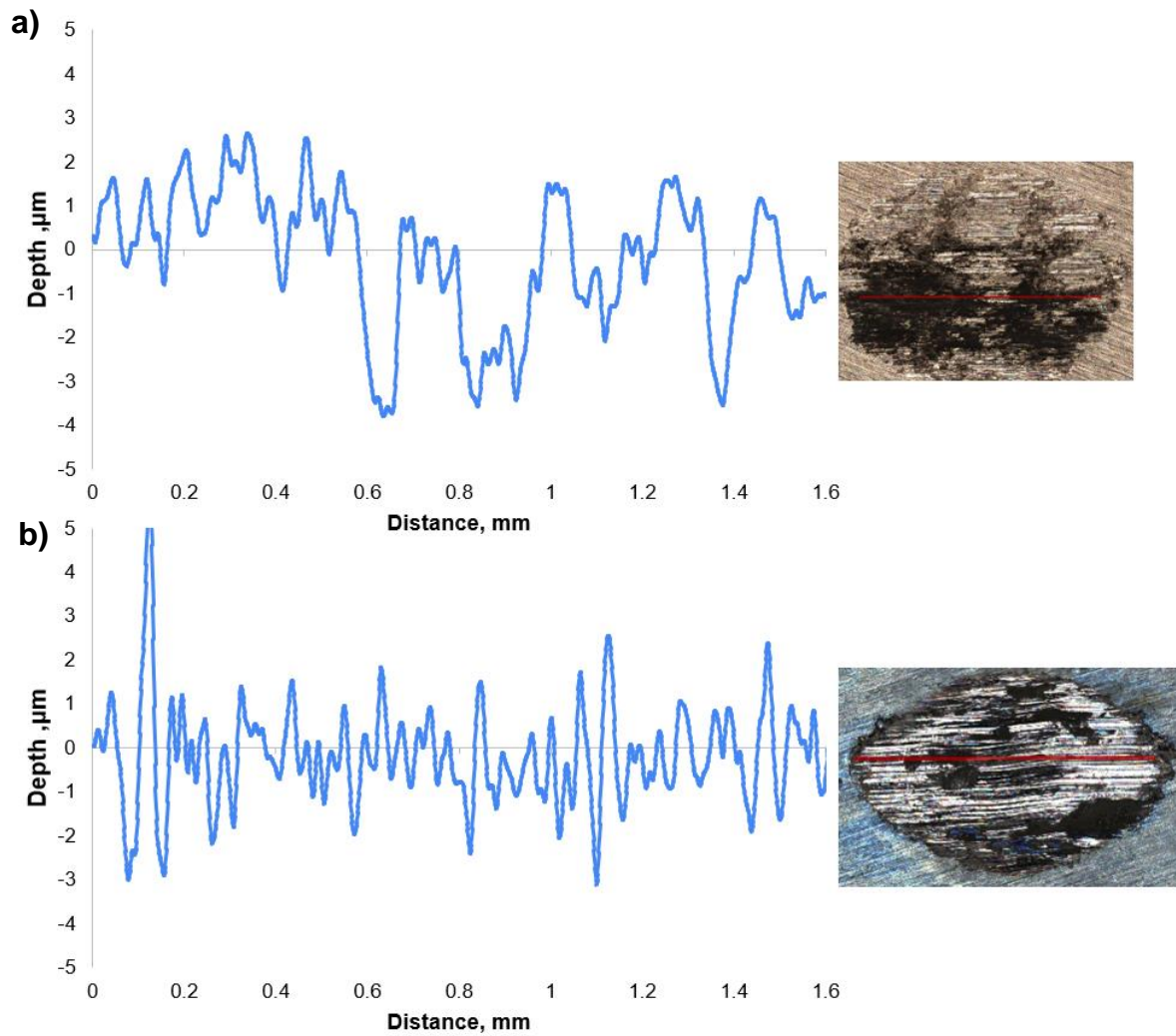
Figure 5-24 Surface profile from C263 disc samples at a normal load of 37.5N post 30,000 cycles at a) 200⁰C b)600⁰C. The corresponding wear scar with red line indicating the profile path (left)

5.5 Haynes 25

5.5.1 Wear scar analysis

5.5.1.1 Wear scar

Figures 5-25 to 5-27 shows the optical images of the wear scar from the Haynes 25 samples using a x5 lens.
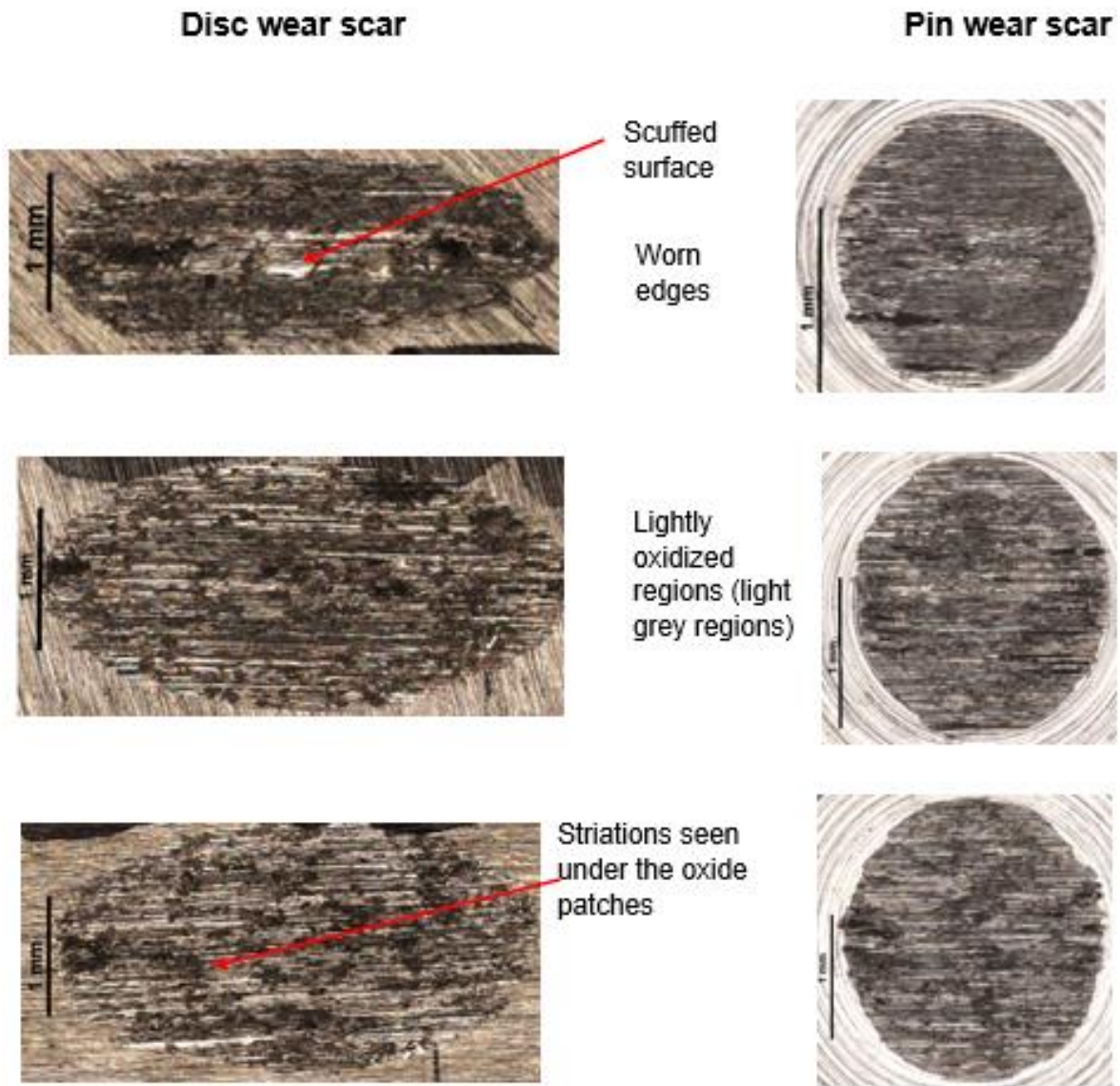
Figure 5-25 Optical images obtained from post test Haynes 25 samples at 200ºC . a,b,c are scars from the disc samples at a normal load of 15,25 and 37.5N respectively. d,e,f are from the corresponding pin samples at a normal load of 15,25 and 37.5N respectively.

Disc wear scar   **Pin wear scar**

Abrasions seen under the oxide patches

Silver/grey regions due to metallic wear or abrasive

Light oxide coverage on the whole scar

Increased oxide coverage
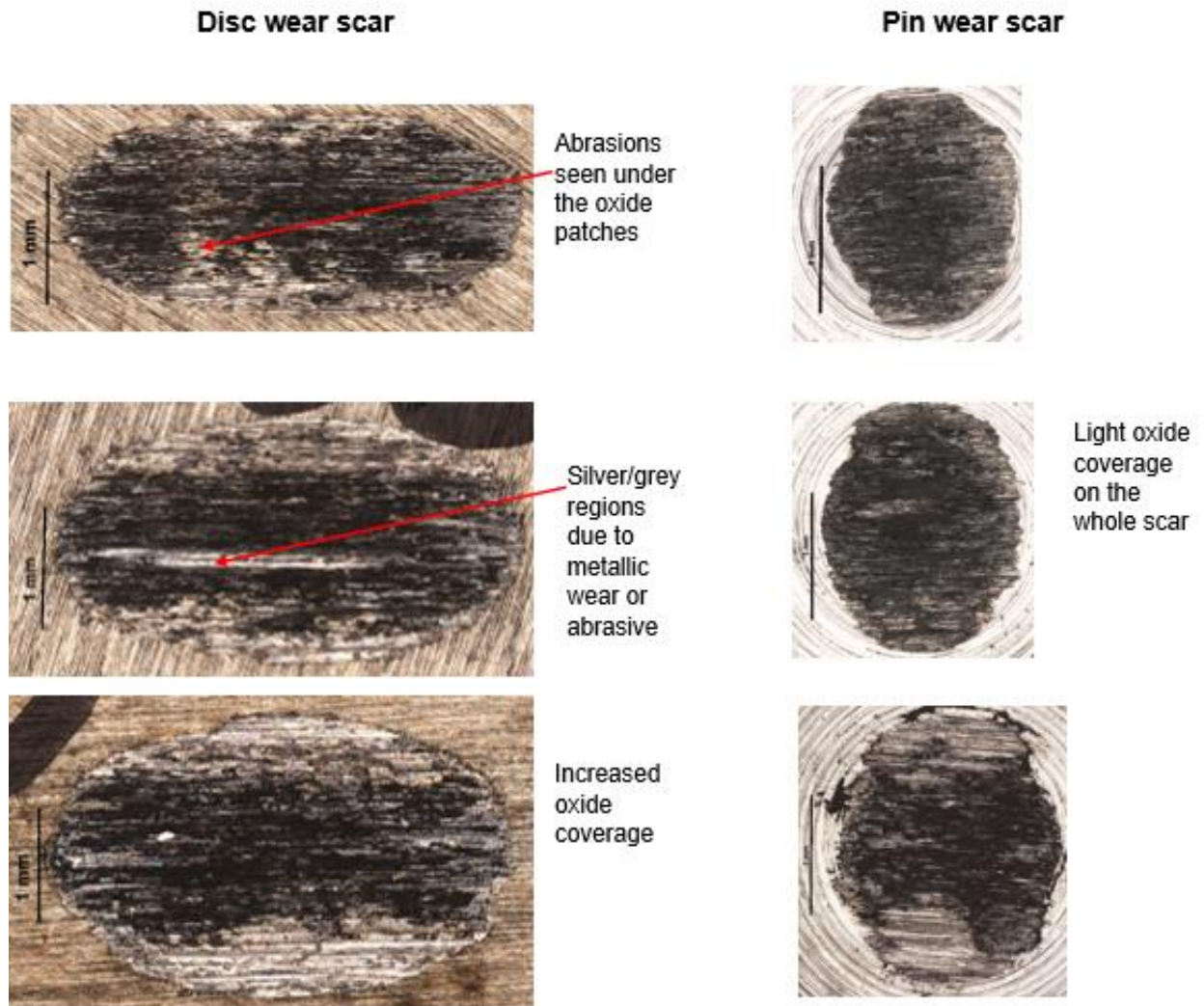
Figure 5-26 Optical images obtained from post test Haynes 25 samples at 400ºC . a,b,c are scars from the disc samples at a normal load of 15,25 and 37.5N respectively. d,e,f are from the corresponding pin samples at a normal load of 15,25 and 37.5N respectively

Figure 5-25 shows the scars from the 200ºC tests. As the load has increased the wear scar width has increased. At the lowest load, scars exhibit mechanical wear with scuffed surfaces and worn edges. Even though there are black oxides present on the surface, no evidence of oxidative wear is seen. As the load is increased, the dimensions of the wear scar has increased and light oxide regions are seen on top of the abrasive marks. At 400ºC (see Figure 5.26), a very different scar is observed when compared to 200ºC. Oxide layers are starting to form on both the pin and disc surfaces. With increasing load, the oxide regions have become denser indicating that thickness of the layers has increased. This is likely because the there is a rise in flash temperature as the load is increased resulting in higher oxidation and sintering of the debris. The wear scars from the 600ºC tests can be seen in Figure 5-27. The coverage

of glaze has increased with increasing load, and glossy/smooth regions are also observed. At the lowest loads, although the scar from the pin samples shows an even distribution of oxide layer, the edges are worn suggesting third body wear. Moreover, on the disc sample, the glaze regions are patchy and concentrated around the middle of the scar at lower loads.
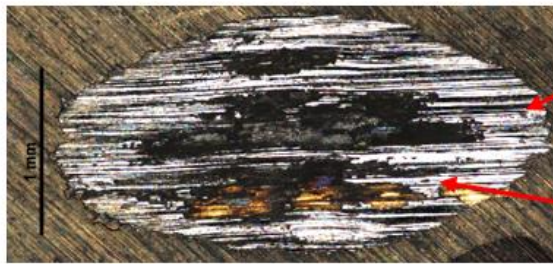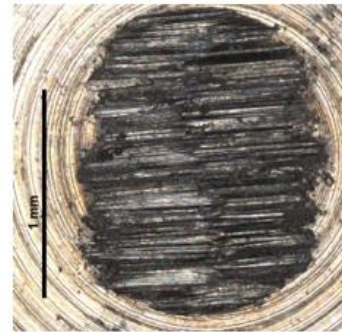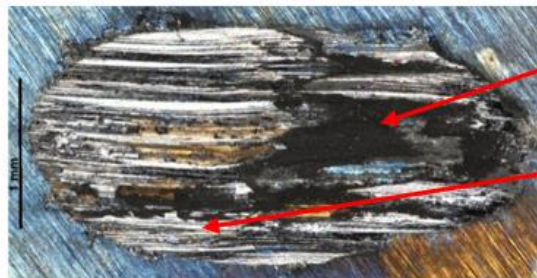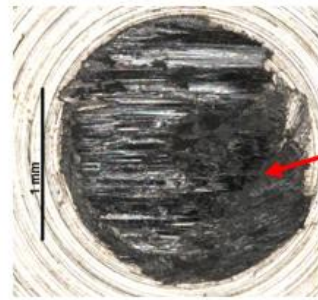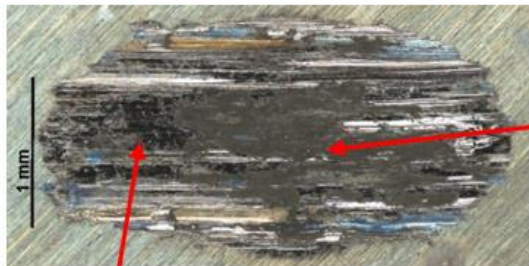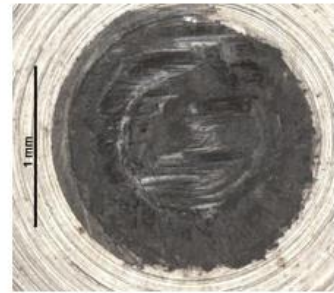
Figure 5-27 Optical images obtained from post test Haynes 25 samples at 600ºC . a,b,c are scars from the disc samples at a normal load of 15,25 and 37.5N respectively. d,e,f are from the corresponding pin samples at a normal load of 15,25 and 37.5N respectively.

Between the different temperatures used, a clear variation in the wear characteristics can be seen. Overall, this is the most significant outcome of these tests, at the lowest temperature, images display mechanical wear with striations and little/no oxide regions and the scar dimensions are relatively small compared to the higher temperatures.

This suggests that the small amount of debris produced is hindering the glaze generation process. At the higher temperature, dense oxide regions are observed, and glossy regions at 600ºC indicating glaze formation. This correlates with the previous studies and oxidation/diffusion kinetics of Co as the activation energy required for Co oxidation is around 550ºC.
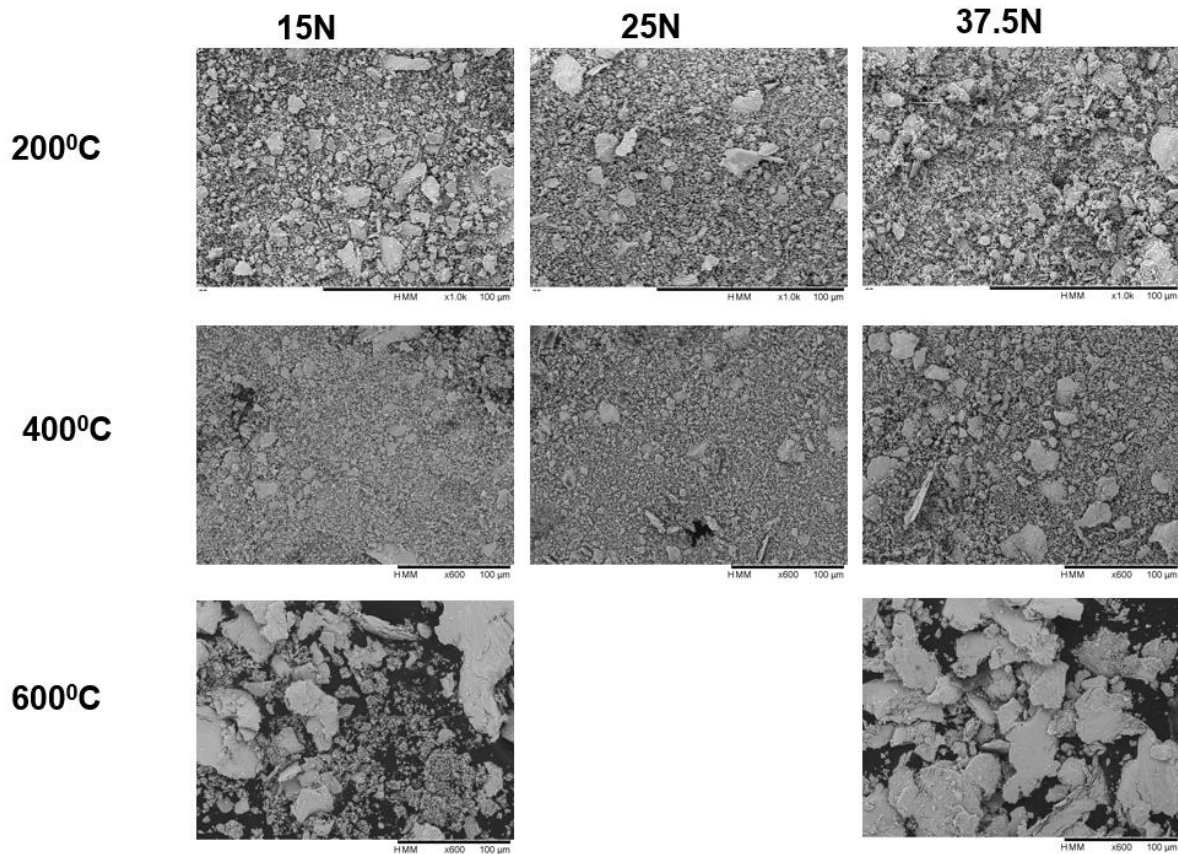
Figure 5-28 SEM image of the wear debris from the Haynes 25 like on like tests at varying temperatures and normal load.

Figure 5-28 displays the wear debris generated from like-on-like tests conducted on Haynes 25 samples at different loads and temperatures. It is evident from the figure that the size of the debris significantly increases with higher loads. Interestingly, unlike with previous materials, finer debris is observed at the intermediate temperature of 400°C. However, the exact reason for this remains unclear. Therefore, further investigation is necessary in this area.

5.5.1.2   Wear volume

Figure 5-29 shows the wear volume lost. Three different wear responses can be observed at the different temperatures indicating different wear mechanisms at each temperature. The highest wear volume is seen at the intermediate temperature of 400ºC, where there is a significant rise in wear volume at the highest load. This is because oxidative wear is occurring as there is enough energy available for oxide layers to be formed on the surface. However, these oxide layers are thin and easily broken down with further sliding resulting in more debris being generated which acts as a third body abrasive particle increasing wear volume. This is evidenced by the wear scar images where a smooth layer can be seen, although the cross sectioned images highlight a MML and debris on top, indicating that oxide layers are being generated with no glaze staying on the surface. Though, the surfaces are damaging at 200ºC, it is not generating as much debris as 400ºC. This means that the third body wear and oxidative wear are limited causing less wear. Finally, at 600ºC, there is a minor decrease in the wear volume with increasing load. With increasing temperature, the flash temperature also rises, so the oxidation and diffusion rates are higher resulting in protective glaze layers being formed on the surface.
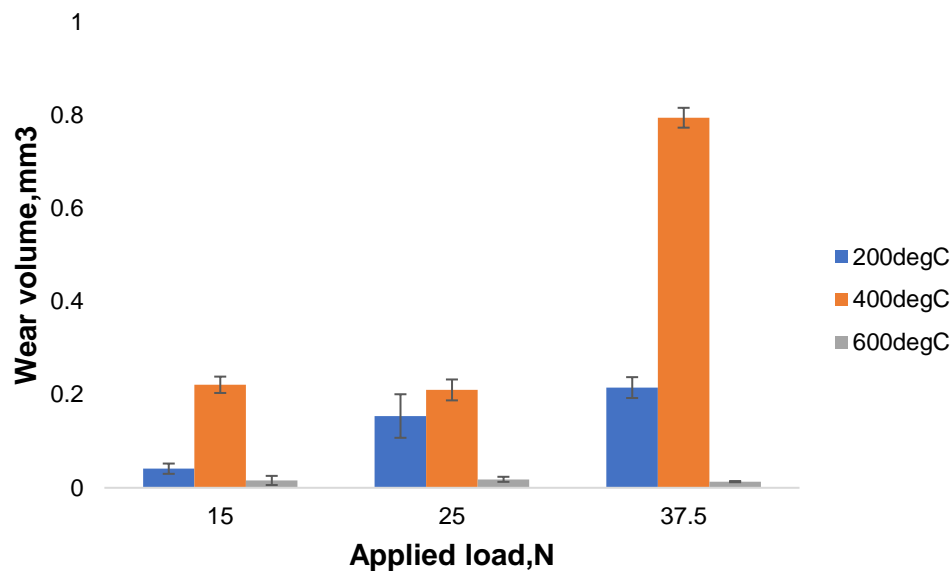
Figure 5-29 The volume lost from Haynes 25 samples at various temperatures

5.5.2 Evolution of coefficient of friction

Figures 5-30 to 5-32 shows the evolution of relative COF for the test duration (i.e. 30,000 cycles) at various load conditions.

Figure 5-30 shows the evolution of COF at 200ºC. An overall increase in the relative COF is seen with increasing load. This is due to being in the initial stage of wear, i.e., mechanical wear causing damage to the surface by ploughing and plastic deformation, but not generating enough debris. This is combined with contact temperature not being high enough to generate the required energy for oxidation and diffusion. A slightly different trend is noticed at the lowest load (i.e.15N) where there is an overall drop in the COF, possibly due to lower production of wear debris when compared to at higher loads leading to less wear by third body particles. There is no evidence of any protective compacted oxide layers forming as steady state COF has not reached at any load conditions.

 The variations in COF at 400ºC can be seen on Figure 5-31. An overall decrease in COF is noticed as the applied load is increased with regions of steady state COF and sharp rises especially at higher loads. The maximum overall drop is achieved at a normal load of 37.5N, falling to 90% of the initial value and 95% at 25N. The steady state COF, seen stable for the longest duration at the highest load, at a maximum of ~5,000 cycles at 37.5N and 3,000 at 25N. This suggests that transient oxide layers are forming and providing some protection. The sharp rises indicate the layers are broken down easily with further sliding.

At the highest temperature of 600ºC, the COF stays reasonably stable at all load conditions. The lowest overall COF is seen at 25N with steady state regions lasting up to 8000 cycles. At the highest load, there is an initial drop in the friction (at around 2500 cycles) meaning protective layers are starting to form. However, as the test progresses, there is a rise in COF, probably due to increased debris in the contact.

An evident distinction in the friction response is seen as the load and temperatures are varied. At higher temperature, evidence of oxide layer formation is seen whereas at lower temperature mechanical wear is observed. Since the changes in wear with load are not as evident as the changes with temperature, an insight is gained into the significance of temperature in glaze formation, as increasing the normal load has not

provided sufficient energy to increase the rate of oxidation and diffusion to produce an effective glaze layer.
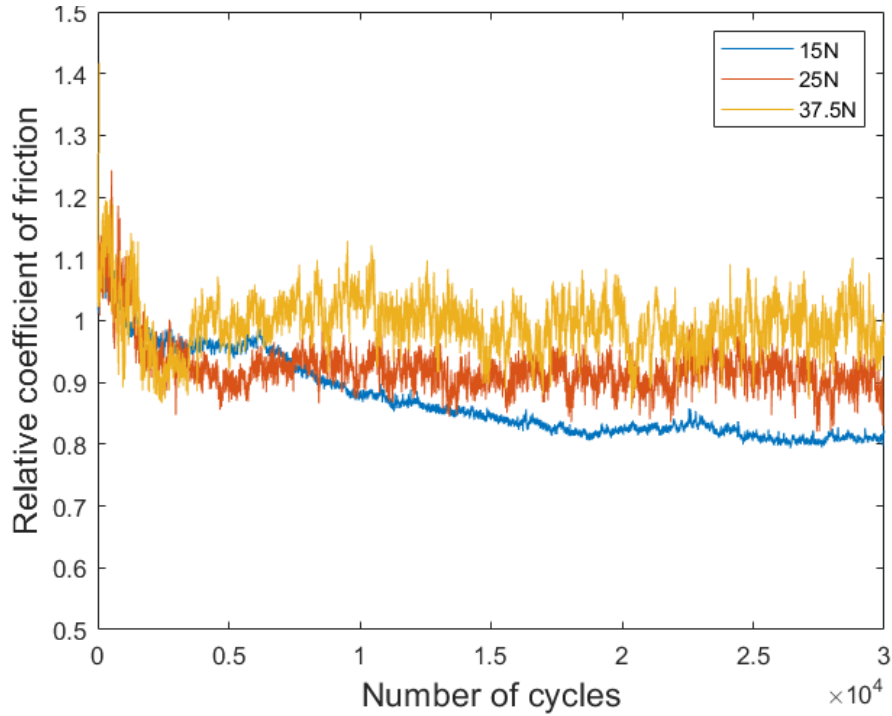
Figure 5-30 The evolution of relative COF over 30,000 cycles at 200˚C at a normal load of 15, 25 and 37.5N on Haynes 25 like on like combination
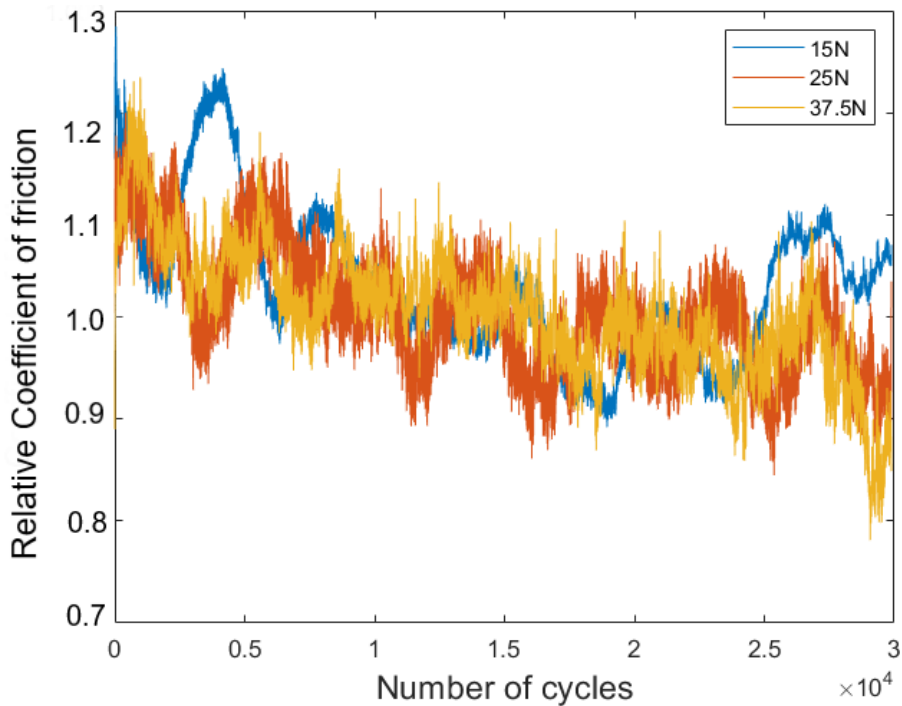
Figure 5-31 The evolution of relative COF over 30,000 cycles at 400˚C at a normal load of 15, 25 and 37.5N on Haynes 25 like on like combination
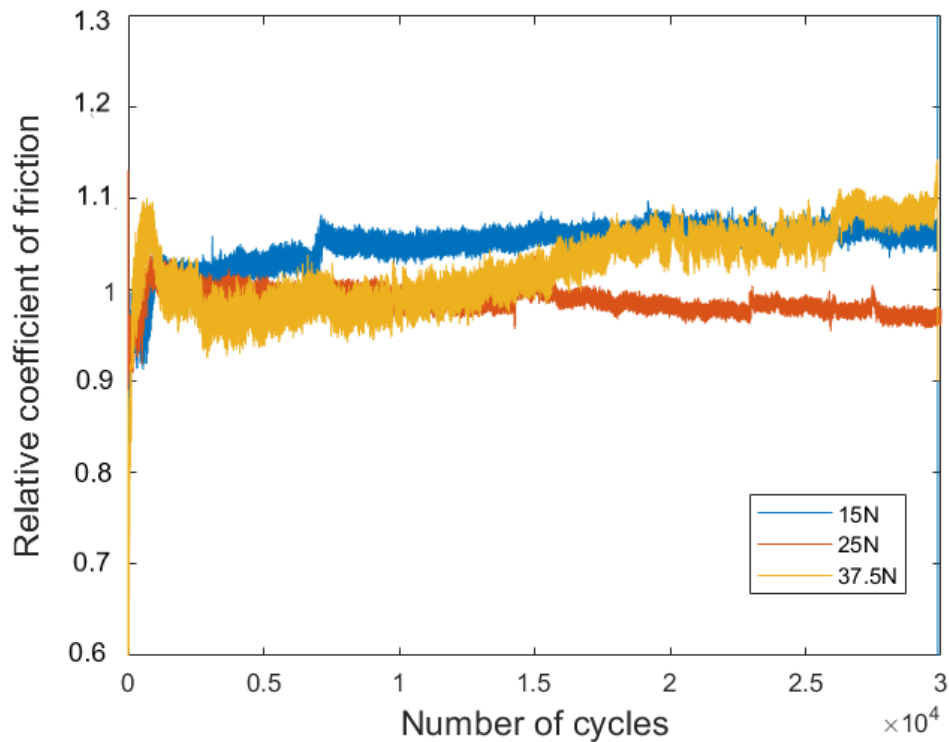
Figure 5-32 The evolution of relative COF over 30,000 cycles at 600˚C at a normal load of 15, 25 and 37.5N on Haynes 25 like on like combination

5.5.3 Surface topography

5.5.3.1 SEM images

Detailed images of the oxidised regions can be seen on Figures 5-33 and 5-34. At the lowest temperature, the images show a very rough surface with adhesive layers and deformed area. As the temperature is increased, transient oxide layers can be seen. At 400ºC, the intermediate load of 25N displays a thin oxide layer with cracks and a mix of large/fine debris on the edges. At the highest temperature a continuous smooth glaze layer is seen at all load conditions. The trend observed in Haynes 25 samples are similar to C263 where a continuous glaze is seen only at 600degC. This further highlights the role of energy availability and diffusion rates (both Haynes 25 and C263 have a high % of Co). The differences in the number of debris seen can be explained with differences in the microstructure of each material which in turn affects the diffusion rate.
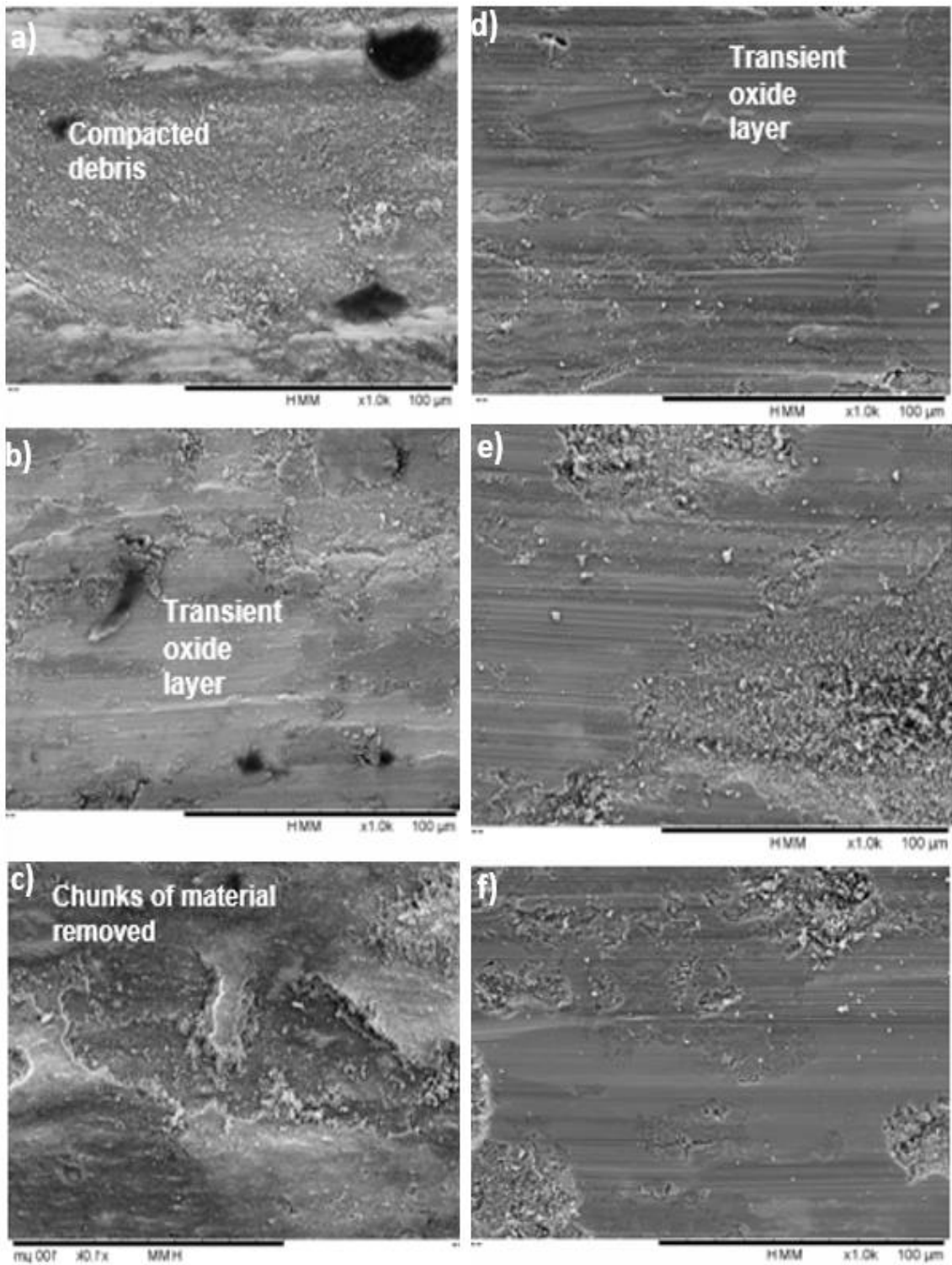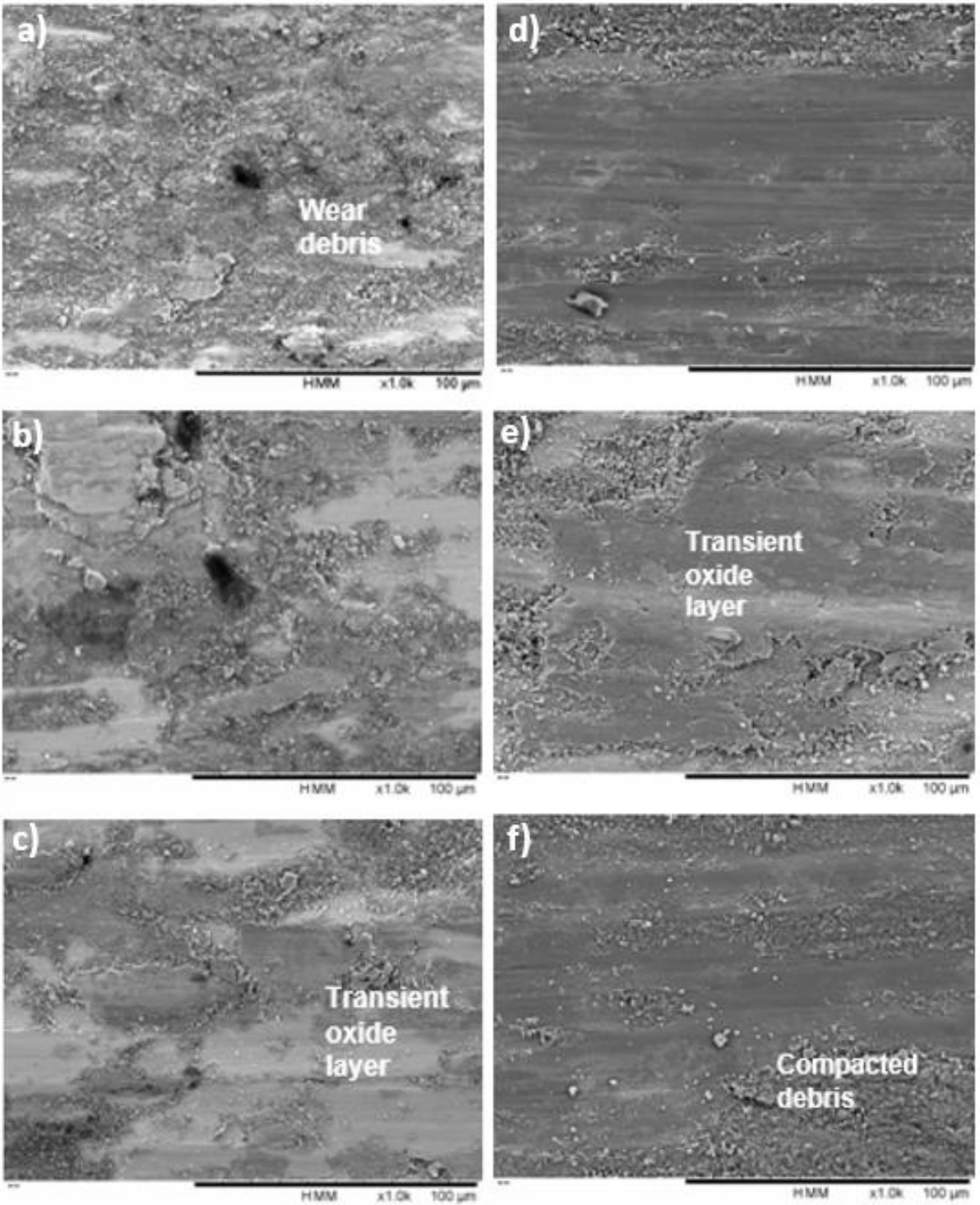
Figure 5-33 SEM images obtained from the oxidised regions on the Haynes 25 samples at x1000 magnification. a,b,c from 200ºC tests and d,e,f from 400ºC tests at and normal load of 15,25 and 37.5N respectively.
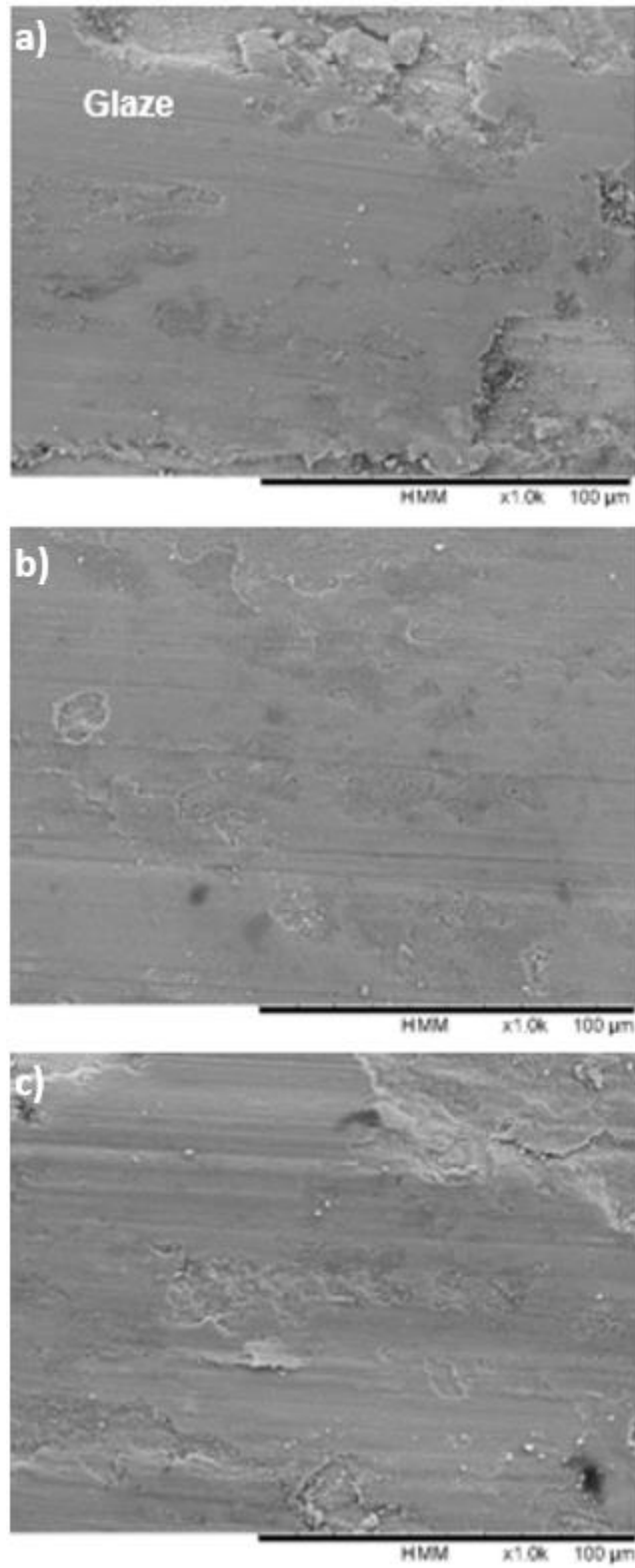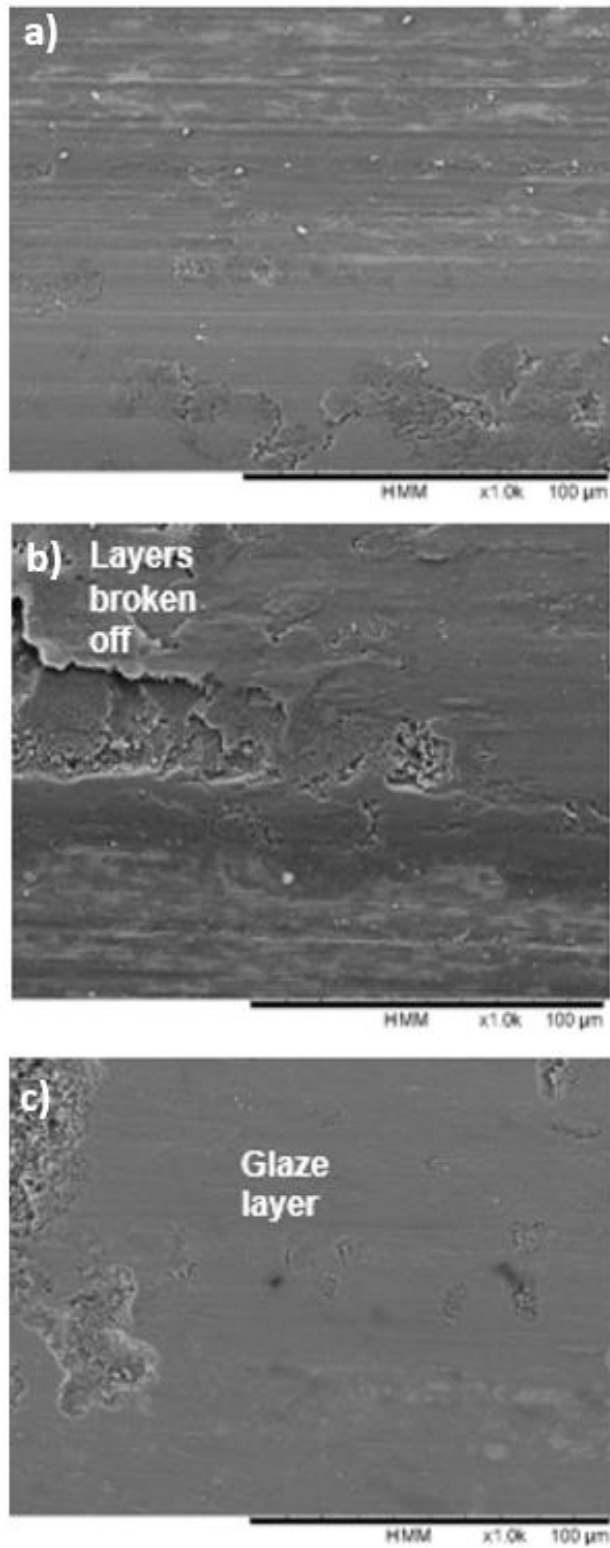
Figure 5-34 SEM images obtained from the oxidised regions on the Haynes 25 samples at x1000 magnification. a,b,c from 600ºC tests at a normal load of 15,25,37.5N respectively.

The sectioned images of the Haynes 25 wear scars are shown in Figure 5-35. At 200ºC, the images shows no sign of oxide layers or MML present, this was reflected on the optical images as well, where the wear scar displayed long striations and mechanical wear. This is likely to be due to severe wear caused by metal to metal adhesions leading to material removal. As the temperature is increased, there is more energy available which allows more diffusion and oxidation. This leads to generation of a mechanically mixed layer and debris being on the surface. Even though, more diffusion is occurring, the rate of breakdown is higher than the rate of generation (as evidenced by the highest wear volume at 400ºC). At 600ºC, a thin layer of glaze is seen and compacted debris as the top layer, this indicates that more debris are to be sintered increasing the thickness and wear resistance of the layers. Since Haynes 25 is a Co-based alloy, and has a higher activation energy, by increasing the temperature, the activation energy is achieved leading to more compaction and sintering of the layers.

200⁰C — Debris layer — N x2.5k 30 μm

400⁰C — MML — N x2.5k 30 μm

**600⁰C** — Compacted debris — Thin layer of glaze — N x2.5k 30 μm
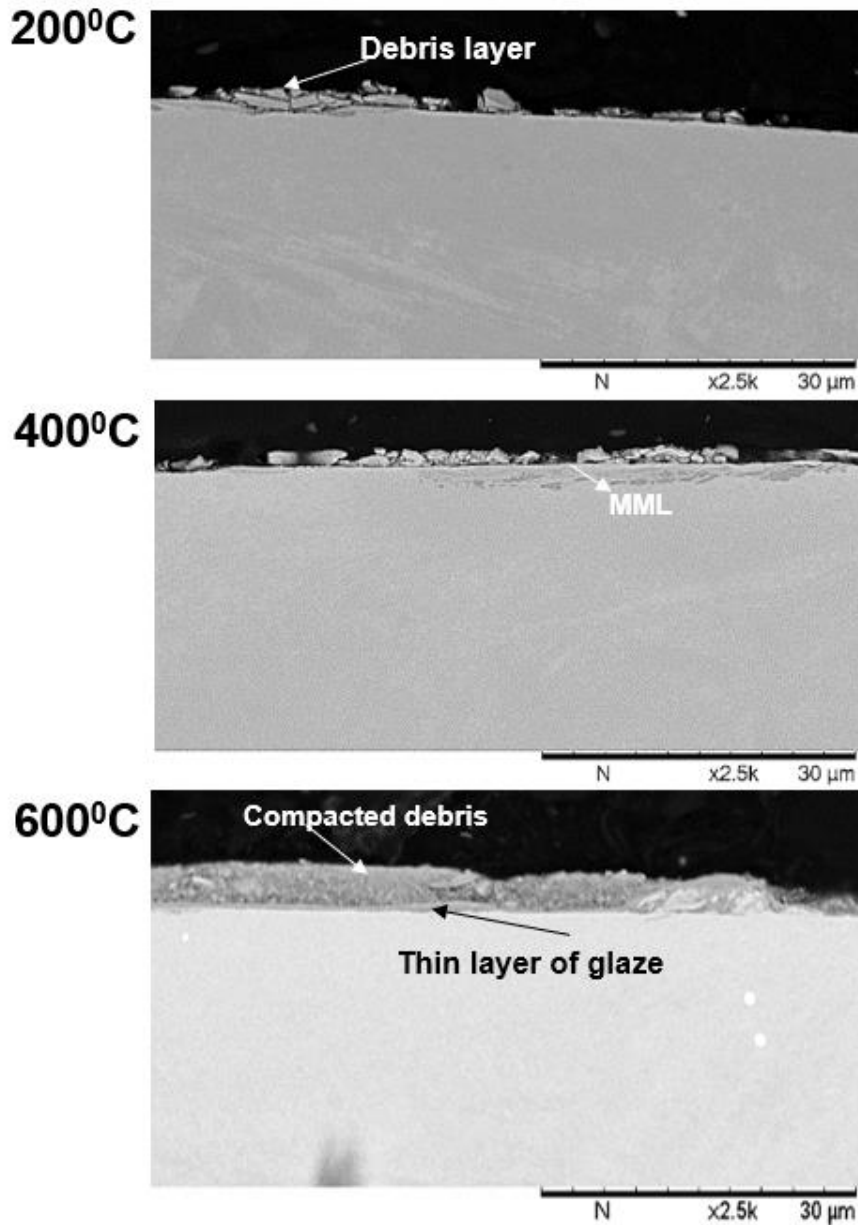
Figure 5-35 Cross sectioned images of the Haynes 25 wear scar at various temperatures at a normal load of 25N.

5.5.3.2   Chemical analysis

Table 5-3 shows the chemical composition of the surface on Haynes 25 at 200ºC, 400ºC and 600ºC. At the lower temperatures (i.e. 200 and 400ºC), there is no changes in the composition even though the wear scars (particularly at 400ºC) have suggested that wear protective layers were forming as patchy regions of oxides were seen and stable COF were observed for short periods of time. The changes in load appear to have no impact on the glaze generation, likely to be due to the fact that the flash temperature rises are not high enough to reach the activation energy. At 600ºC, an

increased Cr and Co concentration is seen. This is because Haynes is primarily consisting of Cobalt which has a higher activation energy than other alloying elements such as Ni, Cr and W. Also, the hardness of Co makes it harder to diffuse elements into the surface as less plastic deformation and cracks are generated preventing oxidation and diffusion.

Normal load, N	Ni/Cr			Co/Cr			Ni/Co		
	200˚C	400˚C	600˚C	200˚C	400˚C	600˚C	200˚C	400˚C	600˚C
Control	0.45	0.45	0.47	2.39	2.39	2.38	0.19	0.19	0.20
15	0.48	0.55	0.56	2.30	2.48	2.80	0.21	0.22	0.20
25	0.49	0.49	0.49	2.34	2.42	3.11	0.21	0.21	0.16
37.5	0.50	0.50	0.47	2.38	2.31	2.83	0.21	0.22	0.16

Table 5.3 Ratio of active elements on the surface obtained from SEM EDX analysis of Haynes 25 samples at various temperatures and load conditions.

5.3.3.3   Surface profiles

Figures 5-36 and 5-37 shows the profiles from the Haynes 25 tests at a normal load of 37.5N. Figure 5-36 shows the results from 200ºC tests where an unstable profile is noticed. This corresponds well with the optical image on the right where only patches of oxidised regions are seen with abrasions indicating wear is occurring. On the other hand, at 600ºC, the scars exhibit a stable region towards the end of the profile suggesting a stable layer is formed as expected for a glaze layer.
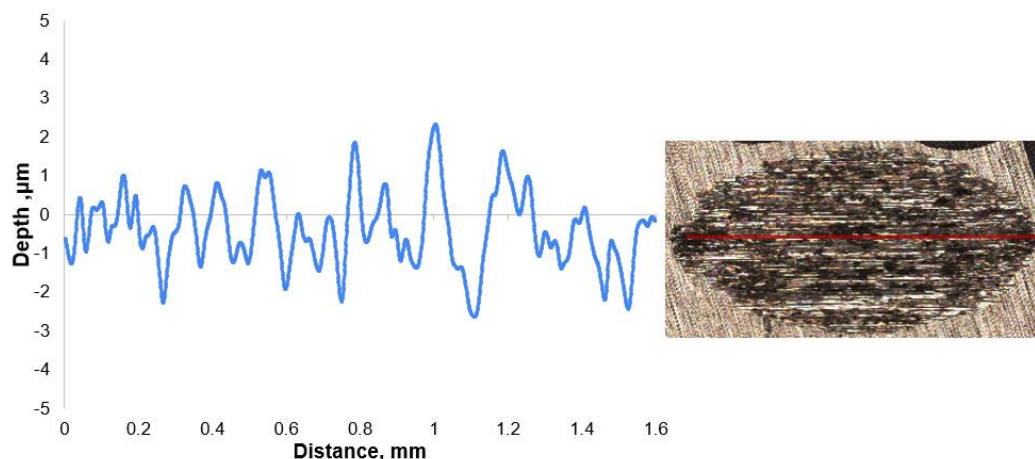
Figure 5-36 Surface profile from Haynes 25 disc samples at a normal load of 37.5N post 30,000 cycles at 200ºC
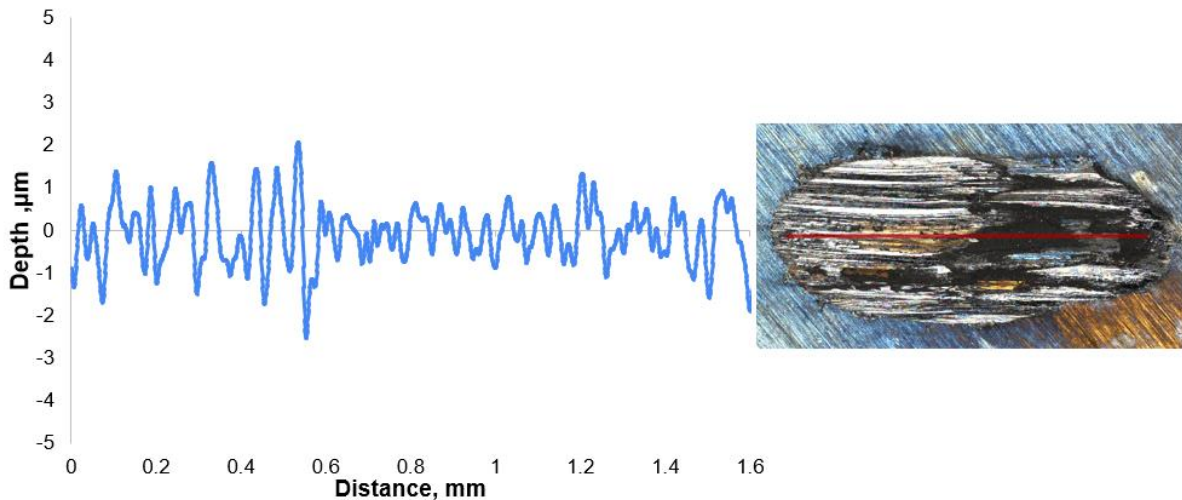
Figure 5-37 Surface profile from Haynes 25 disc samples at a normal load of 37.5N post 30,000 cycles at 600ºC

5.6   Discussion

Reciprocating sliding tests were conducted at various temperatures (ranging from 200ºC to 600ºC) and applied load. The results have emphasised the significance of temperature, load and alloying elements on glaze generation and its effectiveness in protecting the surface. As the temperature is increased, a glossy-smooth surface is noticed with a significant reduction in wear scar dimension and volume. The variations in results between different materials are discussed here.

5.6.1   Influence of temperature

The temperature was varied during the like on like combination test at a normal loading ranging 15 to 37.5N. The results show evident differences in both wear and friction characteristics.

As the temperature is varied, a clear distinction in wear scar is seen in all the materials. At the lower temperature, an even coverage of oxide regions are seen, however, these 'black' oxidised regions are compacted debris rather than a glaze layer, thus increasing the wear volume. As the temperature is raised, smooth-glossy regions have started to appear on the wear scar suggesting a glaze layer. Moreover, a significant reduction in wear volume is also noticed with increased temperature. This is due to the higher oxidation and diffusion rate of the elements involved increasing the rate of sintering. Between the different materials used in this study, the temperature at which

a glazed surface is observed is different, for instance, In718 has started to form 'patchy' glaze regions even at 200ºC whereas on the Haynes 25 samples, glaze is only seen at 600ºC. This is likely to be because different materials generate glazes at different temperatures because of the changes in oxidation/diffusion kinetics behaviour.

At lower temperatures, although a considerable amount of debris are generated, which reduced wear to some extent by preventing metal-metal contact, wear protective oxide layers are not easily developed or maintained throughout the sliding period. These layers formed at low temperatures are not adherent to the substrate thus metal-metal contact is not fully eliminated and easily broken down.

The trends in the COF displays unstable friction characteristics at lower temperatures and a stable COF at the higher temperature. As seen in Figures 5-6, 5-18,5-30, at lower temperatures (i.e. 200 and 400ºC), there are sharp rises and drops in the COF implying that the layers formed are stable for a small period of time, then break down easily generating more debris (peaks in COF). For example, the COF is only stable for ~2500 cycles at 200ºC and 5000 cycles at 400ºC. At the higher temperature (i.e. 600ºC), the peaks and drops are not seen and the COF is staying stable for more than 15,000 cycles (especially for In718). However, as expected for a glaze from some previous studies, a significant reduction in the overall COF is not observed in this study because the wear scar consists of both glazed and non-glazed regions influencing the COF data. This could also be due to the interaction with oxide debris in the contact [91].

Previous studies have shown that there is a critical temperature, also known as the transition temperature, at which a protective layer is formed. However, below this critical temperature, the layers formed are mechanically unstable and prone to detachment and break up due to the differences in thermal contraction rates of the metal and oxide elements. This results in an unprotected surface at lower temperatures

From this study, the influence of temperature can be categorised into two groups- below and above the critical temperature. Below the critical temperature, an overall reduction in COF is seen because a transient oxide layer forms giving some protection against metal-to-metal contact, leading to less adhesion. However, this also causes a

higher wear volume since transient layers are broken down easily, generating more debris, leads to abrasive wear exacerbating the surface. on the other hand, above the transition temperature, regions of stable COF are observed, with no overall drops, because a glaze layer is formed with similar composition so the adhesion between the surfaces is increased. A significant decrease in wear volume is seen as the glaze layers are not broken down easily, causing less damage to the surface.

5.5.2 Influence of load

Increasing the applied load has both positive and negative consequences depending on other important factors that influence the glaze generation process such as the material composition, sliding speed, temperature, etc.

Generally, increasing the applied normal has a positive influence on the glaze generation process by increasing surface and contacting temperatures [38] [40] [92] [93]. Increasing the load leads to plastic deformation and cracks on the surface which aid in the adsorption of oxygen onto the surface promoting the oxidation of the subsurface layers. This leads to a higher rate of glaze generation. The increased load causes greater stresses, which in turn leads to an increased likelihood of producing debris. The same is evident in this study, and it is particularly seen on the Haynes 25 samples at 200ºC where at the lower load (i.e. 15N), the wear scar demonstrates evidence of mechanical wear with scuffing and worn edges, but, as the load is increased, a slightly oxidised surface can be seen on top of the striations with a more rounded edge. This is probably due to rises in flash temperature increasing the oxidation of the surface and debris as increasing the load increases flash temperature. Additionally, the time required to generate these oxides has decreased as the load is increased, presumably associated with a faster rate of oxidation and sintering as the contact temperature is increased due to the load. For instance, C263 at 200ºC, took around 5000 cycles to reach a stable oxide region at 25N whereas, at 37.5N, the stable oxide regions were seen at 2500 cycles.

One of the negative consequences of increasing the load is that as the load increases, the size of the wear debris is also increasing, meaning it will take longer to break down the debris and some of the 'larger' debris is pushed out of the contact, thus increasing wear volume. For example, In718 has shown that an intermediate normal load of 25N

is slightly better than a higher load (as reflected in the wear volume and COF data). This suggests that the rate of breakdown is greater than the rate of formation of glaze.

Previous investigations on varying load have revealed that mechanical wear can be represented with a linear trend in wear volume as the load is increased, and an exponential rise in wear volume if oxidative wear is present. In the present study, different materials show a slightly different response. For instance, In718 presents a linear trend at room temperature, as the temperature has increased a reduction in wear volume is seen between the lower loads and a slight rise as the load is increased. On the other hand, C263 displays mechanical wear with unstable oxide up to 400ºC (and normal load of 25N), beyond which there is a clear reduction in wear volume suggesting a protective oxide layer is formed. Haynes 25 samples display the greatest variation in wear behaviour with varying load with mechanical wear observed at lower temperatures (RT and 200°C) with increasing load, while an exponential increase in wear volume is observed at 400°C due to oxidative wear and the ineffective formation of a glaze layer. Finally, at the highest temperature tested (i.e. 600ºC), the wear volume has decreased with increasing load indicating a wear protective layer has formed, protecting the surface from damage.

It can be concluded that increasing load has a minimal effect on materials with lower activation energy such as IN718 and C263. This is also highlighted by the flash temperature calculations (see Section 3.3.1) which have shown a normal load of 25N will only increase the surface temperature by approximately 40ºC, which may not be enough to generate a glaze layer.

5.5.3 Influence of alloying elements

The composition of the glaze layers formed on the different materials at various load and temperatures are analysed using SEM-EDS to examine the influence of alloying elements. It is seen that at different temperatures the composition of the layers have changed depending on the material leading to variations in friction and wear characteristics.

Table 5.4 shows the main oxide composition of the glaze layer formed at different temperatures at a normal load of 25N. As seen in the table, the composition of the layers have changed with temperature. On the In718 samples, a NiFe (Ni dominant) layer is formed at 200ºC, this is likely the reason for significant reduction in wear

volume as iron oxide formed above 200ºC seems to have better cohesion properties. As the temperature is increased, further iron oxide dominance is observed on the composition, and finally, Cr dependence at the highest temperature. This is because different elements have different activation energy resulting in different diffusion rates. An effective glaze is generated above 200ºC, this links well with the wear scar and volume seen as smooth glossy surface can be seen and drops in wear volume.

On the other hand, C263 exhibits a NiCr layer until 400˚C, suggesting diffusion of Ni and Cr into the surface. One of the other main elements that makes up C263 is Co, and the diffusion of Co is not seen until the temperature is raised to 600˚C. This indicates that Co requires greater energy for diffusion. Previous studies have shown that Ni and Cr formed under certain conditions have poor sintering and adhering properties. The results from Haynes 25 show that there is no change in the composition at 200ºC when compared to the base metal. As the temperature is increased, Ni depletion is seen (almost eliminating Ni presence) at higher temperatures and a Co-Cr layer is seen. As it was previously found that a Co and Cr layer generates an effective glaze, this correlates well with the wear volume seen and scar seen.

	IN718	C263	Haynes 25
200ºC	Ni-Fe	Ni-Cr (>Cr)	Co-Cr-Ni
400ºC	Fe-Ni	Ni-Cr	Co-Cr
600ºC	Cr-Ni	Co-Cr	Co-Cr (>Co)

Table 5.4 The composition of glaze layers formed at various temperatures on In718, C263 and Haynes 25 at a normal load of 25N.

Between the different load conditions used, a significant difference is not seen in any of the materials. This outcome has emphasized the importance of the composition of glaze layers in determining the efficiency of these layers. As seen from the previous studies and this study, the Co and Cr dependent layers are found to be more effective in reducing wear, this is likely due to the fact that the Co-Cr layers adhere to the surface better. Even though Ni-Cr layers are seen at lower temperatures on both IN718 and C263, the oxides formed at different temperatures have different thermal contraction rates, so the detachment can be accelerated at lower temperatures leading to more wear.

5.7   Summary

This chapter has shown that temperature and the composition of the layers have the greatest influence in the effectiveness of the glaze layers generated during sliding. The results from the friction and wear studies show that:

- Distinctive wear and friction behaviour is seen with varying temperature and load conditions at different materials.

- At lower temperatures, a higher wear volume and drops in COF (but unstable) is observed. This is due to less adhesion between surfaces because of the transient oxide layer formation and its break-down resulting in debris in the contact, which in turn prevents metal-metal adhesions. This is not beneficial as the debris act as third-body particles leading to abrasive wear, hence, higher wear volume occurs.

- At higher temperature, a significant drop in wear volume and stable COF for longer periods of time (but an overall rise in COF is observed). At higher temperature, shiny, smooth glaze layers are generated and the composition of both layers are the same or similar. This results in higher adhesion between the surfaces, thus the rise in COF. The glaze layers that are generated at higher temperatures are adherent and wear resistant reducing the wear volume.

- The response from changing the load is different on different materials. A linear trend in wear volume is observed when there is no effective oxide layer present, and an exponential trend when oxidative wear is occurring. The Haynes 25 alloys showed a drop in wear volume with increasing load when a wear resistant glaze layer is present. However, the Ni based alloys presented the lowest wear volume at an intermediate load (400 and 600ºC), likely to be because there is not enough time between the strokes to breakdown the debris, as larger debris are produced at higher loads.

- Between the temperature and load, the results shows that a higher temperature has a higher effect on the glaze generation. The flash temperature rises are not sufficient enough to achieve the required activation energy.

- Different chemical composition of layers is seen at different temperatures. NiCr layers have resulted in oxidative wear as both Ni and Cr oxides exhibit poor adhesion properties. CrFe and CoCr oxides present mean that a wear resistant layer is formed, leading to reductions in wear volume.

Chapter 6   Dissimilar materials

Chapter 6 presents the experimental study of the dissimilar material combination tests conducted at 400 and 600ºC at a normal load of 25N. The tangential load data was recorded throughout the tests, and surface topographical studies were carried out to understand the chemical composition of the layers at different temperatures.

6.1   Introduction

In the previous chapters, the fundamental factors influencing glaze were investigated and discussed. To reduce the complexity of the study, only like-on-like material combinations were used previously. It is clear from the earlier chapters that temperature plays a key role in the glaze generation process. Secondly, the effectiveness of the glaze layer depends on the composition and the thickness of these layers. It is observed that different materials form glaze layers at different temperatures, thus the main objective of this study is to investigate whether dissimilar material combinations could enhance the glaze generation process through the introduction of 'new' alloying elements into the contact and generate an effective glaze even at lower temperatures.

The knowledge of wear and friction behaviour between dissimilar material combinations; whether it is beneficial or disadvantageous to have a certain combination is vital when designing components to ensure that appropriate materials are chosen to achieve design/operational specification. Failure to do so can lead to structural failures, various degradation (corrosion, oxidation etc) leading to premature component failure and risk the safe operation of the engines.

Additionally, it is essential to learn about different material combinations and its wear performance as similar material combinations can lead to severe wear due to adhesive transfer between the materials (see Chapter 1). Due to the high temperatures and load experienced by the aero-engines, the materials are selected so that they meet the demanding requirements of the engines operating conditions. This leads to limited materials being available for certain components, where they often have similar alloying elements, causing adhesive transfer. Thus, coatings are applied on the bulk material to achieve the friction and wear characteristics. However, coatings come with certain risks, such as poor bond between the coating and substrate, defects during application process compromising the integrity of the layer, additional costs/maintenance etc. Hence, knowledge of different material combinations is essential and can improve performance and durability of the engine components.

The test parameters and the set-up are described in Chapter 3, Section 3.4.3. Table 6.1 shows the material combinations used and the temperatures used in this study.

Temperature (˚C)	400, 600
Material combination	• In718 pin and Haynes 25 disc • C263 pin and Haynes 25 disc • In718 pin and C263 disc

Table 6.1 Details the test parameters and the material combinations used in the dissimilar material tests.

6.2   Inconel 718 and Haynes 25

6.2.1   Wear scar analysis

6.2.1.1   Wear scars

Figures 6.1 and 6.2 shows the wear scar acquired from the In718 pin against Haynes 25 disc samples tested at 400 and 600ºC at a normal load of 25N obtained using an optical microscope.
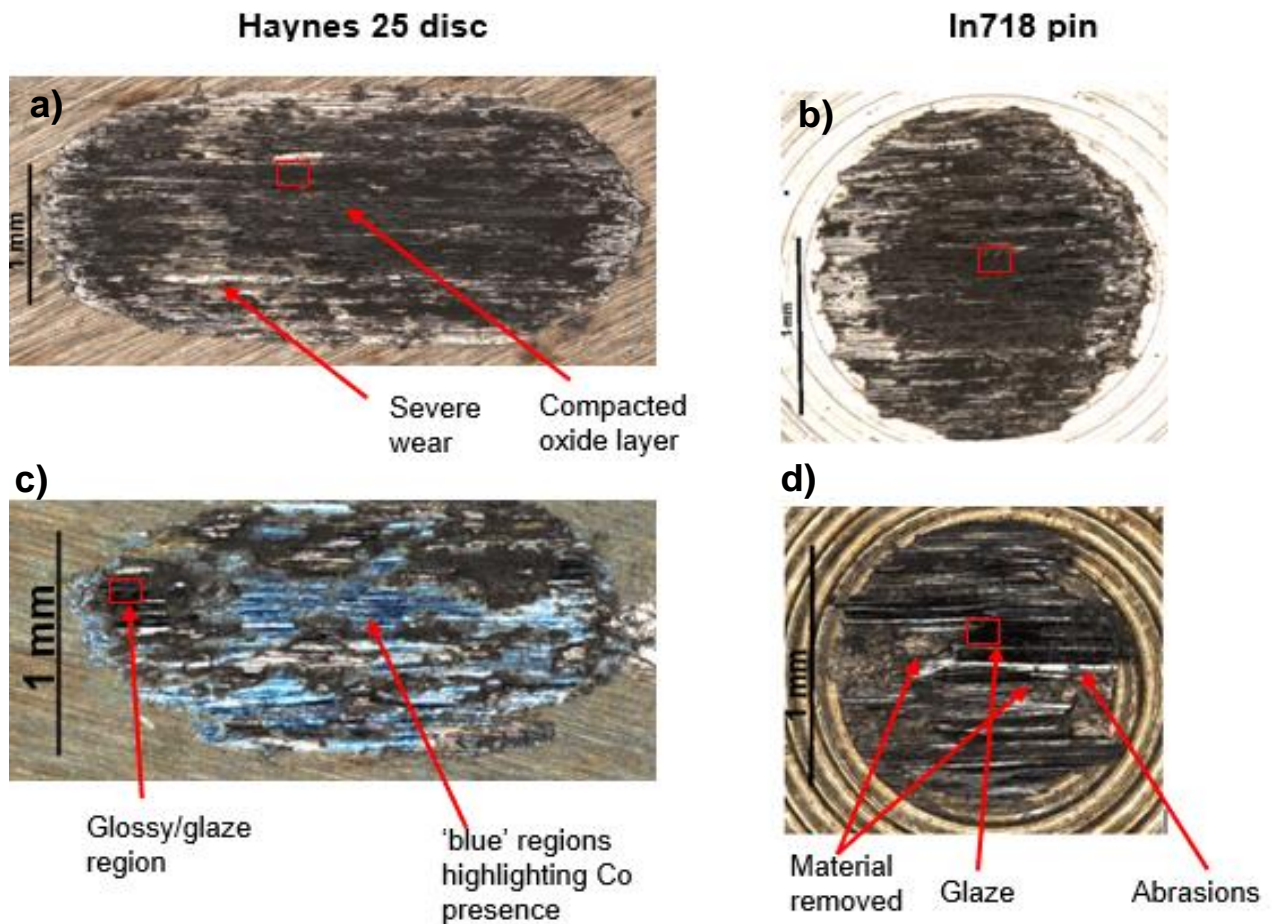
Figure 6.1 The wear scar from tests conducted using Haynes 25 disc and In718 pin and b) at 400 and c and d) at 600ºC at a normal load of 25N.

At 400ºC, the wear scar exhibits an evenly covered oxide layer on both pin and disc. Abrasive marks are visible underneath the lightly covered oxide suggesting that third body interaction and severe wear has occurred. As the thickness of the oxide layer increases, the layers become more wear resistant by preventing metal-to-metal contact. On the pin scar, silver-severe metallic wear regions are visible on the edges. This is likely to be due to reciprocating motion of the pins causing the edges to come into greater contact with the debris, leading to increased interaction between the edges and the debris. At 600ºC, glossy-glazed regions can be seen at the edges. However, severe wear/metallic regions can be seen in the middle of the scar, as highlighted by the 'silver' or 'blue' regions. This suggests that the layers are broken down due to being a thin layer or glaze has not been formed yet. The 'blue' regions indicate the presence of Co, meaning a higher percentage of Co has diffused on to the surface at higher temperature. On the other hand, the In718 pins show an evenly oxidised surface with glazed regions in the middle. As seen in the figure, there are chunks of material being removed from the pin. Moreover, the edges of the pin are worn. This likely to be due to 'harder' oxide particles (Co, Cr) being generated by the disc which in turn act as abrasive particles leading to more wear.

Figure 6.2 shows the SEM images of the regions highlighted in the optical images (see the red square on Figure 6.1). At 400ºC, the wear scar shows metallic wear and adhesive transfers on the disc, whereas a transient oxide layer with fine debris are seen on the edges. With increased temperature a smooth glaze layer is visible on the Haynes 25 disc, however on the In718 pin, abrasive marks can be seen on top of the glaze layer suggesting third body (harder debris particles) interaction from the disc debris. Moreover, the glaze formed on the pin are broken down generating 'rougher' regions.

Between the different temperatures, the key difference is that at 600ºC, the wear scar width has reduced significantly, and glossy regions are visible on the scar. However, the softer material (i.e. In718) shows evidence of broken down glaze layers as a result of abrasive wear at both temperatures.

Haynes 25 disc

a) Metallic wear

HMM x1.0k 100 μm

In718 pin

b) Transient oxide layer

HMM x1.0k 100 μm

c) Glaze

HMMD6.0 x1.0k 100 μm

d)

HMM x1.0k 100 μm

Figure 6.2 Detailed SEM images of the regions of interests highlighted in figure 6.1 (from Haynes 25 against In718 tests. a, b) from 400⁰C and c, d from 600⁰C tests.

6.2.1.2   Wear volume

Figure 6.3 shows the wear volume from both the pin and the disc at varying temperatures obtained by measuring the mass of the pin and the disc before and after the tests.
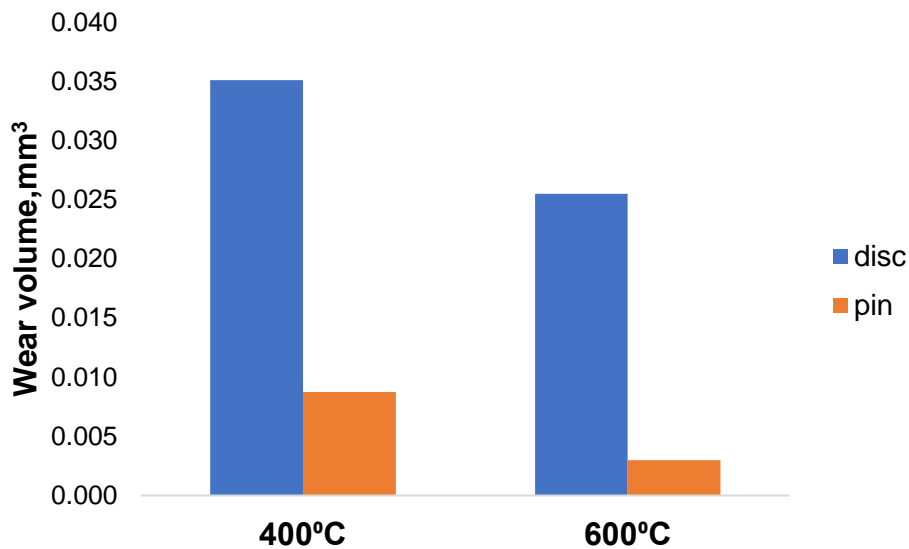
Figure 6.3 Wear volume from both Haynes 25 disc and In718 pin at 400 and 600ºC after sliding for 30,000 cycles.

As seen in the figure, there is an obvious change in the wear volume as the temperature is increased. As the temperature is raised, the wear volume of both pin and disc has reduced, likely to be due to the formation of a wear resistant glaze layer. The rate of drop of wear volume is greater in the pin (In718) when compared with the disc (Haynes 25). This indicates that either an effective glaze layer or a transient oxide layer is formed on In718 pin preventing metal to metal adhesions. Even though, there is evidence of glaze breakdown on the pin scars, the wear volume displays a lower level of wear from the In718, this is likely to be due to the fact that a glaze layer is formed on the In718 (as it has a lower activation energy than Haynes 25), but since the Haynes 25 is 'harder' than the In718, the debris from the disc are causing the glaze to be broken down.

6.2.2 Evolution of coefficient of friction

Figure 6.4 shows the evolution of relative COF at 400 and 600ºC when a In718 pin and Haynes 25 disc is used for tests.
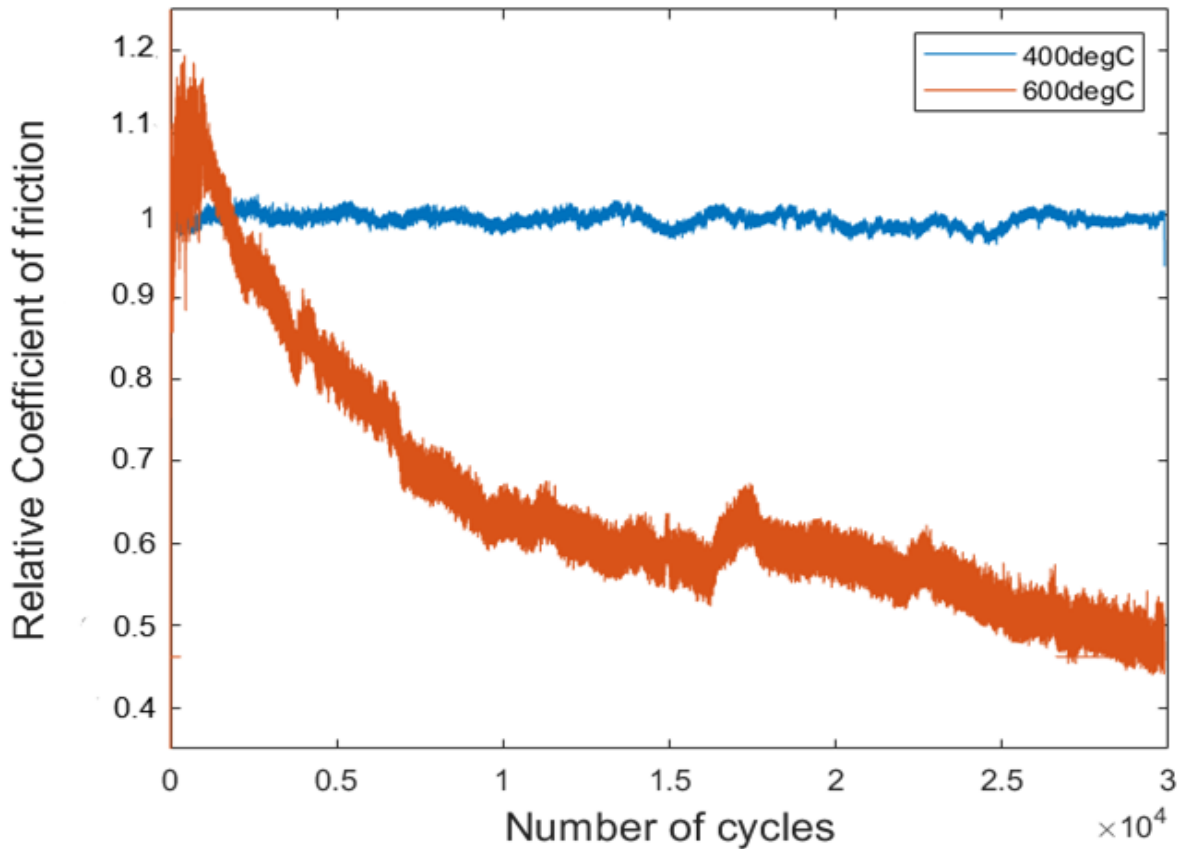
Figure 6.4 Evolution of relative COF as the test is progressed at 400 and 600˚C.

Observable differences in the friction characteristics can be identified at different temperatures. At 400˚C, the COF shows a stable friction behaviour, likely to be the result of debris generated due to severe wear preventing adhesion between the surfaces. At 600˚C, the relative COF has dropped to 0.4, suggesting wear protective layers are generated, preventing surface damage. Since the main alloying elements in the samples are different, the composition of glaze formed on the surfaces are different, resulting in less adhesion between the glazed surfaces leading to reduction in COF.

6.2.3 Surface topography

Figure 6.5 shows the cross sectioned images from the pin and the disc post test at various temperatures acquired using an SEM.
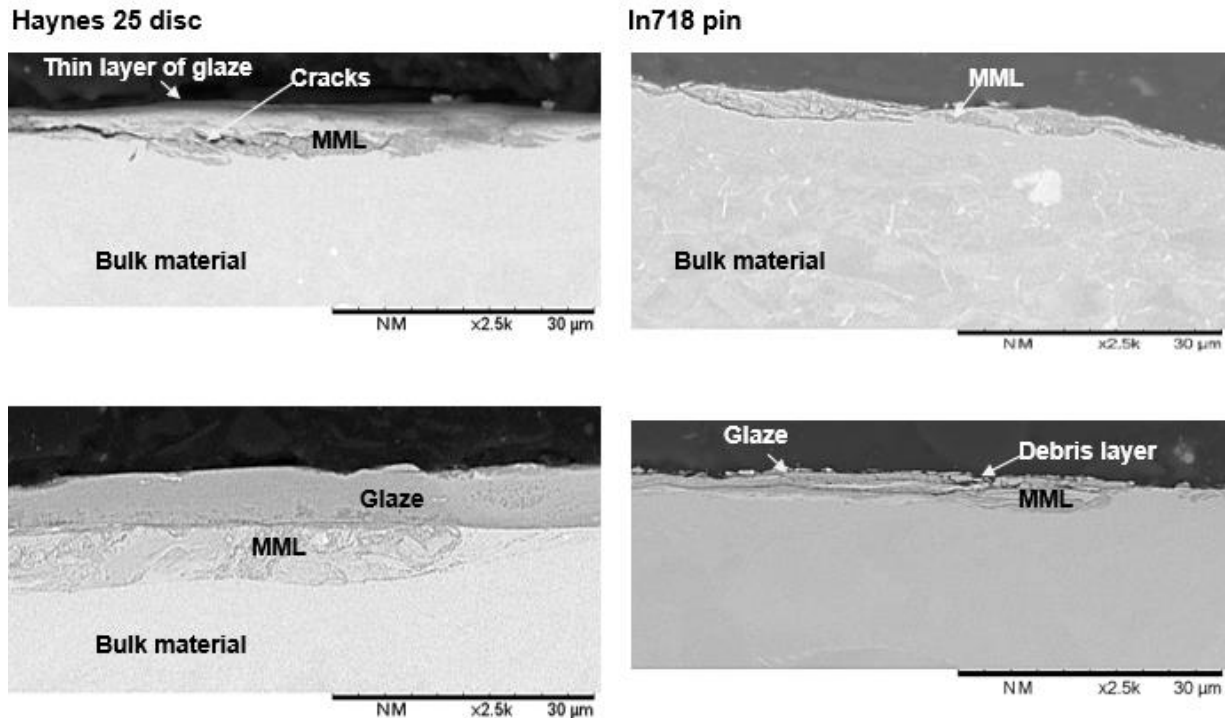
Figure 6.5 The cross sectioned images form the wear scar obtained from Haynes 25 and In718 tested at 400ºC and 600ºC.

The figure shows bulk material, mechanically mixed layer (MML) and glaze layers. At the lower temperature (i.e.400ºC), the wear scar images show a layer of MML on both the pin and disc. Moreover, on the disc, a very thin layer of glaze is seen. Additionally, cracks can be seen along the middle of the MML. This indicates that the MML layers are not strongly adhered on to the bulk material leading to detachment with further sliding. On the pin, no glaze layer is seen and the MML is thin when compared to the disc. This is probably due to Haynes 25 (i.e. disc) debris being 'harder' than the pin, so the layers formed on the pin are easily broken down. Additionally, the disc has higher debris retention capability than the pin leading to increased oxide layer thickness. At the higher temperature, a thick layer of glaze is observed on the Haynes 25 samples, followed by a MML layer. On the In718 pin, a thin layer of MML is seen, with a glaze and debris layer on top. The major difference as the temperature is raised is that the thickness of the layers has increased, leading to a reduction in wear volume as metal-to-metal contact is prevented. Between the different materials, even though the disc seems to have a 'thicker' glaze layer forming, the rate of drop in wear volume

is higher in the pin at higher temperature, this is likely to be because the MML and the glaze on both samples are different leading to a reduction in adhesive wear with the pin being more affected initially due to being softer.

Table 6.2 shows the elemental composition of the layers formed at both 400 and 600˚C. The 'control' data shows the samples prior to the test. The Haynes disc exhibits a NiFe layer at lower temperatures and a CrFe oxide layer at high temperatures. Haynes 25 consists of a very small amount of iron (>5%), and the increase in iron oxide is likely to be due to transfer from the In718 pin. The iron oxide that forms above 200ºC has been found to have good adhesive properties making the layers stable and effective. Moreover, the percentage of iron oxide has increased with temperature indicating that the diffusion rate has also increased with the temperature.

Similarly, the In718 pin generates a CrFe oxide layer. The content of Cr has increased, and this could have been aided by the transfer of Cr atoms from the Haynes 25 as it is made up of 20% of Cr.

Haynes 25					In718 pin				
	Co/Cr	Ni/Co	Ni/Cr	Co/Fe		Ni/Cr	Ni/Fe	Cr/Fe	Ni/Co
Control	2.38	0.20	0.47	26.03	Control	2.58	2.86	1.14	0.00
400˚C	2.20	0.32	0.70	12.75	400˚C	1.08	1.09	0.99	0.58
600˚C	1.06	1.83	1.94	1.73	600˚C	1.20	0.49	2.44	0.77

Table 6.2 The ratios of the main alloying elements (i.e., Ni, Cr, Co, Fe) that forms the glaze layers on Haynes 25 (left) and In718 (right) at varying temperatures.

6.3   C263 and Haynes 25

6.3.1 Wear scar analysis

6.3.1.1   Wear scars

Optical images of the wear scar from the test with a Haynes 25 disc against a C263 pin can be seen in Figure 6.6. As seen in the figure, distinctive features can be seen on both the pin and the disc as the temperature is changed. At the lower temperature, the wear scar displays signs of oxidative wear, as there is an even oxide layer on both the pin and disc samples. However, the disc samples exhibit greater variation in coverage as regions of lightly oxidised regions and dense oxide regions are visible.

This indicates that the thickness of this oxide layer is different at various regions within the contact area. The silver/grey regions suggest that severe wear has happened either as a result of the oxide layer being broken down exposing 'fresh' unoxidised metal or an effective oxide layer has not been formed yet. As the temperature is increased, the obvious feature in the disc wear scar is that there is a blue tint on the surface, this is an indication of Co diffusion into the surface. The rate of diffusion has increased as well as the activation energy for Co diffusion must have been achieved, resulting in more Co atoms diffusing into the surface. Also, patchy glaze regions are seen near the edges of the scar. Likewise, at the lower temperature on the C263 pin scar, an even coverage of oxide is seen with some glossy/glazed patches observed. At the higher temperature, the glazed surface is more obvious, however, there is evidence of scuffing and ploughing due to debris interaction. This can be exacerbated as some of the debris generated by the disc is considerably 'harder' than the pin sample as Haynes 25 has a higher hardness than C263 (see chapter 3 for details).
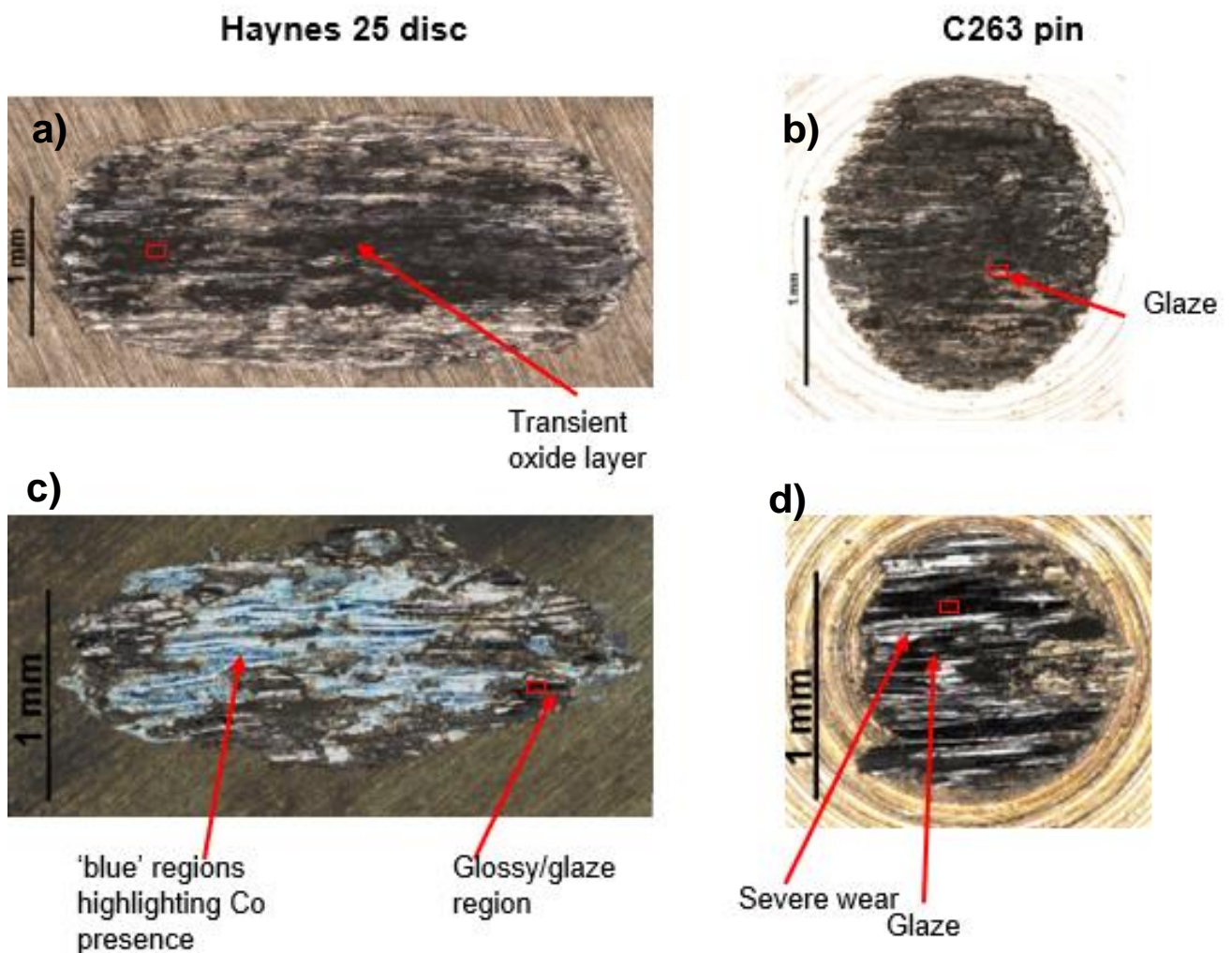
Figure 6.6 The wear scar from tests conducted using Haynes 25 disc and C263 pin at 400 (a and b) and 600ºC (c and d) at a normal load of 25N.

Detailed images of the regions of interests can be seen in Figure 6.7. At lower temperature (i.e. 400ºC), the scar shows a (fine) compacted debris and transient oxide layer. Previous studies have shown that once an oxide layer is formed, the heat transfer from the contact surface to the bulk will be slowed down reducing the thermal softening near the subsurface region. Therefore, when a weak glaze or a transient oxide layer is formed on the surface, it may not be sufficient enough to hinder the heat transfer causing more thermal softening which in turn cannot support new oxide layers that are forming and causes wear [91] [93]. Similarly on the pin sample, transient oxide layers are seen with adhesive layers, probably during the severe wear stage. As the temperature is increased, smooth-glossy continuous layers are seen on the Haynes 25 samples whereas on the pin sample there is evidence of both glaze and broken down layers.
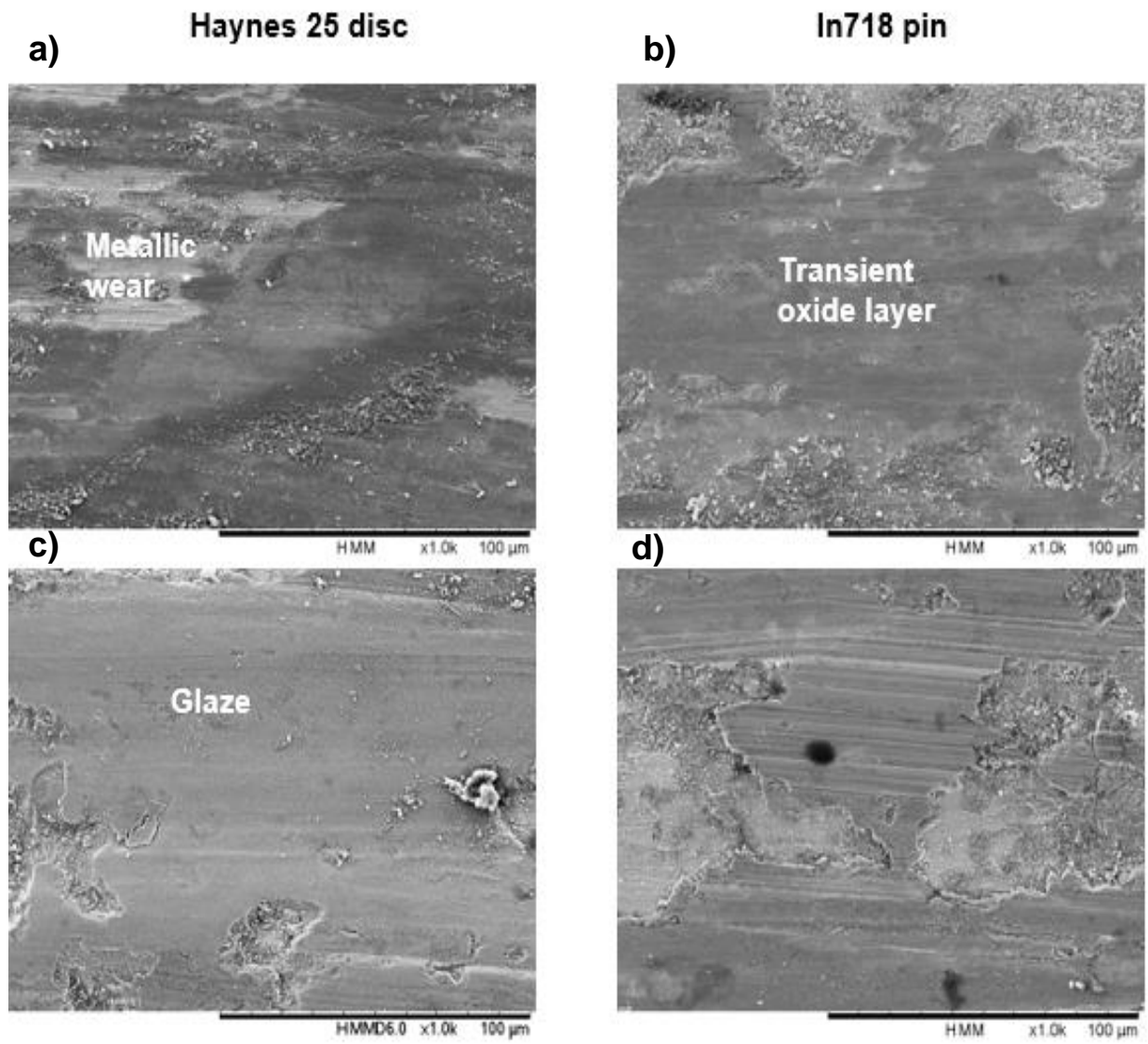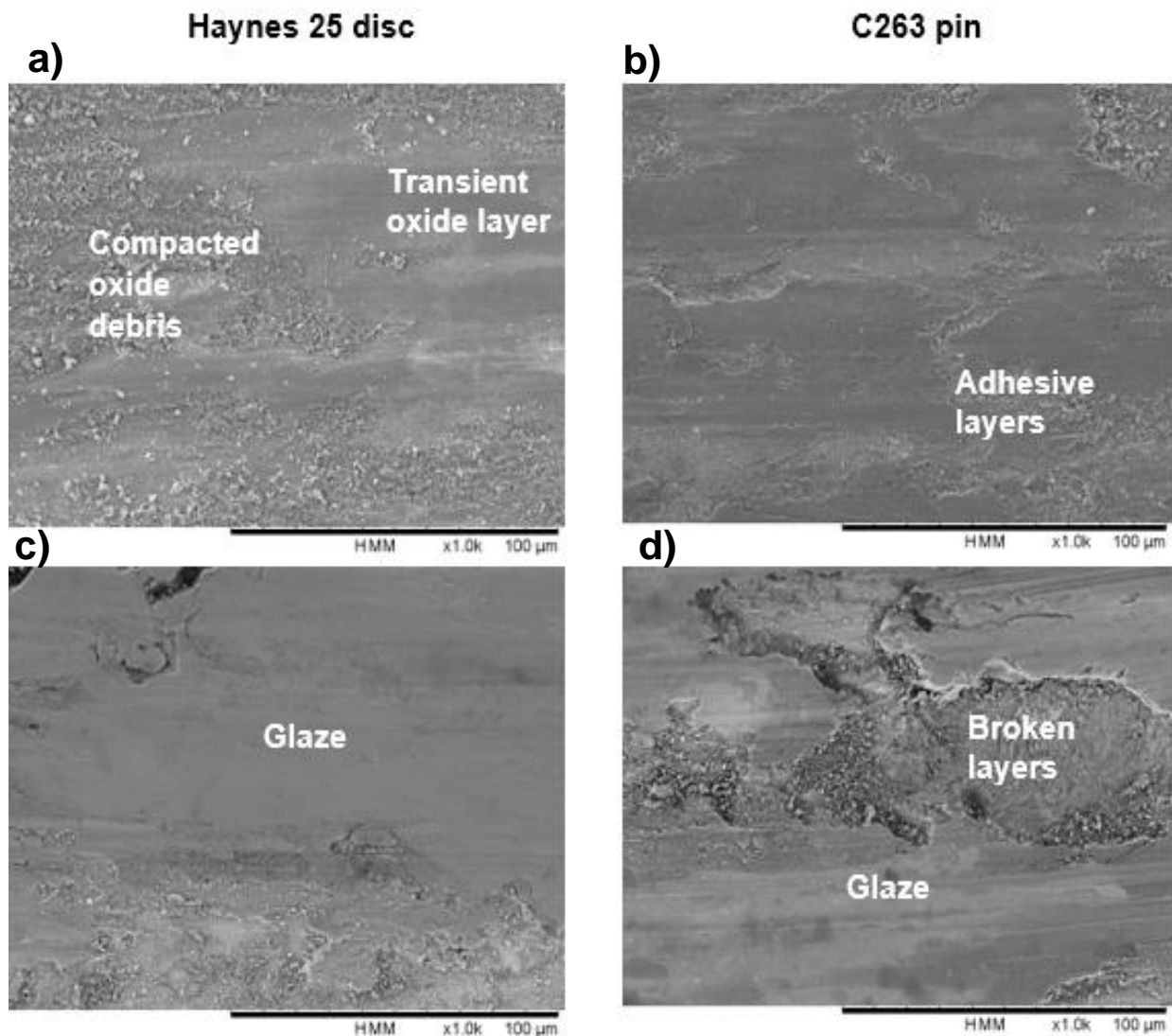

Figure 6.7 Detailed SEM images of the regions of interests highlighted in from Haynes 25 against C263. a) b) from 400˚C tests and c)d) from 600˚C tests.

Between the different materials, both materials form glaze layers at the highest temperature, however, on the C263 samples there is evidence of material removal whereas more continuous glaze layers are seen on the Haynes 25.

6.3.1.2 Wear volume

Figure 6.8 shows the wear volume from Haynes 25 against C263 tests at 400 and 600ºC. As the temperature is increased, a significant drop in wear volume can be seen. At the lower temperature, oxidative wear is occurring (as seen in Figure 6.6 and 6.7). This suggests that a wear protective glaze layer is formed on both pin and disc at 600ºC. The fact that the rate of drop is greater on the Haynes 25 sample, further supports a view that oxidative wear is happening at 400ºC, and a transition is occurring from severe oxidative to mild wear at higher temperatures.
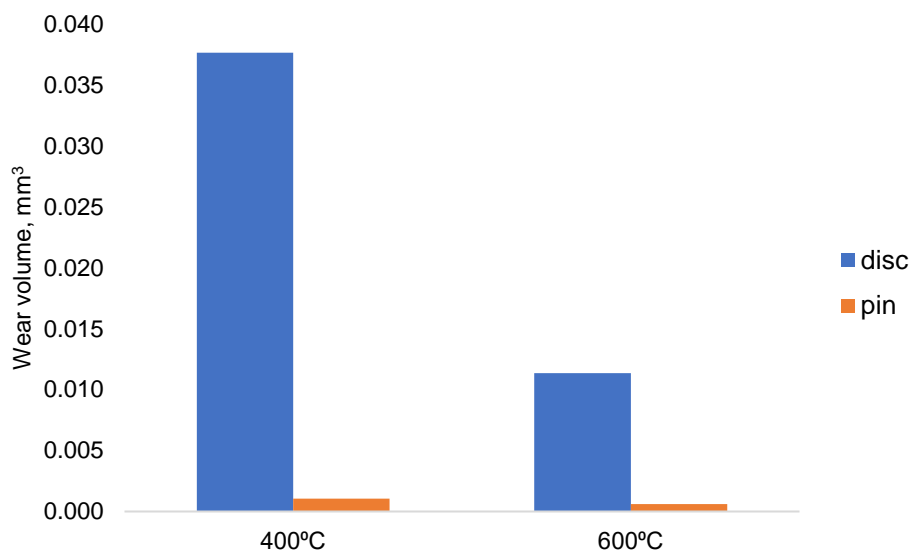
Figure 6.8 Average wear volume from Haynes 25 disc and C263 pin at 400 and 600ºC.

6.3.2 Evolution of coefficient of friction

Figure 6.9 shows the evolution of relative COF as the test progresses. As seen in the figure, at the lower temperature the COF shows a stable region after an initial unsteady period (lasting ~8,000 cycles). The initial unstable region is likely to be caused by the delay in the glaze generation process, as the energy available is insufficient for active elements to diffuse into the surface or oxidation rate is lower. Therefore, over time, the debris will get an opportunity to be oxidised and compacted to form a glaze layer.

Whereas, with increased temperature tests, a rise in the overall friction is seen with some steady state regions towards the end of the cycle. It is probable that this is the result of adhesion between the glaze layers formed on the surfaces as the main alloying elements are similar (only the percentage of the elements differs).
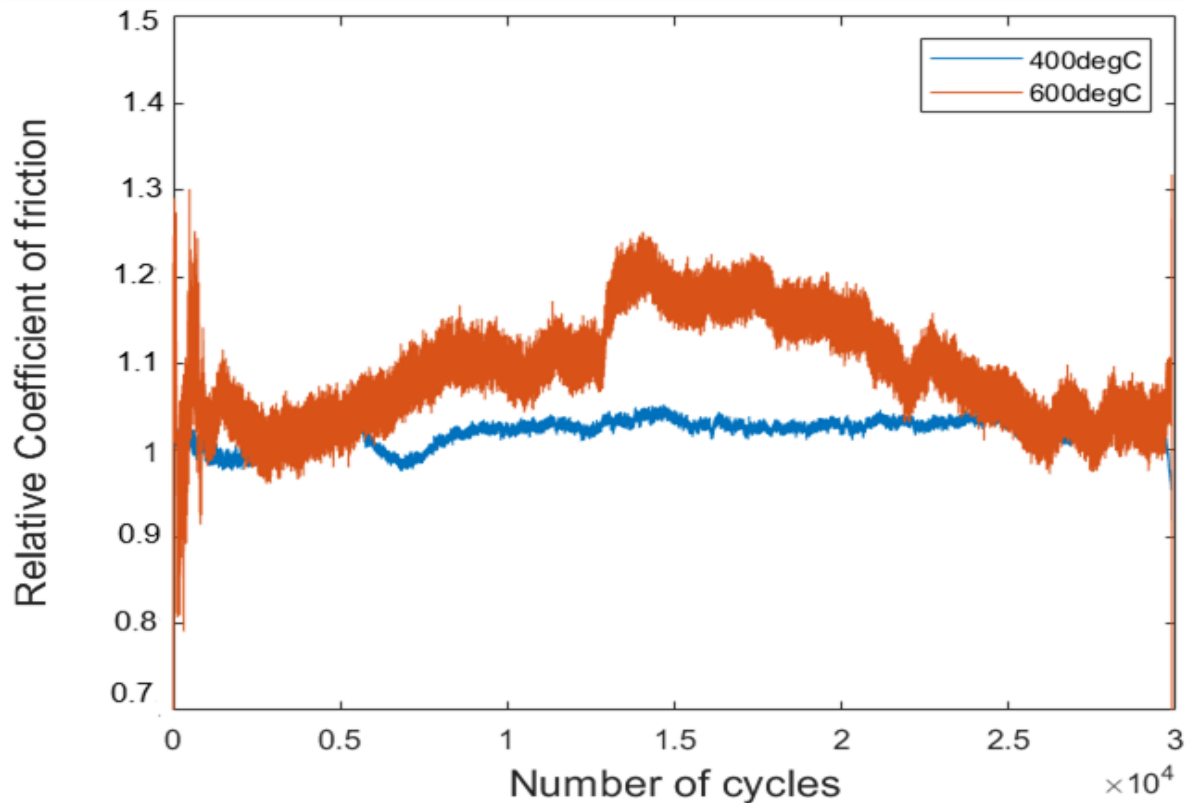
Figure 6.9 The development of relative COF as the test progresses as Haynes 25 disc is rubbed against C263 pins at 400 and 600ºC.

6.3.3 Surface topography

The cross sectioned images of the wear scar from the Haynes 25 against C263 can be seen in Figure 6.10. The thickness of layers are different on the materials at different temperatures. At the lower temperature, the Haynes 25 samples show cracks and 'large' debris on the wear track. There is no glaze or MML layers present suggesting active diffusion of elements is not occurring. The C263 pin sample exhibits a thin layer of MML with glaze on top. Debris are also observed, suggesting both MML and gaze are broken down. This is likely to be because the rate of breakdown is greater than rate of formation of oxide layers leading to increased wear volume and surface damage. As the temperature is increased, a thick MML layer is seen on the Haynes 25 sample, with glaze and debris as the top layer. Similarly, the pin samples consist of a MML and a thin layer of glaze, but the thickness observed on the MML is

less than half of that observed on the disc sample. Also, cracks can be seen indicating that the MML is not adhered properly and is about to detach from the bulk material.
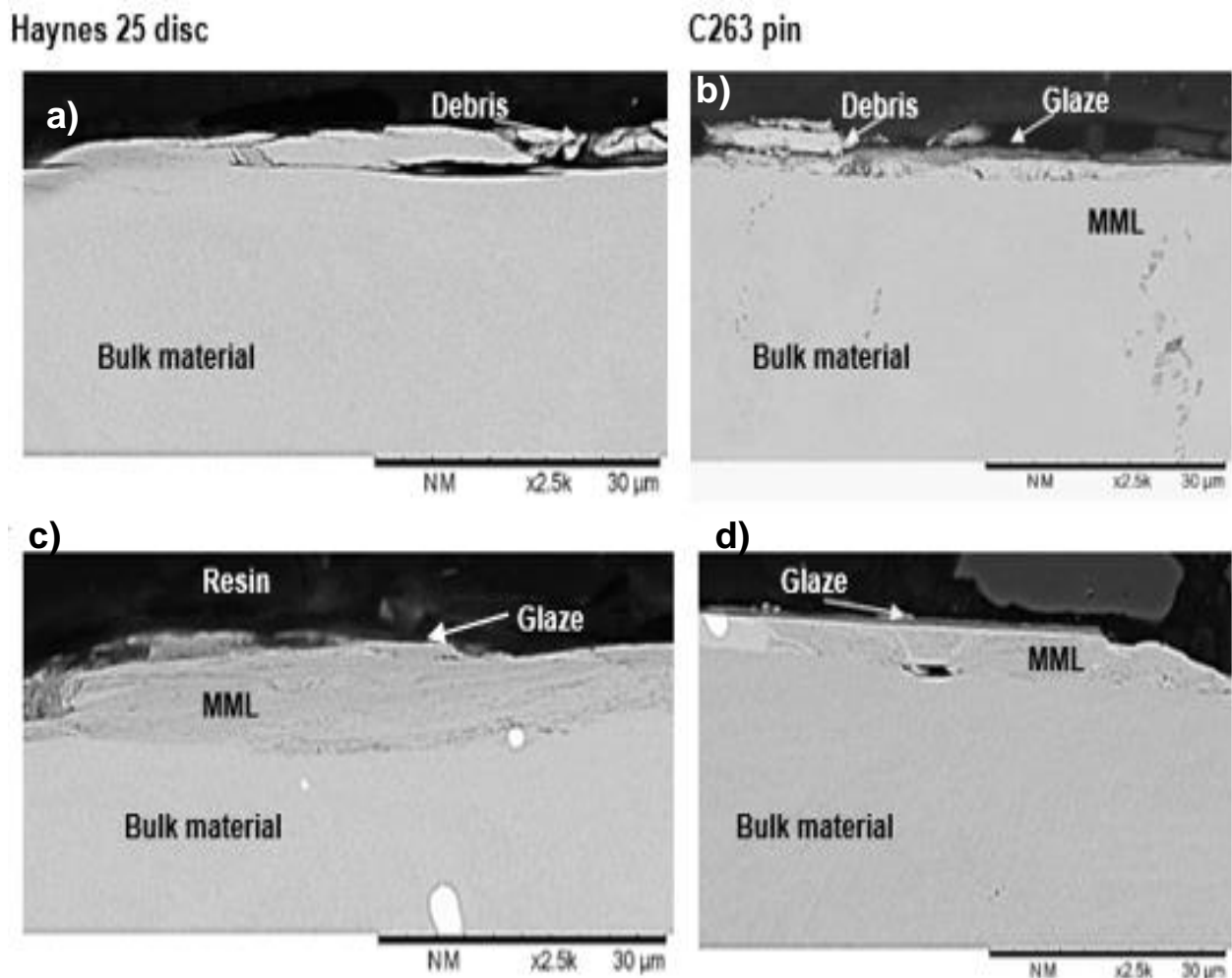
Figure 6.10 Cross sectioned images of the Haynes 25 samples tested against C263 pin at 400 (and b) and 600ºC (c and d).

The chemical composition of the layers formed on Haynes 25 and C263 at 400 and 600ºC can be seen in Table 6.3. The control shows the ratio of the main alloying elements prior to the test. On the Haynes 25 sample, which is a Co-based alloy, no major changes in the composition of the layers are shown when compared to the control. This is probably due to the elements not having enough energy to diffuse into the surface to form a dominant layer. As the temperature is increased, a NiCr dominant layer is seen. Since there is only about 10% of Ni in Haynes 25, it suggests that there is some transfer of Ni from the C263 (which is a Ni based alloy). Moreover, the wear volume from the pin is considerably lower, even at 400˚C, this could be the reason

why no changes in the chemical composition were seen on the disc sample at 400ºC as the availability of debris was limited.

On the pin sample, a CoCr dominant layer is seen at both temperatures. As the temperature is increased, the percentage of Ni has reduced and that of Co has increased. This explains why a smooth glossy layer is seen on the C263 samples at higher temperature. In turn, it is possible that the increase in Co could be from the Haynes 25.

HS25 disc				C263 pin			
	Co/Cr	Ni/Co	Ni/Cr		Ni/Cr	Co/Cr	Ni/Co
Control	2.38	0.20	0.47	Control	2.31	0.91	2.54
400˚C	2.23	0.29	0.65	400˚C	1.27	1.73	0.73
600˚C	0.67	3.09	2.08	600˚C	1.16	1.76	0.66

Table 6.3 The ratios of the main alloying elements (i.e., Cr, Co, Ni) that forms the glaze layers on Haynes 25 (left) and C263(right) at varying temperatures.

6.4   Inconel 718 and C263

6.4.1 Wear scar analysis

6.4.1.1   Wear scars

Figure 6.11 shows wear scars from C263 rubbed against In718 tests at a normal load of 25N and at changing temperatures. At 400ºC, the disc samples (i.e.C263) show metallic wear on the edges and oxide layers in the middle of the scar. The pin sample (i.e., In718) displays an even oxide with some indication of severe wear as debris has abraded into the surface. At 600ºC, the glazed regions are seen on both samples. On the C263 disc, the 'blue' tint suggests that there is diffusion of Co at higher temperature which aids in the generation of an effective glaze layer. On the In718 pins, continuous glaze is seen, but there is evidence of material removal and severe wear, likely to be due to debris interaction.

Detailed images of the regions on interest highlighted in the optical images (see Figure 6.11) can be seen in Figure 6.12. At the lower temperature, both samples exhibit severe wear mechanisms, such as adhesive wear, material removal, compacted debris regions etc. adhesive layers are more dominant in the C263 samples whereas

the In718 specimens shows abrasions and broken down layers (transient oxide layers). With increased temperature, a continuous glaze is seen.

C263 disc

a)

Glossy patches

Severe wear

Compacted debris

In718 pin

b)

Severe wear

Lightly oxidised regions

c)

Abrasions

'blue' regions highlighting Co presence

d)

Material removed

Glaze
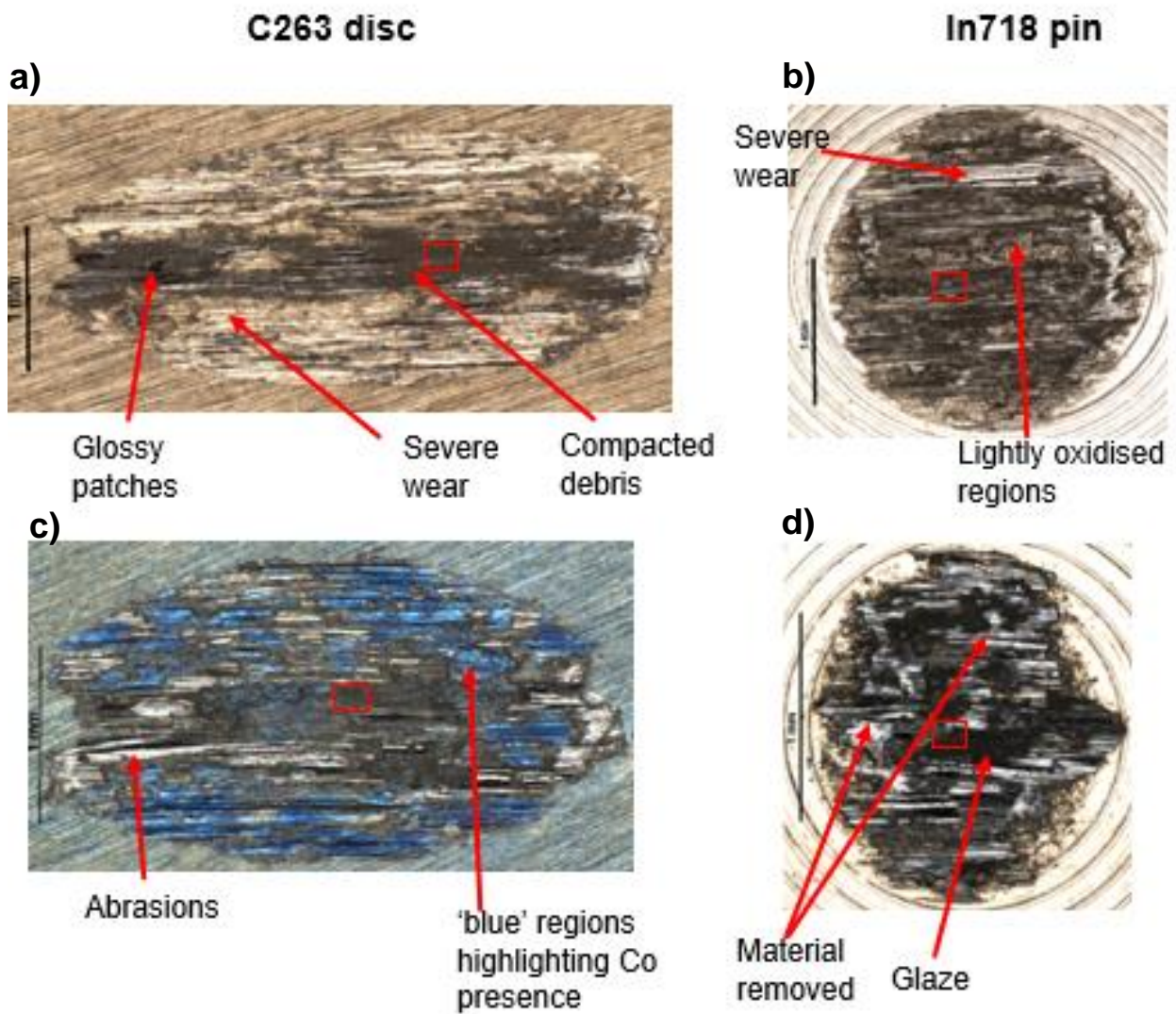
Figure 6.11 The wear scar from tests conducted using C263 disc and In718 pin at 400 (a and b) and 600⁰C (c and d) at a normal load of 25N.

C263 disc

a)

Adhesive layers

In718 pin

b)

Severe wear

Compacted debris

c)

Abrasions on top of glaze

d)

Glaze
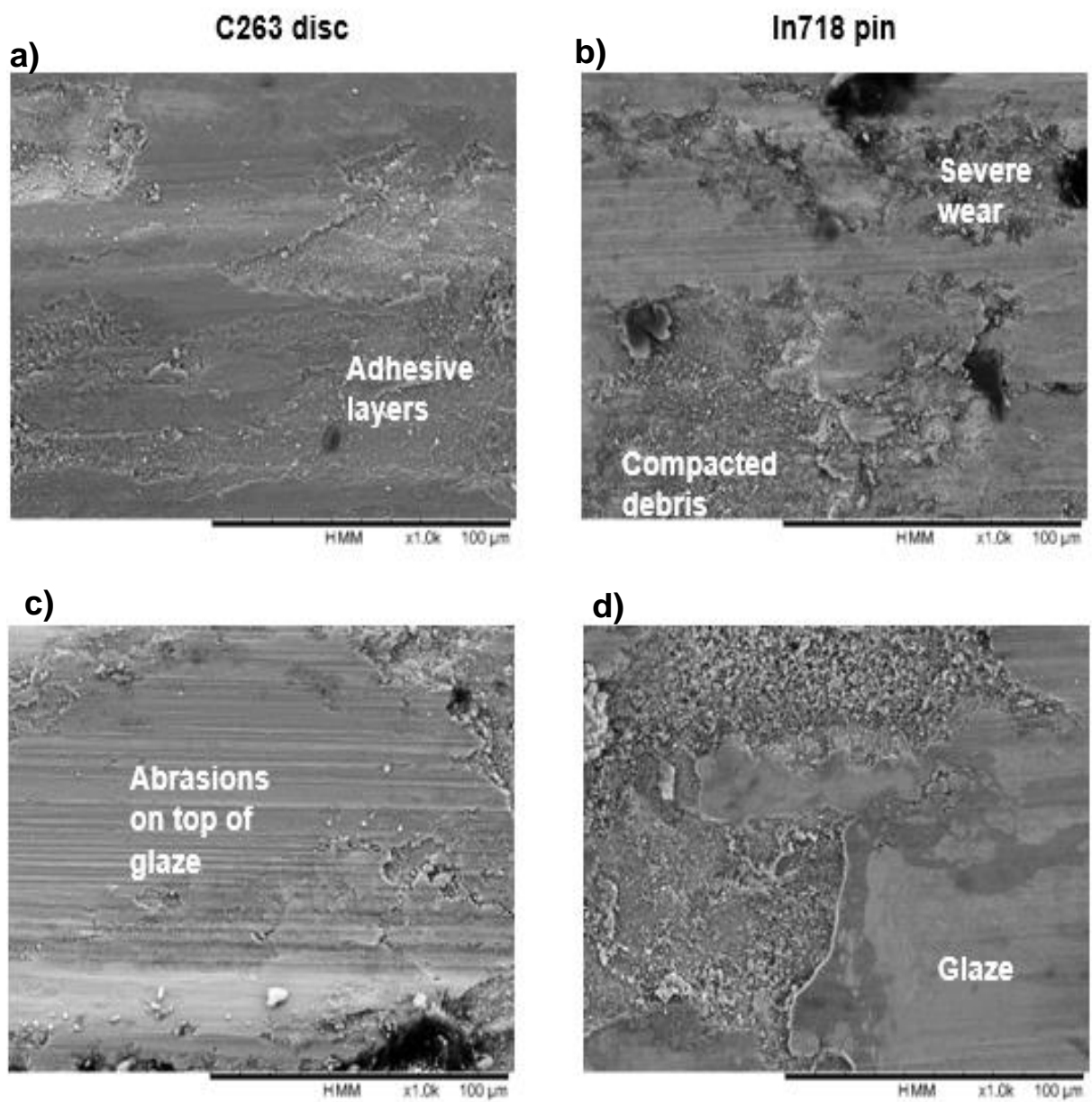
Figure 6.12 Detailed SEM images of the regions of interests highlighted in from In718 against C263 at 400 (a and b) and 600ºC (c and d) at a normal load of 25N.

6.4.1.2   Wear volume

The average wear volume can be seen in Figure 6.13. The loss from the disc is greater than from the pin. Between the different temperatures, the wear volume has dropped, however the rate of reduction in wear volume is higher for In718. This is likely to be due to the generation of an unstable oxide layer which either breaks down easily with further sliding or due to not generating a glaze layer. This correlates well with the C263 scars seen in Figures 6.11 and 6.12, where the cracks seen on the surface indicate that the glaze layers are not thick enough to prevent further surface damage. On the other hand, In718 seems to have formed an effective glaze protecting the surface, thus reducing the average wear volume.
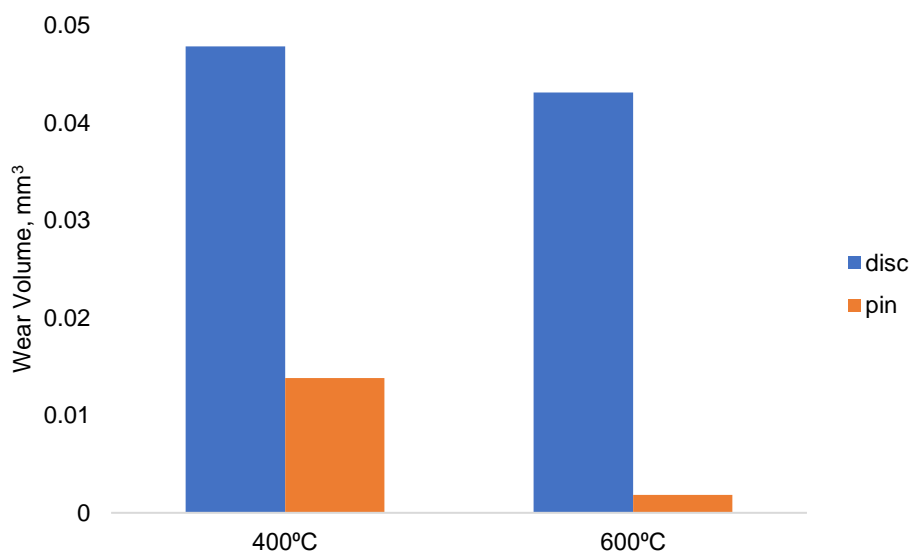
Figure 6.13 Average wear volume from C263 disc and In718 pin at 400 and 600ºC.

6.4.2 Evolution of coefficient of friction

The friction characteristics can be seen in Figure 6.14 showing the changes in COF at different temperatures. Two different trends can be seen in the figure. At the lower temperature (i.e., 400ºC), the COF displays steady state friction lasting for about 5,000 cycles alongside sharp rises/drops. The rises and drops indicate that the oxide layers formed are broken down generating more debris, which in turn is causing more abrasive wear. As the temperature is increased, there is a drop in the COF due to oxide layers forming on the surface which protect against adhesion.
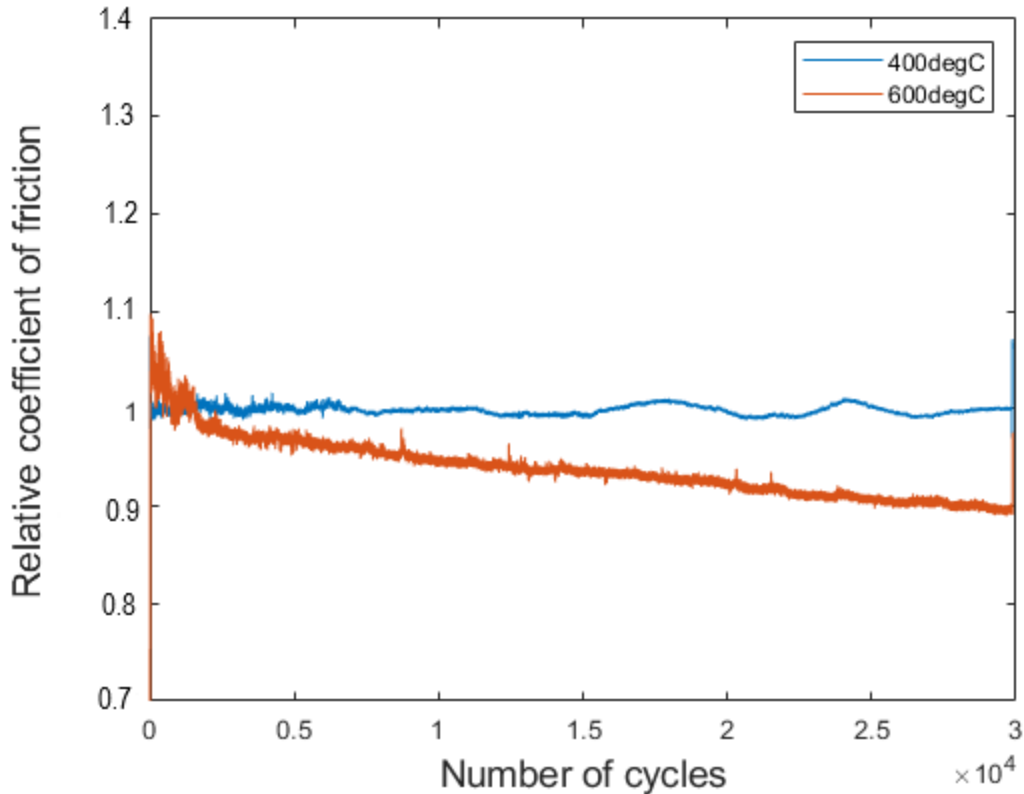
Figure 6.14 Displays the evolution of relative COF as the In718 against C263 test progresses.

6.4.3 Surface topography

Figure 6.15 shows the sectioned images of the wear scars from C263 disc and In718 pin tests. At 400ºC, the layers formed on the scar are mainly composed of MML layer with a thin layer of glaze on the disc scar. On the other hand, at higher temperature, the wear scar displays a glaze layer with a thick layer of MML. The glaze layer is more dominant on the pin sample, compacted debris can be seen as well indicating that either the layers are detaching or more glaze layers are being formed.

The glaze layer is not dominant at the lower temperature, this is likely to be because the rate of breakdown of oxide layer is higher than the rate of generation leading to a higher wear volume (as seen in Figure 6.13). As the temperature is increased, the rate of diffusion and oxidation is higher which leads to higher availability of the required elements in the contact for glaze forming a more effective layer. As a result the rate of glaze breakdown lowers.
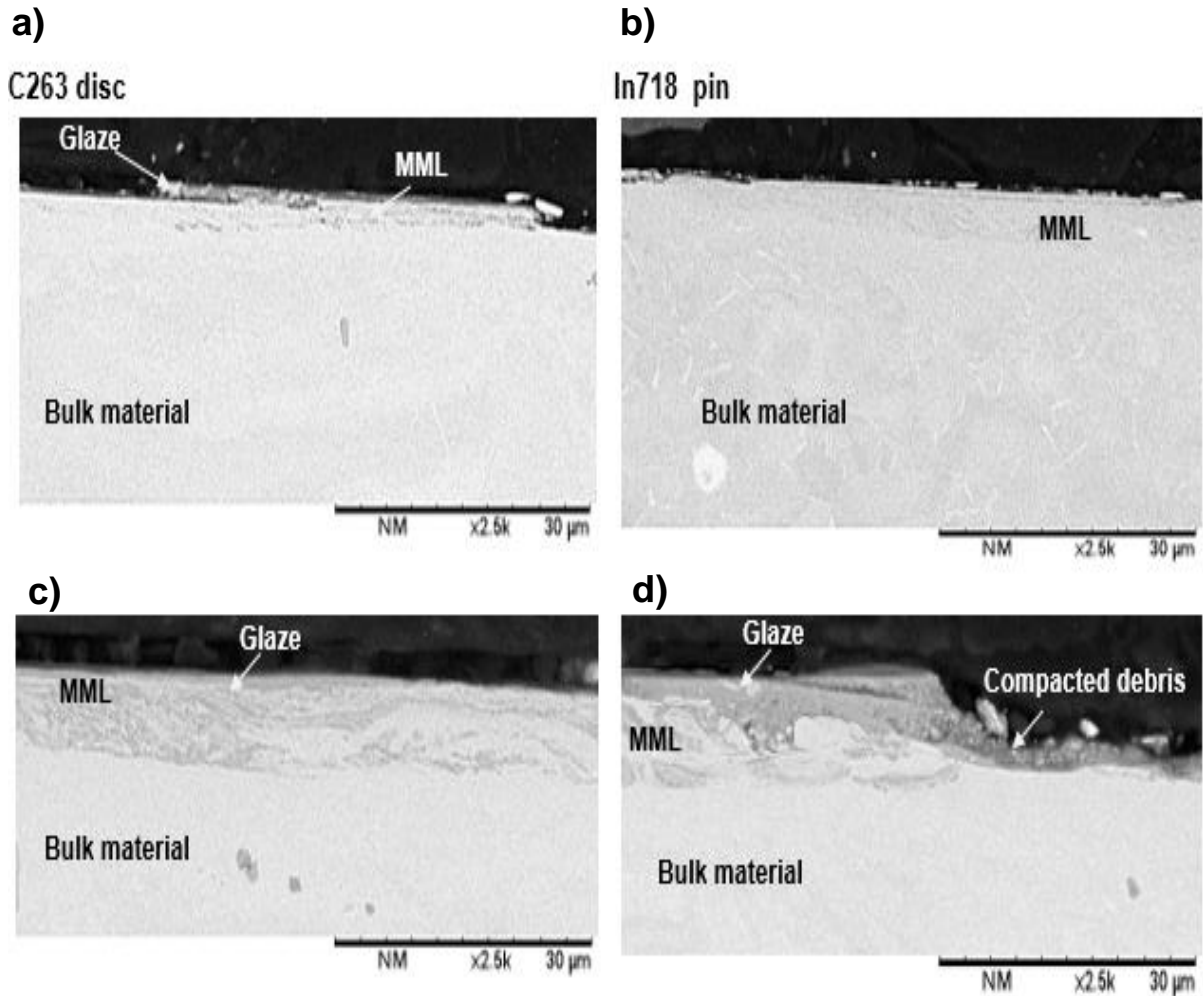
Figure 6.15 Cross sectioned images of the C263 disc rubbed against In718 pins at 400 (a and b)and 600ºC (c and d).

Table 6.4 shows the chemical composition of the layers formed on the In718 pin and C263 disc when tested at 400and 600ºC. The glaze layers formed on the In718 pin are FeCrCo based, which suggests that there has been transfer for Co from the C263. This is likely to be the reason for the reduction in wear volume as CoCr has been found to generate an effective glaze. Between the different temperatures, the percentage of Co content has increased due to increased availability of Co as more Co atoms diffuse into the contact surface as the temperature is increased. The C263 disc samples generate a Ni layer, with a slight increase in Co with increasing temperature. It is observed from the previous studies that Nickel and Chromium have poor sintering and adhering properties, which makes it harder to form an effective glaze leading to more wear as the layers are broken down with further sliding. This explains the trend seen in the wear volume and COF data as a noticeable reduction is not observed. During these tests, it appears that the generation of glaze on C263 is not significantly affected

by the higher temperature, since the rate at which glaze layers break down is greater than the rate of formation.

C263 disc					In718 pin					
	Ni/Cr	Co/Cr	Ni/Co	Ni/Fe		Ni/Cr	Co/Cr	Ni/Co	Ni/Fe	Cr/Fe
Control	2.40	0.93	2.59	74.67	Control	2.87	0.00	0.00	2.88	1.01
400˚C	2.56	0.71	3.63	9.56	400˚C	2.55	0.64	3.96	7.55	2.96
600˚C	2.35	0.76	3.09	15.30	600˚C	2.43	0.90	2.71	44.33	18.22

Table 6.4 The ratios of the main alloying elements (i.e., Cr, Co, Ni, Fe) that forms the glaze layers on C263 (left) and In718 (right) at varying temperatures.

6.5   Discussion

Sliding tests were conducted using dissimilar material combinations at a normal load of 25N and at varying temperatures (400 and 600ºC). The primary aim of this study was to understand the influence of alloying elements and whether having a certain element would aid the glaze generation process even at lower temperatures. Thus, the influence of temperature and the alloying elements are discussed here.

6.5.1   Influence of temperature

The influence of temperature was studied by changing the bulk temperature to 400 and 600ºC. Obvious changes in the friction and wear characteristics are observed with glossy regions seen at higher temperature.

As the temperature is changed, patches of glossy-smooth regions are seen on the different materials. The main difference seen between the different materials is the coverage of glaze on the surface. At lower temperature, all the different material combination displays an evenly covered oxidised regions on the surface, however, abrasive marks are also visible. This indicates the oxide layers formed are not thick enough because the energy available is not sufficient enough to generate a protective glaze layer leading to further wear.

As the temperature is increased, smooth-glossy layers are seen on both pin and disc. The Haynes 25 disc displays patchy glaze with regions of severe wear. Both Haynes 25 and C263 present 'blue' regions on the scar indicating Co diffusion into surface. this means that the rate of diffusion of Co has increased with temperature aiding with the wear protective glaze. The pin scars highlight material removal and severe wear especially at higher temperature. This is likely to be caused by the third body abrasive

particles in the contact. Moreover, the oxide particles are generally 'harder' than unoxidised debris and Co increases the hardness of materials which in turn can plough into the 'softer' material causing more damage.

All the different material combinations display a stable COF at 400ºC when compared to 600ºC. This suggests that the availability of different elements in the surface is preventing the adhesions between the disc and the pin, but the wear volume is higher indicating that the debris are causing abrasive wear. At higher temperatures, different combinations possess a slightly different trend. In718 with Haynes 25 and In718 with C263 combinations displays a reduction in COF because of the higher variations in the elemental composition of the alloys, thus avoiding the adhesion between the layers. The highest rise in COF is observed with C263 and Haynes 25 as there are similar alloying elements leading to generation of surface layers which are alike promoting the adhesion.

When compared to the like-on-like material combinations, the Haynes 25 samples appears to be more beneficial from the dissimilar material. As the thickness of MML and glaze layer has increased even at lower temperature, likely to be due to increased availability of debris and elements into the contact aiding with the formation of oxide layers (see Figure 5.27). The similar material does not seem to be highly benefitted as the glaze and MML appears to be of similar thickness as like on like material combination. The is probably why a high wear volume is observed for In718 against C263 tests when compared to the other combinations.

6.5.2 Influence of the alloying elements

Both disc and the pin samples were examined to determine the chemical composition of the layers formed. Certain material combinations had a positive influence by aiding the glaze generation process.

Figure 6.16 shows the total wear volume from the various material combinations used at different temperature. Between the different materials, the C263 sliding against Haynes 25 has resulted in the lowest material lost and the highest for In718 against C263. Both C263 and Haynes 25 contain a higher percentage of Co and Cr when compared to In718, this attributes to the lowest wear volume seen as a higher percentage of these elements have been previously found to generate a stable glaze, resulting in reduction in wear. The highest wear volume was observed between In718

and C263 samples, as a NiCr layer is formed on both samples. Since Ni and Cr has poor sintering and adhering capabilities, the layers formed were easily broken down with further sliding. Also, the chemically similar layers generated on both interfaces resulted in higher adhesion.

Although the wear volume is relatively high between the In718 with Haynes 25 combination, the wear volume at 400ºC from the Haynes 25 sample was reduced when compared to like-on-like material at 400ºC. This suggests that In718 is aiding the generation of wear protective surface on the Haynes 25 by transferring Fe atoms from the In718 pin.
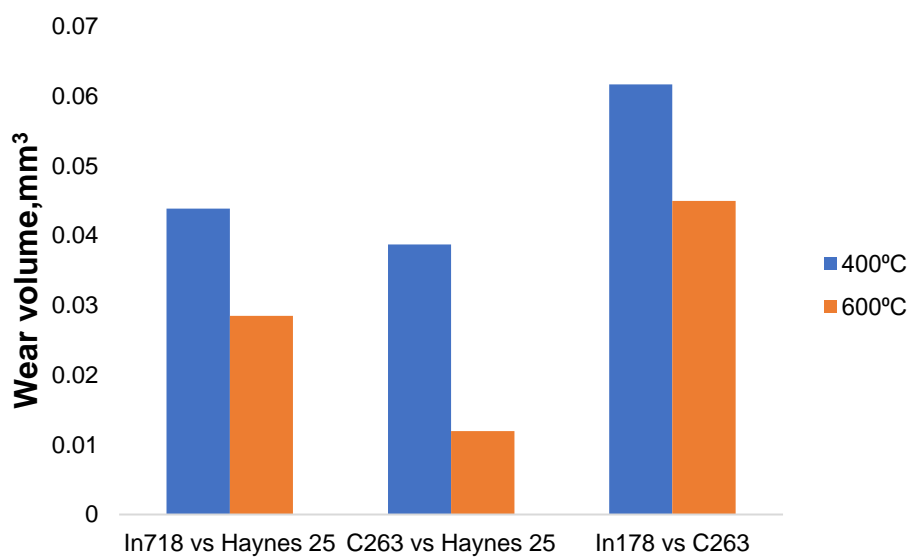
Figure 6.16 The total wear volume from different material combinations at different temperatures.

Overall, it can be concluded the more dissimilar a material is better it is in reducing wear as it benefits from transfer of active elements, given that elements possess good adhesion properties, so it bonds to the substrate reducing the likelihood of detachments. For instance, the limiting factor for glaze generation on Haynes 25 at low temperatures is the availability of debris. It can be seen from Chapters 4 and 5 that In718 generates high volume of debris due to breakdown of transient oxide layers at lower temperatures. This means that there is higher availability of debris, benefiting Haynes 25 sample by generation of an oxide layer, thus preventing further surface damage at 400˚C. It should be noted that the highest wear volume was seen at these conditions on Haynes 25 like on like combination tests. On the other hand, no changes in the chemical composition are observed on Haynes 25 against C263 at lower

temperatures. As the temperature is increased, both the wear scar characteristics and chemical composition of the layer changes indicating that the positive changes observed are temperature dependent. Finally, C263 against In718 tests have resulted in highest wear volume, making them a bad choice. This is due to both samples having a high concentration of Ni (>50%), leading to NiCr layers being formed on the surface which has poor adhesion capabilities.

6.6   Summary

This work mainly studied the friction and wear behaviour when dissimilar material combinations are used. Three different combinations were used and two different temperatures (400 and 600ºC) at a normal load of 25N. The material that is less likely to form a glaze was selected as the disc so better debris entrainment can be achieved. The results from the wear and topography analyses shows that:

- A positive influence is observed on all material combinations with increasing temperature as the wear volume is reduced and the cross sectioned images shows an increased thickness of MML and glaze layer which protects the surface from further damage due to metal-to-metal contact.
- A drop in the COF is seen at 600ºC with In718/Haynes 25 and In718/C263 combinations as the glaze layers formed on the pin and disc are different, thus adhesions are reduced.
- Only a thin glaze layer is noticed on the pin samples, likely to be because of the poor debris retention and the interaction with the debris (as highlighted by the worn edges).
- The combinations with different chemical composition would be more beneficial from introduction of 'new' elements such as like on like tests on Haynes 25 at 400ºC leads to severe oxidative-abrasive wear whereas the introduction of Ni from the In718/C263 results in MML and glaze generation. Conversely, chemically similar materials likely to not have any significant advantages.

Chapter 7 Pre-glazed tests

This chapter presents the results from the pre-glazed tests on In718, C263 and Haynes 25. The results are analysed using wear scar images obtained from optical microscopes and SEM. Also, chemical analysis is carried out to see the effectiveness of the glazed surface.

7.1   Introduction

The fundamental factors affecting glaze formation can be seen in previous chapters. It is seen that severe wear occurs prior to an effective glaze is found, one of the ways to prevent this is by having a pre-glazed surface prior to the test. However, it is not clear from the previous studies and information from industry whether this is always successful. Previous studies [42] have demonstrated that there is a reduction in COF and that it takes less time to form a protective glaze for a pre-glazed surface, even at lower temperatures. If pre-glazing the surface is found to be beneficial in reducing initial wear, then it can be adopted for industrial applications as the temperature and load variations during an aero-engine operation are cyclic allowing the prediction of glaze generation by having the knowledge of the ideal conditions where a wear resistant layer is formed and how it can be replenished before all the layers are removed.

Hence, the aim of this study was to investigate if there is any influence when a glaze has been previously generated in a surface at a certain high temperature and its performance at lower temperature. This enables the discover of whether such a favourable effect exists universally across different materials, and if so, to what degree. Since the effectiveness of a glaze layer is dependent on various factors, the current study is limited to a single normal load condition and only like-on-like material combinations with one load condition is used. This ensures that the results are not influenced by any other factors.

7.2   Test methodology and parameters

Tests were carried out in a button on disc configuration using like on like material combinations. The test set-up and materials used in this study were the same as previously used (as described in Section 3.4.1). The method was slightly altered to investigate the effect of history dependence or pre-glazed samples. Therefore, during this study, the pin samples were rubbed against the disc samples first at a high temperature (i.e. 600ºC), to allow a stable glaze region to be generated on the surface followed by tests at a lower temperature (i.e. 25ºC). Test parameters are detailed in Table 7.1. All the tests were repeated three times for reliability. The tangential force and displacement data were measured throughout the test. Additionally, an image of

the wear scar was taken post high temperature test using a USB microscope to ensure that a glaze is formed on the surface.

Load (N)	25
Frequency (Hz)	8.3
Stroke length (mm)	2.2

Table 7.1 Details the test parameters and the material combinations used in the pre-glazed tests.

7.3   Wear scar analysis

Figures 7.1 to 7.3 show the wear scars of both pin and the disc from the pre-glazed tests. Once the initial high temperature tests are finished, an in situ image is taken of the wear scars to preserve the contact conditions using a USB microscope.

The wear scars from the In718 wear scars are seen in Figure 7.1. Images of the wear scar (disc) post high temperature tests were taken to ensure that a glaze was formed on the surface. As seen in the Figure, black-glossy regions are seen in the middle of the scar, and lightly oxidised regions near the edges indicating either a glaze is broken down or new glaze layers are being generated. Also, there is evidence of metallic wear. The post room temperature test scars show an increased coverage of 'black oxidised regions' with glossy patches in the middle. Abrasive marks are also seen indicating severe wear. The main contrast observed between the tests is that the wear scar width has increased significantly post RT test. This is probably due to the glaze layers being detached as the temperature is varied. On the pin scar, lightly oxidised regions are more dominant, suggesting compacted debris. Silver/grey regions can also be seen near the edges indicating severe metallic wear likely to be as a result of the interaction with oxide/unoxidised debris.
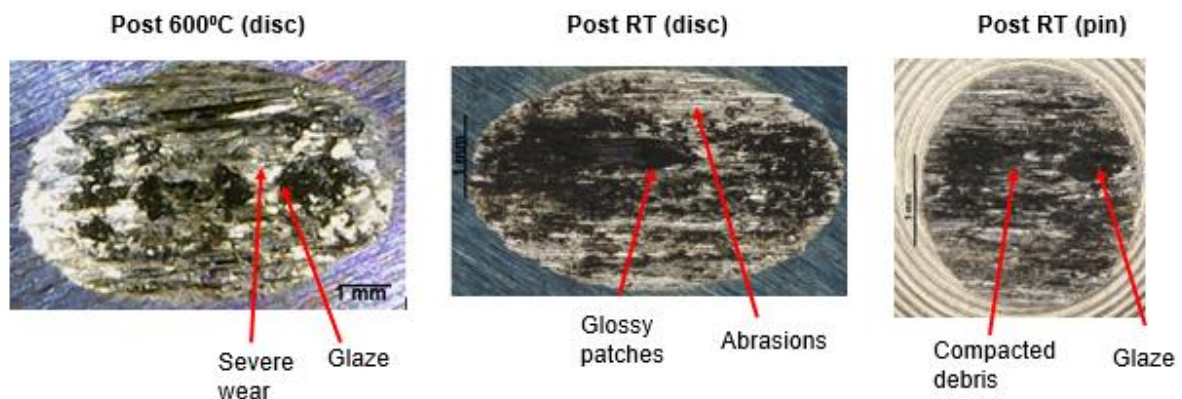
Figure 7.1 The wear scar at various stages of the In718 pre-glazed tests carried out at both 600ºC and room temperature at a normal load of 25N.
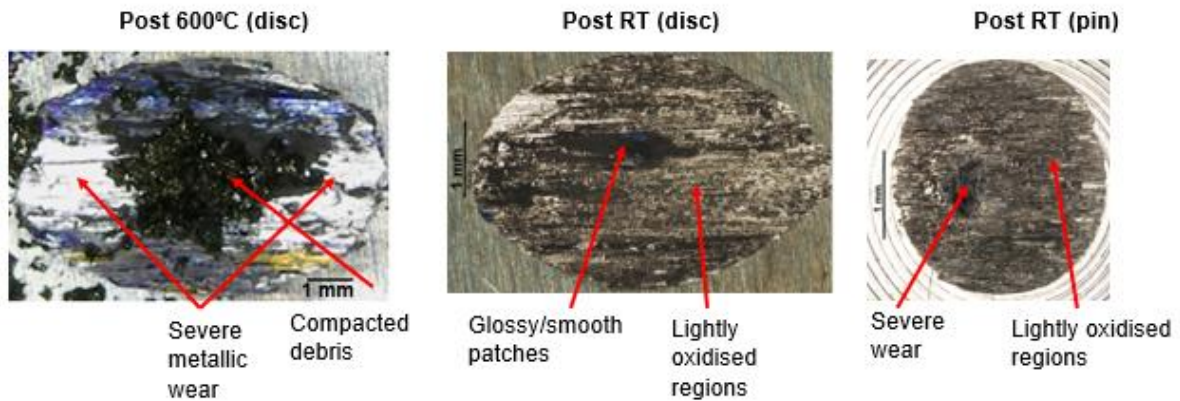
Figure 7.2 The wear scar at various stages of the C263 pre-glazed tests carried out at both 600°C and room temperature at a normal load of 25N.
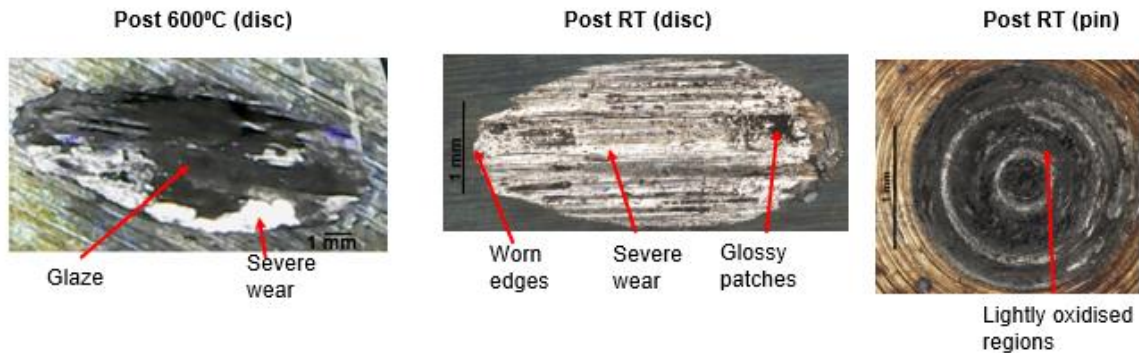
Figure 7.3 The wear scar at various stages of the Hs25 pre-glazed tests carried out at both 600°C and room temperature at a normal load of 25N.

The wear scar from the C263 tests can be seen in Figure 7.2. On the edges of the scar on the disc, severe wear regions (highlighted by metallic silver/grey) are seen, likely to be caused by the debris particles abrading into the surface. Glaze layers are visible in the middle of the scar; however, the extent of layers cannot be fully seen as debris are present over the black oxidised regions. Post room temperature test scar shows an evenly covered light oxide on the surface with 'patchy' glossy regions. Grey/silver regions can be seen underneath the lightly oxidised region on the disc scar, this suggests that new areas are being exposed due to the previously formed glaze being broken and 'new' oxide layers are being formed. Similarly, on the pin scar, an even coverage of light oxide is seen.

Finally, Figure 7.3 shows the scars from the Haynes 25 tests. As seen in the Figure, continuous glaze layers were formed at higher temperature with some metallic wear regions. However, a very different scar is visible post the room temperature tests with

severe metallic wear and abrasive grooves. Almost all of the glaze formed at the higher temperature is destroyed by the end of toom temperature tests, this is likely to be because new glaze layers are not being generated at room temperature, leading to more wear (seen by the increased wear scar width). Additionally, the breakdown of glaze layer is accelerated by the change in the temperature as the rates of thermal expansion changes promoting detachment of the bonded layers. Unlike, the disc scar, the pin shows an even coverage of oxide layer with glossy glaze layers seen.

7.3.1 Wear volume

The total wear volume from individual material can be seen in Figure 7.4.
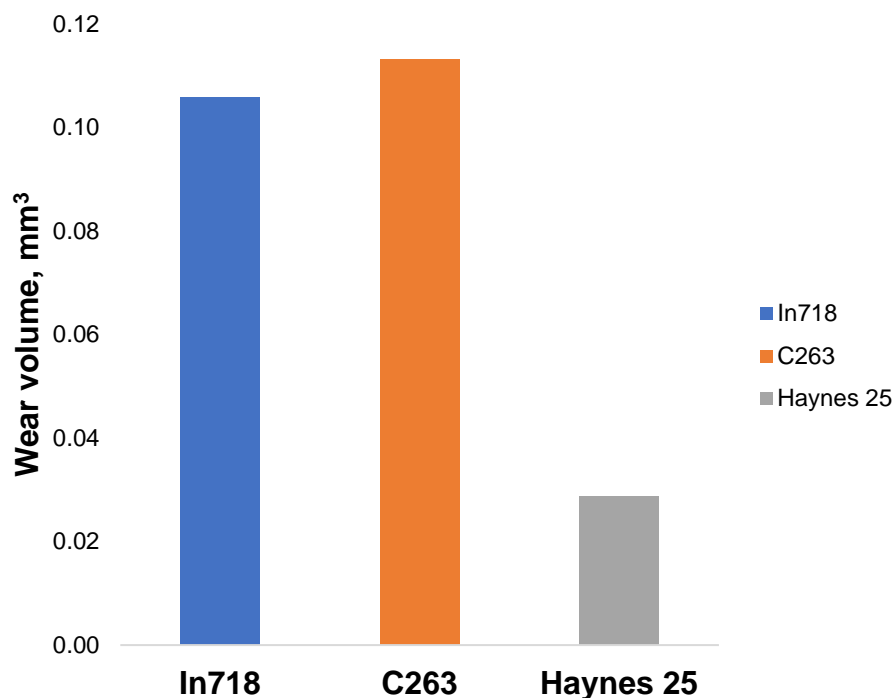
Figure 7.4 The total wear volume from In718. C263 and Haynes 25 when the tests are conducted using a pre-glazed sample at a normal load of 25N.

The highest wear volume was observed for C263 followed by the In718. The lowest wear volume is observed for Haynes 25, and the wear volume is almost three to four times lower when compared with In718 and C263. Glossy glazed regions were visible on all the materials post high temperature tests; this suggests that the glaze layers were protecting from further surface damage until it broke down. Nonetheless, the rate of breakdown was different on different materials as evidenced by the varying level of glaze remaining at the end of the room temperature tests. This is likely to be due to

the differences in chemical compositions and thermal expansion/contraction rates. An effective glaze is seen on the Haynes 25 as the high temperature wear scar exhibits lower scar width and low wear volume at the end of room temperature tests suggesting that Haynes 25 has the highest durability. However, there is a significant drop in the coverage post room temperature test suggesting its inability to replenish the glaze layers that are broken down. This leads to mechanical wear which is causing additional surface damage and subsequently more wear.

7.4   Evolution of coefficient of friction

Figures 7.5 to 7.7 shows the evolution of relative COF as the test progresses and the average absolute COF at the start/end of high temperature, room temperature and pre-glaze room temperature tests. Both high and room temperature(pre-glaze) relative COF results are displayed.
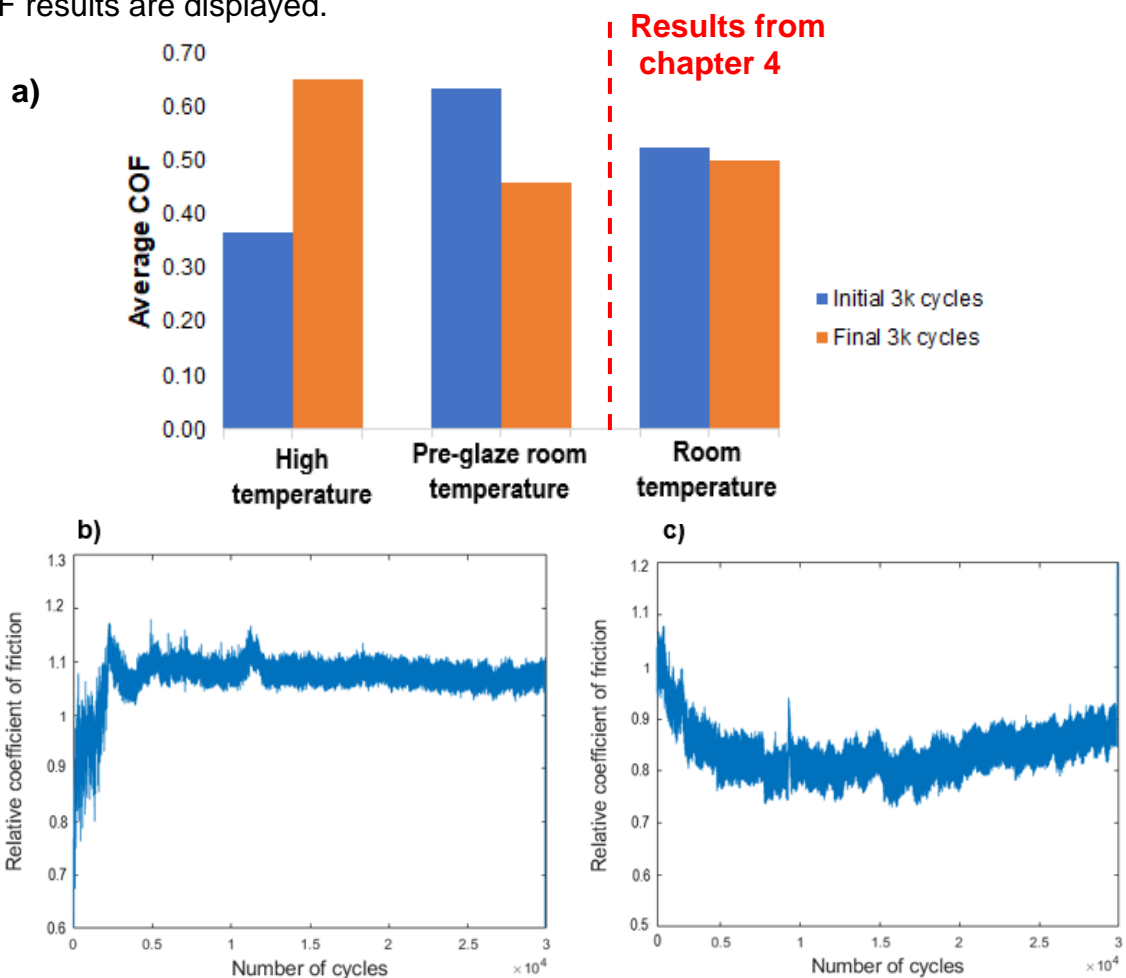
Figure 7.5 The COF data for like on like combination tests on In718 at a normal load of 25N a) the average COF at the initial and final 3k cycles of the test b) the evolution of relative COF at high temperature c) the evolution of COF at room temperature when a glaze layer is already present on the surface.

The evolution of COF from the In718 tests can be seen in Figure 7.5 b and c. As seen in the figure, at higher temperature, a stable COF is seen with an overall rise. This is because of the adhesion between the chemically similar layers formed on the contacting surface. A drop in the COF is observed at lower temperature. Initially, there is a region of stable COF (~7,000 cycles), however, as the test progresses, the COF becomes unstable with peaks and drops in the data indicating that layers are broken down. The overall drop in the COF is likely to be due to third body particles preventing metal-to-metal contact, however this leads to abrasive wear generating more wear and acerating the breakdown of existing glaze layers. Average COF at the start and towards the end of various tests can be seen in Figure 7.5a. There is little variation in the average COF between the start and end of the room temperature where the surface is not pre-glazed, this suggests that a stable layer is not present. On the other hand, the pre-glaze room temperature results shows a high COF at the start of the test and a decrease in COF at the end of the test. As seen in the previous chapters, the drop in COF is due to the presence of third body wear particles in the contact preventing adhesions. Therefore, it can be concluded that the glaze layers are being broken which is also seen in the wear scars.

Figure 7.6 b and c shows the evolution of COF of C263 as the temperature is varied. a similar pattern to In718 is noticed with a stable COF seen at higher temperature and drop in overall COF at lower temperature. Unlike In718, the initial stable COF at lower temperature is lasting ~ 11k cycles, afterwards peaks and drops can been seen with stable regions lasting around 2.5k cycles. A similar trend to In718 is observed with the average COF (Figure 7.6a), where a drop in the average COF is seen when a glaze is present on the surface prior to the room temperature test.

The COF data from the Haynes 25 samples can be seen in Figure 7.7. The stable COF at higher temperature suggests that an effective glaze is formed.an overall reduction in COF is seen at the lower temperature, however unstable regions are seen between 6k to 20k cycles indicating the layers being broken down generating 'rough' surfaces leading to wear. At lower temperature, stable COF is seen between 20k-25k cycles, indicating a glaze layer is formed. This trend was not seen in results without pre-glaze because of limited availability of debris for compaction and sintering to generate a glaze layer. When the glaze layers are broken down leading to more wear, debris are no longer the limiting factor increasing the likelihood of a stable oxide layer.

Figure 7.7c shows the average COF from the tests conducted at different conditions. It can be seen that the COF is significantly lower for room temperature tests than the pre-glaze and high temperature tests. A slight drop in the COF is observed for the pre-glaze room temperature tests suggesting that the layers are starting to break down.
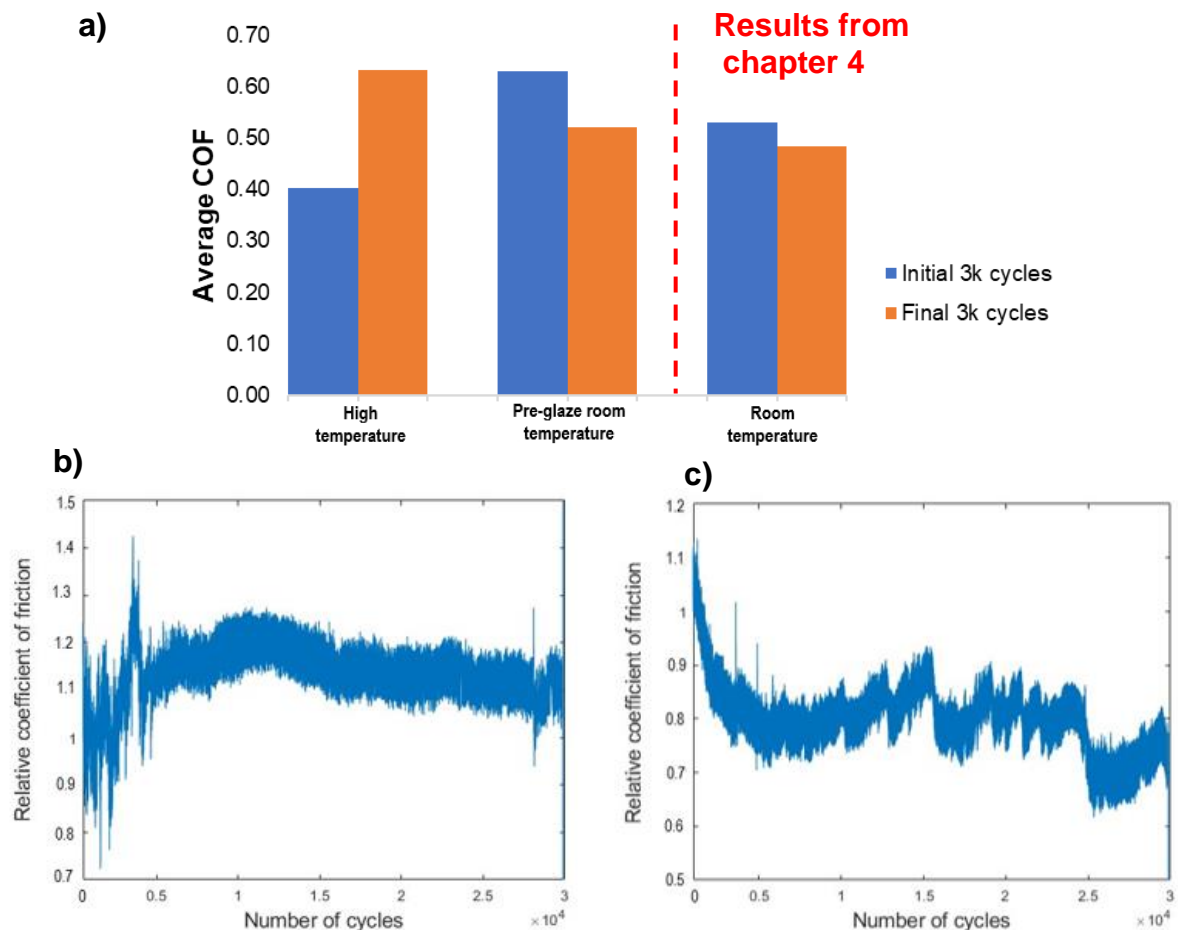
Figure 7.6 The COF data for like on like combination tests on Haynes 25 at a normal load of 25N a) the average COF at the initial and final 3k cycles of the test b) the evolution of relative COF at high temperature c) the evolution of COF at room temperature when a glaze layer is already present on the surface.

The results from chapter 5 (Figure 5-9,5-18,5-27) has shown that In718 forms a continuous glaze layer with a thick MML layer underneath. Whereas on the C263 and Haynes 25 samples , the thickness of MML is lower than In718. The friction data and the wear volume indicates that the wear rate is higher from the In718 samples than the C263 and Haynes 25. This is likely to be because of the different thermal expansion/contraction rates of the glaze layers formed indicating the glaze layers formed on In718 is less stable at lower temperatures when compared to C263 and Haynes 25 leading to detachment and removal of the layers.

It is also important to not that COF values are a combination from both glazed and non-glazed surfaces. Therefore, makes it a challenge to compare COF values between different temperatures or partially glazed surface. These figures are used to study the trends in friction behaviour and the instability of COF at RT tests as the glaze layers are broken down.
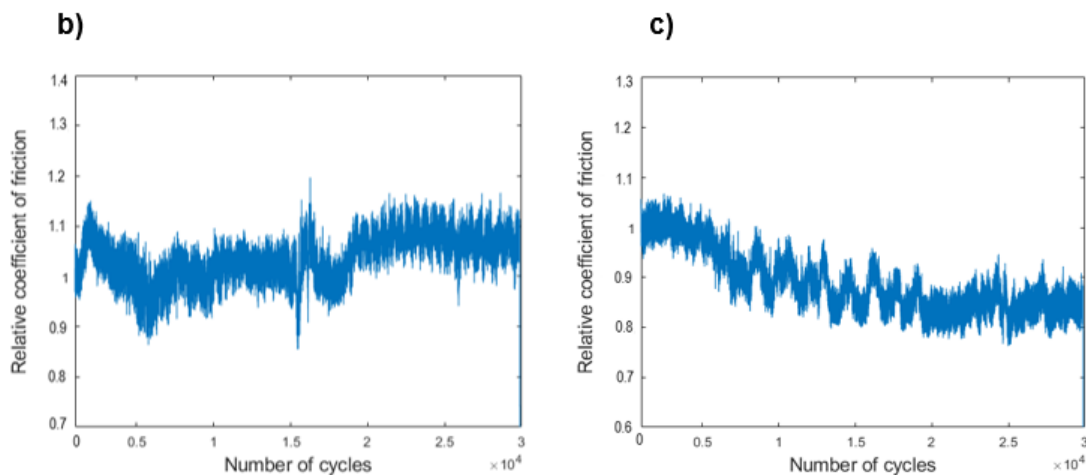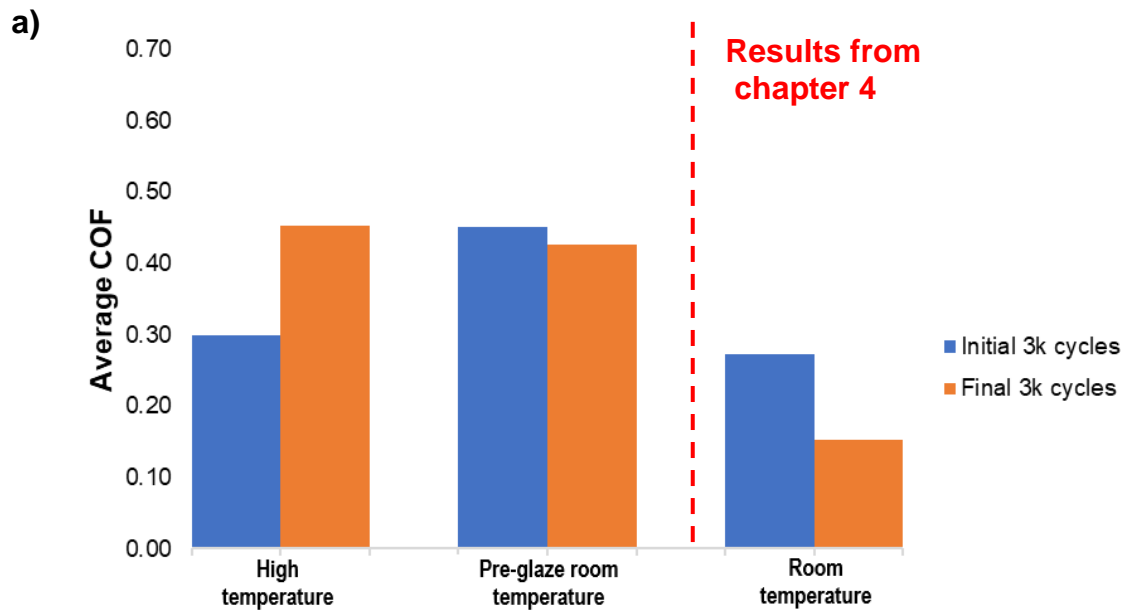
Figure 7.7 The COF data for like on like combination tests on Haynes 25 at a normal load of 25N a) the average COF at the initial and final 3k cycles of the test b) the evolution of relative COF at high temperature c) the evolution of COF at room temperature when a glaze layer is already present on the surface.

7.5   Surface topography

7.5.1   SEM images

The detailed images from the regions of interest can be seen in Figures 7.9 to 7.11, obtained using the Hitachi TM4000 SEM using a mix of BSE and SE detector from the post room temperature tests. The regions of interest are highlighted on the optical images (see Figure 7.8).

Figure 7.9 shows the SEM images of the regions of interests from In718 tests. As seen in the figure, some glaze can be seen underneath the debris and the surface is dominated by the compacted debris. The presence of large cracks along the surface suggests that the oxide layers are thin and can easily break down with further sliding.

SEM images of the wear scars from the C263 tests can be seen in Figure 7.10. Although glaze is observed, it is 'patchy' and not a continuous layer. Debris are visible around the glazed regions indicating the glaze is being broken down. The presence of compacted oxide debris indicates glaze generation is underway and the delay may be due to insufficient energy to sinter the debris.

Figure 7.8 Optical images of the post RT wear scar highlighting regions of interest used for the SEM analysis.
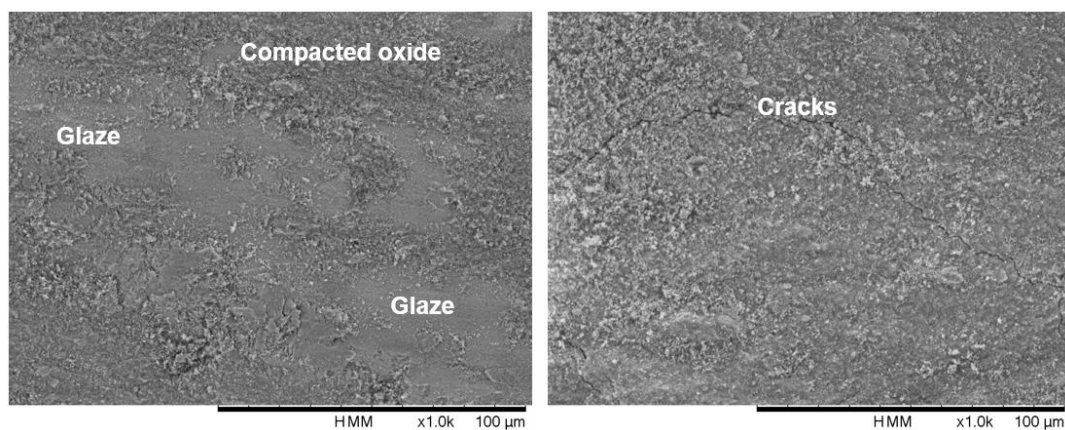
Figure 7.9 SEM images of regions of interest from In718 samples at x1000 magnification.
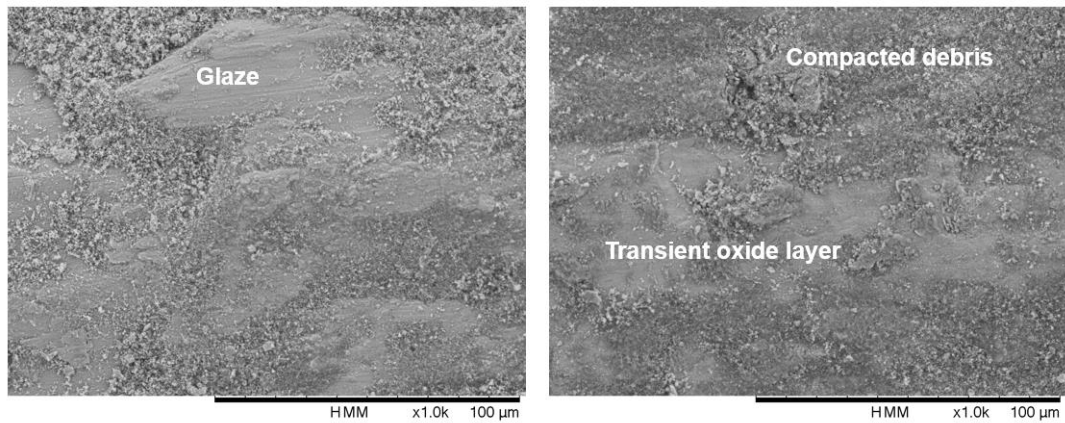
Figure 7.10 SEM images of regions of interest from C263 samples at x1000 magnification.
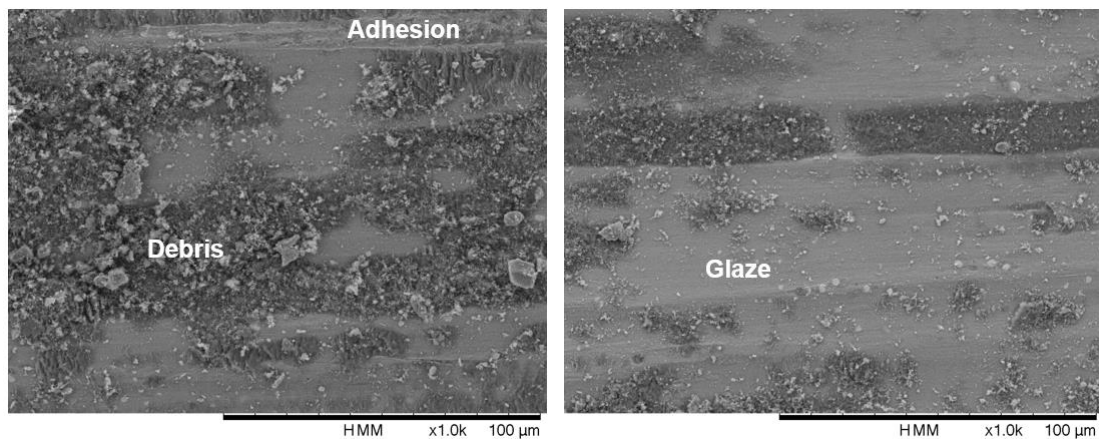
Figure 7.11 SEM images of regions of interest from Haynes 25 samples at x1000 magnification.

Large 'circular' debris are seen on the Haynes 25 scars (see Figure 7.11), this indicates that the glaze layers formed at high temperature are broken down. The glaze is usually 'harder' than the bulk material, therefore the debris cause abrasive wear causing further damage to the surface. Additionally, 'larger' debris will increase the time taken for glaze generation as the debris needs to be broken down and oxidised. Since Co has a higher activation energy, the rate of diffusion and oxidation are lower meaning the glaze generation process is also hindered.

Figure 7.12 shows the cross sectioned wear scars post test. Different layers can be seen on the scar such as a mechanically mixed layer (MML), glaze, bulk material etc. In718 scar exhibit MML with cracks formed indicating that they will be broken off with further sliding creating more debris. Large debris can be seen in the grooves which needs to be further broken down and oxidised before forming 'new' layers. No glaze is observed on the In718, and this indicates that all the glaze that is generated at

higher temperature has been broken down. On the other hand, C263 wear scars show a debris layer, thin glaze layer and MML above the bulk material. Even though a thick layer of MML is noticed, the total wear volume is greatest for the C263, and this indicates that the layers generated are not stable and effective leading to more debris to be generated. This can also be seen by the amount of wear debris seen, as a higher amount of debris is seen for C263 when compared to In718 and Haynes 25. Figure 7.12c shows the cross sectioned scar from the Haynes 25 sample. A layer of fine compacted debris and MML is seen on top of the bulk material suggesting almost all of the glaze has been broken down.

7.5.2 Elemental analysis

The relative changes in the primary elements are used to study the composition of the surface layers. Table 6.2, 6.3 and 6.4 show the control data (i.e.pre-test), post pre-glazed tests (after both 600ºC and room temperature tests), and finally, the room temperature and 600ºC results for comparison.

Table 7.2 shows the results from In718 like-on-like test. as seen in the table, the pre-glazed data shows a slight increase in Cr and Fe content suggesting the layers are primarily made of CrFe. The room temperature data shows no significant difference in the chemical composition compared to the control, whereas at 600ºC, CrFe layer is observed. When compared with the previous tests conducted at room temperature and 600ºC, the data indicates that some of the glaze is retained even after the room temperature tests meaning that pre-glazing the surface would provide some protection against wear. However, the percentage of Cr is lower after pre-glazed tests and the percentage of Fe has increased, this suggests that Fe diffusion is occurring at room temperature. The previous studies have shown that the Fe oxide generating at lower temperatures (>250ºC), will increase wear due to poor adhesive properties, and could be the reason for the high wear volume seen in this study.

The results form the C263 sample can be seen in Table 7.3. As seen in the table, only a slight difference in the chemical composition of the surface layers is observed. A CrCo layer is noticed, as there is a drop in the Ni/Cr and Ni/Cr ratio meaning a Ni depletion. When compared with the room temperature and 600ºC data, pre-glaze data indicates that the glaze is still present protecting the surface, however, the percentage of Co/Cr ratio has decreased suggesting that the rate of Co diffusion into the surface

is decreased hindering the glaze generation process and the glaze layers are not replenished.

Table 7.4 shows the chemical composition of the Haynes 25 surface post pre-glaze test. The results show that there is only a minor change in the chemical composition when compared to the control (i.e., pre test surface). The Ni/Cr and Co/Cr ratio has decreased indicating Cr is still present in the layers. Whereas, at high temperature test, Co rich layer is seen. This links with the wear scar seen where grey/silver regions dominated suggesting the oxide layers have been broken down.
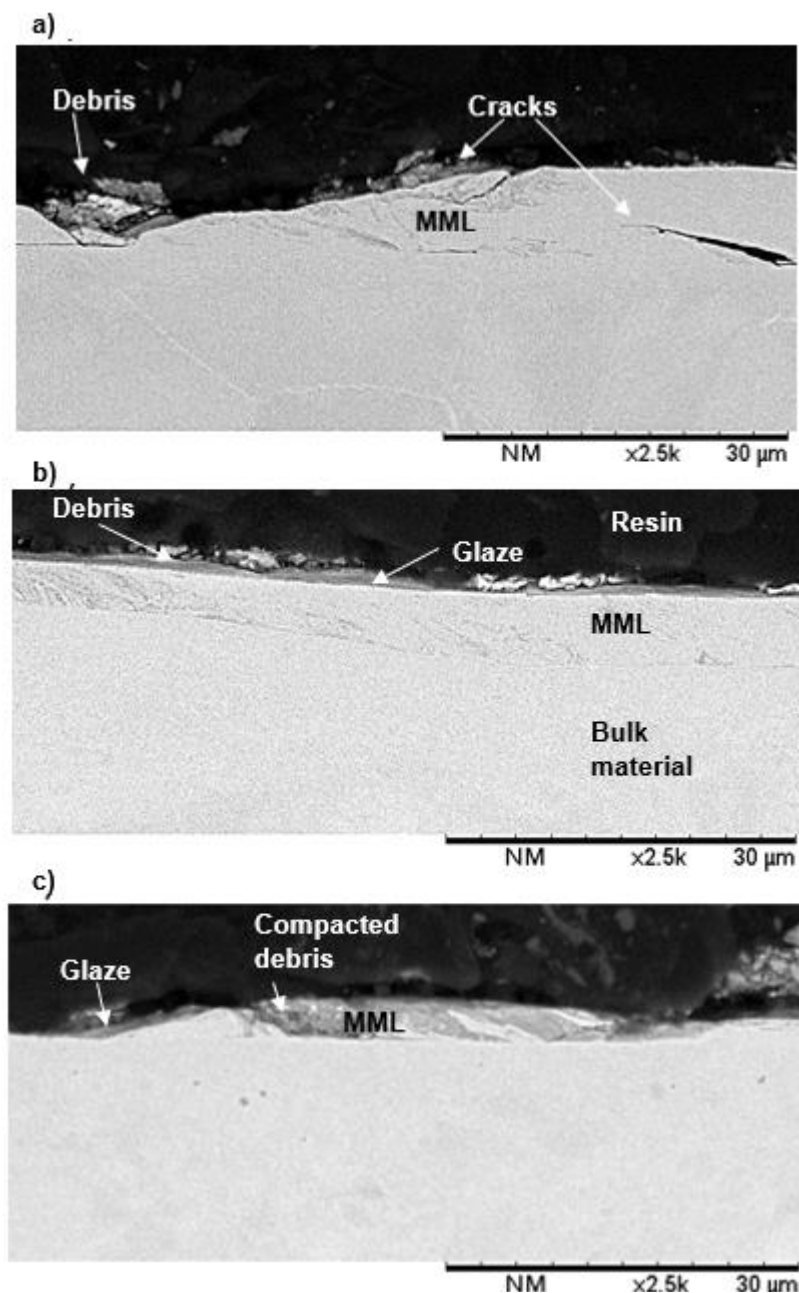
Figure 7.12 Cross sectioned images of the wear scar showing the various layers formed during the tests at a magnification of x2500 a) In718 b)C263 c)Haynes 25

	Ni/Cr	Ni/Fe	Cr/Fe
Control	2.84	2.93	1.03
Pre-glaze test	2.47	2.76	1.12
RT	2.64	2.89	1.27
600˚C	2.24	2.54	1.13

Table 7.2 The elemental analysis of the layers from pre-glazed like-on-like In718 tests. Both RT and 600ºC results are from chapters 4 and 5.

	Ni/Cr	Co/Cr	Ni/Co
Control	2.40	0.94	2.55
Pre-glaze test	2.25	0.90	2.51
RT	4.82	0.35	13.7
600˚C	2.45	1.12	2.19

Table 7.3 The elemental analysis of the layers from pre-glazed like-on-like C263 tests.

	Co/Cr	Ni/Co	Ni/Cr
Control	2.38	0.20	0.47
Pre-glaze test	2.24	0.20	0.45
RT	2.37	0.21	0.49
600˚C	2.83	0.16	0.47

Table 7.4 The elemental analysis of the layers from pre-glazed like-on-like Haynes 25 tests.

7.6   Discussion

Pre-glazed tests were carried out using like-on-like material combinations at a normal load of 25N. A combination of tests are used to ensure that a protective glaze layer is formed, thus an initial sliding test is conducted at 600ºC, followed by tests conducted at room temperature using the same samples. The main aim of the study was to understand the effect of variations in temperature when a glaze is already present on the surface and whether this will reduce the severe wear seen during the run-in period.

The wear scars were assessed post the high temperature and room temperature tests. The post high temperature scars on all the materials show 'black'/glossy regions on

the surface indicating a glaze is formed. However, the quality of the glaze was not checked to preserve the contact conditions. The post room temperature tests showed variability in the oxidised regions observed on the wear scar on different materials. The highest coverage was seen on the In718, followed by C263. The scars from Haynes 25 were dominated by 'grey'/'silver' regions indicating no oxides layers were being formed. This implies that the glaze layers are not replenished at room temperature due to energy being insufficient enough to oxidise, diffuse and sinter the debris.

The COF data shows that a stable glaze is formed at higher temperature as a stable COF is seen as the time is increased. The pre-glaze has shown a reduction in overall COF, however, the COF at room temperature has shown unstable friction behaviour suggesting layers were being broken down. The overall drop is COF is noticed because metal-metal contact is prevented by the glaze layers and the MML as seen in the wear scars. The sharp drops and peaks in COF is likely to be because the layers generated at higher temperature are detached as the temperature is varied leading to more debris in the contact. Unlike C263 and Haynes 25, it should be noted that the pre-glaze COF data from In718 has started to rise towards the end of the test suggesting less abrasions are occurring, and adhesions are increasing. However, it is not clear whether glaze layers were being replenished or not at the present stage.

A significant drop in the pre-glazed wear volume is seen when compared to room temperature tests (see Figure 4-4). The lower wear volume is observed as metal to metal contact is prevented by the glaze on the surface. However, for both In718 and C263, the wear rate has increased relative to the 600ºC like-on-like tests (see Figure 7-13). This indicates as the glaze is broken down, and severe wear is promoted leading to a rise in material loss. Whereas for the HS25 samples, a lower wear rate is noticed, and this correlates well with the trend seen with room temperature tests where a mechanical wear is dominant leading to a higher degree of surface damage compared to In718 and C263. This is also evident in the friction data where an unstable COF is observed as the test progresses indicating that the glaze is being broken down.

The chemical composition of the surface layers from the pre-glazed samples shows that both In718 and C263 shows a different composition compared to room temperature and higher temperature tests, where a CrFe layer is seen on the In718

and CrCo layer on the C263. On both C263 and Haynes 25, the overall Co content has dropped with the temperature, suggesting it is no longer diffusing Co into the surface. Haynes 25 composition is almost same as the control/RT, this indicates that the glaze is destroyed.
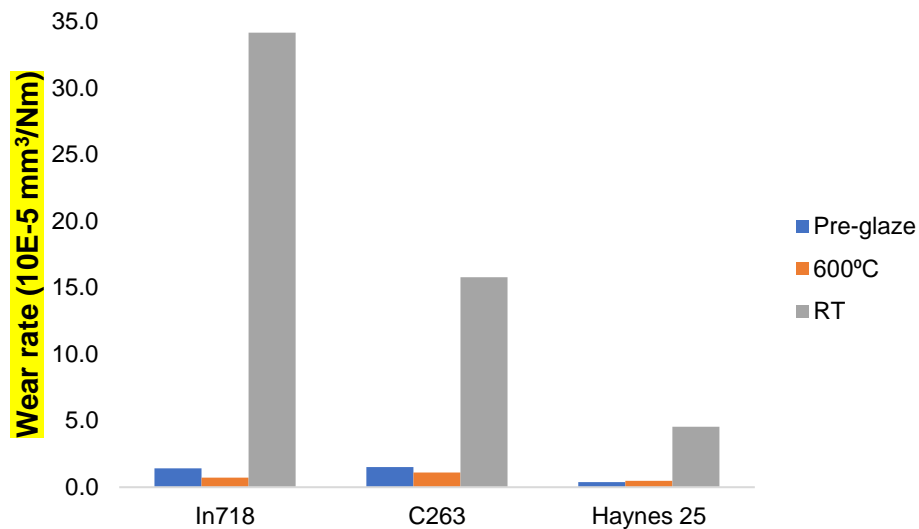
Figure 7.13 The wear rate of pre-glazed, 600ºC and RT tests for comparison

Overall, the pre-glazed tests shows that it can be advantageous and protect the surface to some extent depending on the conditions used such as the temperature, the duration at each temperature, the load etc. it is necessary to conduct further tests to fully evaluate the effectiveness of pre-glazed tests. For example, the current study shows that the glaze layers are destroyed at room temperature and variable amount of MML is seen. MML is currently preventing the metal to metal contact, however, the effectiveness of this layer remain uncertain as glaze layers are not replenished at room temperature. It will be beneficial to see whether raising the temperature to an intermediate level will increase the glaze generation as oxidation/diffusion rates are higher.

7.8 Summary

The aim of the investigations conducted in this chapter was to observe whether there is any influence when a glaze has been previously generated in a surface at a certain high temperature and its performance at lower temperature. Therefore, a combined test method is used- firstly, conduct a test at 600ºC to generate a glaze on the

contacting surface and then carry out the tests under room temperature. It can be concluded from the results that:

- The wear scar images show evidence of severe wear suggesting that the glaze layers are broken down.
- The cross-section images displays a thick layer of MML with very thin or no glaze layer. This was not seen at just room temperature tests as only transient oxide layers were present.
- An overall drop in the COF is observed with the pre-glaze size however, it is unstable indicating, that the layers are broken down producing debris in the contact and the overall drop is likely to be due to less metal-metal contact. This correlates well with the room temperature test results (see Chapter 4).
- The wear rate for pre-glaze tests were slightly higher for Ni based alloys and lower for Haynes 25.
- Although some useful information was collected, the extent of the effectiveness of pre-glazing is not evident. It is needed to study the other factors such as the changing the pressure, temperature or dissimilar material to fully understand the effectiveness of a pre-glaze surface.

Chapter 8   Wear Maps

This chapter summarises the results and findings of the experimental work into a wear map, including the methodology behind the generation of the maps and the statistical analysis of the mathematical model.

8.1   Introduction

As described in the previous chapters, different wear and friction behaviour were seen as the temperature and pressure are varied. The different materials have shown different behaviours, especially the time it takes to generate a wear-resistant layer (i.e. glaze). The post-sliding test samples were analysed using various methods (as mentioned in Section 3.4.4) to understand the different mechanisms and the chemical composition of the layers to determine the effectiveness of the oxide layer that is formed at various operating conditions.

It is clear from the investigations conducted in this study shows that the glaze generation process is a complex process involving various factors, it is a challenge to predict the wear response of a system especially because of the variety of data that needs to be presented/evaluated. One such method of evaluation and prediction can be done via wear maps, thus this chapter focuses on identifying and characterising the different aspects of the wear behaviour that are identified to produce a wear map.

8.2   Construction of wear map

A wear map is a graphical representation of wear analysis from sliding tests using various parameters used in the study. It allows observation of the dependencies of various parameters and allows visualisation of the effective limits of each material at different operating conditions. Moreover, a map can be beneficial to predict the wear performance of a material or material combinations under certain conditions. Therefore, the experimental results from this study were analysed to construct a 3D wear maps [94] [95] [96] [97].

Wear maps are constructed for experiments carried out on like-on-like combinations at various temperature and load conditions. The experimental results are analysed using response surface classification methodology (RSM) in Minitab statistical software. Minitab is utilised because it provides an efficient method for determining the statistical significance of experimental data. RSM is a mathematical and statistical technique used to design experiments in order to optimise a response when several independent variables are involved. The RSM is used for the wear result analysis because it has been used by several researchers to develop a mathematical model to predict the response to identify the main factors influencing the response by carrying out an analysis of variance (ANOVA) [98] [99] [100] [101].

The input parameters used in the analyses were temperature (ºC) and applied load (N) and the target response is wear rate (x10^{-5} mm^3/Nm). These were chosen for the analysis as it was identified as the primary factors influencing glaze generation from the literature review, thus conducted tests varying these factors. Further details on the mathematical models used for the analysis and regression values of each material are detailed in Appendix 8a.

8.3   Inconel 718

Figure 8.1 shows the wear map obtained from the analysis of In718 at temperatures ranging from room temperature to 600ºC. Temperature (ºC) is shown in the x-axis, applied normal load (N) in the y-axis and the contour lines indicate the various wear rates in x10^{-5} mm^3/Nm. The different symbols on the chart represents various wear mechanisms as seen in the wear scar images. The changes in the contour line represent changes in the wear mechanism.

The contour regions are decided using the RSM method as described in the previous section. To be fully confident of these contour positions, more data is needed. A statistical analysis of the current data can be found in Appendix 8a. The contour areas are split into 5 regions. Region A is where the abrasive wear is dominant due to adhesive wear at the initial stages of the test leading to wear particles being released into the contact which in turn results in third body interaction increasing the wear volume. Severe abrasive-oxidative wear is occurring in region B. As the temperature is increased, the rate of oxidation and diffusion of the elements increases leading to more oxide layers being generated. Since the activation energy required for compaction and sintering has not been achieved, the oxide layers are easily broken down with further sliding. Therefore, the rate of breakdown is higher than the rate of generation of layers. Another key factor to consider is the load, the high wear rate seen with a higher load at 200ºC is because the debris generated are oxidised and the oxide particles are considered to be 'harder' than metallic debris damaging the surface more. Region C is where mild oxidative wear is occurring, thin layers of patchy glaze has started to appear on the surface. Even though a glaze layer is forming, it may not be thick enough to provide protection. At the higher load condition (400ºC at 37.5N), it can be seen that the wear mechanism changes to the glaze region, this suggests that the increase in flash temperature has aided to achieve enough energy

for the sintering of the debris. Regions D and E are where a protective glaze is observed.
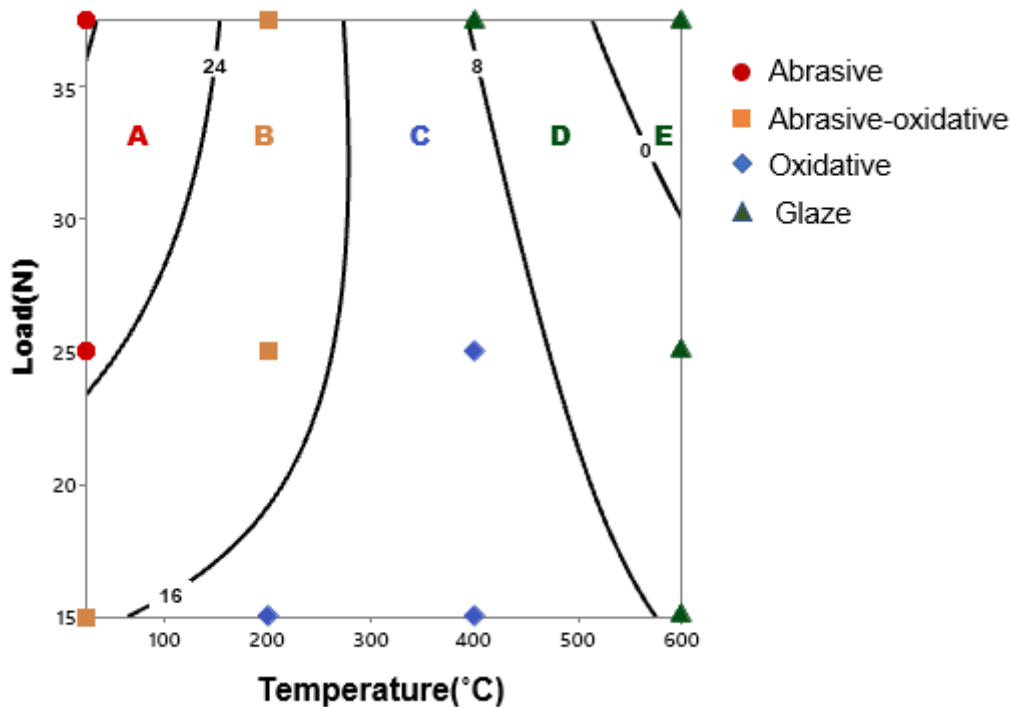
Figure 8.1 Wear map constructed from the experimental data obtained from like on like In718 tests.

8.4   C263

The wear map from the C263 analysis can be seen in Figure 8.2. Similar to the In718 wear map, a positive influence is observed with increasing temperature. However, the area of each contour region (i.e., wear mechanism) is different. Region A is where abrasive wear is happening. As the temperature is increased, the rate of oxidation increases, but there is insufficient energy available for an effective layer to be formed, resulting in severe abrasive-oxidative wear (Region B). Mild oxidative wear is dominant in region C, likely to be due to the formation of a NiCr layer which is considered to have poor adhering properties which makes it prone to detachment and removal of layers. Region D and E are where a glaze layer is seen because of the diffusion of Co into the surface, generating a CoCr layer. The map shows that C263 has a higher energy threshold compared to In718. Since both C263 and In718 are mainly composed of NiCr and displays different wear behaviour highlights the importance of other factors influencing the glaze generations such as the microstructure of the different alloys.
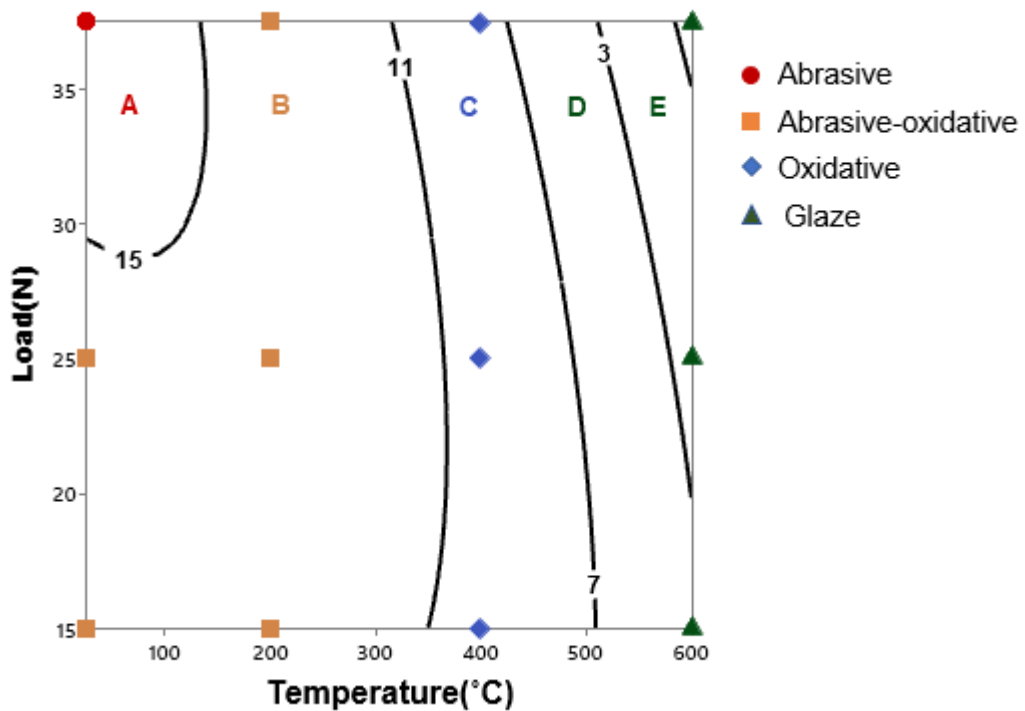
Figure 8.2 Wear map constructed from the experimental data obtained from like on like C263 tests.

8.5 Haynes 25

Figure 8.3 shows the wear map constructed for Haynes 25. A very different trend is seen in Haynes 25 map when compared to In718 and C263 maps. Two regions can be seen with low wear rates; however, distinct wear mechanisms are observed on the wear scars. When the temperature is below 200ºC, mechanical wear is seen with surface damage with striations and the coverage of oxide is low. This suggests that no oxide layers are generated which is evidenced by the no differences seen in the chemical composition. Whereas above 400ºC, a smooth- glaze layer is noticed with a CoCr dominant layer. The middle region can be split into two- mild and severe oxidative wear. Severe wear (Region B) is noticed when the load conditions are high. At high load conditions, the amount of debris produced is higher are oxidised. This results in oxidative wear is abrading into the surface. Region C is where mild oxidative wear is occurring. The oxide layer is preventing the metal-metal adhesions, however, the layers are not sintered to form a glaze layer, thus it is easily destroyed resulting in more wear. Above 400ºC, a wear protective layer is seen, thus the reduction in wear volume.
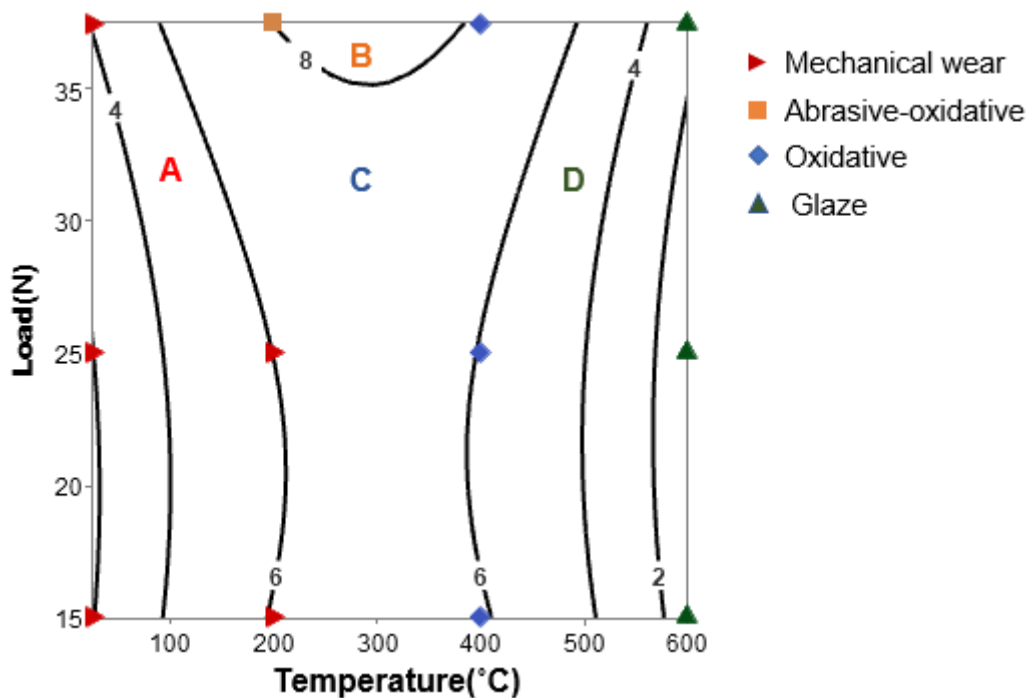
Figure 8.3 Wear map constructed from the experimental data obtained from like on like Haynes 25 tests.

As previously discussed, glaze generation is a complex process involving a variety of variables. This increases the challenge for the prediction and modelling of the wear. During this study, the temperature and pressure are the primary factors studied, but to fully validate the wear maps, a range of temepratures/pressures needs to be examined in order to confirm the predictions by the model. It is also essential to investigate the errors between the experimental and the predicted wear rates at various conditions.

Due to the complexity of laze geration process, the above-presented models can only be used for the conditions used in these tests. Further studies involving other factors such as speed, distance, humidity etc is vital to fully understand and thus produce a detailed wear map. As a result, there are some inaccuracies in the model. Though the regression values for the wear map model are situated between 88 to 92%, further tests are required to validate the model (see appendix 8a).

Chapter 9   Conclusions and further work

This chapter begins with justification of the aims and objectives used in this thesis, then key findings from the various experiments conducted are presented. Finally, the suggestions for future work are given.

9.1   Conclusions

This thesis aimed to investigate the fundamental factors influencing glaze generation and its breakdown. To achieve this aim, the tribological properties were assessed using experimental methods (ball-on-disc tests). Following the literature review (see Chapter 2) and the industry demands, the alloys and test conditions were chosen.

Most of the previous studies on the glaze generation and effectiveness under reciprocating sliding focused on the effect of temperature, since sliding is a complex process involving various mechanisms there are several areas where knowledge is missing. More work is needed to bring an understanding of other factors in glaze generation. Thus, this thesis examined the influence of temperature and the normal load on three different aerospace alloys (In718, C263 and Haynes 25). Both C263 and In718 are nickel based whereas Haynes 25 is a cobalt-based alloy, enabling to observe the effect of different elements in glaze generation.

The key findings from this thesis are as follows:

- From the literature review, it was clear that one of the primary factors impacting glaze generation is temperature as this influences the rate of oxidation and diffusion which are essential for the formation of glaze layers. Therefore, like-on-like material combinations were tested at a range of temperatures varying from room temperature to 600º C.
    1. A positive influence is observed on the materials as the temperature is increased.
    2. At lower temperatures, a higher wear volume and drops in COF (but unstable) is observed. The overall drops in COF is due to less adhesion between surfaces because of transient oxide layer formation. Since transient layers are broken down easily, generating debris, this leads to abrasive wear and a higher wear volume.
    3. At higher temperatures, a significant drop in wear volume and stable COF for a longer period of time (but not drops in overall COF). This suggests there is a high level of adhesion between the layers formed on both the pin and the disc because of the similar chemical composition of the layers. Also, because the glaze is not broken down easily, so less damage to the surface, and thus a reduction in the wear volume.

4. As the temperature changes, the rate at which the glaze is formed is different on various materials due to the differences in rates of oxidation and diffusion with In718 starts to glaze above 200ºC and Haynes 25 at 600ºC.

- The temperature can be increased either by increasing the bulk temperature or due to the flash temperature as the samples are rubbed. Hence, the applied load was altered (15 to 37.5N).

    1. As the load increases, the size of the wear debris increased, meaning it will take longer to break down the debris or some of them are pushed out of the contact, thus increasing wear volume.

    2. Previous studies have shown a linear trend in wear volume with increasing load where there is mechanical wear and exponential increase when an oxide layer is present. The experimental results from this study have shown a linear trend when there is no effective oxide layer present and exponential wear when oxidative wear is occurring. The Haynes 25 alloys showed a drop in wear volume with increasing load when a wear resistant glaze layer is present. However, In718 presented the lowest wear volume at an intermediate load (400 and 600ºC), likely to be because there is not enough time between the strokes to breakdown the debris as larger debris are produced at higher loads.

    3. Pressure can also affect the microstructure of the alloy, which can impact the formation and growth of the oxide layer. Specifically, higher pressure can lead to greater deformation of the material, which can create defects and dislocations in the crystal structure. These defects can provide sites for the nucleation and growth of the oxide layer.

    4. The surrounding environment usually has lower temperatures to form a glaze, so by increasing the pressure will increase the flash temperature. But experimental results and flash temperature calculations have shown the flash temperature rises are not high enough to achieve the required activation energy. Furthermore, leads to larger debris being generated which takes longer to breakdown.

- The chemical composition of the layers determines the effectiveness of the layer. Hence, EDS analysis were carried out to establish the chemical composition of the layers formed at various temperatures and load.

    1. As the temperature is increased, the chemical composition of the layers have varied resulting in wear mechanisms to change.
    2. NiCr layers have resulted in oxidative wear as both Ni and Cr oxides exhibits poor adhering properties. On the other hand, a CrFe and CoCr oxides presents a wear resistant layer is formed leading to reductions in wear volume.
    3. At a specific temperature, there were no significant differences in the composition observed among the various load conditions used.

- Overall, this study shows that temperature plays a more significant role in glaze generation than pressure. Though a rise in pressure can be beneficial by increasing the flash temperature so providing energy for oxidation and diffusion.

- The dissimilar material allowed the observation of the wear behaviour when two different alloys are used. A significant drop in the wear volume is seen at 400ºC, especially on the Haynes 25 sample against both C263 and In718 where a thick MML is noticed when compared to the like-on-like combination at the same conditions. However, at 600ºC, the results have not shown a major difference as both materials forms a glaze a 600ºC.

- One of the options to reduce the severe wear occurring during the run in stage is by pre-glazing the surface. The experimental results from the pre-glazed tests shows a drop in the wear volume and COF is seen when compared with room temperature tests, however, the extent of the wear resistance is not clear as the post room temperature data on reglazed samples and wear scar images indicate that the glaze layers have broken down due to changes in the thermal contraction/expansion rate resulting the detachments.

- Wear maps were constructed using a response surface methodology with temperature and load as the input parameters and wear rate as the target response. Both C263 and In718 show a similar response though the area of each wear mechanism was different, whereas Haynes 25 data shows a different pattern with two regions of low wear rate.

9.4   Further work

The experimental work and the results presented in this thesis provide clarifications on the role of some of the key factors influencing glaze formation. As previously mentioned, sliding is a complex phenomenon with various mechanisms, thus further work is needed to map the complete tribological performance of the materials used in this study.

- Currently, the tests have only conducted on simple geometry, therefore, further tests need to be conducted on more representative contacts to understand how debris are retained and the pressure changes can be further studied.
- The current study presented a fundamental analysis of the influence of alloying elements. Since oxidation and sintering are an essential part of the glaze formation process, this needs to be further studied. A Focused Ion Beam (FIB) analysis would be beneficial to understand the composition of each layers.
- Since temperature is only one of the factors affecting the diffusion of elements, other factors affecting diffusion and oxidation rates needs to be further investigated.
- In order to simplify and focus on the dissimilar material combination, only one load condition is used, so further tests are needed to understand the effect of flash temperature. Moreover, the pin/disc samples needs to swap to observe the impact of debris availability and retention on glaze generation.
- To validate the wear map model, more wear tests at regular temperatures and load conditions are needed. Since glaze generation involves a range of different processes, other factors such as sliding distance, speed, environmental factors etc needs to be investigated.
- An in-situ glaze progression/degeneration visualization method to understand how the layers are broken especially at pre-glazed conditions. This will also enable to observe any changes in the debris (such as the size, the movement etc).

References

[1]   R. Rajendran, "Gas turbine coatings - An overview," Engineering failure analysis, vol. 26, pp. 355-369, 2012.

[2]   "Aeroengine Safety," Institute of Thermal Turbomachinery and Machine Dynamics, Graz University of Technology, 2022. [Online]. Available: https://aeroenginesafety.tugraz.at/doku.php?id=6:62:62. [Accessed 1 November 2022].

[3]   A. Dreano, S. Fouvry and G. Guillonneau, "Understanding and formalization of the fretting-wear behavior of a cobalt-based alloy at high temperature," Wear, Vols. 452-453, pp. 203-297, 2020.

[4]   T. Howard, "HP/IP Spherical Wear Test Report," The Leonardo Tribology Centre, Sheffield, 2014.

[5]   S. R. Rose, "Studies of the high temperature tribological behaviour of some superalloys," PhD thesis, University of Northumbria at Newcastle, 2000.

[6]   K.S.Anastasiou, "Optimization of the aluminium die casting process based on the Taguchi method," Proceedings of Institute of Mechanical Engineers, vol. 216, no. 7, pp. 969-977, 2002.

[7]   G. W. Stachowiak, Engineering tribology, 3 ed., Amsterdam;Boston: Elsevier Butterworth-Heinemann, 2005.

[8]   C. Mate, Tribology on the Small Scale: A Bottom Up Approach to Friction, Lubrication, and Wear, Oxford: Oxford University Press, 2007.

[9]   B. Bhushan, Introduction to tribology, 2 ed., Hoboken: John Wiley & Sons Inc, 2013.

[9]   Hölscher and e. a. Hendrik, " Principles of Atomic Friction: From Sticking Atoms to Superlubric Sliding," Philosophical Transactions: Mathematical, Physical and Engineering Sciences, vol. 366, no. 1869, p. 1383–1404.

[10]   K. Holmberg and A. Matthews, Coatings Tribology: Properties, Mechanisms, Techniques and Applications in Surface Engineering, Oxford: Oxford: Elsevier Science & Technology., 2009.

[12]   E. N. J. Pedro M.D. Santos, "A state-of-the-art review on roughness quantification methods for concrete surfaces," Construction and Building Materials, pp. 912-923, 2012.

[13]   S. L. Casey Q. LaMarche, "Method of quantifying surface roughness for accurate adhesive force predictions," Chemical EngineeringScience, vol. 158, pp. 140-153, 2017.

[14]   A. Merkle and L. Marks, "Dynamic In-situ TEM Investigations of Tribological Interfaces," Microscopy and Microanalysis, vol. 12, no. S02, pp. 950-951, August 2006.

[15]   "The Tribology Laboratory," Lehigh University , [Online]. Available: https://www.lehigh.edu/~intribos/. [Accessed 10 August 2020].

[16]   K. Anantheshwara, A. J. Lockwood, R. K. Mishra, B. J. Inkson and M. Bobji, "Dynamical Evolution of Wear Particles in Nanocontacts," Tribology letters, vol. 45, no. 2, pp. 229-235, 2012.

[17]   J. F. Archard and W. Hirst, "The Wear of Metals under Unlubricated Conditions," Proceedings of the Royal Society of London. Series A, Mathematical and Physical Sciences, vol. 236, no. 1206, pp. 397-410, 1956.

[18]   J. T. Burwell, "Survey of possible wear mechanisms," Wear, vol. 1, no. 2, pp. 119-141, 1957.

[19]   H. R, Electric Contacts: Theory and Application, Newyork: Springer-Verlag, 1967.

[20]   R. Aghababaei, " On the origins of third-body particle formation during adhesive wear," Wear, vol. 426, pp. 1076-1081, 2019.

[21]   R. Aghababaei, D. H. Warner and J.-F. Molinari, "Critical length scale controls adhesive wear mechanisms. Nat Commun. 7(1), p11816.," NAture communications, vol. 7, no. 11816, 6 June 2016.

[22]   K. Holmberg and A. Matthews, Coatings Tribology: Properties, Mechanisms, Techniques and Applications in Surface Engineering, Oxford: Oxford: Elsevier Science & Technology., 2009.

[23]   T. F. J. Quinn, "Oxidational wear modelling: I," Wear, vol. 153, no. 1, pp. 179-200, 1992.

[24]   T. F. J. Quinn, "Review of oxidational wear: Part I: The origins of oxidational wear," Tribology International, vol. 16, no. 5, pp. 257-271, 1983.

[25]   F. H. Stott, " The role of oxidation in the wear of alloys," Tribology International, vol. 31, pp. 61-71, 1998.

[26]   F. H. Stott, D. S. Lin and G. C. Wood, "The structure and mechanism of formation of the 'glaze' oxide layers produced on nickel-based alloys during wear at high temperatures," Corrosion Science, vol. 13, no. 6, pp. 449,IN443,455-454,IN446,469., 1973.

[27]   J. K. Lancaster, "The formation of surface films at the transition between mild and severe metallic wear," Wear, vol. 6, no. 5, p. 417, 1963.

[28]   J. Jiang, F. H. Stott and M. M. Stack, "The role of triboparticulates in dry sliding wear," Tribology international, vol. 31, no. 5, pp. 245-256, 1998.

[29]   J. Jiang, F. H. Stott and M. M. Stack, "Some frictional features associated with the sliding wear of the nickel-base alloy N80A at temperatures to 250 °C," Wear, vol. 176, no. 2, pp. 185-194, 1994.

[30]   F. H. Stott, "High-temperature sliding wear of metals," Tribology International, vol. 35, no. 8, pp. 489-495, 2002.

[31]   A. Iwabuchi, K. Hori and H. Kubosawa, "The Effect of Oxide Particles Supplied at the Interface Before Sliding on the Severe--Mild Wear Transition," Wear, vol. 128, no. 2, pp. 123-137, 1988.

[32]   A. Iwabuchi, H. Kubosawa and K. Hori, "The dependence of the transition from severe to mild wear on load and surface roughness when the oxide particles are supplied before sliding," Wear, vol. 139, no. 2, pp. 319-333, 1990.

[33]   K. i. Hiratsuka and K. i. Muramoto, " Role of wear particles in severe–mild wear transition. Wear," Wear, vol. 259, no. 1, pp. 467-476, 2005.

[34]   F. P. Bowden and P. H. Thomas, "The Surface Temperature of Sliding Solids," Proceedings of the Royal Society of London. Series A. Mathematical and Physical Sciences, vol. 223, pp. 29-40, 1954.

[35]   D. Kuhlmann-Wilsdorf, "(1985). Flash temperatures due to friction and Joule heat at asperity contacts," Wear, vol. 105, no. 3, pp. 187-198, 1985.

[36]   F. S. M. S. Jiaren Jiang, "A generic model for dry sliding wear of metals at elevated temperatures," wear, vol. 256, pp. 973-985, 2004.

[37]   F. P. Bowden and P. H. Thomas, "The Surface Temperature of Sliding Solids," Proceedings of the Royal Society of London. Series A. Mathematical and Physical Sciences, vol. 223, pp. 29-40, 1954.

[38]   F. H. Stott and M. P. Jordan, " The effects of load and substrate hardness on the development and maintenance of wear-protective layers during sliding at elevated temperatures," Wear, vol. 250, pp. 391-400, 2001.

[39]   F. S. M. S. Jiaren Jiang, "A generic model for dry sliding wear of metals at elevated temperatures," wear, vol. 256, pp. 973-985, 2004.

[40]   Z.-m. L. Yun-fei, "Influence of Normal Load, Sliding Speed and Ambient Temperature on Wear Resistance of ZG42CrMo," Journal of Iron and Steel Research, vol. 19, no. 4, pp. 69-74, 2012.

[41]   F. Alkelae and S. Fouvry, "Identification of parameters influencing the glaze layer formation and stability at high temperature for a Waspaloy/René125 contact under fretting wear conditions," Wear, vol. 390, pp. 41-48, 2017.

[42]   R. Wohltat, "Trent 1000 : Results of Coefficient of Friction testing on 1N718 (REW), 1N713 (QDC) and MarMOO2 (QPD) - MERO6O200," Rolls-Royce, Germany, 2018.

[43]   J. Jiang, F. H. Stott and M. M. Stack, "The effect of partial pressure of oxygen on the tribological behaviour of a nickel-based alloy, N80A, at elevated temperatures," Wear, vol. 203, pp. 615-625, 1997.

[44]   D. Klaffke, "On the repeatability of friction and wear results and on the influence of humidity in oscillating sliding tests of steel-steel pairings," Wear, vol. 189, pp. 117-121, 1995.

[45]   L. Xin, Z. Wang, J. Li, Y. Lu and T. Shoji, "Microstructural characterization of subsurface caused by fretting wear of Inconel 690TT alloy," Materials Characterization, vol. 115, pp. 32-38, 2016.

[46]   A. Viat, A. Dreano, S. Fouvry, D. B. B. M.-I and J.-F. Henne, "Fretting wear of pure cobalt chromium and nickel to identify the distinct roles of HS25 alloying elements in high temperature glaze layer formation," Wear, vol. 376, p. 1043, 2017.

[47]   A. Dreano, S. Fouvry, S.-J. S, J. Galipaud and G. Guillonneau, "The formation of a cobalt-based glaze layer at high temperature: A layered structure," Wear, vol. 440, p. p203101, 2019.

[48]   E. Rabinowicz, "Friction and wear of materials," Journal of Lubrication Technology – Transactions of the ASME, vol. 103, pp. 188-194, 1981.

[49]   S. Hsu, Y. Yang and R. Munro, "Quantitative wear maps as a visulaisation of wear mechanism transitions in cermaic materials," Wear, 1980.

[50]   M. F. Ashby and S. C. Lim, " Wear-mechanism maps," Scripta Metallurgica et Materiala, vol. 25, no. 5, pp. 805-810, 1990.

[51]   M. Okoshi and H. Sakai, " Research on the mechanism of abrasion. Report III, mechanism of abrasion of cast iron and steel," Trans. JSME, vol. 7, pp. 29-47, 1941.

[52]   I. A. Inman and P. S. Datta, " (2010a). Studies of high temperature sliding wear of metallic dissimilar interfaces III: Incoloy MA956 versus Incoloy 800HT," Tribology International, vol. 43, no. 11, pp. 2051-2071, 2010.

[53]   G. Zheng, J. Zhao and Y. Zhou, "Friction and wear behaviors of Sialon–Si 3 N 4 graded nano-composite ceramic materials in sliding wear tests and in cutting processes," wear.

[54]   A. Dreano, S. Fouvry and G. Guillonneau, "Understanding and formalization of the fretting-wear behavior of a cobalt-based alloy at high temperature," Wear, Vols. 452-453, pp. 203-297, 2020.

[55]   M. Cadeddu, "An Investigation of Molybdenum Disulphide Dry Film Lubricant Coatings," The University of Sheffield, Sheffield, 2021.

[56]   A. S.T.M. (ASTM), "G133 Standard Test Method for Linearly Reciprocating Ball-on-Flat Sliding Wear.," ASTM, 2016.

[57]   "Pin on disk test," TriboNet, [Online]. Available: https://www.tribonet.org/wiki/pin-on-disk-test/. [Accessed 14 November 2019].

[58]   NeoNickel, "Alloy C263," [Online]. Available: https://www.neonickel.com/generate-alloy-pdf/?id=114. [Accessed 12 May 2020].

[59]   A. Materials, "Nickel Alloy C263," [Online]. Available: https://www.azom.com/article.aspx?ArticleID=9485. [Accessed 12 May 2020].

[60]   H. International, "Haynes 25," [Online]. Available: https://www.haynesintl.com/alloys/alloy-portfolio_/High-temperature-Alloys/haynes-25-alloy/chemical-composition. [Accessed September 2021].

[61]   Ulbrich, "Inconel 718 (Alloy 718)," [Online]. Available: https://www.ulbrich.com/alloys/inconel-718-uns-n07718/. [Accessed 12 May 2020].

[62]   A.S. metals, "Special Metals Inconel 718," [Online]. Available: http://asm.matweb.com/search/SpecificMaterial.asp?bassnum=NINC34. [Accessed 12 May 2020].

[63]   A. Ravikiran and S. Jahanmir, "Effect of contact pressure and load on wear of alumina," Wear, vol. 241, no. 1-12, pp. 980-984, 2001.

[64]   A. Rudnytskyj, "Simulations of contact mechanics and wear of linearly reciprocating block-on-flat sliding test," Luleå University of Technology , 2018.

[65]   S. Kucharski and Z. Mroz, "Identification of wear process parameters in reciprocating ball-on-disc tests," Tribology International, vol. 44, pp. 154-164, 2011.

[66]   M. H. Nazir, Z. A. Khan, A. Saeed, V. BAkolas, W. Braun and R. Bajwa, "Experimental analysis and modelling for reciprocating wear behaviour of nanocomposite coatings," Wear, Vols. 416-417, pp. 89-102, 2018.

[67]   J. J. Ayerdi, A. Aginagalde, I. Llavori, J. Bonse, D. Spaltmann and A. Zabala, "Ball-on-flat linear reciprocating tests: Critical assessment of wear volume

determination methods and suggested improvements for ASTM D7755 standard,," Wear, Vols. 470-471, 2021.

[68]   V. Hegadekattea, N. Huberb and O. Krafta, "Modeling and simulation of wear in a pin on disc tribometer," Tribology Letters, vol. 24, no. 1, pp. 51-60, 2006.

[69]   ASTM, "G115-10 Standard Guide for Measuring and Reporting Friction Coefficients," p. 13, 2018.

[71]   A. R. Warmuth, W. Sun and P. H. Shipway, "The roles of contact conformity, temperature and displacement amplitude on the lubricated fretting wear of a steel-on-steel contact," Royal Society, vol. 3, no. 10, 2016.

[72]   T. Dick, C. Paulin, G. Cailletaud and S. Fouvry, "Experimental and numerical analysis of local and global plastic behaviour in fretting wear," Tribology International, vol. 39, no. 10, pp. 1036-1044, 2006.

[73]   S. Fouvry, P. Duo and P. Perruchaut, "A quantitative approach of Ti–6Al–4V fretting damage: friction, wear and crack nucleation," Wear, vol. 257, no. 9-10, pp. 916-929, 2004.

[74]   D. ,. K. M. O. A. N. D. a. H. D. Mulvihill, "Investigation of non-Coulomb friction behaviour in reciprocating sliding," Wear, vol. 271, no. 5-6, pp. 802-816, 2011.

[75]   K. Thomas, "Image processing as applied to medical diagonostics," University of Oregon, 2010.

[76]   B. a. s. Scotland, "Segmentation," [Online]. Available: https://www.bioss.ac.uk/people/chris/ch4.pdf. [Accessed November 2021].

[77]   Y. Li, J. Sun and C.-K. Tang, "Lazy Snapping," ACM Transactions on Graphics, vol. 23, no. 3, pp. 303-308, August 2004.

[78]   L. Kempenaers, "The Basics of Elemental Analysis with XRF – Q&A," Malvern Panalytical, 7 January 2020. [Online]. Available: https://www.materials-talks.com/the-basics-of-elemental-analysis-with-xrf-qa/. [Accessed November 2021].

[79]   Fischer, "FISCHERSCOPE   X-RAY   Series," [Online]. Available: https://www.helmut-fischer.com/fileadmin/content/1-filebase/3-products/2-pdf/4-x-ray/en/BROC_952-008_X-RAY-Overview-en.pdf. [Accessed June 2021].

[80] Buehler, Buehler SumMet, The Sum of our experinece, A guide to Materials preparation & Analysis, 2018.

[81] E. a. A. K. Gulbransen, "Kinetics of the Oxidation of Chromium," Journal of The Electrochemical Society, vol. 104, no. 6, 1957.

[82] F. H. Stott and M. P. Jordan, "The effects of load and substrate hardness on the development and maintenance of wear-protective layers during sliding at elevated temperatures," Wear, vol. 250, no. 1-12, pp. 391-400, 2001.

[83] A. Dreano, S. Fouvry, S. Sao-Joao, J. Galipaud and G. Guillonneau, "The formation of a cobalt-based glaze layer at high temperature: A layered structure," Wear, Vols. 440-441, 2019.

[84] I. A. Inman and P. S. Datta, "Development of a simple 'temperature versus sliding speed' wear map for the sliding wear behaviour of dissimilar metallic interfaces II," Wear, vol. 265, no. 11-12, pp. 1592-1605, 2008.

[85] Helmi Attia, A. d. Pannemaecker and G. Williams, "Effect of temperature on tribo-oxide formation and the fretting wear and friction behavior of zirconium and nickel-based alloys," Wear, vol. 476, 2021.

[86] M. M. De OliveiraJunio, H. L. Costa, Silva Junior and J. De Mello, "Effect of iron oxide debris on the reciprocating sliding wear of tool steels," Wear, Vols. 426-427, pp. 1065-1075, 2019.

[87] A. P. Mouritz, Introduction to aerospace materials, 1 ed., Cambridge;Philadelphia,;New Delhi: Woodhead Publishing, 2012.

[88] A. Tewari, "Load dependence of oxidative wear in metal/ceramic tribocouples in fretting environment," vol. 289, 2012.

[89] A. Laureys, M. Pinson, T. Depover, R. Petrov and K. Verbeken, "EBSD characterization of hydrogen induced blisters and internal cracks in TRIP assisted Steel," Materials Characterization, vol. 159, 2020.

[90] K. J. Kozaczek, B. G. Petrovic, C. O. Ruud, S. K. Kurtz and A. R. McIlree, "Microstructural modelling of grain-boundary stresses in Alloy 600," Journal of Materials Science, vol. 30, pp. 2390-2400, 1995.

[91]   K. Bhansali, "Adhesive wear of nickel- and cobalt-base alloys," vol. 60, no. 1, 1980.

[92]   Y. P. H.-m. L. Y.-f. L. Jian ZHANG, "Influence of Normal Load, Sliding Speed and Ambient Temperature on Wear Resistance of ZG42CrMo," vol. 19, no. 4, 2012.

[93]   K. Bhansali, "Adhesive wear of nickel and cobalt base alloys," Wear, vol. 60, no. 1, pp. 95-110, April 1980.

[94]   Hsu, Stephen, Wang, Y.S. and Munro, "Quantitative Wear Maps as a Visualisation of Wear Mechanisms Transition in Ceramic Materials," Wear, vol. 134, no. 10, pp. 1-11, 1989.

[95]   H. Zhou, P. Yao, Y. Xiao, K. Fan, Z. Zhang, T. Gong, L. Zhao, M. Den, C. Liu and P. Ling, "Friction and wear maps of copper metal matrix composites with different iron volume content," Tribology International, vol. 132, pp. 199-210, 2019.

[96]   S. M. HSU, D. S. LIM, Y. S. WANG and R. G. MUNRO, "Ceramics Wear Maps: Concept and method developments," Lubrication Engineering, vol. 41, no. 1, pp. 49-54, 1991.

[97]   X. Zhang, K. Zhang, X. Kang and L. Zhang, "Friction maps and wear maps of Ag/MoS2/WS2 nanocomposite with different sliding speed and normal force," Tribology International, vol. 164, 2021.

[98]   R. Siriyala, G. Alluru, R. Penmetsa and e. al., "Application of grey-taguchi method for optimization of dry sliding wear properties of aluminum MMCs," Frontiers of Mechanical Engineering , vol. 7, pp. 279-287, 2012.

[99]   S. Basavarajappa, G. Chandramohan and J. P. Davim, "Application of Taguchi techniques to study dry sliding wear behaviour of metal matrix composites," Materials & Design, vol. 28, no. 4, pp. 1393-1398, 2007.

[100]   S. Chelladurai, M. K., A. P. Ray, M. Upadhyaya, V. Narasimharaj and G. S, "Optimization of process parameters using response surface methodology: A review," materialstoday:proceedings, vol. 37, no. 2, pp. 1301-1304, 2021.

[101]   K.S.Anastasiou, "Optimization of the aluminium die casting process based on the Taguchi method," Proceedings of Institute of Mechanical Engineers, vol. 216, no. 7, pp. 969-977, 2002.

[102]   D.A.Rigney, L. Chen, M. Naylor and A. Rosenfield, "Wear processes in sliding systems," Wear, vol. 100, no. 1-3, pp. 195-219, 1984.

[103]   D. A. Rigney, "Large strains associated with sliding contact of metals," Material Research Innovations, vol. 1, pp. 231-234, 1998.

Appendix
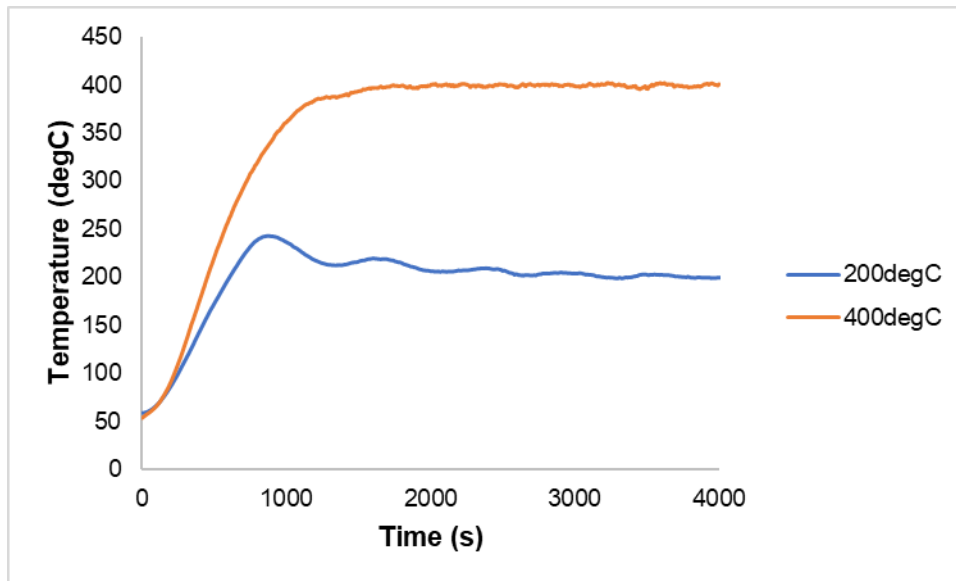
3a   Heater output data

Figure 3a-1 heater controller output data from 200 and 400ºC tests.
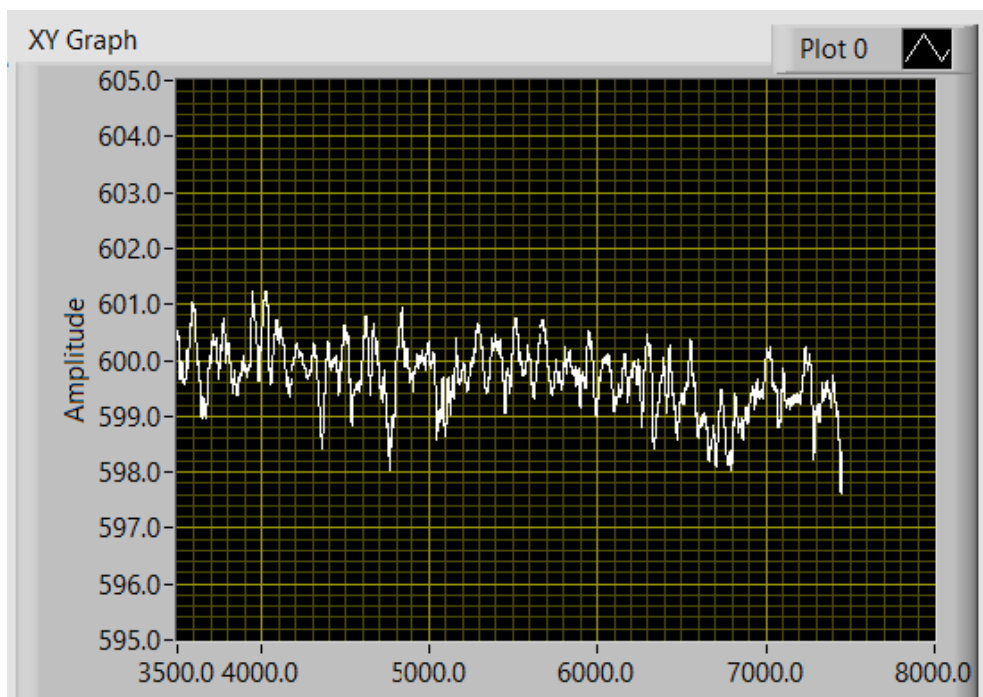

Figure 3a-2 heater controller output data from 600ºC tests.

3b: Fretting loops

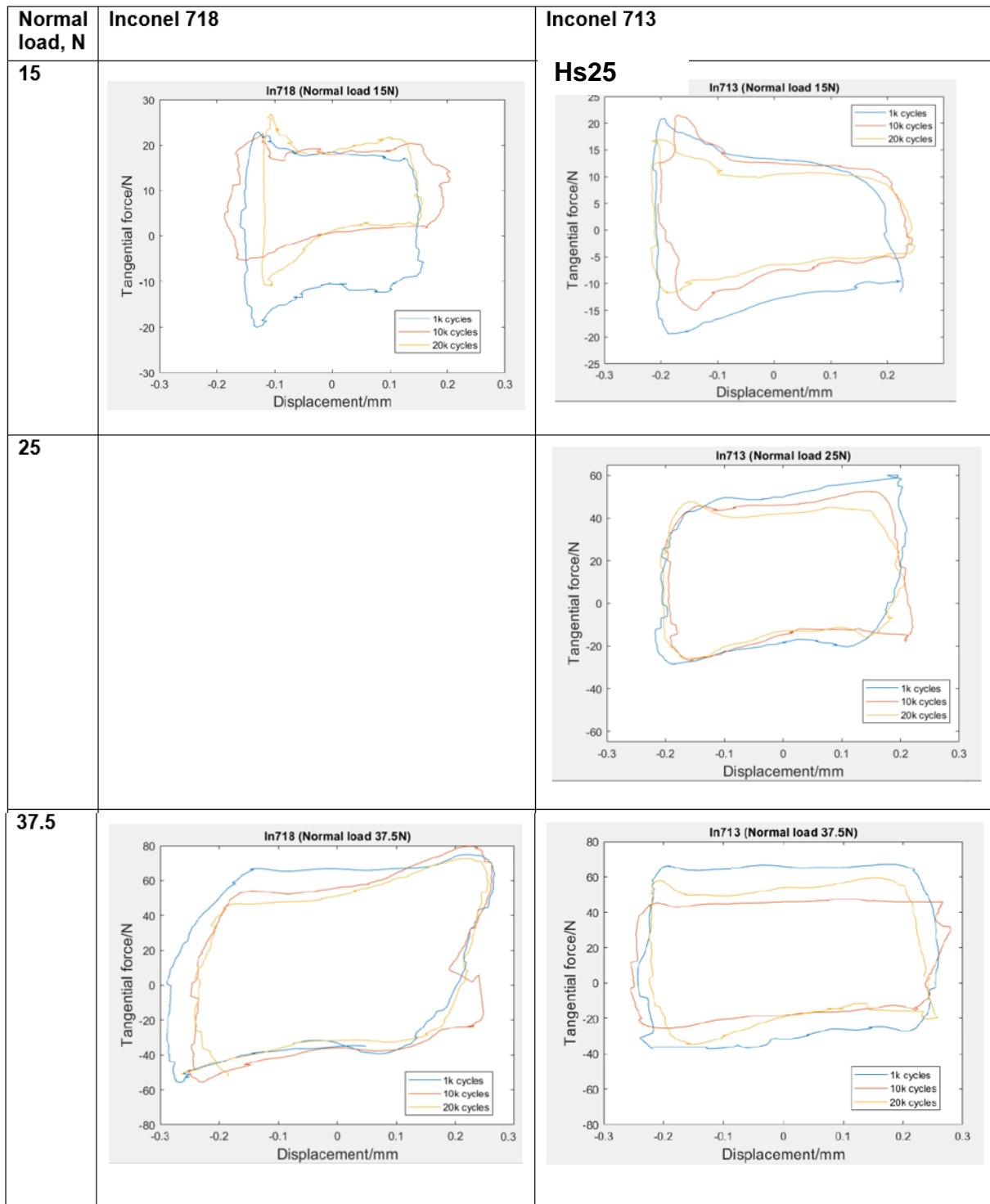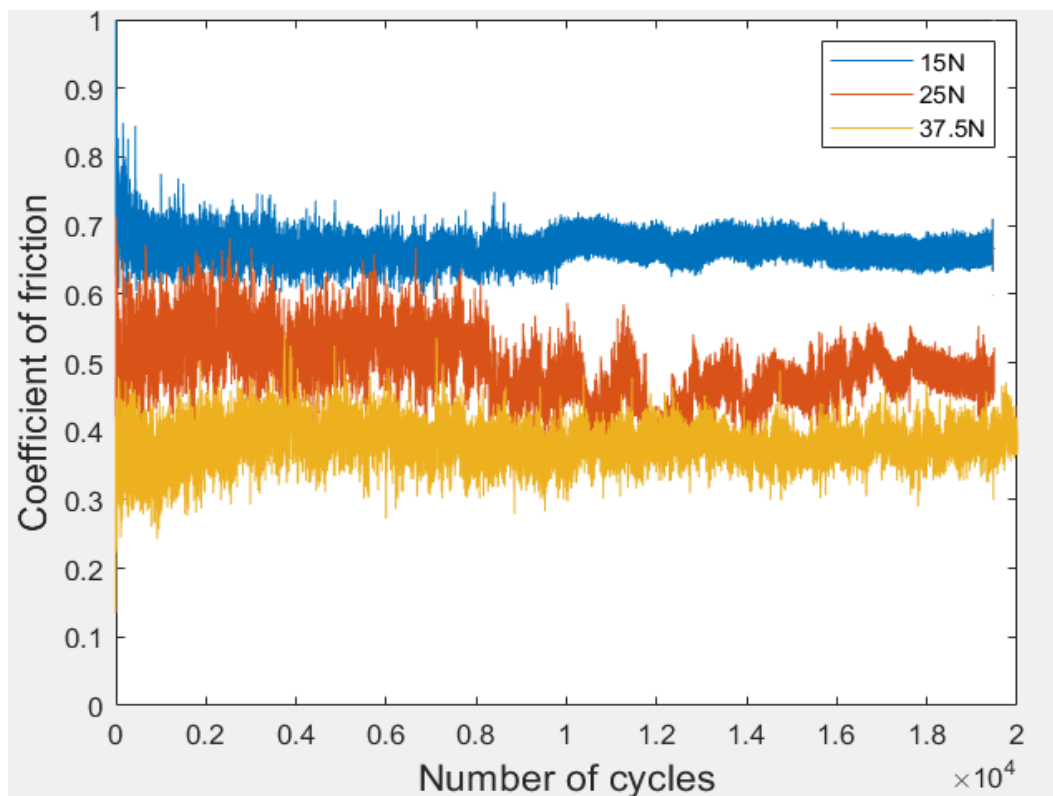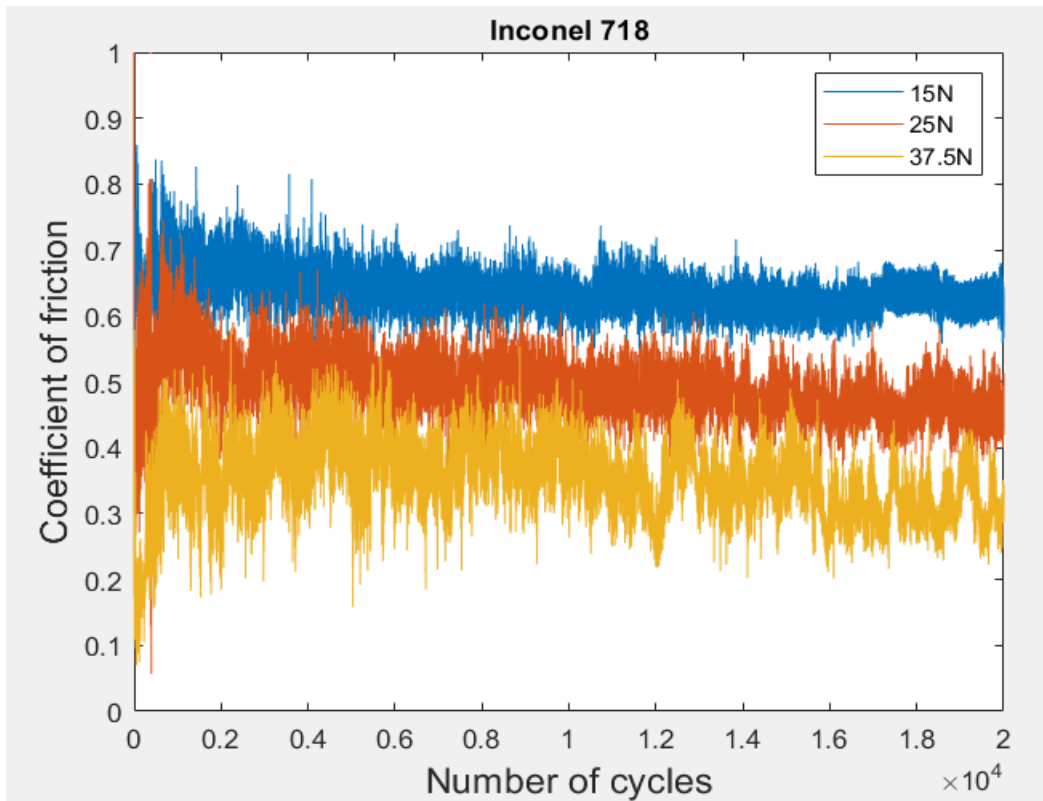| Normal load, N	Inconel 718	Inconel 713
15		**Hs25**
25		
37.5		

Figure 3b-1 fretting loops.

4a: Evolution of COF with time

The variation in COF throughout the test. As seen in the figure, the starting point of each test is different, and it is due to the rig inaccuracies at lower loads. Relative COF was calculated to avoid the errors due to the rig.
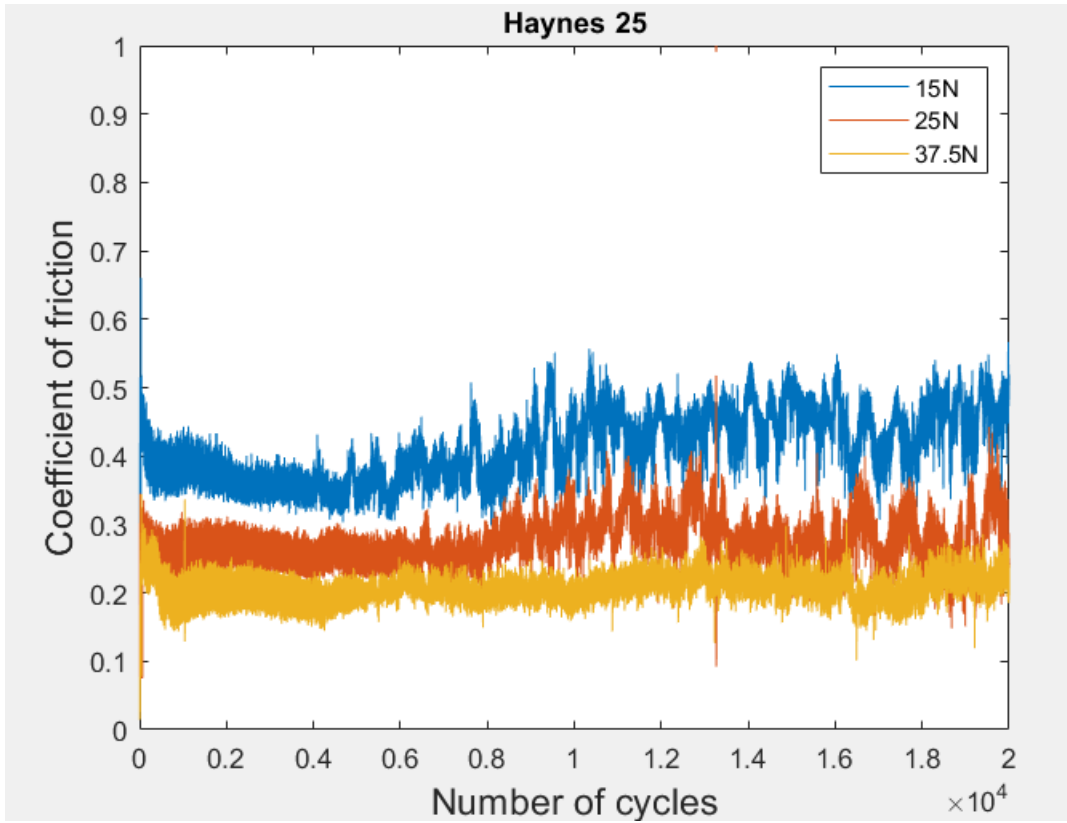
Figure 4a-1 The progression of COF without taking the irregularities in the test rig.

4b: Haynes 25 elemental analysis

Table 4c-1 shows the chemical composition of the layers formed on the Haynes 25 samples at room temperature. As seen in the table 4c-2, there is not much difference the ratios of the elements, meaning no glaze layers were formed. Additionally, the availability of oxygen was considerably lower even at 'black oxidised' regions suggesting either the plastic deformation or cracks are not developed on the surface to allow oxygen diffusion.

Haynes 25		Ni	Cr	Co	O	W
	Control	10	19.8	46.8	0	13.6
15N	no glaze	10.2	20.4	48.6	0	14.2
	Initial glaze	10	19.8	47.8	1.3	14.2
	glaze	8.6	17.6	41.6	9.6	12.7
25N	no glaze	9.8	19.7	46.6	0	13.5
	Initial glaze	8.0	16.4	38.7	11.2	11.2
	glaze	7.3	20.2	34.7	6.2	10
37.5N	no glaze	5.0	20.5	49.9	16.9	13.9
	Initial glaze	8.2	19.1	34.9	15.6	12.7
	glaze	9.2	21.9	38.4	20.5	11.8

Table 4b-1 the percentage of main alloying elements at varying load and different regions of interests from the room temperature tests.

Haynes 25	Ni/Cr	Co/Cr	Ni/Co
Control	0.51	2.36	0.21
15	0.49	2.36	0.21
25	0.36	1.72	0.21
37.5	0.42	1.75	0.24

Table 4b-2 the ratios between the main alloying elements from the glaze layers formed on Haynes 25 room temperature tests.

5a: Interrupted test at 200ºC
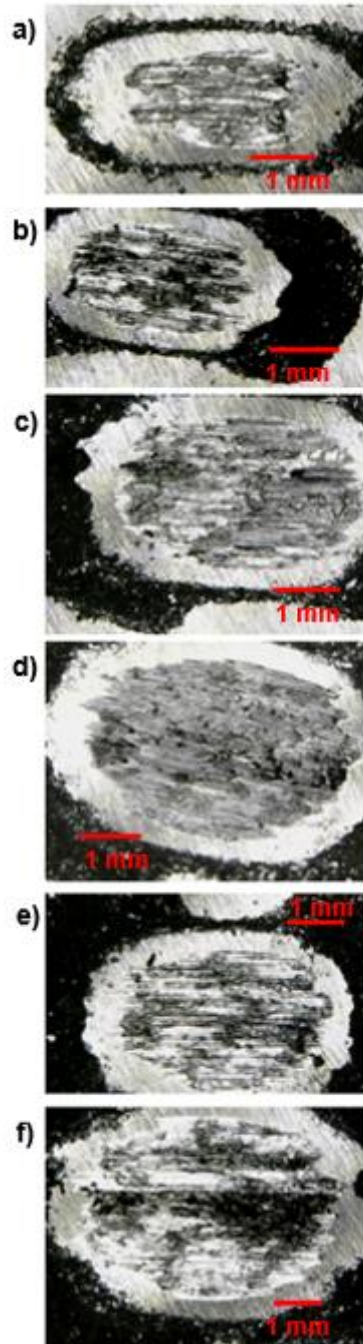
8a   Mathematical model for wear prediction using RSM

Three different models are developed for the different materials as the wear responses were different. But, the input and the response parameters are kept same.

Regression equation:

- (In718) Wear rate x10e-5 (mm^3/Nm)= -1.0 + 0.0177 Temperature(ºC) + 1.38 Load(N)+0.000001Temperature(ºC)*Temperature(ºC)-0.0115Load(N)*Load(N) - 0.00227 Temperature(ºC)*Load(N)

- (C263) Wear rate x10e-5 (mm^3/Nm)= 3.5 + 0.0298 Temperature(ºC) + 0.594 Load(N)-0.000050Temperature(ºC)*Temperature(ºC)-0.0071 Load(N)*Load(N) - 0.000777 Temperature(ºC)*Load(N)

- (Haynes 25) Wear rate x10e-5 (mm^3/Nm)= 3.7 + 0.0390 Temperature(ºC) - 0.29 Load(N)   -   0.000063   Temperature(ºC)*Temperature(ºC)+0.0075 Load(N)*Load(N) - 0.000060 Temperature(ºC)*Load(N)

-

Analysis of Variance (In718)

Source	DF	Adj SS	Adj MS	F-Value	P-Value
Model	5	1161.33	232.267	2.14	0.191
Linear	2	952.09	476.045	4.38	0.067
Temperature(ºC)	1	948.26	948.260	8.72	0.025
Load(N)	1	3.67	3.673	0.03	0.860
Square	2	5.54	2.771	0.03	0.975
Temperature(ºC)*Temperature(ºC)	1	0.02	0.019	0.00	0.990
Load(N)*Load(N)	1	5.52	5.523	0.05	0.829
2-Way Interaction	1	243.66	243.659	2.24	0.185
Temperature(ºC)*Load(N)	1	243.66	243.659	2.24	0.185
Error	6	652.24	108.707		
Total	11	1813.58			

Analysis of Variance (C263)

Source	DF	Adj SS	Adj MS	F-Value	P-Value
Model	5	337.652	67.530	7.11	0.017
Linear	2	271.515	135.757	14.29	0.005
Temperature(ºC)	1	271.106	271.106	28.53	0.002
Load(N)	1	0.437	0.437	0.05	0.837
Square	2	42.341	21.171	2.23	0.189
Temperature(ºC)*Temperature(ºC)	1	40.257	40.257	4.24	0.085
Load(N)*Load(N)	1	2.084	2.084	0.22	0.656
2-Way Interaction	1	28.461	28.461	3.00	0.134
Temperature(ºC)*Load(N)	1	28.461	28.461	3.00	0.134
Error	6	57.016	9.503		
Total	11	394.668			

Analysis of Variance (Haynes 25)

Source	DF	Adj SS	Adj MS	F-Value	P-Value
Model	5	74.433	14.8865	0.84	0.567
Linear	2	8.481	4.2407	0.24	0.795

Temperature(ºC)	1	2.101	2.1014	0.12	0.742
Load(N)	1	6.370	6.3705	0.36	0.571
Square	2	64.936	32.4682	1.83	0.240
Temperature(ºC)*Temperature(ºC)	1	62.629	62.6290	3.53	0.109
Load(N)*Load(N)	1	2.307	2.3073	0.13	0.731
2-Way Interaction	1	0.171	0.1710	0.01	0.925
Temperature(ºC)*Load(N)	1	0.171	0.1710	0.01	0.925
Error	6	106.440	17.7399		
Total	11	180.872			

Material	R squared (%)
In718	92.3
C263	85.5
Haynes 25	83.1